Targeting Complex Topologies with Dynamic Combinatorial Chemistry

Eilbigi Dehkordi, Mehrafarin

Award date:
2018

Awarding institution:
University of Bath

Targeting Complex Topologies with Dynamic Combinatorial Chemistry

Mehrafarin Eilbigi Dehkordi

A thesis submitted for the degree of Doctor of Philosophy

University of Bath

Department of Chemistry

May 2018

Abstract

Dynamic combinatorial chemistry (DCC) is a powerful tool for synthesising molecules with complex topologies and identifying unexpected receptors, catalysts and ligands. This work explores its use towards synthesising various [2]catenanes.

Chapter 1 outlines the concept of DCC and its applications, exploring how the folding and arrangement of molecules such as catenanes takes place. The DCC evolution is discussed and how donor-acceptor interactions have affected the synthesis of complex topologies.

Chapter 2 describes the discovery of a new generation of donor-acceptor [2]catenanes in aqueous dynamic combinatorial systems. More importantly, a mechanism that explains and predicts the structures formed is provided, giving a fundamental insight into the role played by the hydrophobic effect and donor-acceptor interactions in this process. It also explores in further detail how subtle variations in the building block design influence the selective formation of [2]catenane.

Chapter 3 describes the assembly of new [2]catenanes in aqueous libraries using NDI dumb-bell building blocks, where linkers with two nitrogen atom influence the libraries distribution.

In Chapter 4, a new dithiol acceptor building block is introduced and the interaction of this molecule with different acceptors moieties and a donor building block is studied.

Chapter 5 underlines both the advantages and the limitations of the method developed in Chapters 2, 3 and 4.

After a short conclusion (Chapter 5), Chapter 6 provides experimental details.

Acknowledgements

First of all, I would like to thank my supervisor, Dr Dan Pantoș, for his kindness and support throughout the time I worked with him. I can say he is one of the greatest people and as the previous students used to call him “The King”.
Dan’s dedication to work is inspiring and I have learnt so much from him. Working with him was a valuable experience, fun, and lots of stressful times (but still fun).

I would like to especially thank Dora Răsădean for her support and patient, for working with me late hours so I can finish my work and for being so kind and helpful every step of the way.
I also would like to thank Tiberiu Gianga (Tibi) for testing my patience every day and being the calmest person on earth. I thank Tibi for his help in daily work and useful discussions about mass spec and NMR.
I will definitely miss Simone Limberti – my coffee buddy–; the coffee breaks we took to chat and gossip about the Pantoș group. Also, I thank Dr Giles Prentice, who was a great support and help during the time he spent in the Pantoș group.

I also thankful to all the colleagues in the Department of Chemistry in 1South that made workplace enjoyable and for all the moments we laughed and shared experiences: Dr Fabienne Pradaux-Caggiano, Dr Adam Sedgwick, Toby Nash, Ben Alexander and George. My thanks go to Dr John Lowe for valuable help with NMR studies set up.

I am grateful to my family for always being there for me. My sister, Bahar, for spoiling me with gifts and trips and being more excited about my PhD than her own. My dad, who without my life is not possible and every day I am grateful for having him, maybe far (Kuwait), but he is always in my mind and heart. My mum, for comforting me at difficult times with her kind words and unconditional support. And my husband, Dooman, who makes me a better person ever day and I am grateful for his unconditional love and support, which makes me feel so lucky. The journey throughout my PhD was more joyful having him next to me.

Finally, I would like to thank my friends in Bath: Nooshin, Nikan, Mahsa, Behnood, who made the experience of living and working in this beautiful city so great and fun and also my friends in London: Shaharzad, Sara, Khale Shahnaz, Sanaz and Sahar who I always had a great time with them.
I gratefully acknowledge the University of Bath for funding.

Abbreviations

1D One dimensional

2D Two dimensional

A Acceptor

A-A Acceptor-Acceptor

COSY Correlation spectroscopy

CT Charge transfer

D Donor

D-A Donor-Acceptor

DCC Dynamic Combinatorial Chemistry

DCL Dynamic Combinatorial Library

DCM Dichloromethane

D-D Donor-Donor

DMF Dimethylformamide

DMSO Dimethylsulfoxide

DN Dialkoxynaphthalene

DNA Deoxyribonucleic acid

Eq. Equation

Equiv. Equivalent

ESI-MS Electrospray ionisation mass spectrometry

FTMS Fourier transform mass spectrometry

HOMO Highest occupied molecular orbital

HPLC High performance liquid chromatography

K Kelvin

Ka Association constant

LUMO Lowest unoccupied molecular orbital

LC-MS liquid chromatography-mass spectrometry

MS Mass spectrometry

MS/MS Tandem mass spectrometry

MW Microwave

m/z Mass to charge ratio

NDA Naphthalenedianhydride

NDI Naphthalenediimide

NMI Naphthalenemonoimide

NMR Nuclear Magnetic Resonance

NOESY Nuclear Overhauser enhancement spectroscopy

RT Room temperature

ΔS Change in entropy

TFA Trifluoroacetic acid

UV-vis Ultra violet-visible

VT Variable temperature

Table of Contents

Chapter 1

Dynamic Combinatorial Chemistry and Donor-Acceptor Catenanes

1.1 Dynamic Combinatorial Chemistry

Dynamic combinatorial chemistry (DCC) is a field in supramolecular chemistry that has extensively been studied in the recent years. DCC under thermodynamic control, has been used as a tool to access unexpected molecules with highly organised and complex topologies through reversible processes. These reversible reactions can have covalent as well as a non-covalent character. DCC allows the efficient synthesis of libraries containing structures with complex topologies whose individual properties are recognised through the library's response to the external stimuli.[1–6]

A dynamic combinatorial library (DCL) consists of relatively simple molecules (building blocks), which are continuously interconverting and going through reversible processes.

In DCC, every constituent within the library is in equilibrium, and their distribution depends on their thermodynamic stability, meaning that the most thermodynamically stable molecule is selected and amplified from a pool of potential targets. When a particular library member is amplified, its free energy is lower than the rest of library members. The libraries' distribution can be altered by introduction of an external stimulus such as addition of a suitable template or change in the environmental conditions: temperature, pH,[7] light[8] or electric fields.[9] The addition of an appropriate template to a library can significantly modulate the libraries' distribution and amplify the formation of one particular molecule at the expense of the others. This means that a particular library member has the best interaction with the template, and this can be advantageous as it allows the formation of the desired product in a good yield. Since all of the library members are linked through a set of equilibria, the amplification of one member can influence the others and the new amplified molecule can change the behaviour of the system.[10]

DCC has been used to synthesise new interlocked molecules,[11–13] catalysts,[5,14] sensors and receptors,[15] inhibitors and dynamic materials. It has also been used to make stable aggregates formed due to interactions between combinations of library members.[16–18]

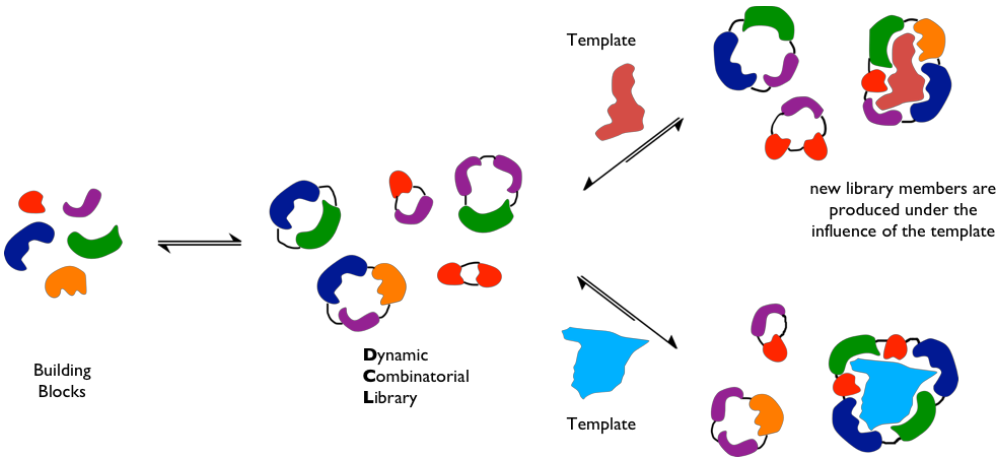

Figure 1-1. Cartoon representation of a general DCL. Small molecules (building blocks) interact in a DCL to make new structures and the addition of a template can amplify the formation of the most stable structure.

Designing an efficient dynamic combinatorial system to generate a diverse collection of products is a key step. Choosing an appropriate template to rule the system and building blocks who can interact with the template is essential. The building blocks cannot be chosen randomly, and they need to be able to go through reversible reactions, therefore having suitable functional groups is vital. This way, the outcome has better predictability and thus, the use of an appropriate template can help to amplify the desired product.

DCC explores reversible reactions in contrast with the conventional synthetic chemistry, in which the desired molecule is synthesised in such a way, so it does not revert back to the starting material or any other product. The aim of the classical routes is usually to form one product in each reaction and the formation of by-products is not desirable as it shows the poor design of the synthetic route. Distinctively, in DCC, the larger the library, the greater the chance to discover an interesting species amongst the many products.

In mid-1990s, the concept of DCC was independently created and developed by the Sanders and Lehn groups. DCC has opened new avenues for the synthesis of interlocked molecules such as catenanes, which would otherwise be difficult and challenging to achieve through conventional synthetic methods.

The dynamic combinatorial synthesis of different catenanes, Solomon links, and knots, with some of their history, is covered in this chapter.

1.2 Catenanes

The name "catenane" comes from the Latin word *catena*, which means "chain", and in chemistry, it denotes molecules that are made of two or more mechanically interlocked rings. The two-ring catenane is the simplest catenane and is referred to as a [2]catenane, which is topologically non-trivial. Catenanes[19–25] are molecules composed of two or more interlocked rings with mechanical bonds connecting them, and thus cannot be separated unless one bond breaks. These mechanically interlocked molecules have new properties (structural and functional) that are significantly different to their original components.[26]

The catenanes possess internal mechanical motion generated by either a circumrotation movement or pirouetting which is the rotation of one ring in the other ring or around the other ring. In the catenanes field, the [2]catenanes are the most common mechanically interlocked molecules; the literature reports several main routes towards their synthesis. The first method which is called the statistical catenation, involves the threading of a chain into another ring followed by the closure of the chain and formation of the [2]catenane (Figure 1-2). This approach relies on the macrocyclisation factor (*i.e.* low yields), and its limitations were recognised by Lüttringhaus and Schill in 1964, who attempted to use covalent bonds to direct the formation of [2]catenanes.[27]

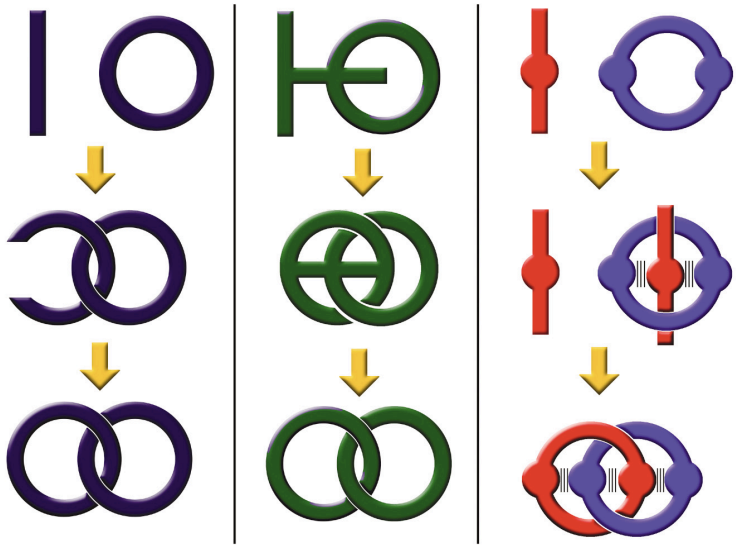

Figure 1-2. Different routes to synthesise a [2]catenane.[26]

The second route (covalent-directed catenation) involves the catenane formation *via* a covalent interaction, in which the ring and thread are joined by one or more covalent bonds that are cleaved after the formation of catenane.[28,29] This route requires long synthetic pathways while achieving very small yields and, when the directed covalent bonds breaks the strong interaction

between the species is lost. The last route, which is called template-directed catenation, relies on non-covalent (e.g., donor/acceptor interactions, π–π stacking and hydrogen-bonding) or coordinative bonding interaction.[30–32] This route is the most popular method as it produces the catenane in high yields compare to the other two methods. It works when one ring acts as a non-covalent template during the formation of the second ring.

In 1960, Wasserman was the first to report the synthesis of a catenated molecule,[19] and one year later, Wasserman and Frisch published a paper, which introduced a series of novel topologically complex molecules. They also established that the mechanically interlocked species are molecules rather than assemblies of different moieties and so introduced the concept of mechanical bond.[33] Since then, many researchers started to explore the topological aspect of molecules as well as bond geometry and atom connectivity.

A few years later (1967) from the discovery of the first synthetically generated catenane, the discovery of the first naturally occurring catenane composed of DNA strands was revealed. This was isolated from the mitochondria of HeLa cells and human leukaemic leucocytes, being constructed of circular DNA. [34]

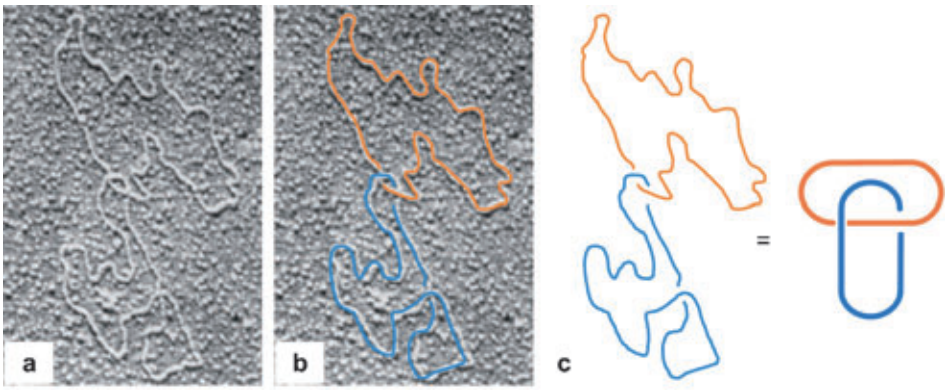

Figure 1-3. (a) Electron micrograph (EM) of circular DNA showing a catenane topology, (b) and c) highlighting the two rings of the DNA catenane as a Hopf link.[35]

Ever since, a range of different interlocked DNA topologies have been discovered and synthesised.[36] Efforts have been made to control the relative motion of the rings in synthetic DNA catenanes for their use as molecular machines. Protein catenanes have also been successfully synthesised, despite the challenges brought by design and synthesis issues.[37]

The initial approaches to synthesise mechanically interlocked molecules (statistical catenation and covalent-directed catenation) were suffering from long and laborious synthetic routes and low yields. The researchers' efforts have paved the way towards the use of templated synthesis of catenanes, enabling their formation in larger scale. The use of templates is an ideal approach for synthesising molecules with complex topologies due to their role in bringing molecules

together into organised species with superior yields and relatively short synthetic routes. Such templates include π-π interaction, solvophobic effect,[38] donor acceptor interactions,[23,39–41] metal anion template,[42–44] metal cation template,[24,45–48] anion template, hydrogen[49–52] and halogen bond.[25] The templated approach has further fuelled the area and expanded the number of reported [2]catenanes as well as other molecules with complex topologies.[53,12,26]

Some of the groups that have laid the foundations of this field and started to explore these complex topologies are those led by Sanders,[2,3,10,47,54] Stoddart,[20,53,22,55–58] Otto,[3,10,59,60,4] Sauvage[30,31,45,61,62] and Leigh.[50,63–68]

1.3 Supramolecular Interactions

1.3.1 π - π Interaction in Aromatic Systems

DCC has been an efficient approach in accessing unpredictable complicated structures through supramolecular interactions (non-covalent) such as hydrogen bonding, electrostatic and π-π interactions, van der Waals forces, solvophobic effect, *etc*.

π-π interactions[69,56] are relatively weak interactions which concern π-systems of aromatic molecules. These π-π interactions play an important role in the supramolecular chemistry present in the biological realm, because it can determine the structure and properties of the molecular assemblies in structures such as proteins and DNA.

In 1990, Hunter and Sanders proposed an electrostatic model to explain the geometry and stacking behaviour of aromatic molecules (Figure 1-4).[70]

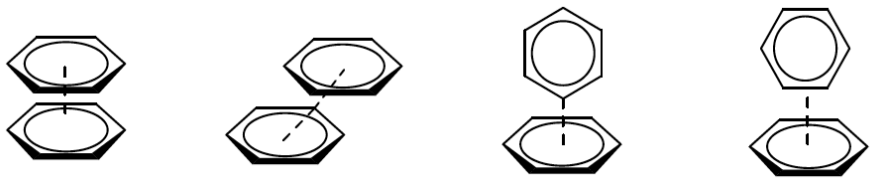

Figure 1-4. The electrostatic model of benzene, from left to right: the face-to-face geometry-repulsive, offset geometry-attractive, and T-shaped and edge-to-face geometry-attractive.

In an electron neutral aromatic molecule such as benzene, there are negatively charged π-clouds around the positively charged σ framework, which makes an edge-to-face, T-shaped or an offset stacking favourable, resulting in π-σ interactions. However, because the negative charges repel each other, a non-offset face-to-face interaction between unpolarised aromatics is not favourable.

The π-π interaction between aromatic moieties is strongly modulated by the substituents around the π-rings, resulting in favourable or unfavourable interactions between π-systems.

The Hunter and Sanders theory suggests that the substituents on the π-ring can inductively withdraw or add electron density to the π-system, and therefore, changing the electrostatic interaction.[70] This effect is called nonlocal and indirect as the substituent affects the second ring through the π-system of the first ring (substituted ring). For example, in the presence of heteroatoms or other functional groups that can polarise the aromatic system, face-to-face interactions could become favourable. Due to a decrease in π–repulsion, attractive interactions such as local electrostatics, van der Waals force, face-to-face stacking of π–donor and π–acceptors can also become favourable. Similarly, face-to-face interactions between π–acceptors are favoured. On the other hand, the stacking between π-donors is not favourable as in the case of unpolarised aromatics and would result in edge-to-face or T-shape geometry.

A more recent theory introduced by Wheeler and Houk suggests that, unlike Sanders and Hunters theory, there is a direct interaction between the substituent and the second benzene ring. This computational study also suggests that the C-X σ bond is more polarised than C−H and this can affect the interaction energy between the two Ph rings (see Figure 1-5). This effect is local, both direct and indirect and it has been shown to dominates the π- π stacking.[71]

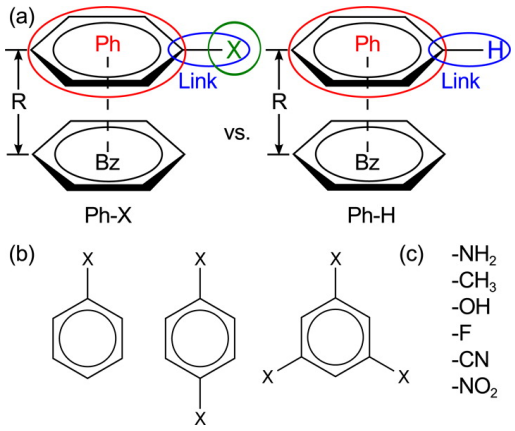

Figure 1-5. (a) Shows the polarised Ph−X σ bond compare to Ph−H, (b) different number of substituents that can affect the π- π interaction and (c) different possible substituents on the Ph ring.[71]

This work also discusses the effect of number of substituents on the polarity of substituted ring (Figure 1-5b) and the effect of electron-withdrawing and electron donating-moieties on the ring (Figure 1-5c).

The 1,4,5,8-naphthalenetetracarboxylic diimide (NDI) and 1,5-dialkoxynaphthalene (DN) model is a good example of how the stacking of the aromatic regions between electron-rich and electron-deficient molecules occur. Iverson *et al.*[72] reported that the strength of donor-acceptor interactions and the solvent environment is closely related. NDI and DN have clearly the strongest interaction in water, ca. 2045 M^{-1}, and ca. 12 M^{-1} in chloroform. As expected, the D-A interactions are much stronger than A-A interactions (ca. 200 M^{-1} in water, $K < 1\ M^{-1}$ in chloroform); and the least favourable interaction is the donor-donor one (ca. 20 M^{-1} in water, $K < 1\ M^{-1}$ in chloroform).

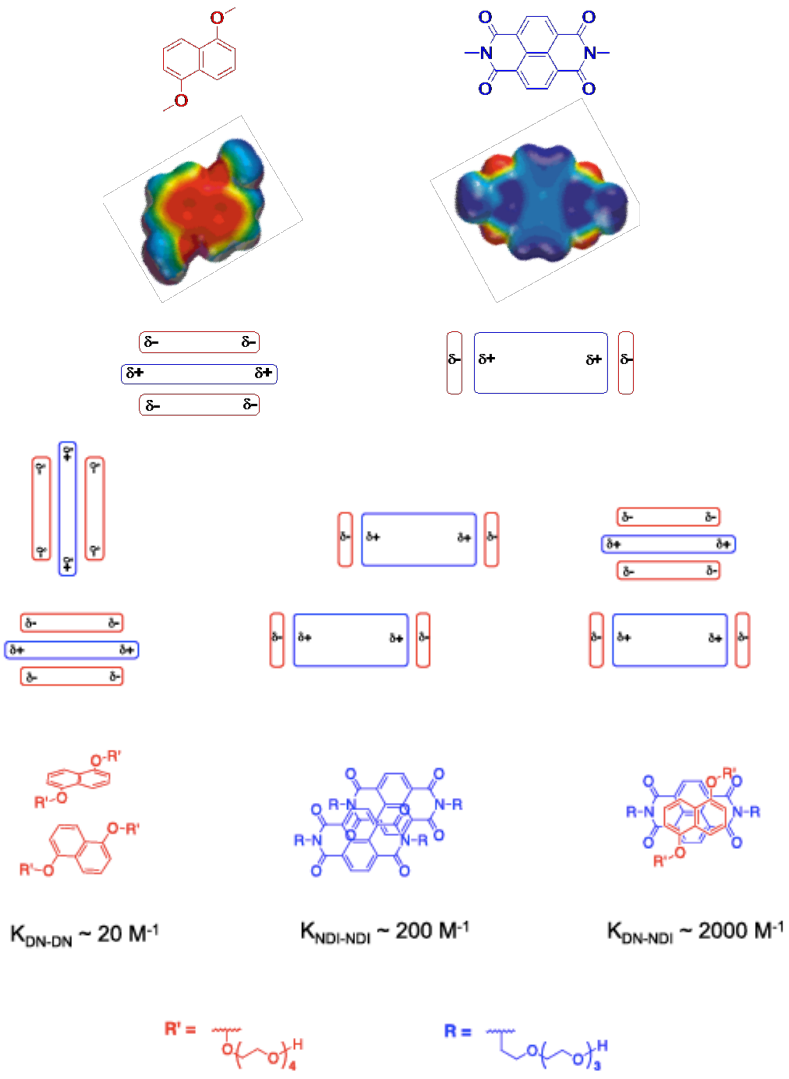

Figure 1-6. The model of electrostatic interaction of electron deficient naphthalenediimide (NDI) in blue and electron rich 1,5-dialkoxynaphthalene (DN) in red.[72]

1.3.2 π - π Donor-Acceptor Interaction

A π-π donor-acceptor interaction (D-A) is the electrostatic interaction between the π systems of an electron-rich aromatic (donor) molecule and electron-deficient aromatic (acceptor) molecule.[73–79] This D-A interaction is a specific form of the general π-π interaction. it involves the optimum overlap of π-deficient and π-rich systems to reduce the solvent-exposed surface area.

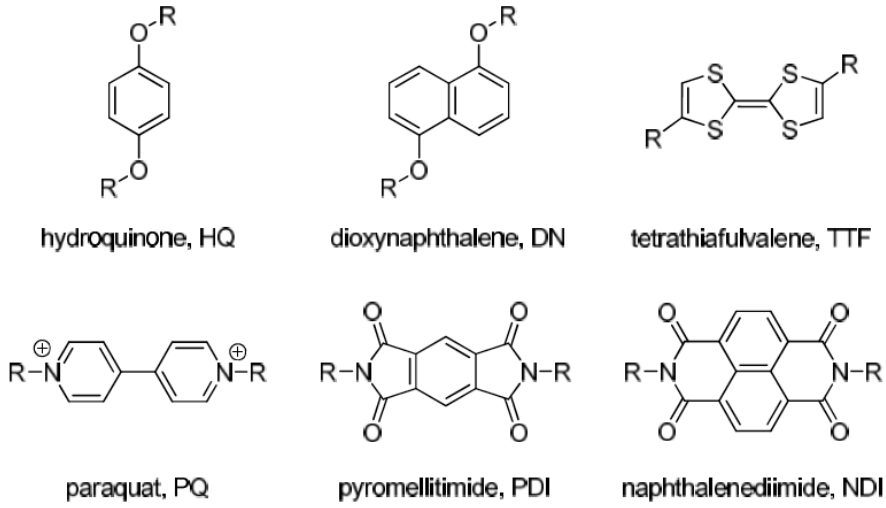

Figure 1-7. Examples of commonly used π-acceptors and for π–donors.

The D-A interaction occurs due to an overlap between the aromatic systems of donor and acceptor molecules. The charge transfer happens by the overlap of the high energy HOMO of the donor to the low-lying LUMO of the acceptor, which results in a bright colour change.

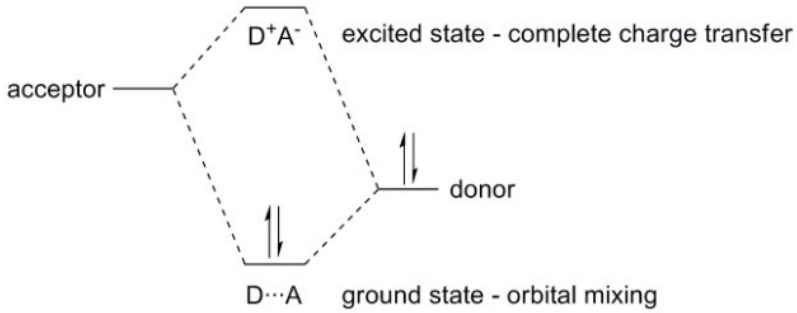

Figure 1-8. The orbital diagram of a donor-acceptor charge transfer complex.

The D-A interaction is better described as the sum of van der Waals, solvophobic effect, local electrostatic and charge transfer.[26,58,80] Even though the vivid colour change is an indication of the charge transfer, it is not the main driving force in favourable stack of π –donor to π – acceptor.

In 1980s, Stoddart and co-workers were the first to use D-A interactions as template to obtain interlocked molecules with complex topologies.[81–83] The idea came after the synthesis of 1:1 inclusion complex between electron rich crown ether and electron deficient guest, paraquat (PQ) (**1.1**). Another D-A 1:1 complex (**1.2**) was produced from cyclobis(paraquat)*p*-phenylene acting as π –deficient host and a hydroquinone (*p*-dimethoxybenzene) as the π–rich guest. Ever since, this template has become significantly important in synthesising different interlocked molecules, such as catenanes.[83]

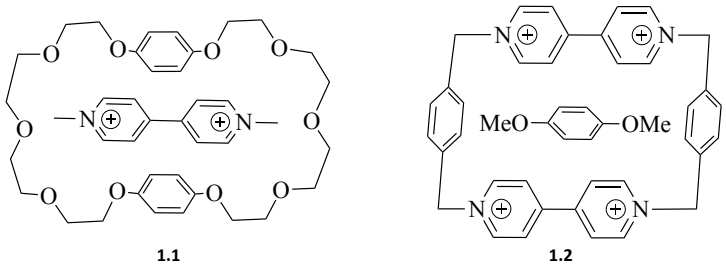

1.1 1.2

Figure 1-9. The inspiration for Stoddart's D-A catenanes came from these complexes (**1.1** and **1.2**).

A discovery reported by Liu and co-workers showed the formation of a highly organised D-A complex by solid state grinding. Upon grinding, a purple colour started to appear, which was an indication of charge-transfer complex between the electron-rich crown ether and electron-deficient pyridine-NDI. The X-ray diffraction analysis revealed an infinite stack of pseudorotaxane with alternative D-A units.[84]

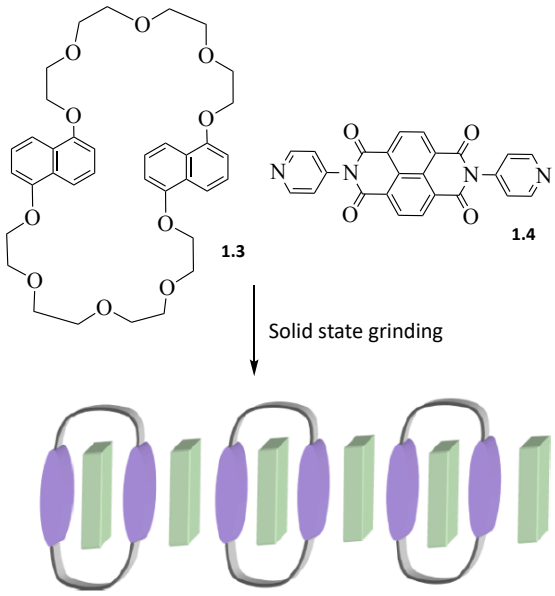

Figure 1-10. Solid-state D-A complex, formed from grinding the **1.3** and **1.4**.[84]

A remarkable illustration of the charge transfer between donor and acceptors and the way by which geometry influences the orbital overlap, thus the colour of the D-A complex, was developed by Stoddart's group. They used 'ExBox^{4+}' that functions as a high affinity scavenger for polyaromatic hydrocarbons (PAHs) to show a variety of D-A complexes. ExBox^{4+} has a box-like geometry and is composed of electron poor 1,4-phenylene-bridged bipyridinium units ExBIPY^{2+}.[85]

The crystals of ExBox•4PF6 are almost colourless by themselves; however, the occurrence of different colours for each insertion complex is extraordinary. The charge transfer interactions between the host and guests results in the colour change, with the exception of **1** because no charge-transfer band was observed.

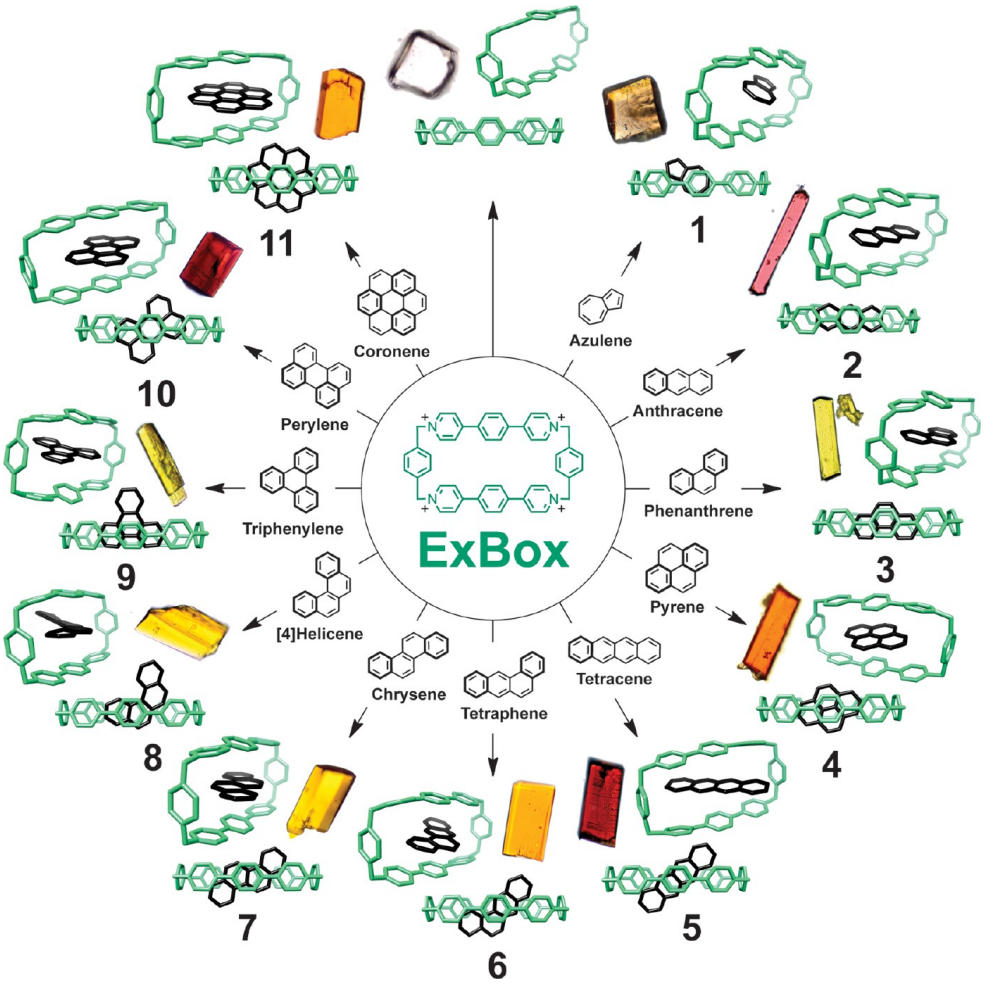

Figure 1-11. The figure shows the ExBox^{4+} Scavenger and variety of crystals formed.[85]

In 1989, Stoddart *et al*. reported for the first time in the literature the synthesis of an electron rich and an electron deficient donor-acceptor [2]catenane (Figure 1-11). A mixture of bis(pyridinium) salt $2PF_4$ (**1.5**), bis(bromomethyl)benzene (**1.6**) and bisparaphenylene-34-crown-10 (**1.3**) in acetonitrile was stirred for two days. The product was a [2]catenane showing a deep red colour solid (due to the presence of charge transfer) over 70% yield.[86]

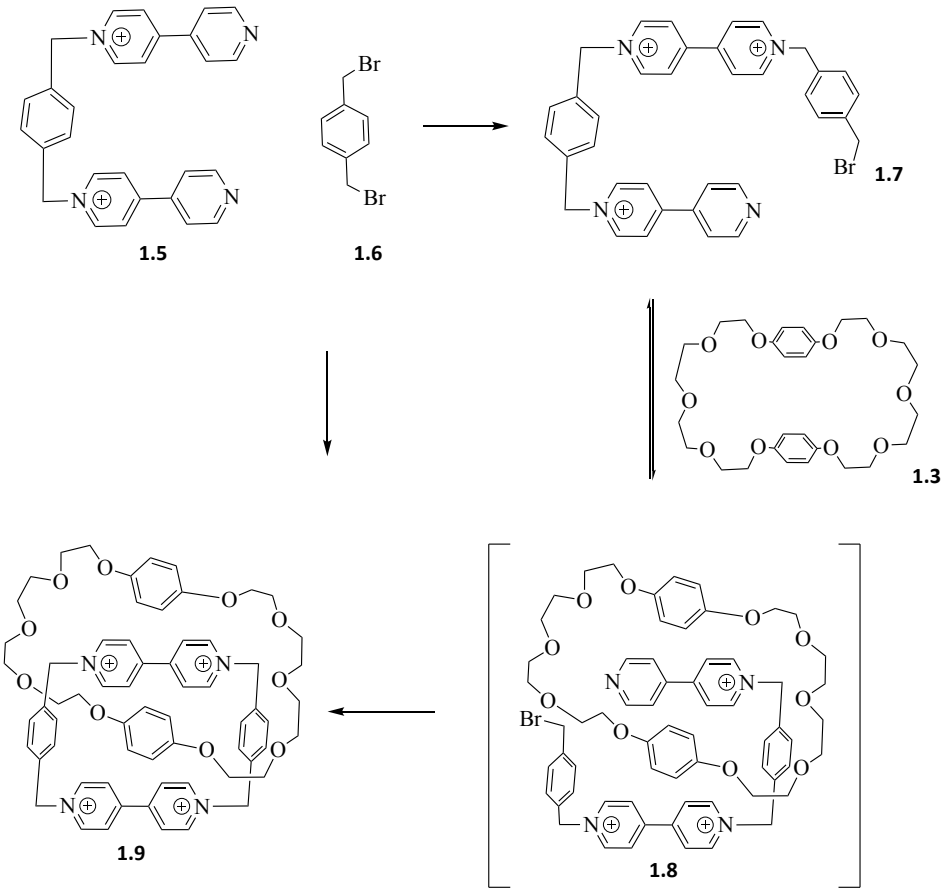

Figure 1-12. The first [2]catenane achieved through donor-acceptor interaction by Stoddart's group.

It is now considered that the main driving force for the formation of this [2]catenane is hydrogen bonding between the acidic α-carbon hydrogen of bipyridinium cation and the oxygen atoms in the polyether chain of the bisparaphenylene-34-crown-10.[87]

In 1998, Stoddart and co-workers reported an unsymmetrical [2]catenane, containing both dioxynaphthalene (DN), and tetrathiafulvalene (TTF) as electron-rich moieties. The paraquat (PQ) binds stronger to TTF than DN, therefore the TTF is located inside the ring and DN is at periphery. However, this can be altered by two electron oxidations of TTF to TTF dication. This leads to electrostatic repulsion between PQ and TTF dication which results in rotation of the ring, brings the DN inside the cavity and TTF dication outside the ring. This can be diverted back to the original stacking of TTF inside the PQ by reduction.[88]

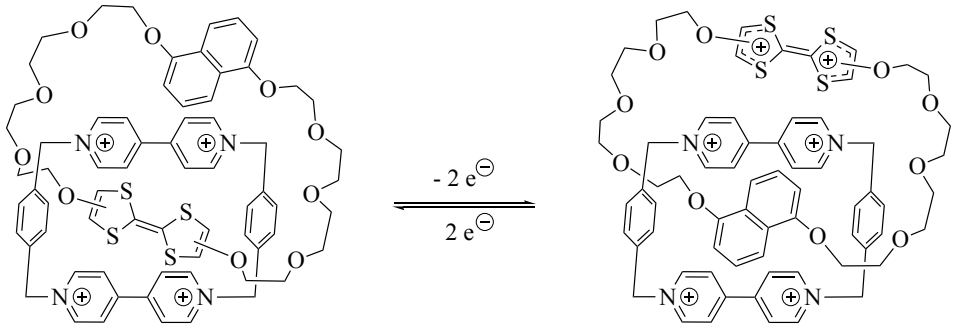

1.20

Figure 1-13. The unsymmetrical [2]catenane with two different donor moieties.

In 2007, Liu and co-workers[89] also reported an unsymmetrical [2]catenane containing pyromellitimide (PDI) and PQ as the two acceptor moieties sandwiched between an ether macrocycle as the donor moiety.[90] However, switching between PDI and PQ has not been reported.

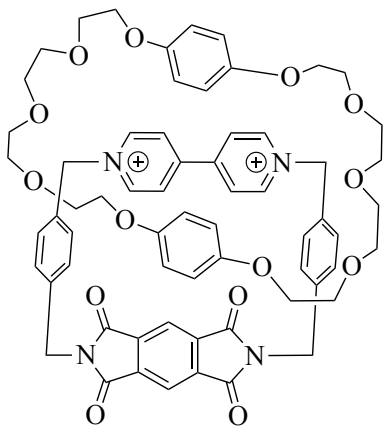

Figure 1-14. The unsymmetrical [2]catenane with two different acceptor moieties.

Formation of [3]catenane,[91] [5]catenane[92,93] and [7]catenanes[94] was also achieved using similar building blocks. By replacing the phenylene linker with biphenylene, the size of the cavity in acceptor is large enough to accommodate two donor building blocks **1.21**.[93]

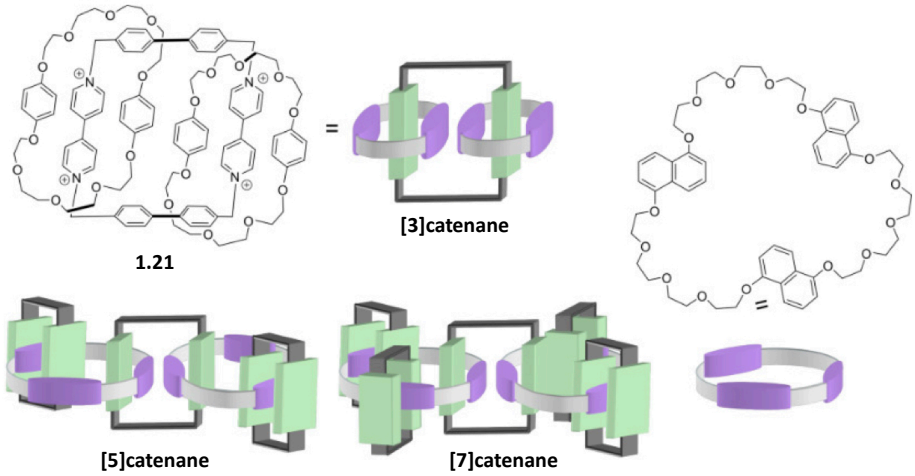

Figure 1-15. Examples of [3], [5] and [7]catenanes.

In 2016,[95] Au-Yeung and his team synthesised a series of new [3], [4] and [6] catenanes. The new strategy employed supramolecular interactions (metal–ligand coordination, ion dipole and hydrophobic interactions) to synthesise the [3]-, [4]- and [6] catenane in >80% yield.

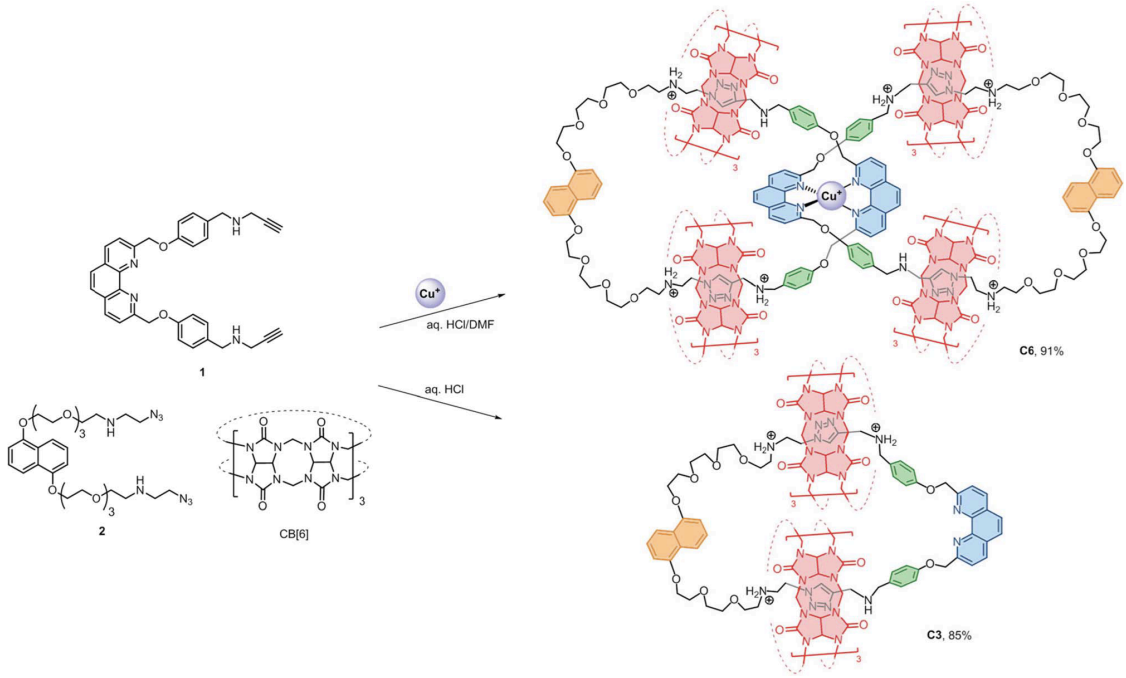

Figure 1-16. The synthesis of [3] and [6]catenanes. Structures of [3] and [6]catenane are shown as the +7 and +3 ions which are the most stable form of the catenanes.[95]

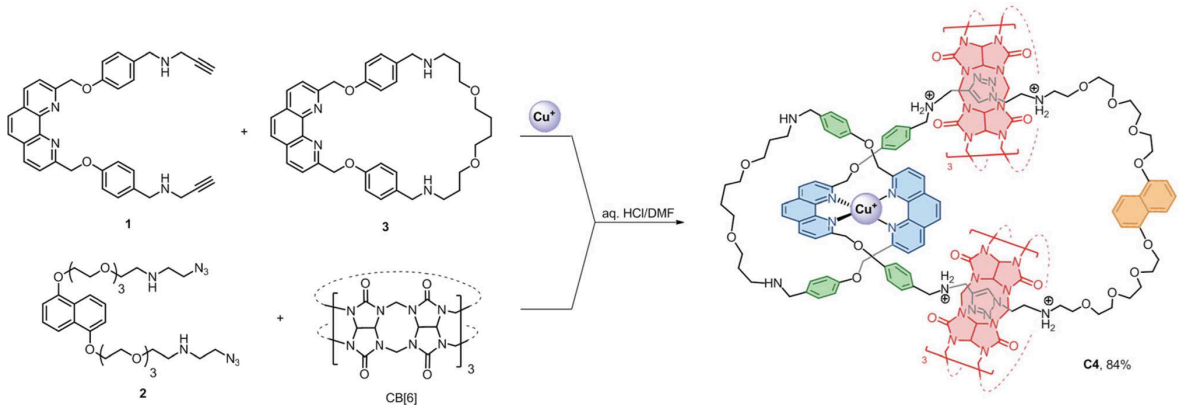

Figure 1-17. Synthesis of a [4]catenane. The structure is shown as the +5 ion which is the most stable and abundant form of the catenane.[95]

1.3.3 Hydrophobic Effect

The D-A interactions in DCC are also influenced by the solvophobic effect. The aqueous dynamic systems give a fundamental insight into the role played by solvophobic effect (in this case called hydrophobic) and D-A interactions when building a complex architecture. The hydrophobic effect[96–98] brings the aromatic region of the molecules together in order to reduce the total solvent-exposed surface area; the efficient desolvation of the aromatic systems plays a crucial role in this process. The strength of solvophobic effect is strongly dependent on the solvent polarity. As the solvent becomes more polar the association constant increases from ca. 12 M^{-1} in chloroform to ca. 2000 M^{-1} in water as described above for the DN – NDI pair.[72] Also, addition of salts such as $NaNO_3$, Na_2SO_4, Na_2HPO_4 *etc*. have an important influence on system's polarity. The addition of salt is a great way to increase the ionic strength of the solvent, bringing together of the hydrophobic region of molecules and reducing their contact with the solvent.

1.4 Reversible Reactions in DCC

The reactions involved in the formation of CDLs must be reversible to allow the exchange between the building blocks. To initiate this exchange within a library, a suitable reversible reaction compatible with the library conditions is required. These reversible reactions must meet some criteria, such as the timescale the reaction happens at. Sometimes the reversible reaction is fast, and the formation of cyclic species is the indication of that intramolecular reaction; however, the intermolecular interaction could be slow, and the library requires a long time to reach equilibrium even if the reversible reaction is fast. Therefore, in an ideal DCL, it is essential for the equilibration and selection to take place simultaneously, and the conditions

required for the reversible reactions must be compatible with the non-covalent interactions for the selection process. Mild reaction conditions are preferred in reversible reactions, so to not disturb the non-covalent interactions. Reversible reactions should also be possible to stop, so the desired product can be isolated and analysed.

There are three types of exchange reaction used in DCLs: reversible covalent reactions, noncovalent interactions and metal – ligand coordination. In DCC, reversible covalent reactions have been the most extensively used. Even though noncovalent interactions and metal – ligand coordination have faster exchange rate and shorter equilibration time, their products are usually less stable and more difficult to isolate and analyse.

Different reversible reactions have been studied and used over time to promote the formation of complex molecules, out of which several became very successful and useful in the field of DCC. The range of reversible exchanges used in DCC is continuously growing; the most prominent and extensively studied reversible reactions in DCC to make molecules with complex topologies are disulfide,[10,47,99–102] hydrazone[8,103,104] and imine exchanges[105–108] (Figure 1-18).

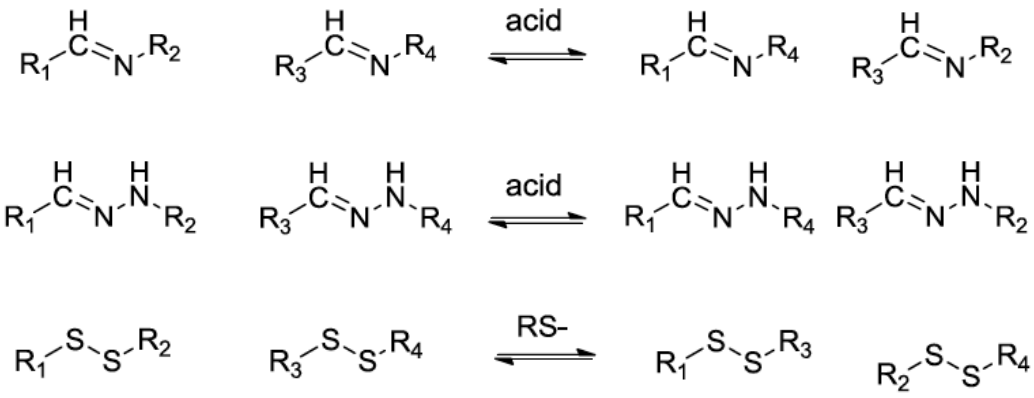

Figure 1-18. Some of the main reversible reactions used in DCL.

These exchange reactions have extensively been used for generating catenanes or other interlocked molecules through DCC. The hydrazone and imine exchange require mild conditions: either in aqueous buffers (pH between 5.0 and 8.5), or in organic solvents in the presence of weak acids namely oxalic acid for imine exchange, and TFA in CH_3Cl for the hydrazone exchange.

1.4.1 Hydrazone Exchange in DCC

In a study conducted by Sanders, Otto and co-workers, a series of macrocycles were made using peptide-based building blocks. They obtained a range of macrocycles up to the cyclic hexamer by using the peptide building block (pPFm) **1.22**, with TFA in a mixture of chloroform and DMSO solution.[103]

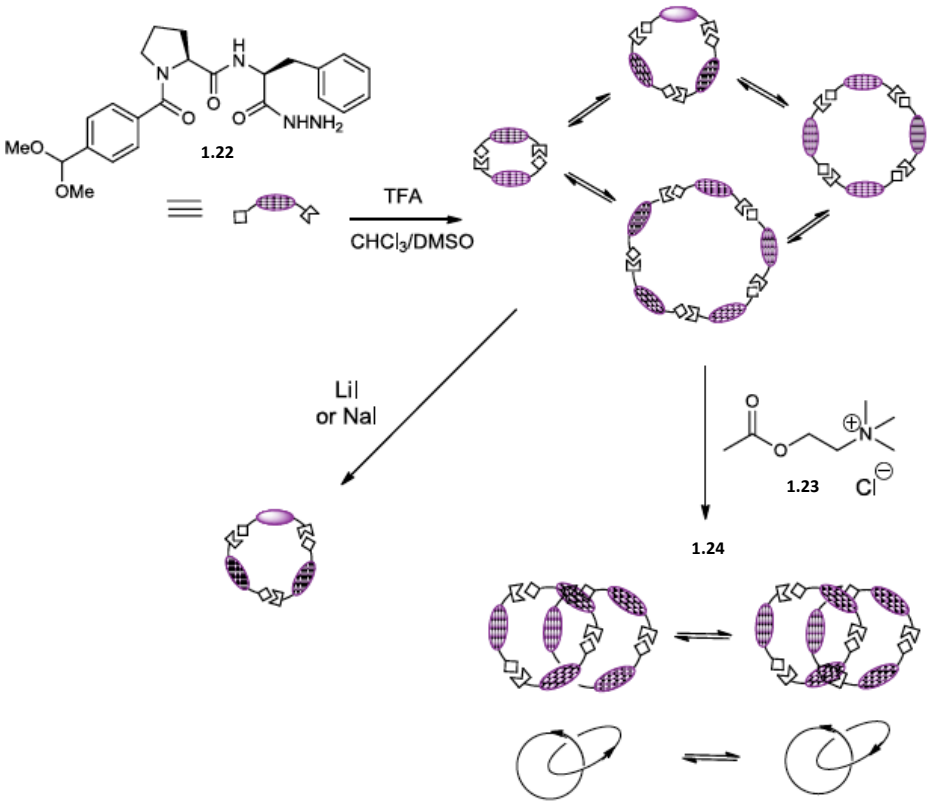

Figure 1-19. The pPFm DCL, where addition of Acetylcholine chloride **1.23** amplifies the formation of [2]catenane **1.24**.

The peptide building block underwent hydrazone exchange; the library reached equilibrium after three days forming a series of macrocycles. However, the libraries' distribution was drastically changed when acetylcholine chloride **1.23** was introduced as a template, leading to the formation of a new product **1.24**, which was isomeric with the cyclic hexamer. The formation of this [2]catenane occurred very slowly (after 44 days, 70% yield was achieved).

1.4.2 Imine Exchange in DCC

An imine-based [2]catenane was recently synthesised by Cougnon and his team through DCC in water from a dialdehyde (**A**) and aliphatic diamines ($\mathbf{B_n}$). The formation (self-assembly) of these [2]catenanes was driven merely by hydrophobic forces. The change in the length of the aliphatic diamine chains affected both the conformation and yield of the [2]catenane synthesised. The range of diamines used varied (n = 4 – 9), and the odd-even character of diamines had a significant effect on the catenanes distribution (odd numbers diamines favoured the formation of [2]catenane and the even number diamines disfavoured).[109]

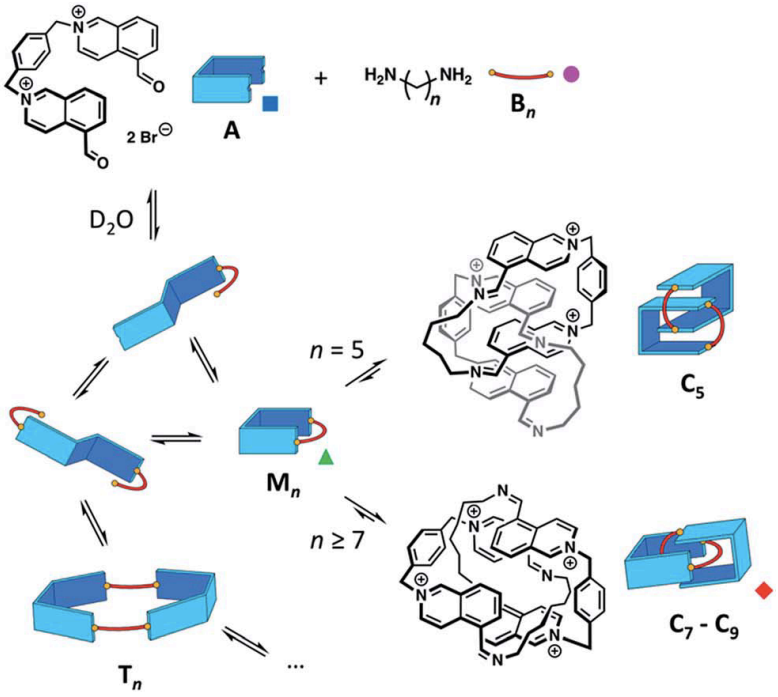

Figure 1-20. Synthesis of imine-based DCLs in water.[109]

Since that imine condensation is not favourable in pure water, the formation of these [2]catenanes has been a great achievement.

This work demonstrated the impact of hydrophobic effect in the synthesis of interlocked molecules. The self-assembly of these [2]catenanes did not even require the use of templates such as complementary donor–acceptor π-π stacking or metal coordination. The hydrophobic effect also overcomes the charge repulsion between the positively charged moieties.

1.4.3 Disulfide Exchange

Disulfide exchange was one of the first exchanges used in DCC and has been the most favoured reversible reaction due to its robustness and functionality under mild conditions (in water and under air). The exchange starts with the fast oxidation of thiols to disulfides, and a subsequent nucleophilic attack of thiolate anion on another disulfide bond to release another thiolate. The exchange ends once all the thiolate anions have been oxidised to disulfides, or by protonation of thiolate anions; at this stage the library components are frozen, *i.e.* they do not change their composition.

Disulfide exchange can also take place in organic solvents in the presence of organic bases such as triethylamine to deprotonate the thiols to thiolate anions and start the exchange. The first disulfide-based DCL was reported by Hioki[110] and Still in 1998, followed by further exploration in 2002 by Sanders and co-workers.

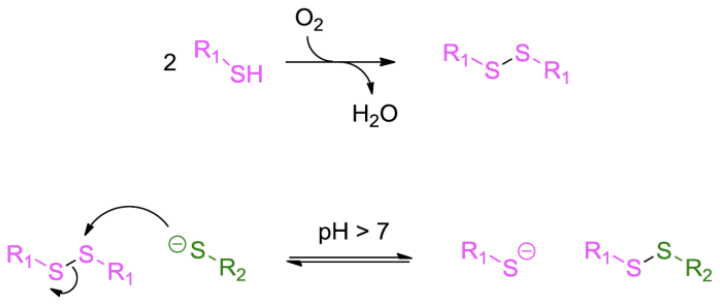

Figure 1-21. Mechanism of disulfide exchange.

In 2008, Otto *et al*. discovered an unexpected [2]catenane composed of two interlocked tetramers.[111] This catenane was made in a disulfide-based DCL containing the naphthalenedithiol **1.25**. The formation of the [2]catenane, **1.26**, was mainly driven by the hydrophobic forces. This catenane was decatenaned by addition of *N*-trimethyladamantyl ammonium. This moiety acted as a guest inside the cavity and prevented the formation of the [2]catenane, resulting in tetrameric square **1.27**.

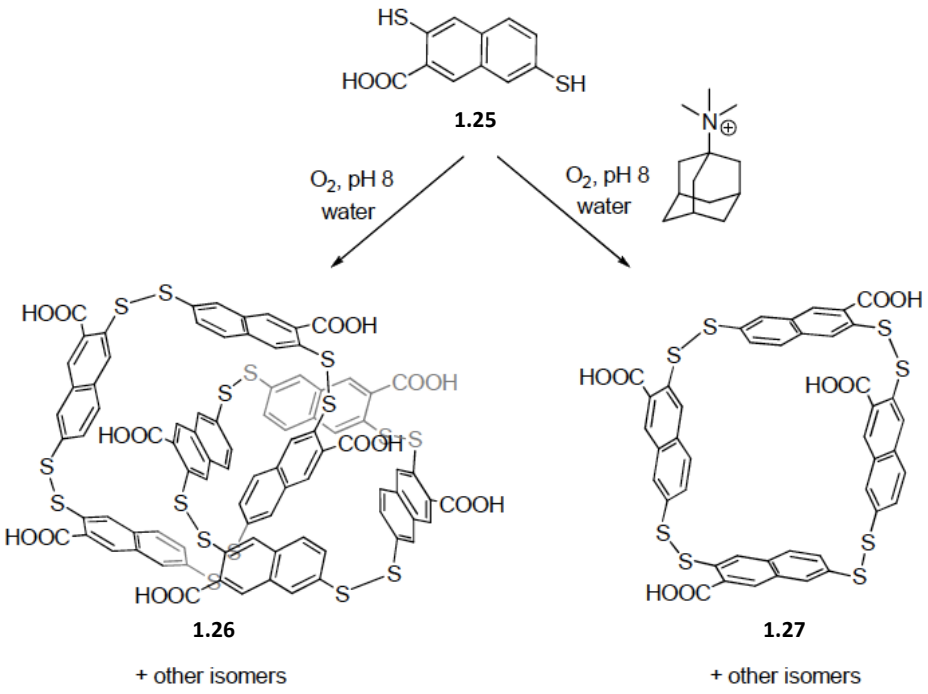

Figure 1-22. Dynamic catenane (**1.26**) assembled from naphthalenedithiol **1.25**.[111]

1.5 Donor-Acceptor [2]Catenanes Through Disulfide Exchange

Using disulfide exchange, Sanders and Pantoș groups have reported the synthesis of a range of [2]catenanes[23,80] as well as other complex topologies such as [3]catenanes,[58] Solomon link,[112] a figure-eight knot and the first organic trefoil knot. The main building blocks employed in the synthesis of the catenated species were the π-acceptor 1,4,5,8-naphthalenediimide thiol (NDI, labelled as A) and the π-donor dialkoxynaphthalene thiol (DN, labelled as D), which enabled the production of disulfide-based libraries. The experimental conditions employed a slightly basic pH (8) under air to promote the oxidation process. Using D-A stacks in a compact face-to-face geometry has widely been used as template for complex structures such as foldamers[113–115] rotaxanes,[41,99,116] and catenanes.[23,80,117] Sanders *et al*. have extensively studied the versatile nature of D-A interactions of NDI and DN building blocks.

The two building blocks (NDI and DN), due to their electronic properties, undergo donor-acceptor interactions during which a charge-transfer from the HOMO orbitals of the donor to the LUMO of the acceptor occurs, triggering a bright colour change of the library solution. This property has been used as a template to promote more versatile libraries.

These molecules (NDI and DN) have a cysteine moiety at the peripheral positions, whose role is to deliver better water solubility through the carboxylate groups. The cysteine provides the thiols for the disulfide exchange, allowing the formation of new and interesting structures. This

project was initiated by Au-Yeung, who discovered that the D-A libraries set up in water under air oxidation conditions generated a variety of macrocycles and D-A catenanes.[23,80,117] The isolation of the [2]catenanes from the reaction mixture has allowed their comprehensive characterisation. The molecules have self-assembled under a novel aromatic stacking arrangement not previously observed: DAAD (**1.28**) and DADD (**1.29**), as shown in Figure 1-19. It is intriguing to observe that these molecules have not adopted the conventional DADA arrangement, owing to hydrophobic effects overcoming the repulsive donor-donor or less favourable acceptor-acceptor interactions.[118]

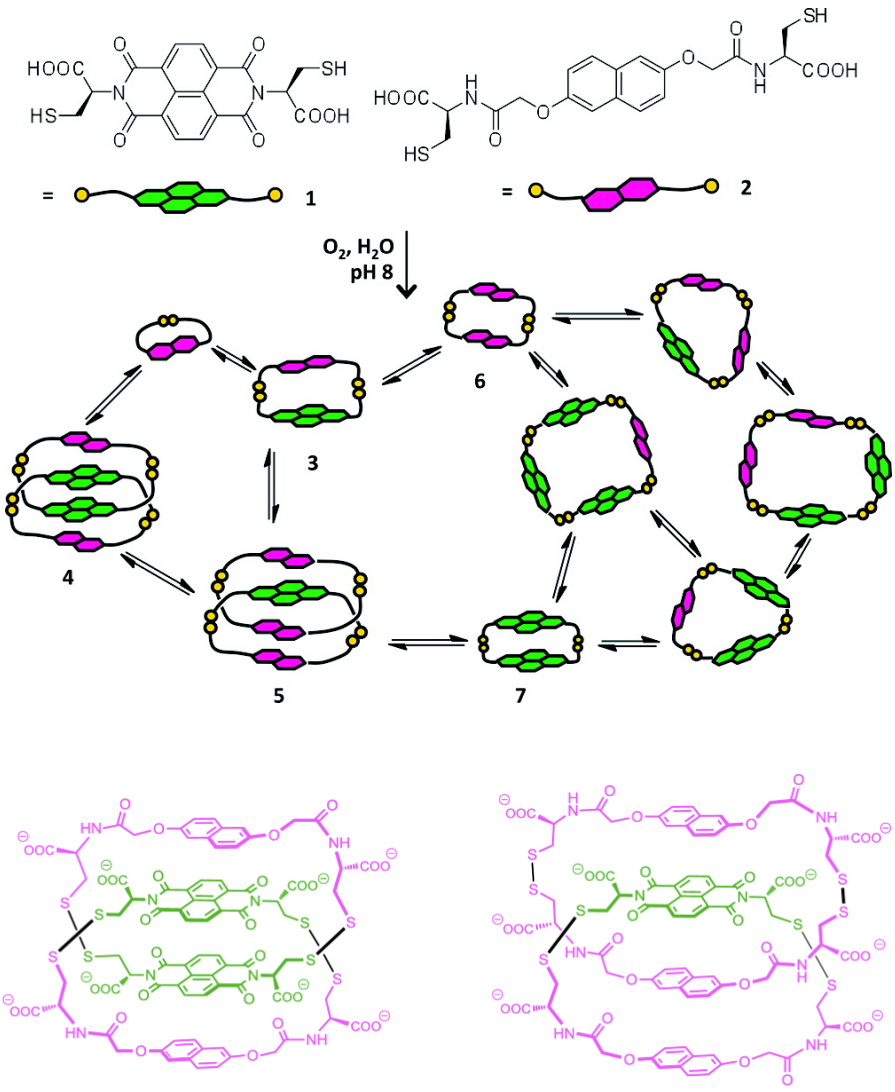

1.28 **1.29**

Figure 1-23. DCL of NDI acceptor (1) and DN (2) which results in formation of the novel arrangement: DAAD (**1.28**) and DADD (**1.29**).[119]

That DAAD arrangement of **1.28** became possible due to the rigidity of NDI molecule and the available space within the small cavity of the NDI dimer which does not allow for the hydrophobic core of DN to fit in, making the DAAD stacking the most stable conformation.

The catenane **1.28** is also more stable than **1.29**, since all the stackings are favourable (two donor-acceptor and one acceptor-acceptor interaction). The **1.29** has two favourable D-A interactions and one less favourable D-D interactions, thus emphasising that the hydrophobic effect could be the main driving force for the formation of this [2]catenane.

This idea was continued by F. B. L. Cougnon and N. Ponnuswamy in Sanders group; their work has taken advantage of the versatility of these building blocks. They have introduced different linkers in between the NDI moieties, further developing this idea by connecting two NDI cores with different linkers. Thus, by expanding the range of acceptor-building blocks, a variety of interlocked molecules such as [2]catenanes with distinct compositions and topologies (namely AAAA, DADD, AADA, and DAAD stacking), [3]catenanes, trefoil knot, Solomon link and figure-eight knot have been produced.[2,120,121]

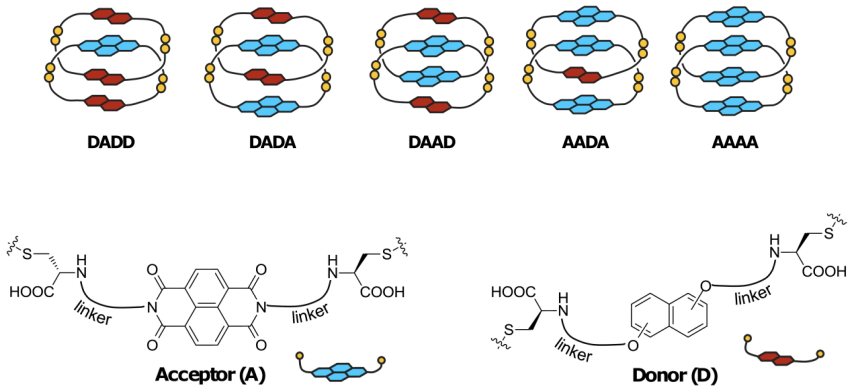

Figure 1-24. Possible arrangements of the π units of a donor-acceptor [2]catenane.[122]

Each catenane illustrated in Figure 1-24 represents a major synthetic challenge using classical kinetics driven chemistry but has been achieved using the DCC strategy. By tailoring the size of the building blocks and using different linkers such as alkyl chains or amino acids, the composition of the DCL is dramatically changed, leading to the formation of distinct interlocked species. This area of research is far from being exhaustively studied, as even more intriguing structures could be potentially formed using this strategy.

1.5.1 Donor-Acceptor [3]catenanes

The formation of highly ordered interlocked structures such as a [3]catenanes is not trivial, and it requires precision in designing the building blocks. Considering its versatility, the NDI scaffold has been classified as an appropriate building block. The modification of its structure by the addition of a flexible butyl chain to connect the two hydrophobic NDI cores provided a good platform for this idea. Figure 1-25 shows the DCL of two electron deficient NDIs connected by a butyl chain with a donor dihydroxynaphthalene in 1:2 ratio in water, under air at pH 8.[123]

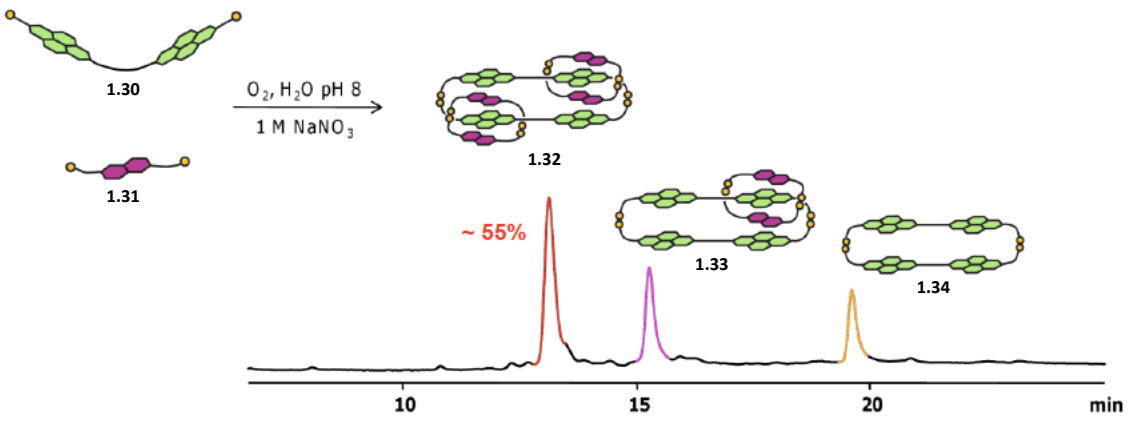

Figure 1-25. HPLC analysis of the library containing NDI (**1.30**) and DN (**1.31**) in 1:2 molar ratio (5 mM total concentration). The HPLC analysis was performed in the presence of 1 M $NaNO_3$, recorded at 383 nm.[124]

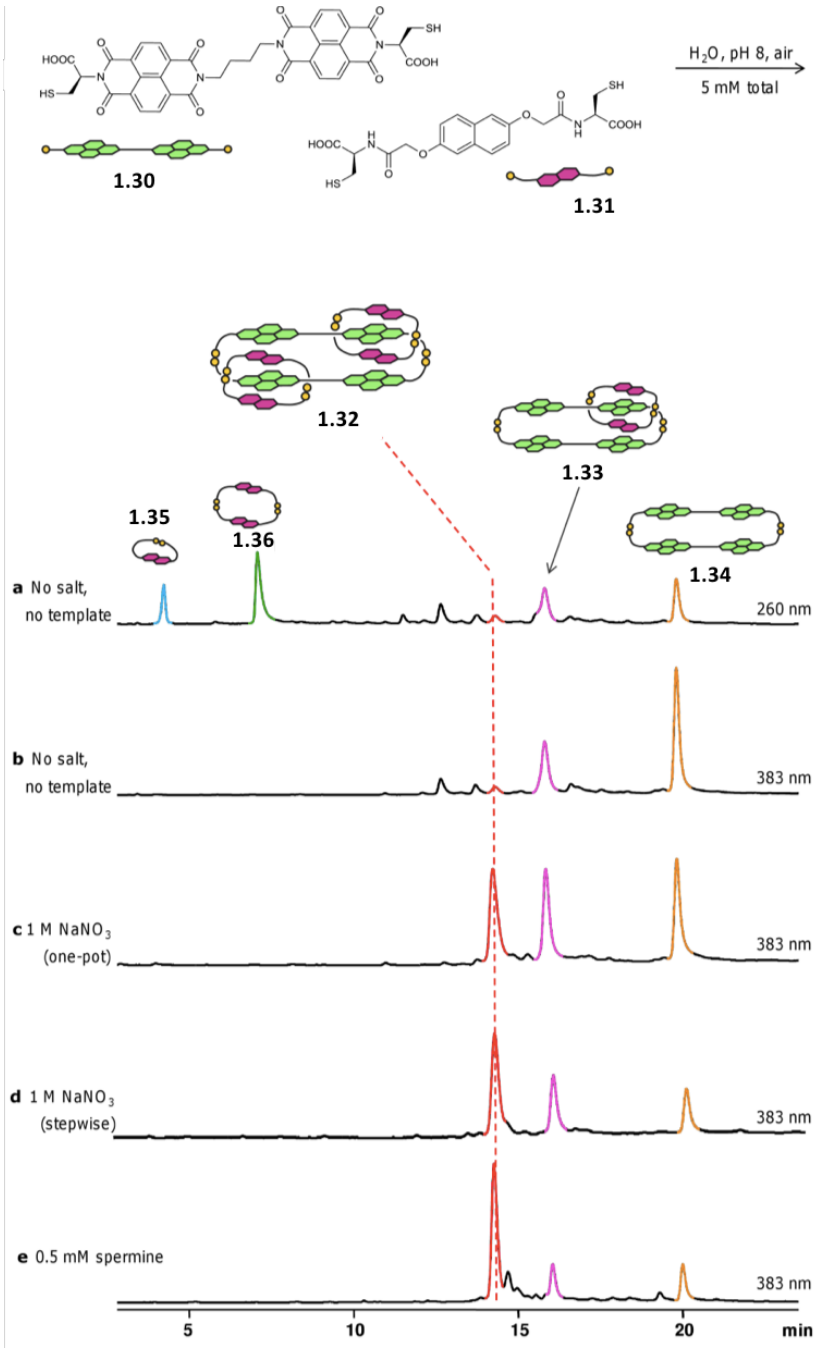

Figure 1-26. HPLC analysis of the library containing NDI and DN in 1:2 molar ratio (5 mM total concentration). In (a) 383 nm and (b) 260 nm the HPLC was performed in the absence of $NaNO_3$. The library was also prepared in presence of 1 M of $NaNO_3$, (c) in one-pot or (d) after stepwise addition of DN (absorbance recorded at 383 nm). (e) The library in the presence of 0.5 mM of spermine (absorbance recorded at 383 nm).[123]

As shown in Figure 1.26, the formation of [3]catenane **1.32** is promoted (amplified) in the presence of 1 M $NaNO_3$ from a small amount to 33% and this concentration increased to 55% after stepwise addition of DN. The salt enhances the system's polarity, and therefore the hydrophobic regions tend to get "buried", restricting the contact with the solvent due to molecule's close-packed geometry. The $NaNO_3$ is supporting the solvophobic effect driven

synthesis of these molecules and shows how by increasing the ionic strength the library distribution can change. Thus, the [3]catenane, **1.32**, has the most appropriate structure to minimise the exposure of hydrophobic cores to the medium.

Spermine was also used as a template in this library, amplifying the formation of [3]catenane to 60% due to the favourable interaction between the polycation and the carboxylate groups of the catenane.

1.5.2 All-acceptor [2]Catenane

The synthesis of the first all-acceptor [2]catenane using NDI-based building block was achieved by Dr N. Ponnuswamy in Sanders group. The study has provided an understanding of the role played by hydrophobic effect in DCC, which can bring the non-polar molecules in close geometry limiting their interaction with the aqueous solvent towards obtaining catenanes. This all acceptor [2]catenane does not have the conventional arrangement where all aromatic units are stacking, instead the hydrophobic alkyl chain is between the electron-deficient aromatic units. This is a direct proof that the hydrophobic effect can overcome the less favourable π-σ interaction and enable the synthesis of an all-acceptor [2]catenane.[112]

The synthesis of an all-acceptor building block is based on the same design concept as for the [3]catenane DCLs, where the two NDI hydrophobic cores are connected by a flexible aliphatic chain. Eight aliphatic chains (diamines) were used (from 1,2-diaminoethane to 1,9-diaminononane), and the formation of the all-acceptor [2]catenane was observed only when n ≥ 8, being the dominant species in the library when n = 9. This suggests that the longer the length of the hydrophobic chain is, the more favourable the formation of all-acceptor species would be.

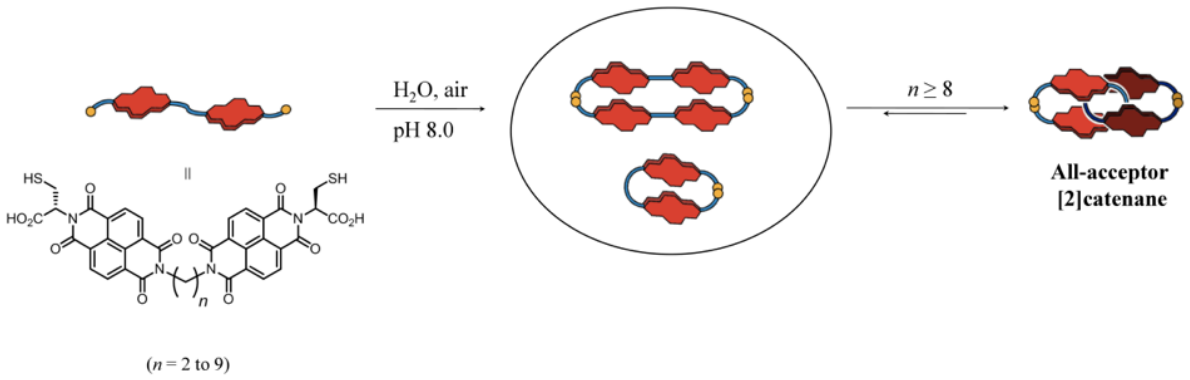

Figure 1-27. DCL of an all-acceptor [2]catenane formed using the electron deficient NDI building block.[112]

All these studies have paved the way towards a comprehensive understanding of how these molecules interact and fold into structures that have not been possible to achieve through conventional synthetic methods.

Another example for an all-acceptor [2]catenane was reported by Li and co-workers based on perylenediimide **1.35**. the synthesis of catenane **1.37** was achieved by dynamic molecular assembly. For the synthesis of this [2]catenane, they took advantage of the disulfide exchange to form the cyclic dimer which becomes the immediate major product. This cyclic dimer then guides the formation of a dimer-dimer [2]catenane **1.37**, which becomes the second major product.[125]

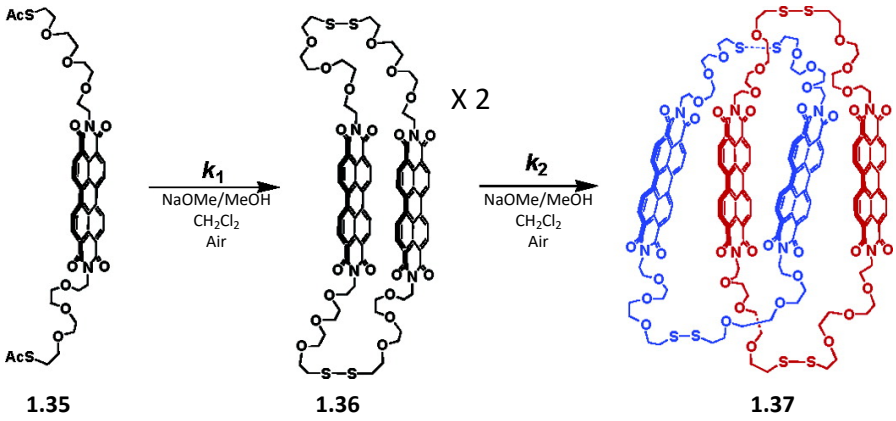

Figure 1-28. Self-assembly of an all acceptor [2]catenane via disulfide exchange.[125]

The synthesis of this all-acceptor [2]catenane **1.37** was carried out in CH_2Cl_2. Using the π-π stacking of perylene's large aromatic surfaces, the dimer **1.36** self-assembled to form the all-acceptor [2]catenane.

1.6 Synthesis of Higher Order Structures Using Disulfide Exchange with NDI-based Molecules

In DCC, reversible reactions have the benefits of overcoming the formation of kinetic side products. In reversible chemistry, by using simple building blocks in suitable library conditions, molecules that are capable to assemble or fold into knots and links can be formed.

1.6.1 Knots

Molecular knots were observed for the first time in proteins and in DNA.[34,37] The synthesis of such complex structures happens in Nature mostly, with a few examples where these complicated structures have been achieved synthetically.

Using current synthetic methods to create these complex structures is very difficult and it requires precise and accurate synthetic steps. The knots have been categorised by the number of crossing points using the Alexander Briggs notation. For example, a trefoil knot has three crossing points, therefore, it is depicted as 3_1.

In the Sanders group, a few molecular knots were synthesized and characterized, such as the trefoil knot[38] and figure-eight knot, along with a Solomon link.[112]

1.6.2 All-acceptor Trefoil Knot

Sanders and co-workers were the first ones to report the stereoselective synthesis of a purely organic trefoil knot from an all-acceptor building block in water. This trefoil knot was made from an NDI-based building block and its formation was mainly driven by hydrophobic effects.[38]

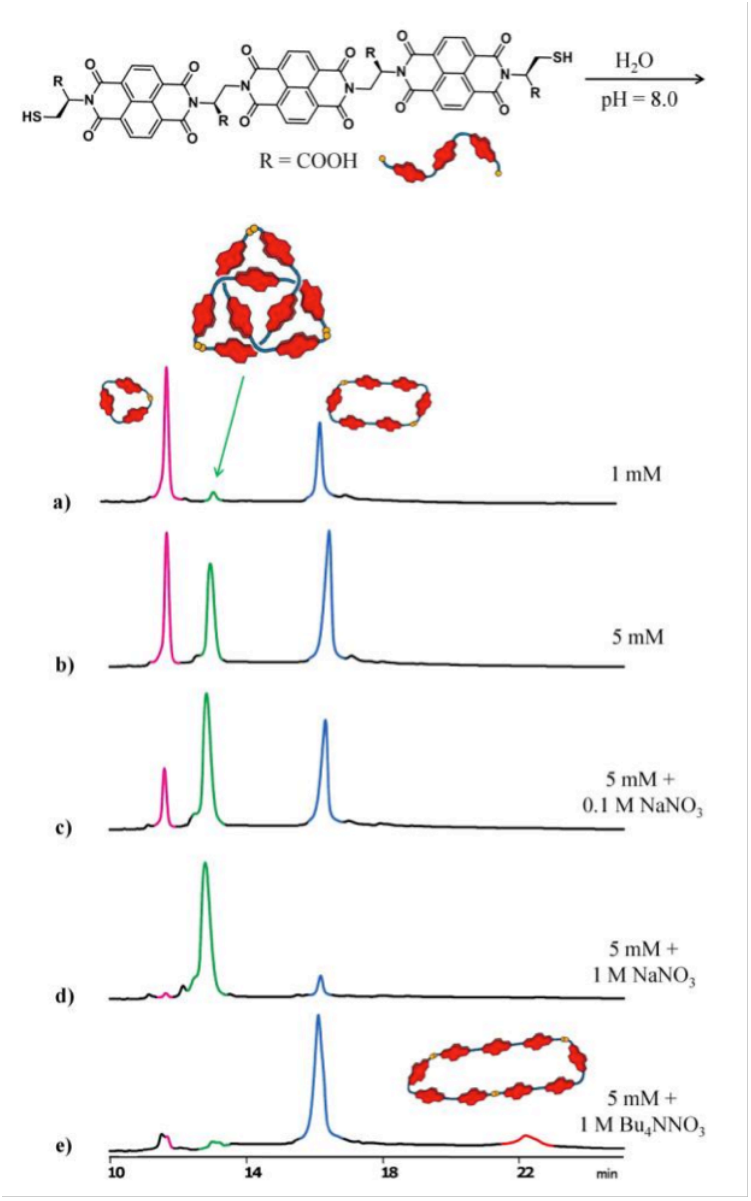

Figure 1-29. HPLC analysis of libraries at (a) 1 mM and 5 mM of the LLLL building block, in the absence of $NaNO_3$ (b) and presence (c-e) of different inorganic salts. Absorbance was recorded at 383 nm.[38]

The short retention time of trefoil knot gave the first insight of complexity of the structure. As observed in Figure 1-29, the addition of 1 M $NaNO_3$ significantly amplified the formation of trefoil knot, which is because of the enhanced polarity of the medium and the hydrophobic effect. However, by addition of 1 M Bu_4NNO_3, the formation of trefoil knot was significantly reduced, and the formation of cyclic dimer drastically amplified due to the solvation of NDI surfaces by Bu_4NNO_3. Therefore, the Bu_4NNO_3 is acting as a negative template for the trefoil knot.

This knot shares many common properties with protein folding, since the primary structure of the building block is composed of hydrophobic and hydrophilic moieties, which instructs the folding into the secondary knotted structure.

The molecular structure of the trefoil knot is the smallest topology in this library; it can bury the hydrophobic surfaces and minimize their exposure to the solvent, while the hydrophilic regions are exposed to the solvent. The hydrophobic forces are the main driving force in formation of this trefoil knot.[96,98]

The trefoil knot naturally has a chiral topology. All the amino acids forming the knot is L-isomer, therefore the right-handed and left-handed knots are diastereomers. The knot's enantiomer was also made from all D-amino acids. However, the diastereomeric building block containing L-cysteine and D-amino-alanine mainly formed the dimer and did not form the knot (Figure1-30).

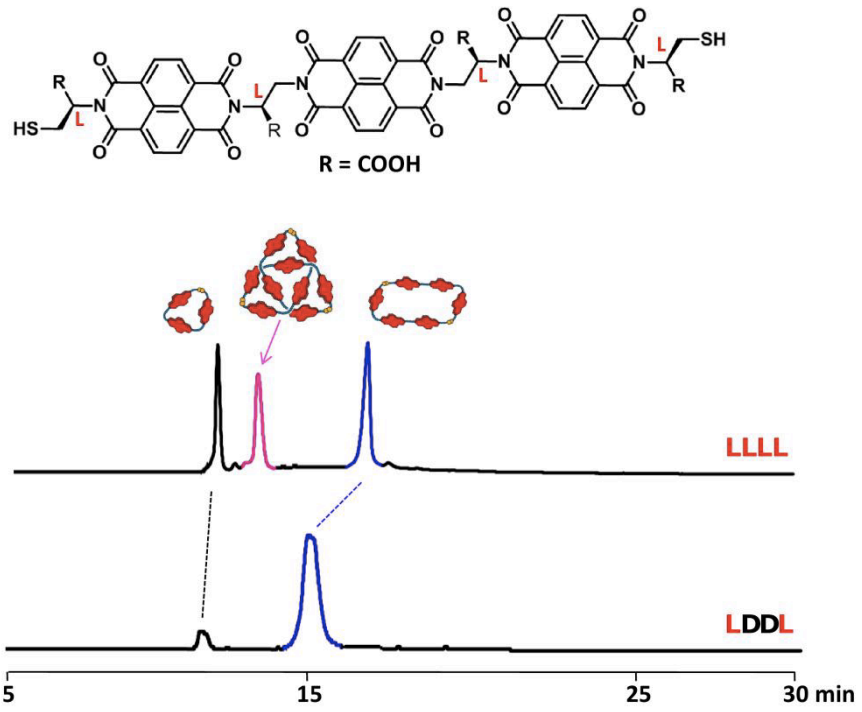

Figure 1-30. The HPLC analysis of (a) LLLL chiral centres and (b) LDDL chiral centres.[126]

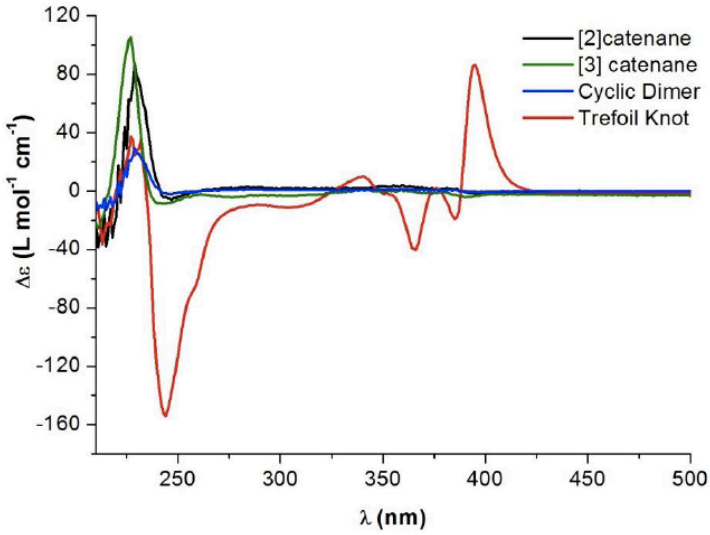

Figure 1-31. The CD signal of the all-L knot is orders of magnitude stronger than in related interlocked structures.[126]

The CD study shows a strong positive band in the NDI absorption region (385 nm) and a strong negative band in the imide region (245 nm). The CD signal is much stronger than for the previously published [2], [3] catenanes or the cyclic dimer by the Sanders group. [122,123,126]

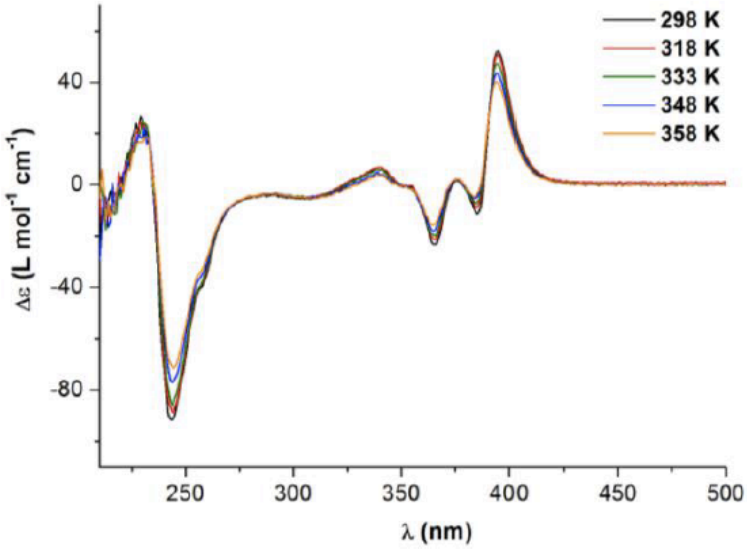

Figure 1-32. CD of the all-L knot (H_2O) at variable temperatures from 298 K to 358 K.[126]

The variable temperature (VT) CD experiment shows that upon increasing the temperature the knot keeps its topology and does not unwind.

1.6.3 All-acceptor Figure Eight Knot and Solomon Link

The syntheses of a purely organic Solomon link, (60% measured by HPLC) and figure-of-eight knot (18% measured by HPLC) from a single dithiol building block in an aqueous dynamic combinatorial library were reported by Sanders group. The formation of both structures evidences the hydrophobic effect as a powerful tool for construction of a range of complex topologies. The DCL consists of the all-acceptor building block (two NDIs connected *via* a hexyl chain and terminated by two L-cysteine). The LC-MS results reveal the presence of dimer, trimer and four tetramers (T1, T2, T3 and T4 where T=tetramer). However, by making a library of a racemic mixture of building blocks (LL building block in red and DD building block in orange), a new tetramer was formed (T5) which has a more stable structure, assigned as a *meso* figure eight knot. It is remarkable how by changing the chirality on the cysteine (using both L and D building blocks) the libraries distribution changes to make near-quantitative T5.[112]

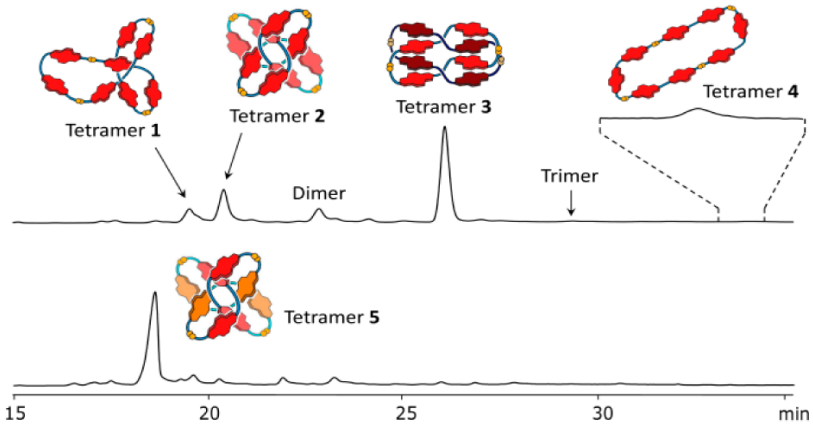

Figure 1-33. HPLC analysis of a library at 5mM of building block, in water at pH 8.0. Absorbance was recorded at 383 nm.[112]

These results show a correlation between the chirality of the terminal amino acid residue and the topological chirality of the final structures formed.

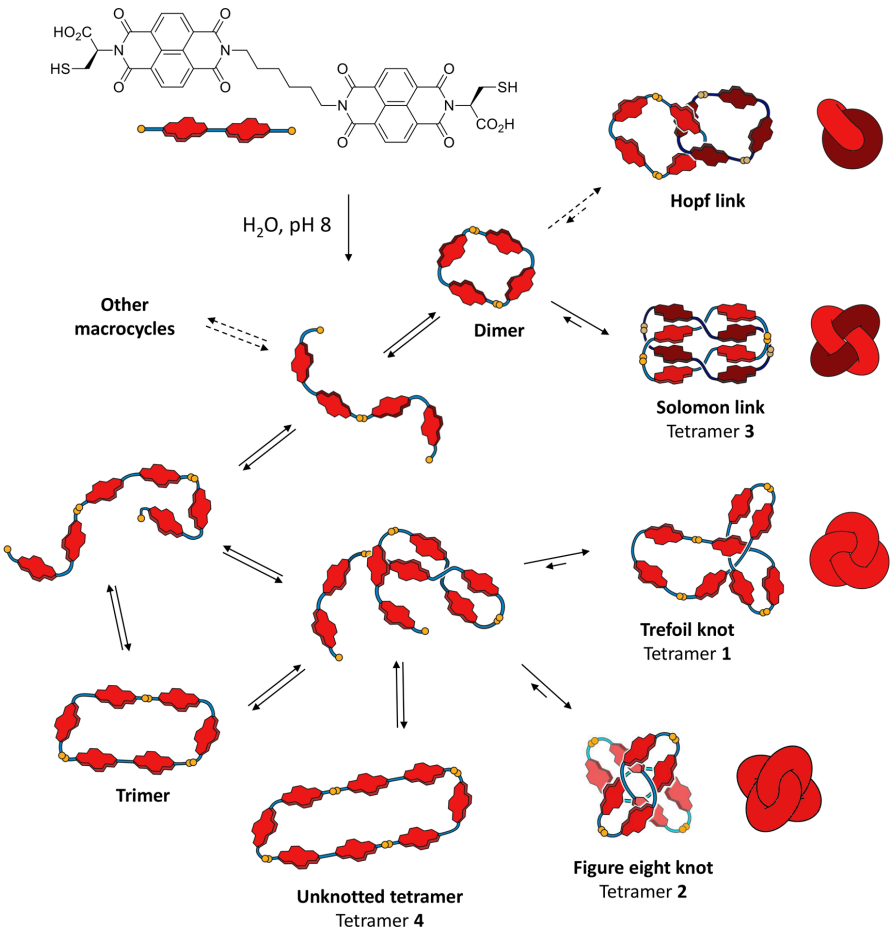

Figure 1-34. The topological isomers (knots and links) possible in the disulfide DCL (T1, T2, T3 and T4). The cartoon yellow dots represent the sulfur atoms of the building blocks.[112]

The formation of different knots and links from just a simple building block proves the relationship between the structure of the building block (the size, flexibility and solubility) and the topology that is finally formed.

1.7 A Selection of Other Remarkable Interlocked Molecules

1.7.1 Five Crossings Molecular knot (Pentafoil):

Leigh and co-workers have reported a five (pentafoil) and an eight crossing knots. The five-crossing knot (pentafoil) was prepared in one-pot, starting from five bis-aldehyde (**1.38**), five glycol linker, 2,2′-(ethylenedioxy)bis(ethylamine) building blocks (**1.39**) and five metal cations and one chloride anion which all self-assembled to form the molecular pentafoil knot in 44% yield.[127]

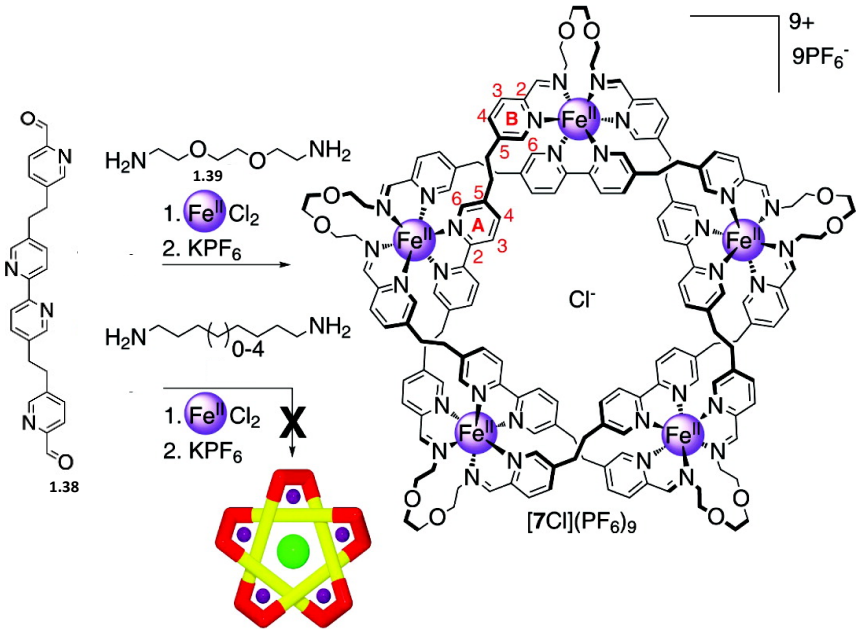

Figure 1-35. The synthesis of molecular pentafoil knot.[127]

The assembly of building blocks to form a molecular pentafoil knot was mainly driven by introducing a diamine (**1.39**) that could form a low-energy turn due to the gauche effect on its glycol linkers.

1.7.2 Eight Crossings Molecular knot:

The eight-crossing molecular knot[128] is another complex interlocked molecule reported by Leigh group, and its formation includes the assembly of four building blocks into three braided ligand strands. The position of the three strands at each crossing point is controlled by the octahedral iron(II) ions.

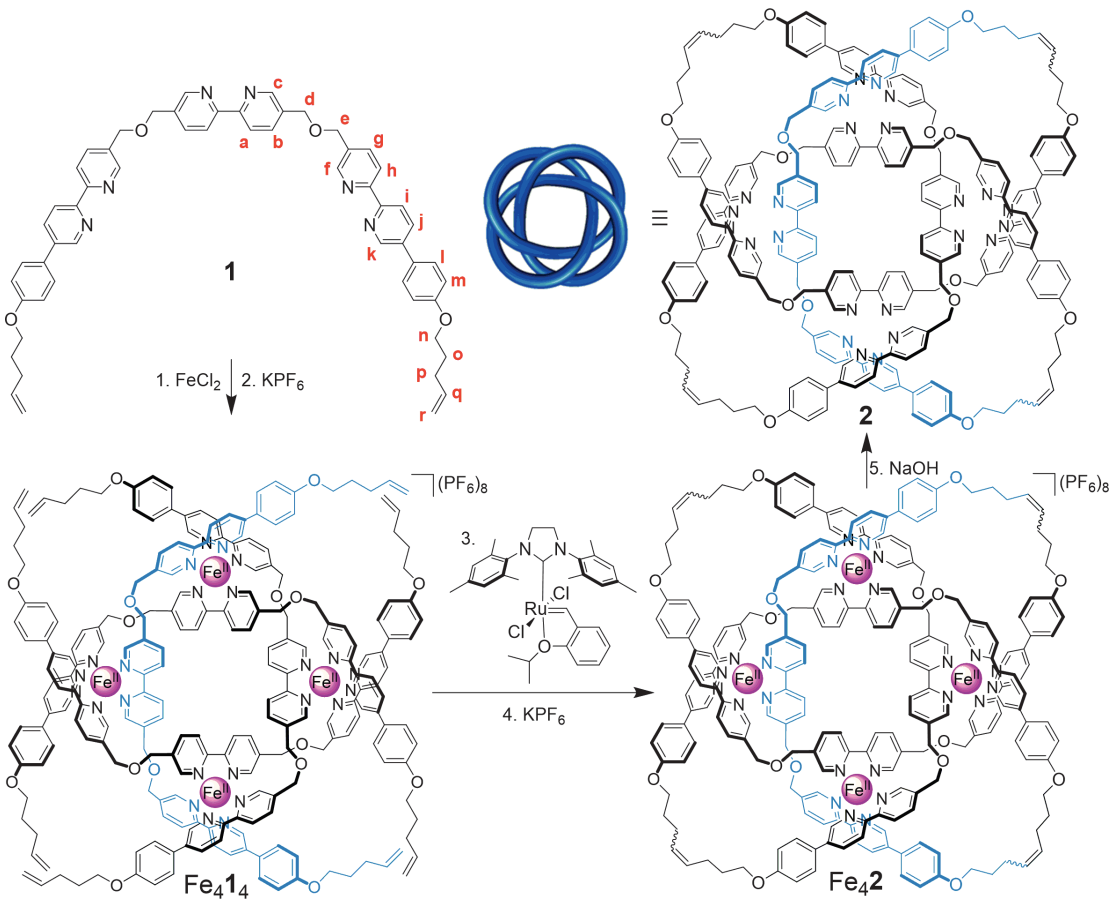

Figure 1-36. The synthesis of eight crossing molecular knot.[128]

1.7.3 Three-Dimentional (3-D) Tetrahedral Polycatenanes

Sanders and Nitschke have achieved a 3-D tetrahedral polycatenane from three reversible interactions (imine exchange, donor-acceptor interaction and metal-ligand coordination), which lead to the formation of a cage-like tetrahedral [7]catenane. These metal-cages can form [n]catenanes upon threading with crown ethers (acting as donor building blocks).[129]

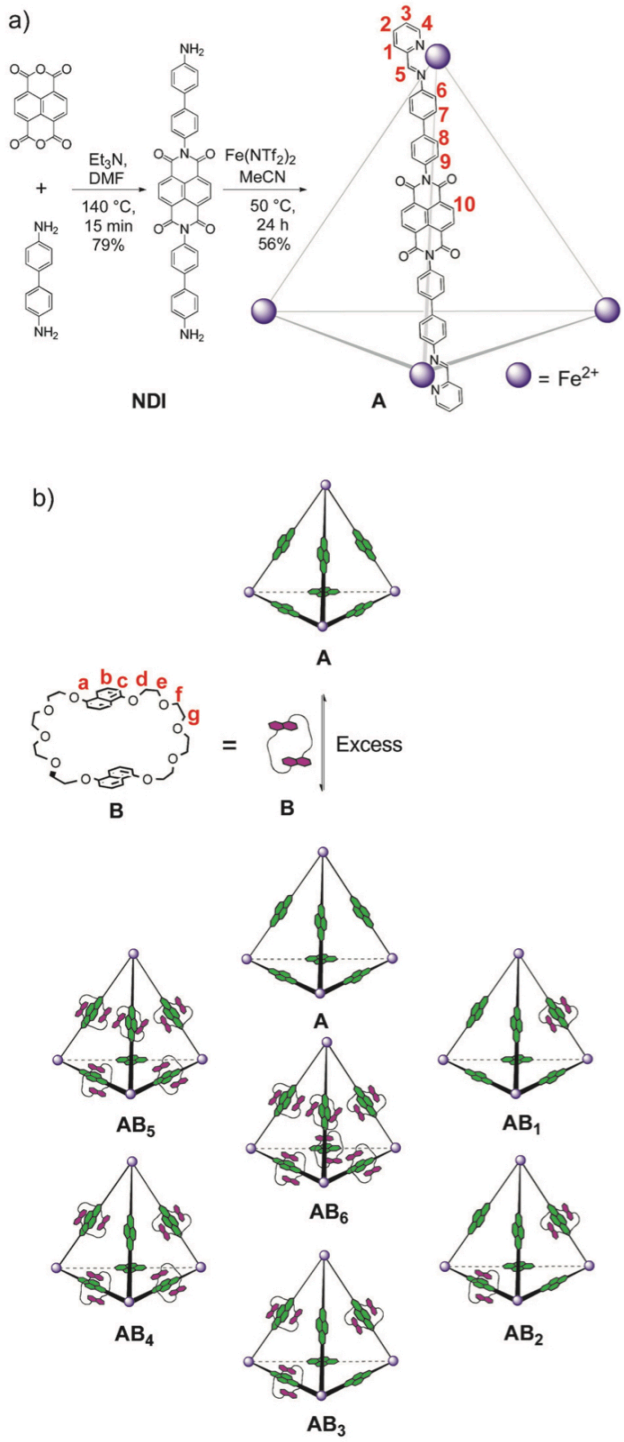

Figure 1-37. (a) The synthesis of 3-D tetrahedral cage and (b) the DCL of **A** with excess **B** (crown ether).[129]

Conclusion

In summary, this chapter discussed dynamic combinatorial chemistry and its applications. DCC has established to be a powerful tool for accessing molecules with complex topologies through simpler building blocks. This has been proven by a large number of studies performed in this field, and thus, various interlocked species with phenomenally complex topologies have been reported. Taking advantage of supramolecular interactions (such as Hydrogen bonding, π–π stacking, donor-acceptor interaction, hydrophobic effect) has paved the way for accessing these complex topologies.

The interest in this area is continuously growing, and the use of appropriate building blocks and tailored experimental design will allow further molecules otherwise inaccessible to be discovered.

Aim of Study

The aim of this project was to explore the donor-acceptor interaction between the electron rich dioxynaphthalene (DN) and electron poor naphthalenediimide (NDI) in aqueous dynamic combinatorial chemistry.

In the next three chapters we go through the synthesis of variety of [2]catenanes based on donor-acceptor interactions of the π systems. All these [2]catenanes are made using disulfide chemistry. This work differentiates itself from previous work done by the Sanders group by using new functionalities in the NDI building blocks and using other, less studied donor building blocks. In this project, we incorporate polyamines in the structure of the building blocks in order to promote self-templation and study the influence of the hydrophilic groups in the linker on the DCLs distribution.

The presence of nitrogen atom in the alkyl chains can change the solubility, flexibility and reactivity of the building blocks. It is expected to see changes in hydrophobicity of building blocks and how the building blocks are going to interact and assemble. We will use a broad range of polyamines to explore the effect of numbers of nitrogen as well as the length of polyamine on the DCLs composition.

Chapter 2

Studying the Formation of Donor-Acceptor [2]Catenanes in Aqueous Dynamic Combinatorial Libraries

2.1 Building Block Design

In this study, the acceptor building blocks were composed of two large hydrophobic NDI electron-deficient π-systems, connected by flexible polyamine chains which differ in the length and number of nitrogen atoms in the linker. Six consecutive polyamines were used as the source of flexible linkers with increasing length.

The donor building blocks vary in length of the side chain and in the substitution arrangement of the central core (1,5- or 2,6-derivatives).

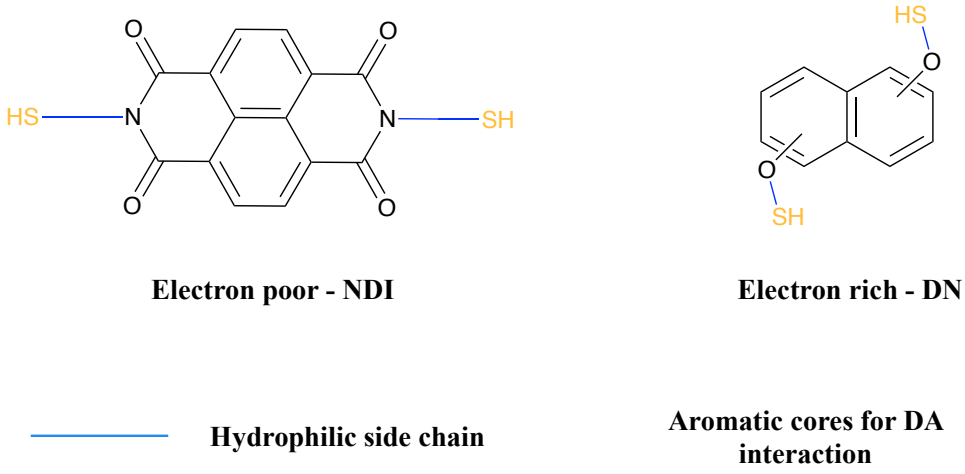

Figure 2-1. General design for Donor and Acceptor building blocks.

2.2 Building Block Synthesis

The first step of the synthetic protocol was to produce naphthalenemonoimide (NMI). The reaction involved the mono-substitution of naphthalenedianhydride (NDA) with 1 equivalent of trityl protected L-cysteine. The cysteine moiety was added only to one side of the NDA molecule, which allowed for the further functionalisation with the polyamine moiety, thus connecting the two NMI building blocks together.

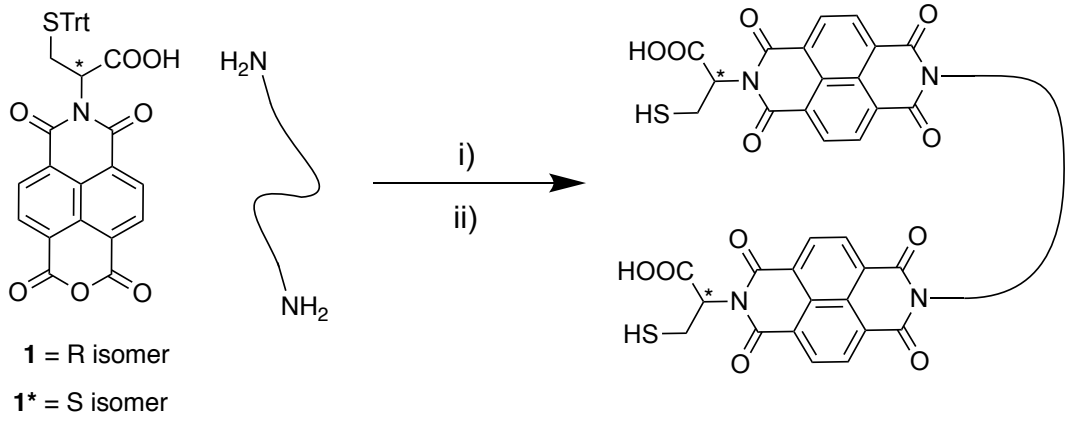

Figure 2-2. The synthetic route to acceptor building blocks (shown as a generic structure, for precise structures see experimental section) *via* different linkers. Reaction conditions: i) Et_3N, DMF, 120°C, μW, 5min; ii) CF_3COOH, Et_3SiH, CH_2Cl_2, 30 min. **1** and **1*** represent the NMI with L or D cysteine. The overall yield for each new compound is presented in Figure 2-3.

The same procedure was used for all the polyamines: the first step was the reaction of amine chain with naphthalenemonoimide under microwave irradiation followed by deprotection of trityl-cysteine.

The objective was to explore the behaviour of these molecules in aqueous solution by themselves, with template and also in the presence of donor building blocks. The donor building blocks were synthesised following a previously published protocol by Dr Au-Yeung.[120]

Acceptor building blocks

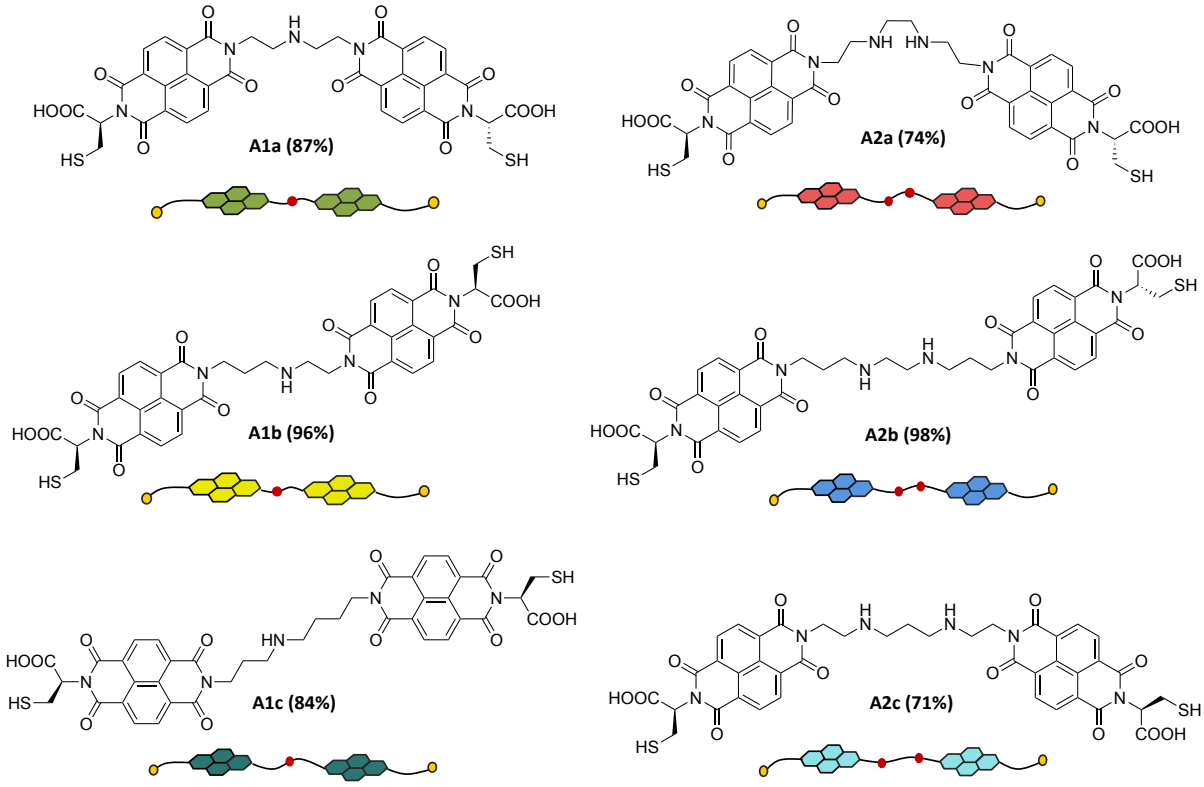

Donor building blocks

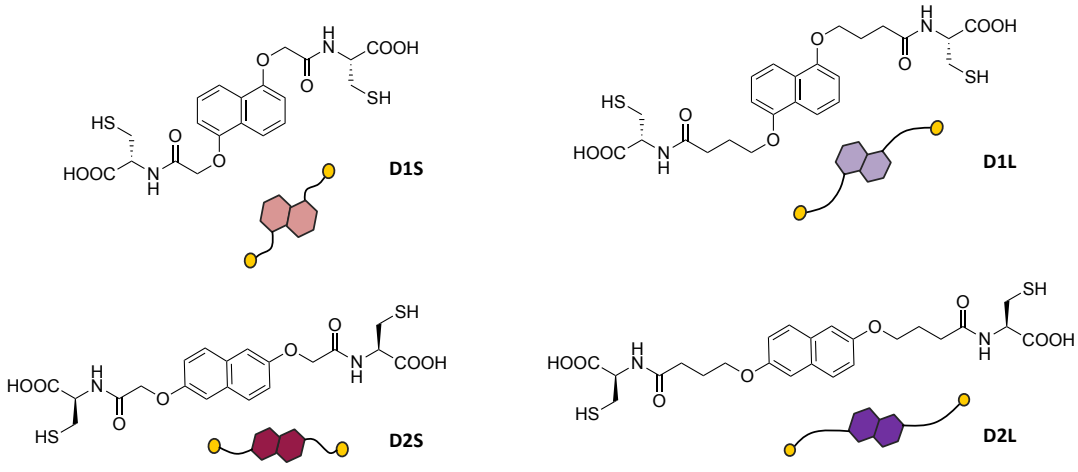

Figure 2-3. Acceptor (A) and Donor (D) building blocks synthesised and used in this chapter with their corresponding cartoon representations and acronyms. The overall yield for each new acceptor molecule is also presented.

In this work, two sets of polyamines were used: the ones with one nitrogen atom in their linker (**A1a**, **A1b** and **A1c**) and the ones with two nitrogen atoms (**A2a**, **A2b** and **A2c**), each having different number of carbon atoms in their linker. The aim was to compare the effect of number of nitrogen atoms in the polyamine on the library's distribution. For example, **A1c** and **A2a** have the same number of atoms (n = 8) in their linker; however, the **A1c** has one nitrogen atom and **A2a** has two. In the previous studies reported by Sanders group, all acceptor [2]catenanes using an alkyl chain (n = 8) as linker have been achieved. The length of these polyamines was also another focus of the current study. The shorter polyamines such as **A1a** or **A2b** have only 5 or 6 atoms in their linkers, respectively, and from previous studies this leads to the formation of cyclic dimers and formation of interlocked structures namely [2] or [3]catenanes.

2.2.1 Proposed mechanism for the formation of catenanes in aqueous DCLs

Considering the structural features of acceptor building blocks with the two hydrophobic NDI cores, the formation of conventional DADA [2]catenane is expected. The disulfides at the end of the NDI will oxidise to form a cyclic monomer. Once the first ring with an appropriate cavity size forms, the threading of a DN building block inside the cavity is favoured, thus making a stable aromatic stack through donor-acceptor interactions. However, a second pathway has been considered for the formation of these catenanes, and that is by formation of a DN dimer first and subsequent threading of the acceptor molecule (NDI) through the ring cavity and closing the catenane by oxidation of thiols. This serves as a pseudorotaxane precursor for the formation of the [2]catenane with DADA arrangement (Figure 2-4).

Previous studies on a DCL composed of donor and acceptor building blocks in pure water have shown that it does not usually lead to the formation of catenanes, with only traces of complex structures identified. This suggests that in water the sum of donor-acceptor and hydrophobic interactions is not sufficient enough to bring stacks of building blocks in the close proximity necessary for catenation or the assembly of any other complex structure. However, by increasing the polarity of the medium by involving high salt concentration libraries (*e.g.* 1 M $NaNO_3$), the formation of structures such as catenanes and knots was promoted. The hydrophobic effect plays an important role in the formation of such topologies and we made use of it in the design of our products. To identify the parameters promoting efficient formation of the catenanes in the libraries, the first step is the formation of a dimer with a large enough cavity to allow an aromatic core threading through. Once the aromatic surfaces are in optimum overlap the catenane formation is favoured and occurs through donor-acceptor and

hydrophobic interactions. This step requires each ring forming the catenane to be relatively tight; when the rings are too flexible, catenanes are not formed or formed in very small yields.

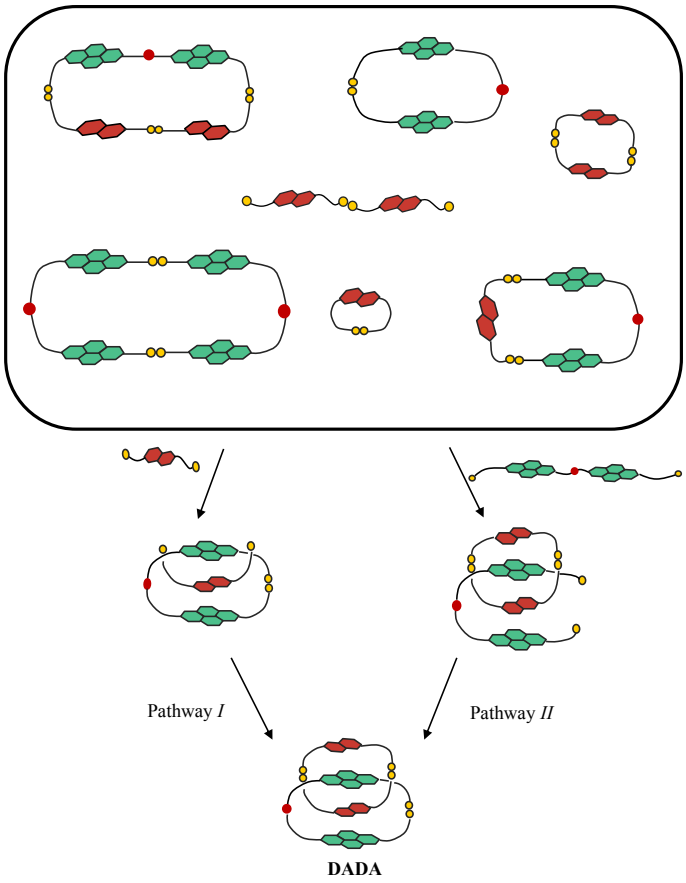

Figure 2-4. The cartoon representation of possible arrangement to form in a D-A library and proposed mechanism for the formation of dynamic combinatorial donor-acceptor [2]catenanes.

In pathway *I*, the formation of catenanes in donor-acceptor libraries occurs through formation of NDI cyclic monomer, and subsequent threading of a DN monomer, followed by linking another DN monomer and closing the catenane. Distinctly, in pathway *II*, the three sequential steps are: the formation of a DN dimer, threading of a linear NDI into the dimer's cavity, and closing the catenane. The process is more likely to undergo a mechanism as shown in pathway *I* due to favourable intramolecular cyclisation of NDI over the intermolecular dimerisation of DN represented in pathway *II*. In these libraries the DADA stacking sequence is strongly favoured because the NDI cyclic monomer is highly likely to occur and thus allows the threading of the donor building block. This restricts the possibility of non-classical stacking (e.g. DAAD and DADD).

2.2.2 NDI-based Building Blocks in This Chapter: A1a, A1b and A1c

In this chapter, three new dumb-bell NDI-based building blocks are introduced, all of which have one nitrogen atom in their linker. These three molecules differ in the number of carbon atoms in their linker (with shortest being **A1a** with five atoms in total in the linker, and longest **A1c** with eight atoms in the linker). The length of the linker will have a significant effect on the flexibility of the molecule. The nitrogen atom in the linker can reduce the solubility of the molecule in water however, it increases the flexibility of the molecule when compared to an all alkyl chain. For each of these molecules, a library of the building block by itself in water was prepared in order to investigate their potential towards the formation of complex topologies without the DN building blocks.

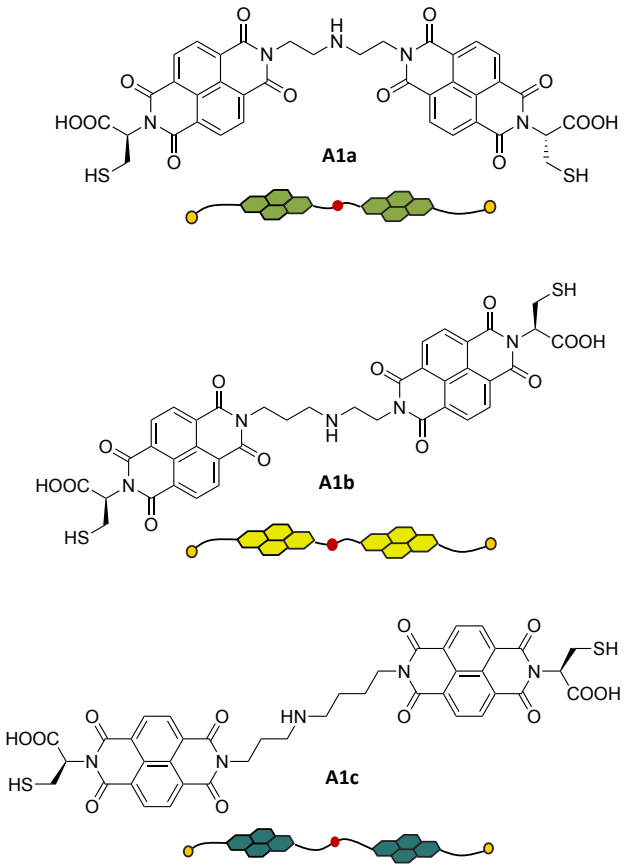

Figure 2-5. The three NDI-based molecules discussed in this chapter (**A1a**, **A1b** and **A1c**).

2.3 DCL of A1a-Dithiol Acceptor

The DCL of **A1a** acceptor was generated by dissolution of the building block in water (5 mM concentration) and the pH was adjusted to 8 using an aqueous solution of 100 mM NaOH. The library was stirred for one day under air in a capped vial to allow full oxidation of the thiols.

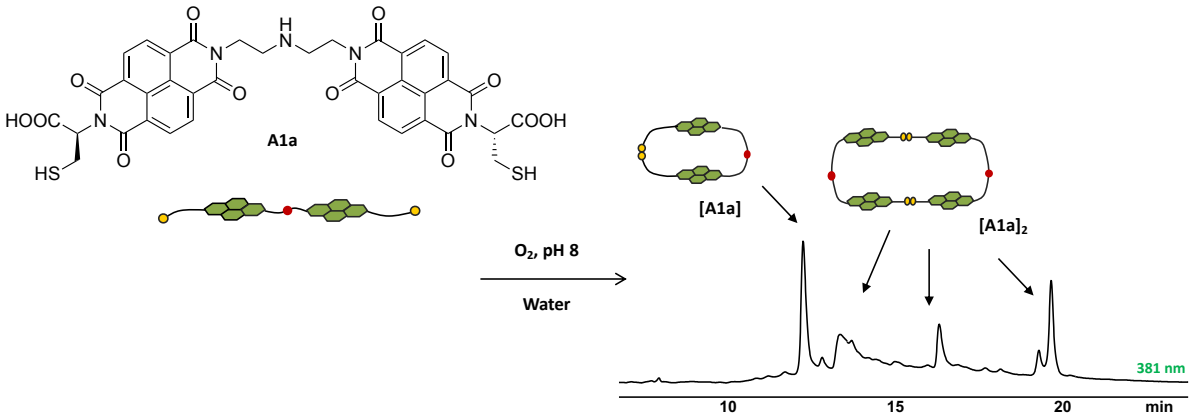

Figure 2-6. The HPLC analysis of **A1a** library in water. Absorbance was recorded at 381 nm.

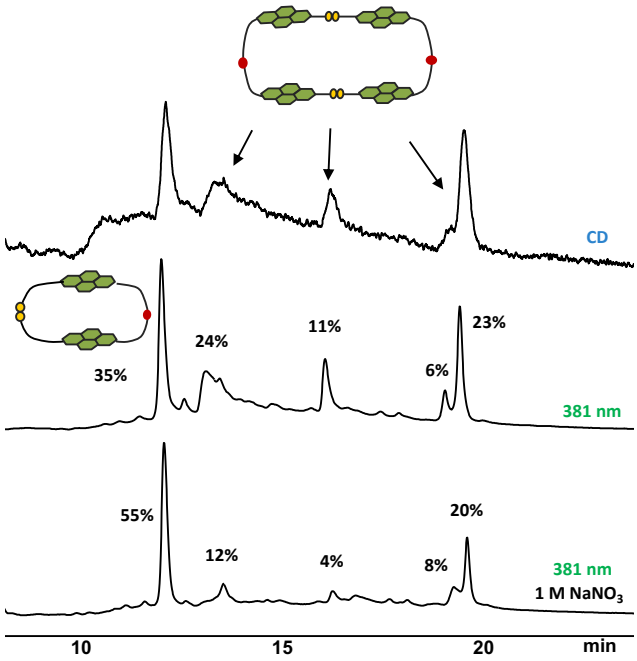

Figure 2-7. The HPLC analysis of **A1a** library in water with and without $NaNO_3$. Absorbance was recorded at 381 nm and CD was also recorded at 381 nm. Estimated yields are indicated above the corresponding peaks. The yields are calculated based on the integration of HPLC peaks.

The libraries were analysed using a HPLC instrument equipped with a diode array detector (DAD). A CD detector was connected in series with the DAD detector, thus all the retention times in CD are 0.6 min longer than in DAD and the peaks are broader.

Using the DAD, the NDI (λ_{max} = 381 nm) chromophores was monitored, and the CD detection at 381 nm allowed us an early identification of species in which the chirality of the cysteine has been effectively been transferred to the NDI chromophore. Our previous experience has shown that interlocked or conformationally restricted molecules have a CD signal on the NDI absorbance, while flexible macrocycles or linear species do not. As can be seen on Figure 2-7, all four peaks representing the **A1a** macrocycles show CD signals, and that is due the chirality being transferred from the cysteine onto the aromatic core.

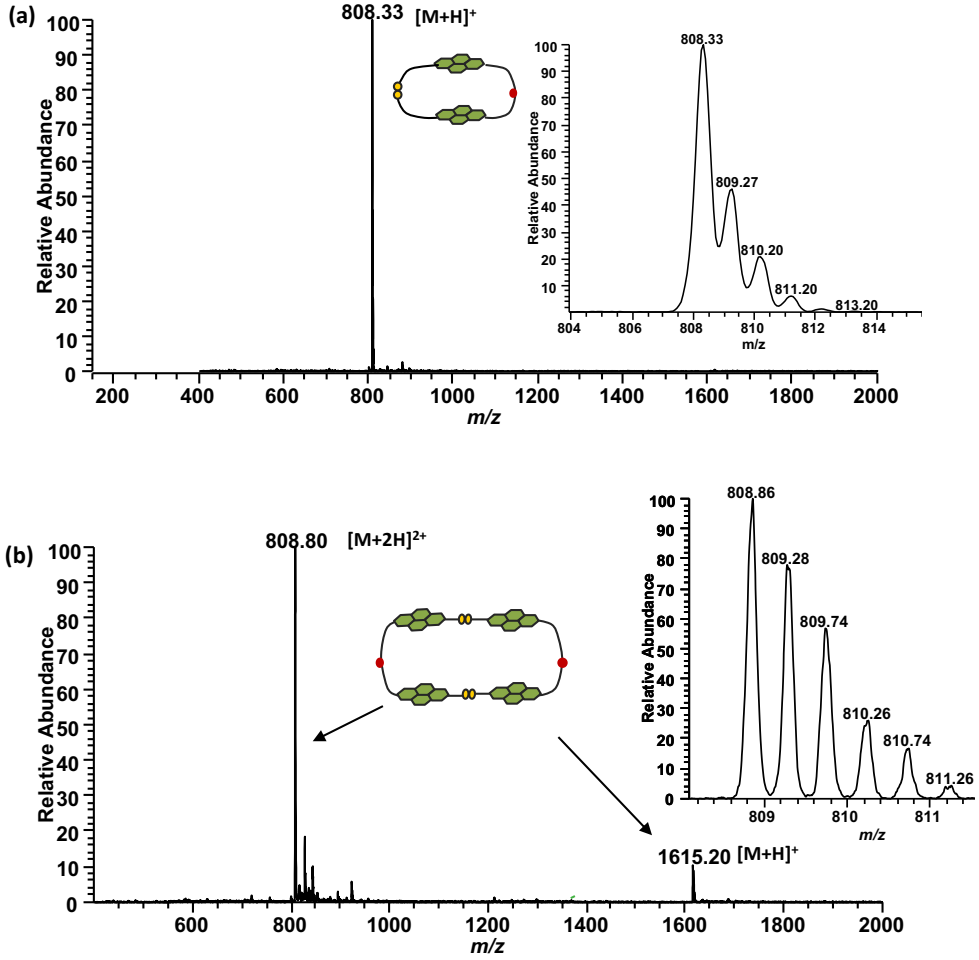

Figure 2-8. ESI-MS (*+ve*) spectra of (a) **[A1a]** cyclic monomer (as singly charged cation), (b) the **[A1a]**$_2$ cyclic dimer (as doubly charged cation). Expansions of molecular ions are shown as inserts.

Two major components have been at equilibrium in this library: the cyclic monomer **[A1a]** and cyclic dimer **[A1a]**$_2$. The three separate peaks that correspond to the cyclic dimer have the same *m/z* value, isotopic pattern, and fragmentation behaviour in MS. This can be due to the different, yet stable conformations of the dimer, which slowly interconvert and will be separated by the conditions used in the HPLC analysis.

The analysis of this library by HPLC and LC-MS shows no sign of molecules with complex topologies, just macrocycles being formed. This can be because of linker's flexibility (having the nitrogen atom in the linker), consequently easily closing up to form a monomer or a dimer. The library with increased polarity (containing 1 M $NaNO_3$) allowed the formation of **[A1a]** species to increase to 55%. This is because the **[A1a]** has a tighter packing in comparison to the dimer, and therefore, the hydrophobic effect favours its formation. The hydrophobic effect has a great influence on libraries' distribution and relative stability of the macrocycles. This reveals that the tight conformation of the monomer is the best to minimise the exposure of hydrophobic surfaces when the ionic strength of the solvent is increased.

2.3.1 Introducing the DN building blocks

After the analysis of **A1a** building block by itself, new DCLs were set up using DN building blocks (**D1S**, **D2S**, **D1L** and **D2L**) and the effect of these electron rich moieties on the libraries was studied.

The library set up was very similar to the **A1a** DCL. The DCL of **A1a** with DNs was generated by dissolution of the building blocks in water (5 mM concentration) and the pH was adjusted to 8 using an aqueous solution of 100 mM NaOH. The solutions were mixed in a 1:2 ratio (**A1a**:DN) and stirred for one day under air in capped vials to allow full oxidation of the thiols. At the event of mixing the two building blocks, an immediate colour change was observed from yellow / colourless to bright red. This was the case for every donor building block that was used. The colour change is usually the first indication of the donor-acceptor interaction and the charge transfer from HOMO of the donor to the LUMO of the acceptor. Thus, implying a molecular or supramolecular system in which the NDI and DN building blocks are in close proximity (core distance under 3.5-4Å).

The libraries were analysed using HPLC and LCMS. We used the DAD as it allowed us to monitor both the NDI (λmax = 381 nm) and DN (λmax = 254 nm) chromophores simultaneously while the CD was recorded at 381 nm.

2.4 D-A DCL of A1a Acceptor and D1S Donor

The first D-A DCL, consisted of **A1a** species and the rigid donor building block **D1S**. The analysis has revealed the presence of macrocycles of **A1a**, **D1S** and **A1a-D1S**.

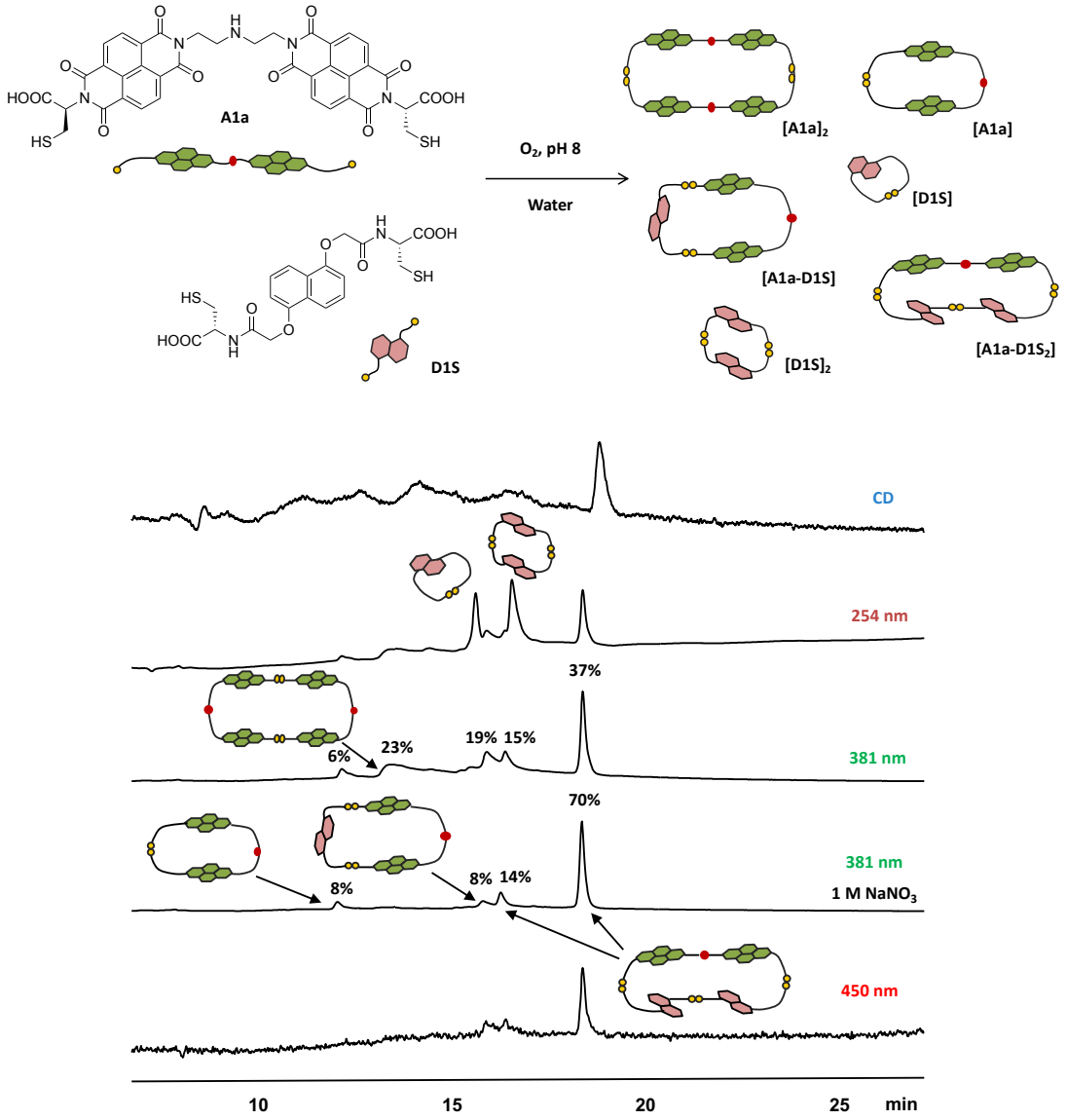

Figure 2-9. The HPLC analysis of **A1a** and **D1S** library (1:2 molar ratio, 5 mM total concentration). From top to bottom: CD detected at 381 nm, UV-Vis detected at 254, 381, 381 with 1 M $NaNO_3$ and 450 nm as indicated above the chromatograms. The wavelengths correspond to the main absorbance of the **D1S** (254 nm), **A1a** (381 nm) and the D-A charge-transfer complex (450 nm). Estimated yield is indicated above the corresponding peaks.

The HPLC and LC-MS analyses show a mixture of **A1a** and **D1S**, which have led to the formation of series of macrocycles. The MS data indicated that the species eluting in the first 15.0 min are a **A1a** cyclic monomer and dimer, then at 15.7 min the **D1S** cyclic monomer starts to appear, followed by the heterodimer **[A1a-D1S]** at 15.9 min and **D1S** cyclic dimer at 16.6

min. The **[A1a-D1S]** heterodimer contains one NDI and one DN, and the heterotrimer [**A1a-D1S$_2$]** was formed by one NDI and two DNs.

The heterotrimer **[A1a-D1S$_2$]** at 18.4 min is the major species (37%) in this library and its concentration increases up to 70% by addition of 1 M $NaNO_3$. This indicates that **[A1a-D1S$_2$]** has the tightest arrangement compare to the rest of the macrocycles, therefore its formation is favoured under more polar environment.

At 16.3 min, a small peak with the same mass as the peak at 18.4 min is observed, also representing the DA trimer. The two peaks both show identical MS and MS/MS data, and this suggests that the **[A1a-D1S$_2$]** heterotrimer has an isomer that appears earlier on the HPLC chromatogram.

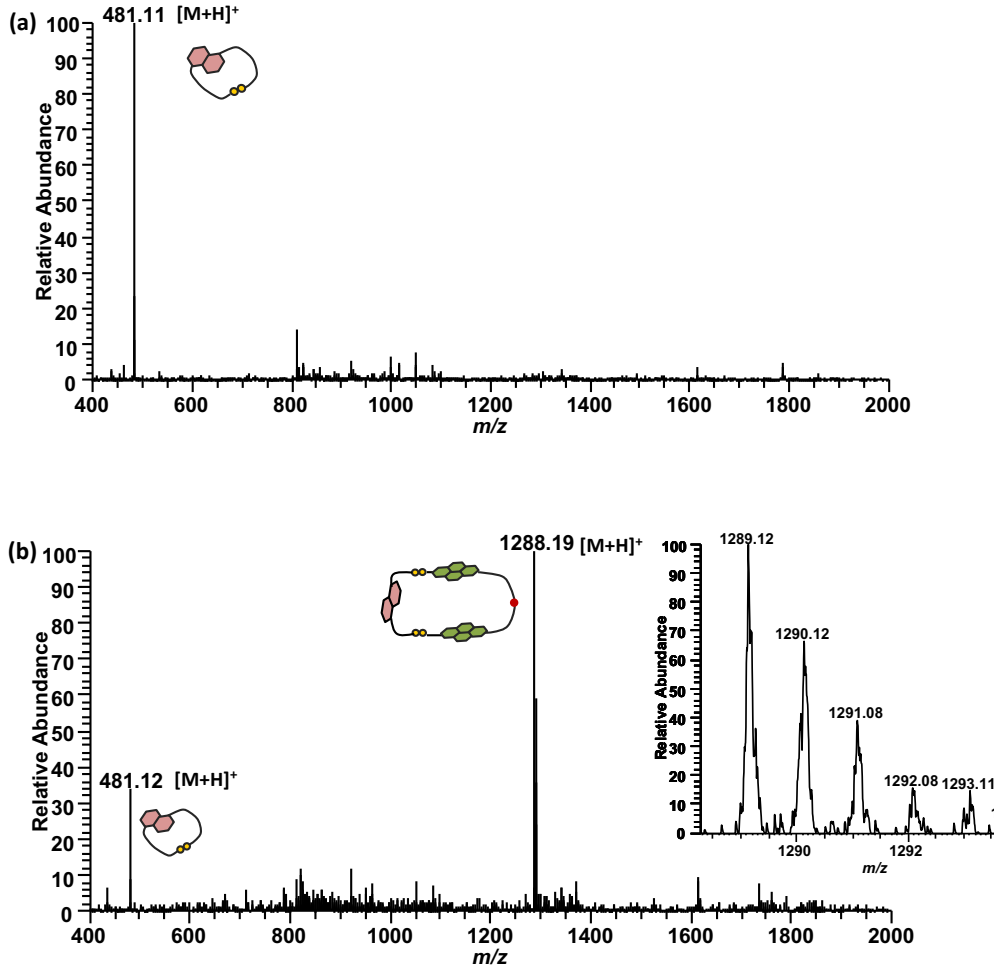

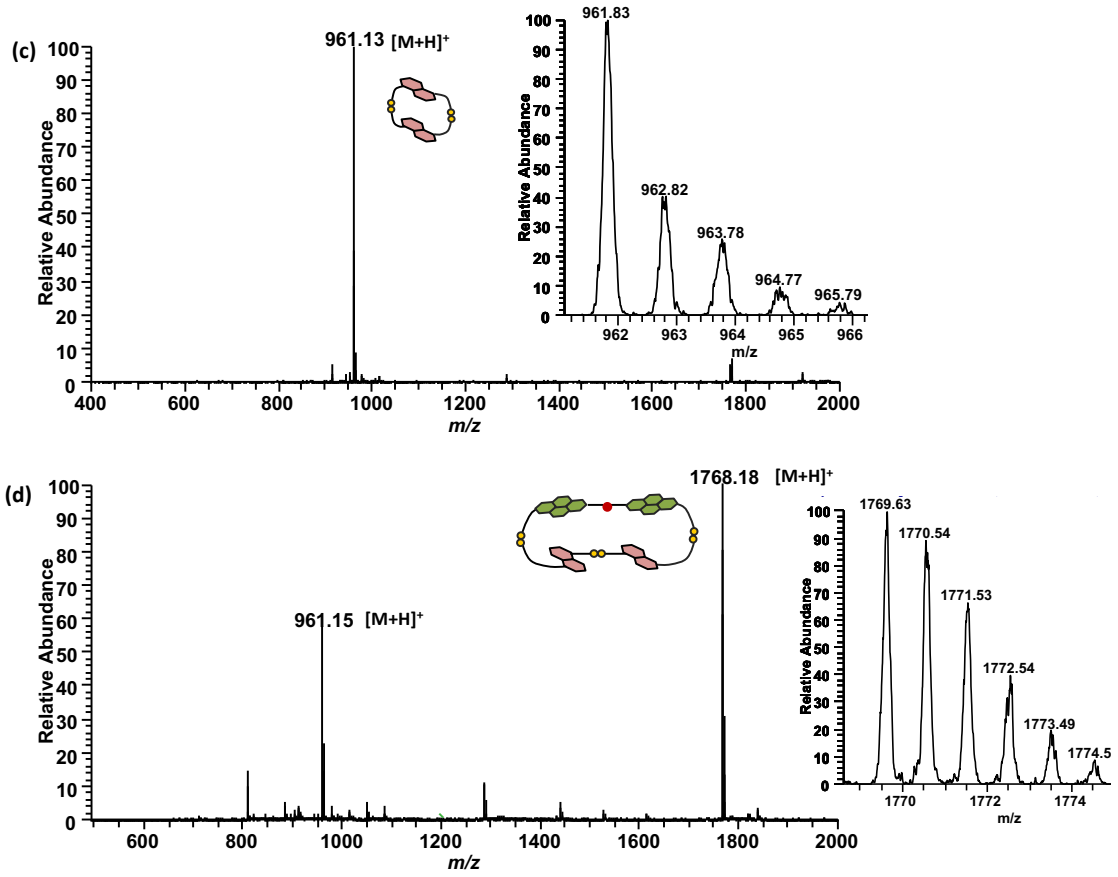

Figure 2-10. ESI-MS (*+ve*) spectra of (a) DN cyclic monomer **[D1S]** (as singly charged cation), (b) the heterodimer **[A1a-D1S]** (as singly charged cation), (c) the DN dimer **[D1S]$_2$** (singly charged cation), (d) the heterotrimer **[A1a-D1S$_2$]** (singly charged cation). The expansion of parent molecular ion is shown as insert.

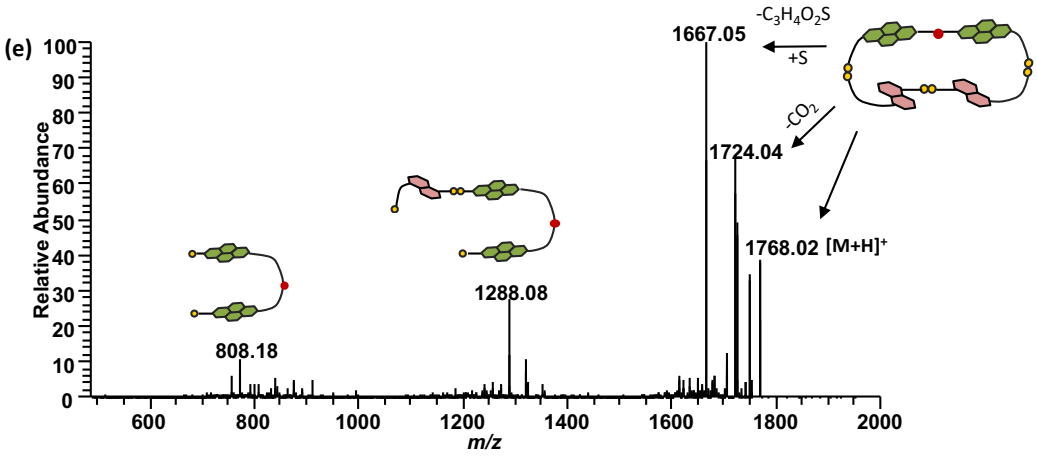

Figure 2-11. MS/MS fragmentation spectra of DA trimer **[A1a-D1S$_2$]**.

Following these results, we have explored how the rigidity of DN and the length of polyamine in NDI can affect the library's distribution. The cyclic monomer of **A1a** is too tight to fit a DN moiety in its cavity therefore it is not possible to form a DADA [2]catenane with these two building blocks.

2.5 D-A DCL of A1a Acceptor and flexible D2S Donor

A new D-A DCL consisting of **A1a** and **D2S** was set up, in which the electron-rich component, **D2S**, is less rigid compare to **D1S**, expecting to yield a more diverse library. However, the analysis has revealed that library's composition is very similar to the one with **D1S**, in which different macrocycles of **A1a** and **D2S** have been obtained.

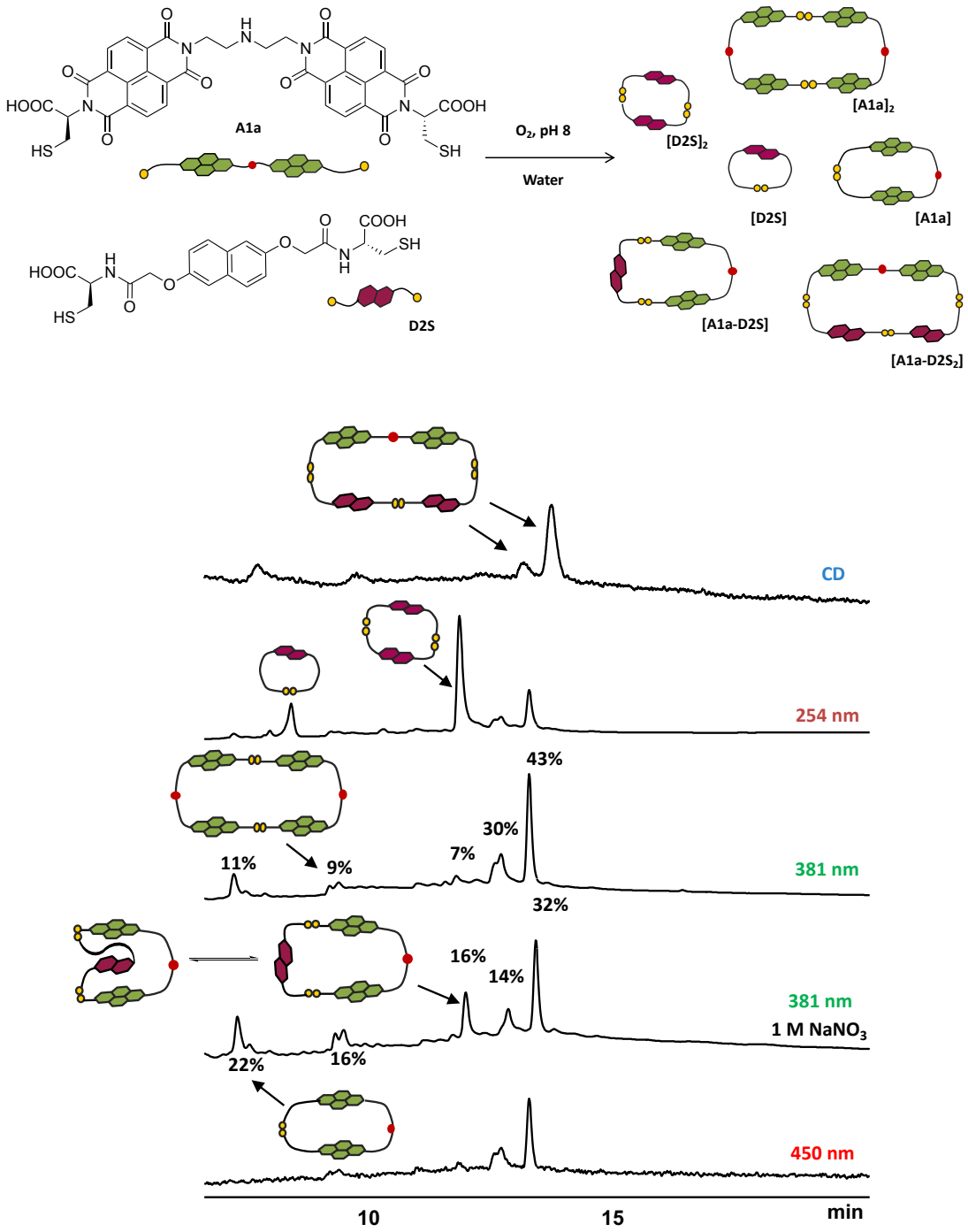

Figure 2-12. The HPLC analysis of **A1a** and **D2S** DCL (1:2 molar ratio, 5 mM total concentration). Estimated yield is indicated above the corresponding peaks.

At equilibrium, the library consists of series of macrocycles: **A1a** cyclic monomer and dimer, **D2S** cyclic monomer and dimer, as well as heterodimer **[A1a-D2S]** and heterotrimer **[A1a-D2S$_2$]**. The distribution of these macrocycles in presence of 1 M $NaNO_3$, is slightly different to the library without salt. In the library with $NaNO_3$, the concentration of heterotrimer **[A1a-D2S$_2$]** decreases from 43 to 31%, and the concentration of **A1a** cyclic monomer, dimer and heterodimer **[A1a-D2S]** increases by 10, 7 and 9%, respectively. The peak representing the heterodimer **[A1a-D2S]**, shows two possible arrangements for the molecule which can be in equilibrium. The hydrophobic effect favors the more compact structure as it has a smaller solvent accessible area.

The addition of salt appeared to have an opposite effect on the **[A1a-D2S$_2$]** and **[A1a-D1S$_2$]** macrocycles. This can be explained based on the connectivity of the DNs: in cyclic structure the 1,5-derivative is more rigid than the 2,6-isomer, and consequently the macrocycle of **[A1a-D1S$_2$]** has a tighter arrangement than **[A1a-D2S$_2$]**. Therefore, the formation of **[A1a-D2S$_2$]** is less favorable in more polar solvent due to its flexible packing.

The distribution of this library shows two peaks representing the **[A1a-D2S$_2$]**: one small peak at 12.9 min and one larger at 13.4 min. The two peaks exhibit identical MS and MS/MS data, and this suggesting that the **[A1a-D2S$_2$]** heterotrimer has a stable isomer that can be separated through HPLC and elute earlier on the chromatogram.

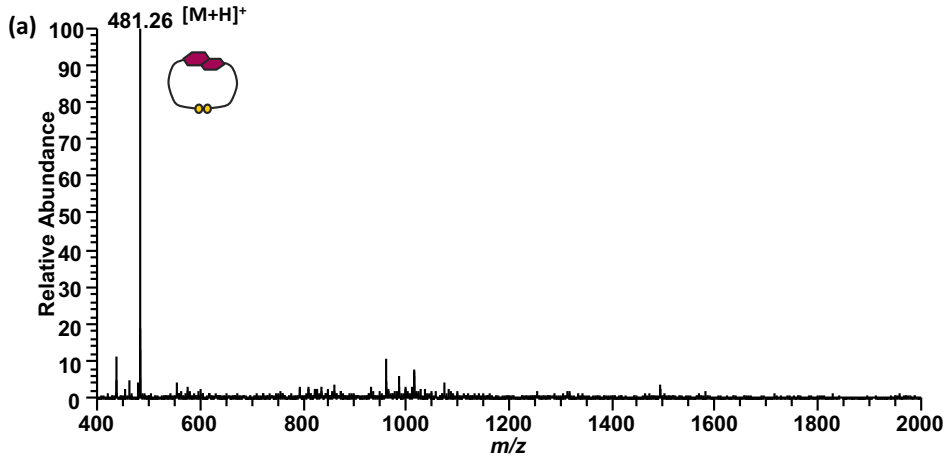

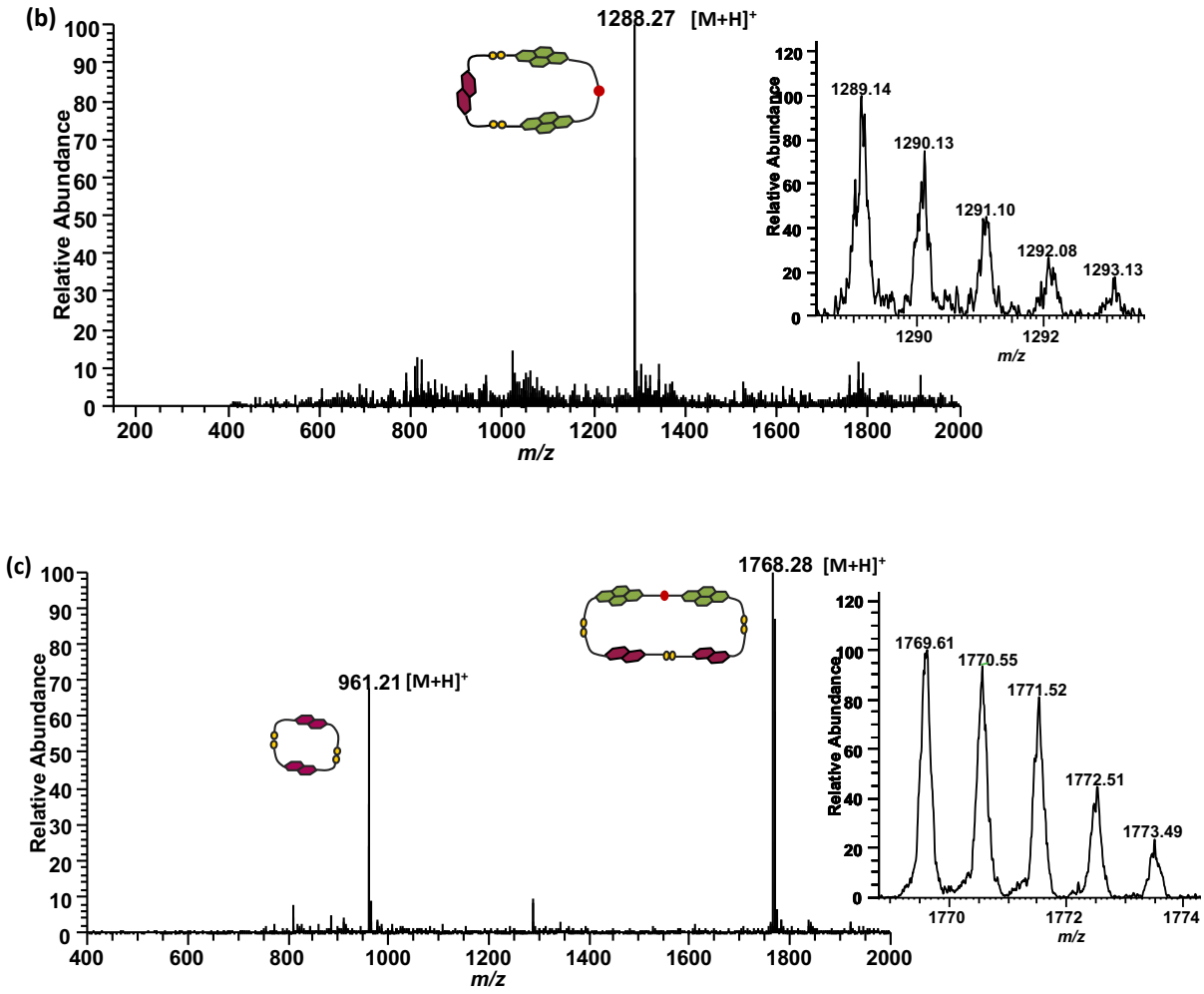

Figure 2-13. ESI-MS (+*ve*) spectra of (a) DN cyclic monomer **[D2S]** (as singly charged cation), (b) the heterodimer **[A1a-D2S]** (as singly charged cation), (c) the DN dimer **[D2S]$_2$** (as singly charged cation) and the heterotrimer **[A1a-D2S$_2$]** (as singly and doubly charged cation).

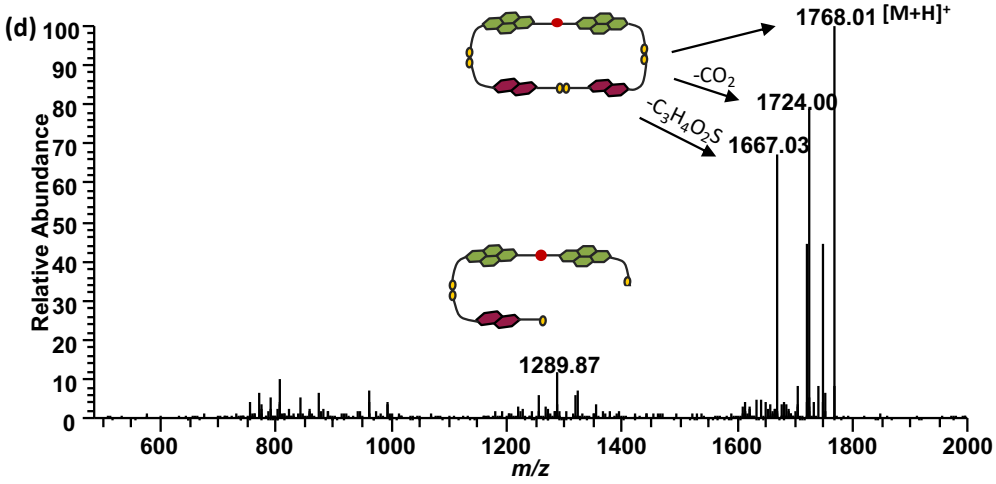

Figure 2-14. MS/MS fragmentation spectra of D-A trimer **[A1a-D2S$_2$]**.

In previous studies working with the same DN building blocks, it was proven that the DNs with the short side-chains result in a [-D-D-] dimer whose small cavity size enables a relatively good interaction with an acceptor moiety. However, in these sets of libraries, the tight [-A-A-] cavity does not favour the threading, hence no catenation.

In a conceptually similar work reported by Dr Fabien B. L. Cougnon,[123] employing such acceptor molecules, where the two NDIs are connected *via* an alkyl chain (NDI-$(CH_2)_n$-NDI), leading to formation of [3]catenane and [2]catenane in the presence of **D2S**. In is shown that when ($n \leq 6$), the dimerization of the NDI is favoured followed by threading of two **D2S** moieties into its cavity and closing up to form a [3]catenane. The formation of giant macrocycles and larger [2]catenanes using the 1,5-isomer (**D1S**), is also observed.

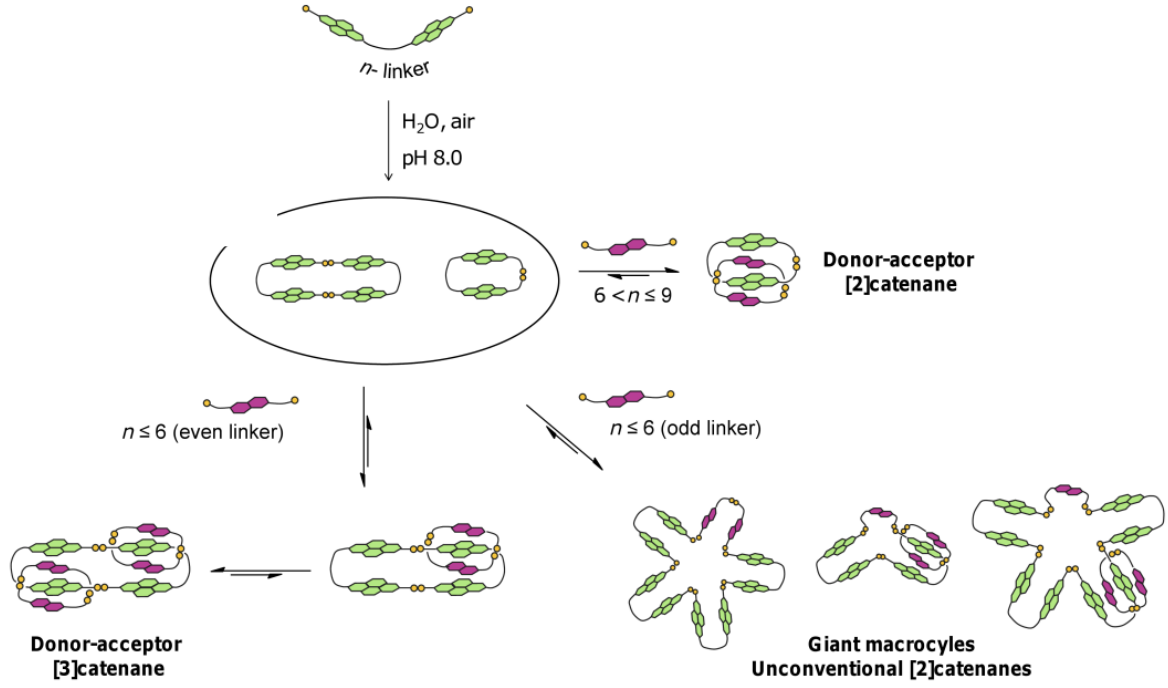

Figure 2-15. HPLC analysis reveals the different types of [2] and [3]catenanes formed in dynamic combinatorial libraries from the electron-rich (**D1S** and **D2S**) and the electron-deficient (**A**) building blocks.[124]

The data obtained from the libraries of **A1a** with **D1S** and **D2S** do not indicate the presence of a [3]catenanes or [2]catenanes. This can be explained by the presence of the nitrogen atom in the linker, making the molecule too flexible and bringing the hydrophobic surfaces closer together. This inhibits the threading of the DN moiety to threat through the cavity and form a catenane. This theory is only valid for **A1a** building block for having the shortest polyamine linker compared to the rest of acceptor moieties.

D-A DCL with Flexible DNs

The next set of DN building blocks used to set up libraries were **D1L** and **D2L**. These DNs are more flexible in comparison to **D1S** and **D2S**. The side-chain is two carbons longer in length, increasing the possibility to obtain interlocked molecules.

2.6 D-A DCL of A1a Acceptor and D1L Donor

This library consists of **A1a** acceptor and **D1L** donor building block. At equilibrium, the library consists of **A1a** and **D1L** cyclic monomers and dimers as well as D-A heterodimer **[A1a-D1L]** and heterotrimer **[A1a-D1L$_2$]**.

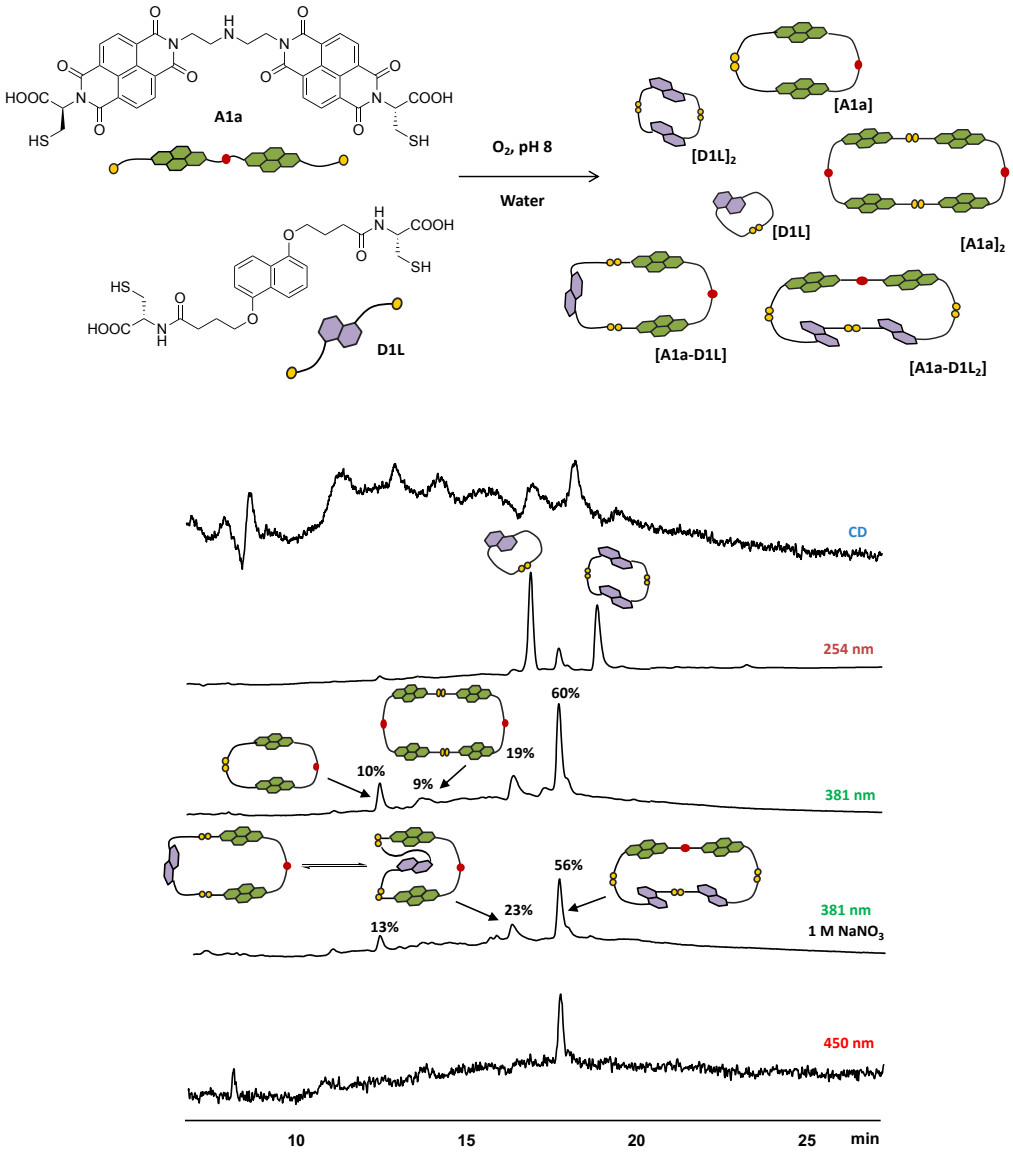

Figure 2-16. The HPLC analysis of **A1a** and **D1L** library (1:2 molar ratio, 5 mM total concentration). Estimated yield is indicated above the corresponding peaks.

The increase in polarity of the medium with 1 M $NaNO_3$ did not significantly changed library's composition, suggesting that the polarity plays a minor effect on this DCL.

The CD signals in this library are very broad compared to the DNs with the short side-chain. The shorter DNs formed tighter packing as shown in the previous libraries, and consequently displayed sharper CD signals. This supports the theory that the chirality transfers better through the tighter packing to give sharper Cotton effects.

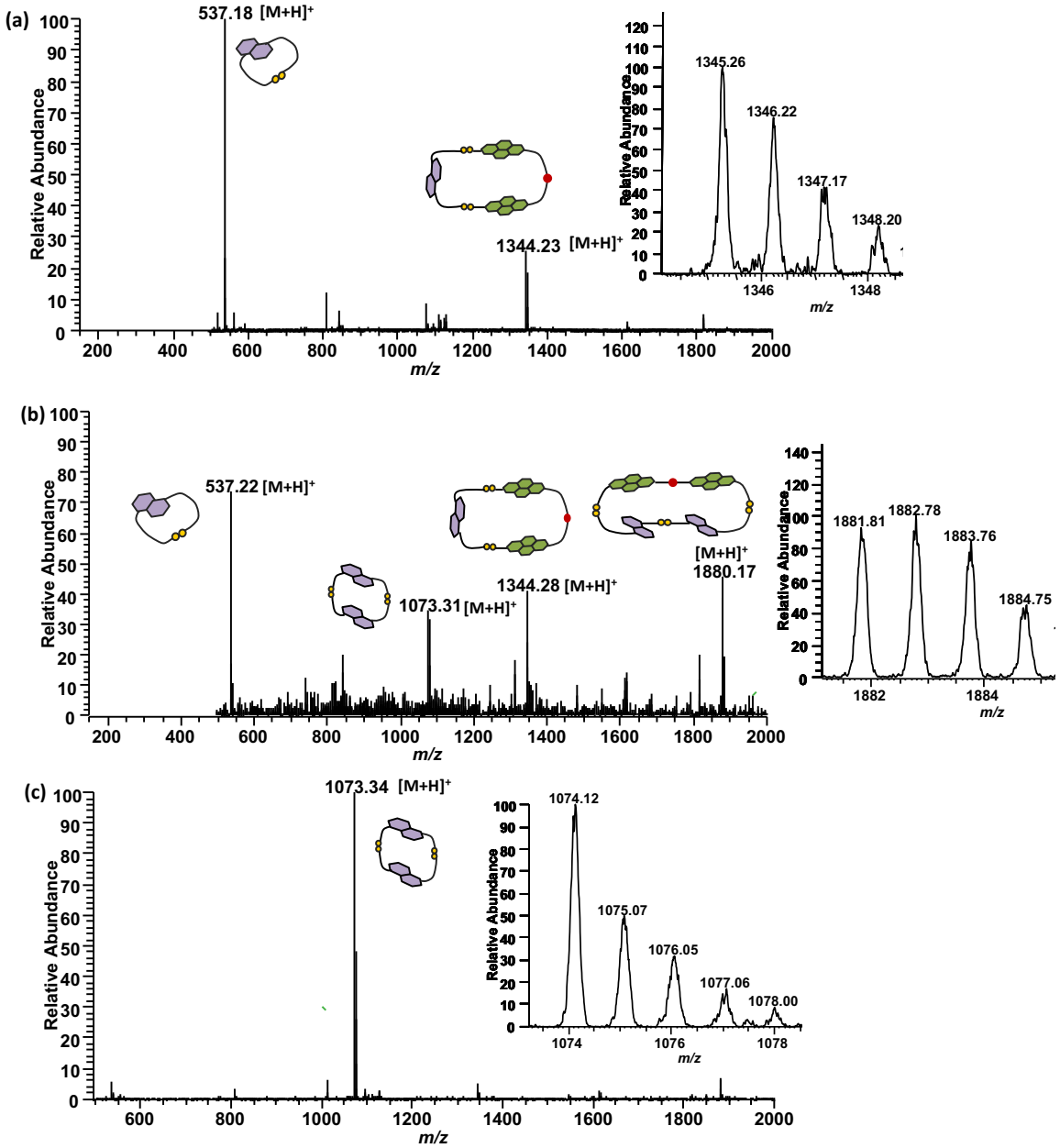

Figure 2-17. ESI-MS (+*ve*) spectra of (a) DN cyclic monomer **[D1L]** (as singly charged cation) and the heterodimer **[A1a-D1L]** (as singly charged cation), (b) the heterotrimer **[A1a-D1L$_2$]** (as singly charged cation) also the **[D1L]**, **[D1L]$_2$** and **[A1a-D1L]** was observed due to peak overlap (c) the DN dimer **[D1L]$_2$** (as singly charged cation). The expansion of parent molecular ions is shown as inserts.

Some of the peaks in the HPLC chromatogram appear very close to each other, so the MS data shows the overlap of some of the peaks.

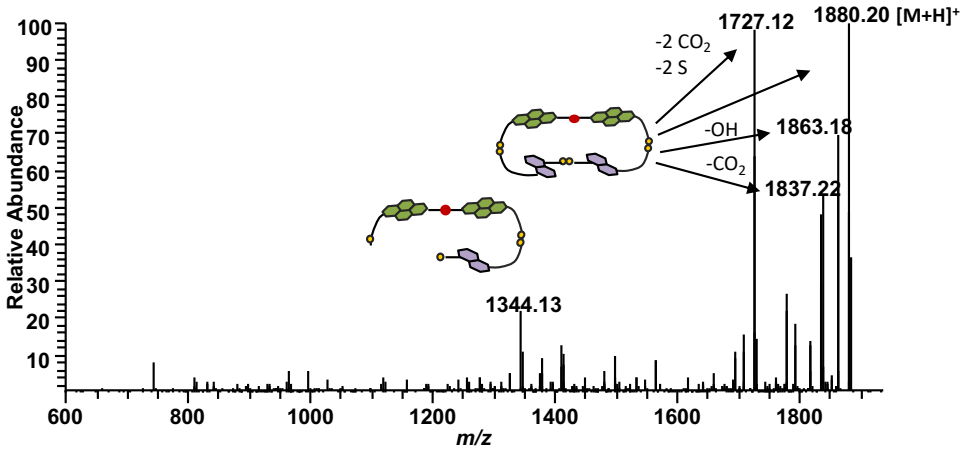

Figure 2-18. MS/MS fragmentation spectra of D-A heterotrimer **[A1a-D1L$_2$]**.

The library's composition is very similar to what is observed for the DNs with short side chain, with the HPLC / LC-MS analyses indicating a series of macrocycles due to the small cavity in **A1a** cyclic monomer.

2.7 D-A DCL of A1a Acceptor and D2L Donor

The last library with **A1a** acceptor employed the **D2L** donor building block. With the flexibility of the DN (due to its 2,6- connectivity), and its greater length, a more versatile library was expected to form. However, analysing the library by HPLC / LC-MS (Figure 2-19 and 2-20), has revealed a series of macrocycles.

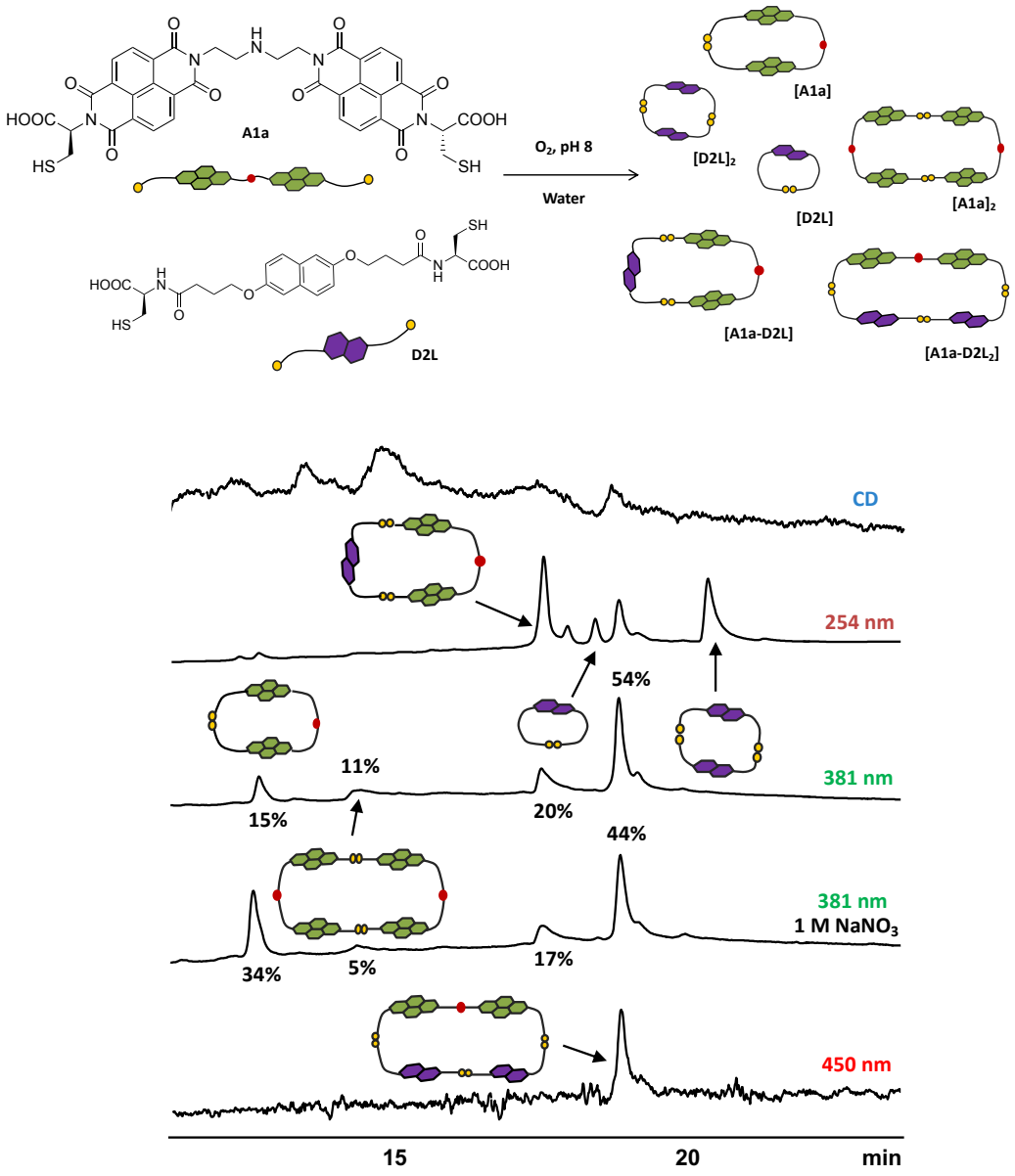

Figure 2-19. The HPLC analysis of **A1a** and **D2L** DCL (1:2 molar ratio, 5 mM total concentration). Estimated yield is indicated above the corresponding peaks.

In all the libraries studied with different DN building blocks, a series of macrocycles have been identified, which have similar sequence in appearance on HPLC chromatogram. The distribution of species in this library is very similar to the library with **D2S**. In this library as

well, the concentration of heterotrimer **[A1a-D2L$_2$]** decreases at the expense of **[A1a]** in the presence of $NaNO_3$ (from 54 to 44%).

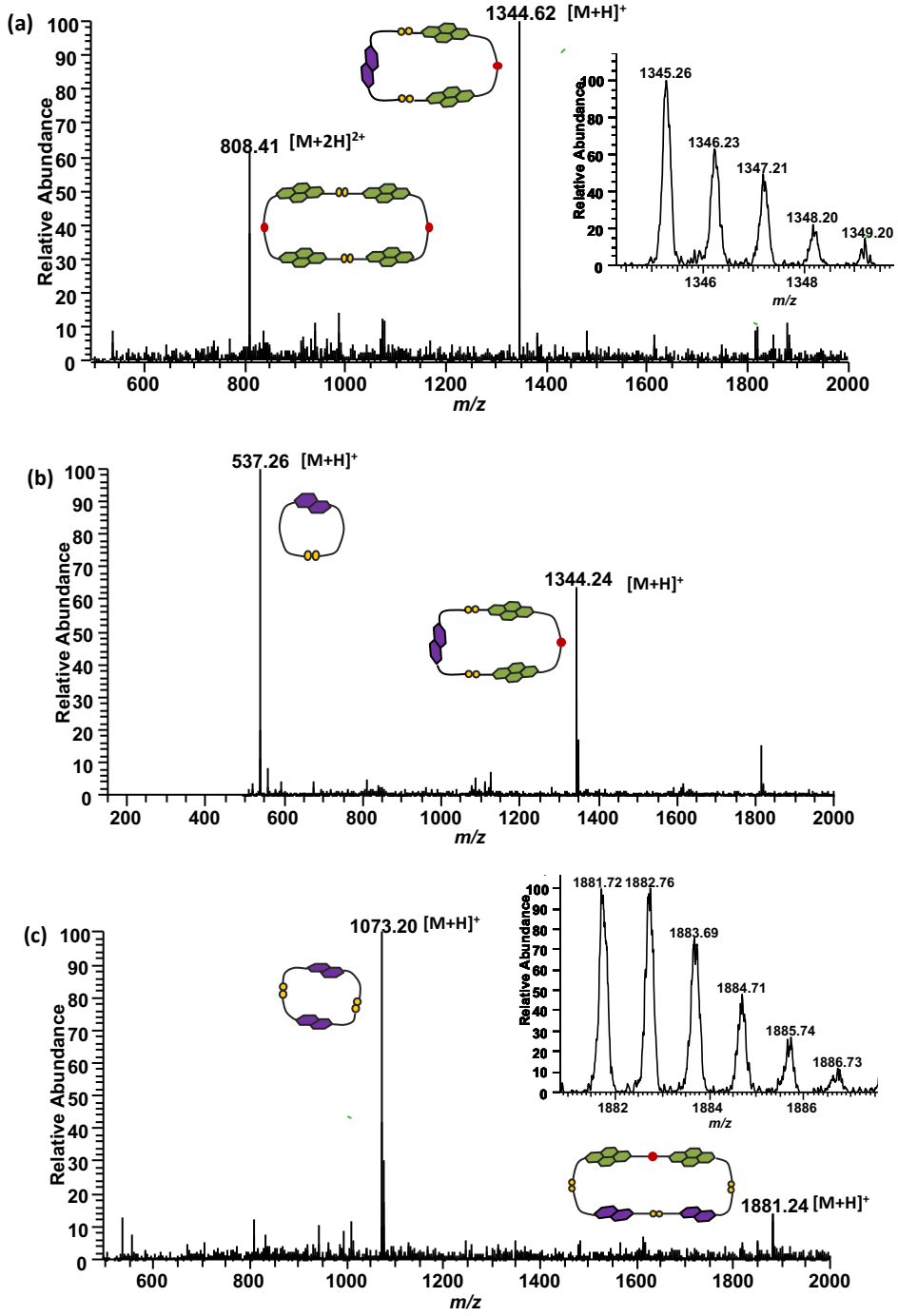

Figure 2-20. ESI-MS (+*ve*) spectra of (a) **[A1a]$_2$** (doubly charged cation) and heterodimer **[A1a-D2L]** (as singly charged cation) (b) **[D2L]** (as singly charged cation) and heterodimer **[A1a-D2L]** (as singly charged cation), (c) **[D2L]$_2$** (as singly charged cation) and the heterotrimer **[A1a-D2L$_2$]** (as singly charged cation). The expansion of parent molecular ions is shown as inserts.

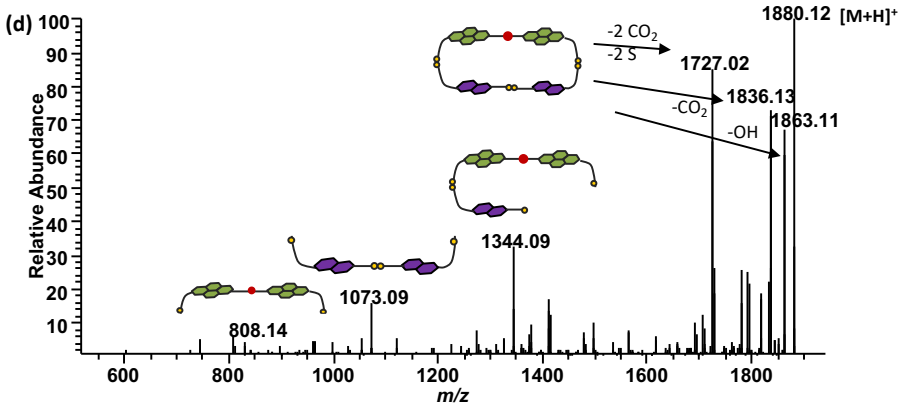

Figure 2-21. MS/MS fragmentation spectra of D-A trimer **[A1a-D2L$_2$]**.

Comparing the DCLs behaviour of the four donor building blocks (**D1S**, **D2S**, **D1L** and **D2L**) with the acceptor (**A1a)**, it was found that changing the length of DN side chain or the connectivity (1,5- / 2,6-) did not lead to formation of any interlocked molecules and we observe a range of macrocycles being formed.

To summarise the results in this section, a series of macrocycles of which D-A heterodimers and heterotrimers were obtained. None of the DCLs made with the **A1a** acceptor showed the formation of catenane or any other complex molecules. The formation of DN dimers over monomers within DCLs with short side chain DNs is more efficient, and vice versa for DNs with long side chain. It has been concluded that the diethylenetriamine in **A1a** acceptor is too short and makes a very tight cyclic monomer; consequently, the cavity between the two NDIs is not large enough to fit a DN molecule. Also, the presence of nitrogen atom in the linker makes the **A1a** dimer too flexible and the aromatic surfaces can form close contacts, preventing another aromatic moiety to enter inside the cavity. This section provides valuable information about the importance of the length and flexibility of the polyamine although these sets of species have not led to interlocked molecules.

2.8 DCL of A1b Dithiol Acceptor

The second building block synthesised, **A1b**, has consisted of six atoms in the linker (five -CH_2 and one -NH), which is one carbon more than **A1a**. Using a polyamine which is only one carbon longer than the previous building block, could change the libraries' distribution and lead to molecules other than macrocycles.

The DCL of **A1b** was generated by dissolution of the building block in water (5 mM concentration) and the pH was adjusted to 8 using an aqueous solution of 100 mM NaOH. Two libraries were set up, one with $NaNO_3$ and one without, and stirred for one day under air in capped vials to allow full oxidation of the thiols. The libraries were analysed using HPLC and LC-MS instruments.

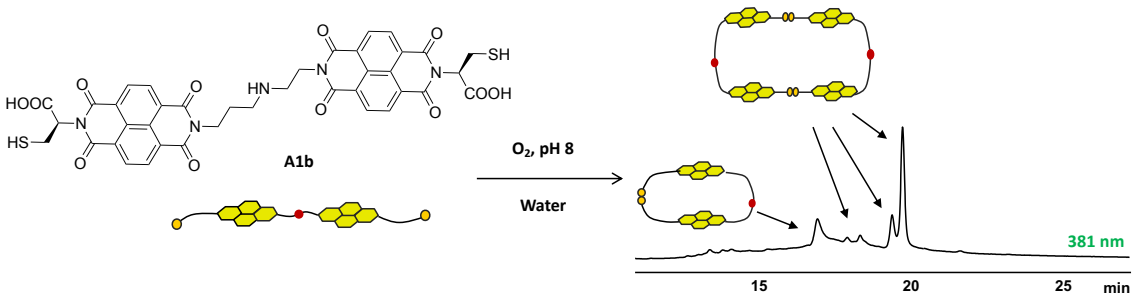

Figure 2-22. The HPLC analysis of **A1b** library in water. Absorbance was recorded at 381nm.

In Figure 2-23, two major components were at equilibrium in this library: cyclic monomer **[A1b]** and cyclic dimer **[A1b]$_2$**.

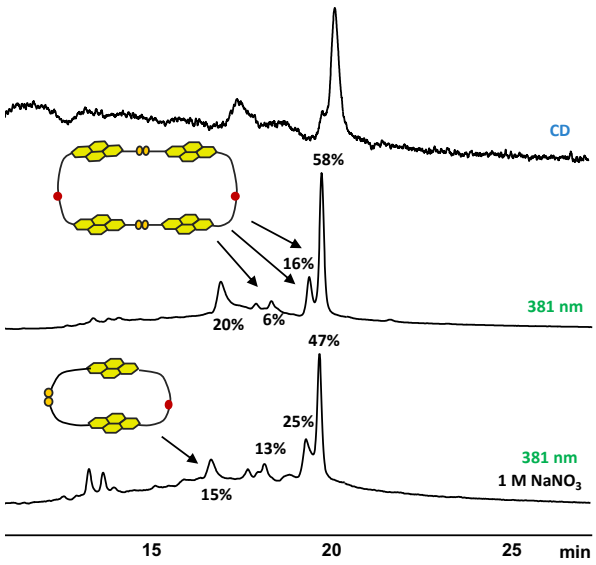

Figure 2-23. The HPLC analysis of **A1b** library in water with and without 1 M $NaNO_3$. Absorbance was recorded at 381 nm.

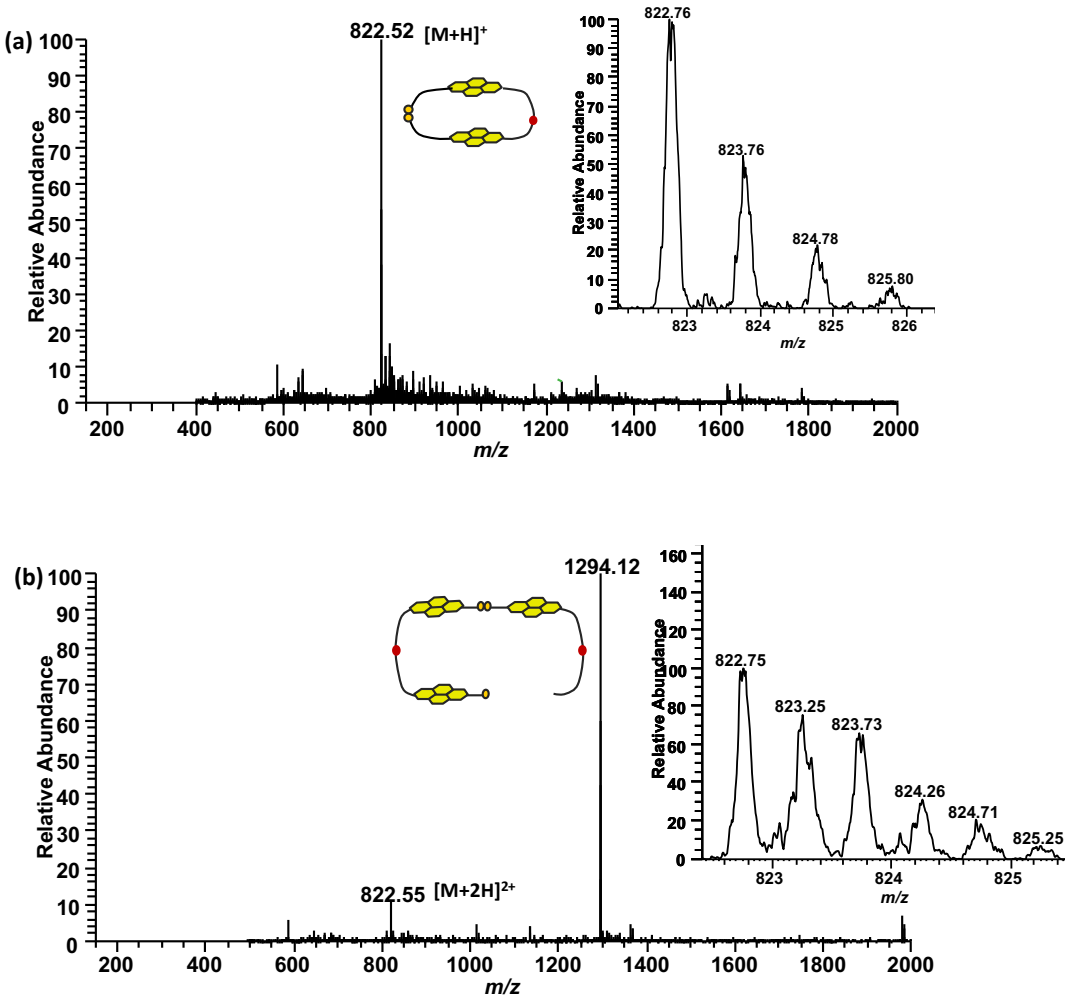

Figure 2-24. ESI-MS (+*ve*) spectra of (a) cyclic monomer **[A1b]** (as singly charged cation) and (b) a fragment of **A1b** cyclic dimer (as singly charged cation). Expansions of molecular ions are shown as inserts.

The library of **A1b** by itself has led to formation of two major molecules: cyclic monomer **[A1b]** and cyclic dimer **[A1b]$_2$**. This library shows three peaks at 18.3, 19.4 and 19.7 min representing the **A1b** dimers. This could also mean that the **A1b** dimer has more than one stable conformation, which are slowly interconverting and separated under HPLC conditions.

2.9 D-A DCL of A1b with D1S

The first D-A DCL of **A1b** with **D1S** that has the least flexibility in terms of length of the side chain and connectivity (1,5-isomer). The **A1b** and **D1S** form a series of macrocycles, and no catenane or other complex molecules were observed. In this library, the formation of heterodimer **[A1b-D1S]** was significantly decreased in the library with 1 M $NaNO_3$, and the concentration of heterotrimer **[A1b-D1S$_2$]** was increased 26% (Figure 2-25). This set of DCL makes progress towards our goals when using **D2S** donor, which allows the formation of the first [2]catenane. This provides the understanding that more flexible DN and longer NDI are potential candidates for the formation of interlocked molecules.

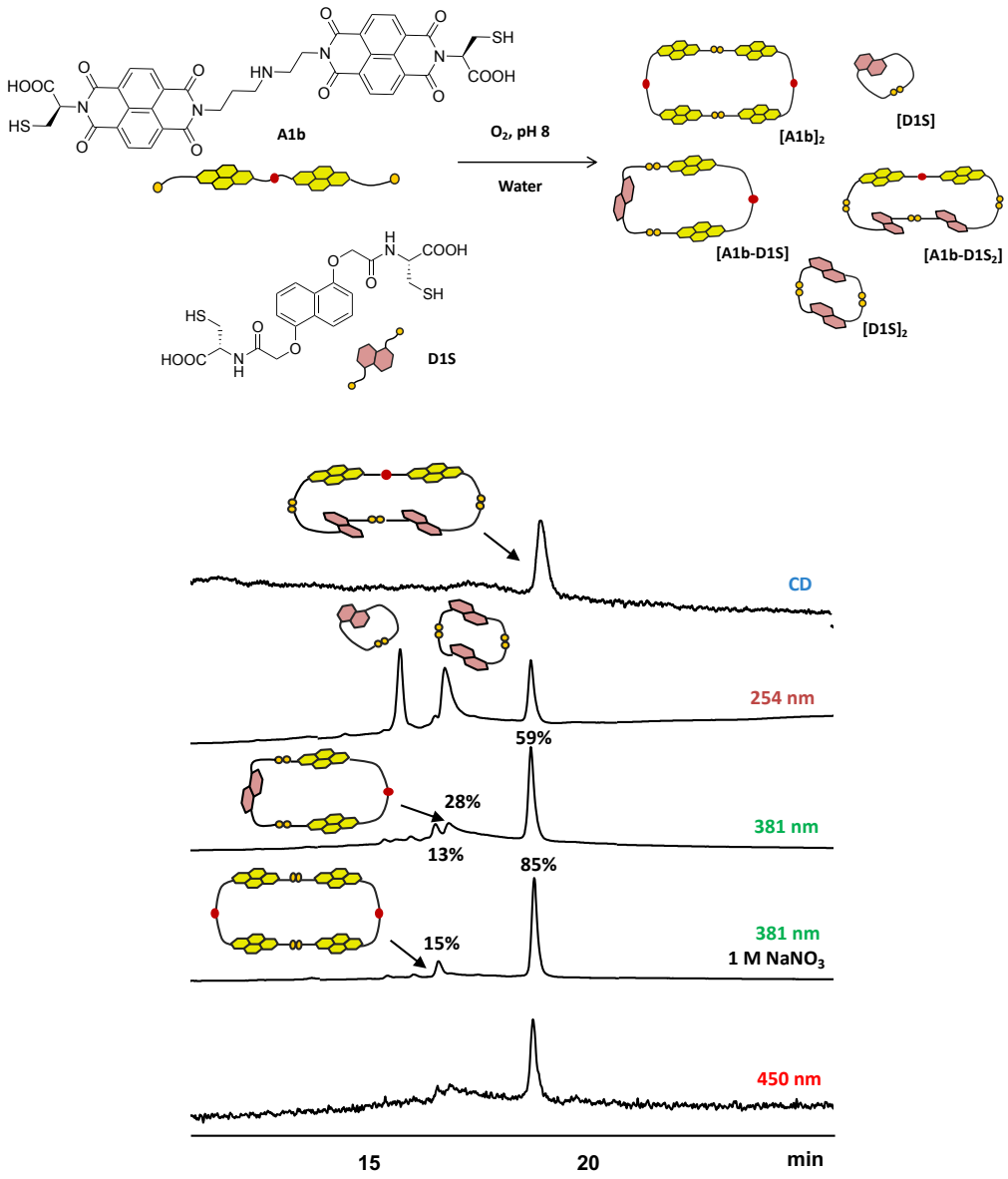

Figure 2-25. The HPLC analysis of **A1b** and **D1S** DCL (1:2 molar ratio, 5 mM total concentration). Estimated yield is indicated above the corresponding peaks.

The rigidity in **D1S** dimer prevents the threading of NDI through its cavity even though **A1b** has a slightly larger cavity than **A1a**.

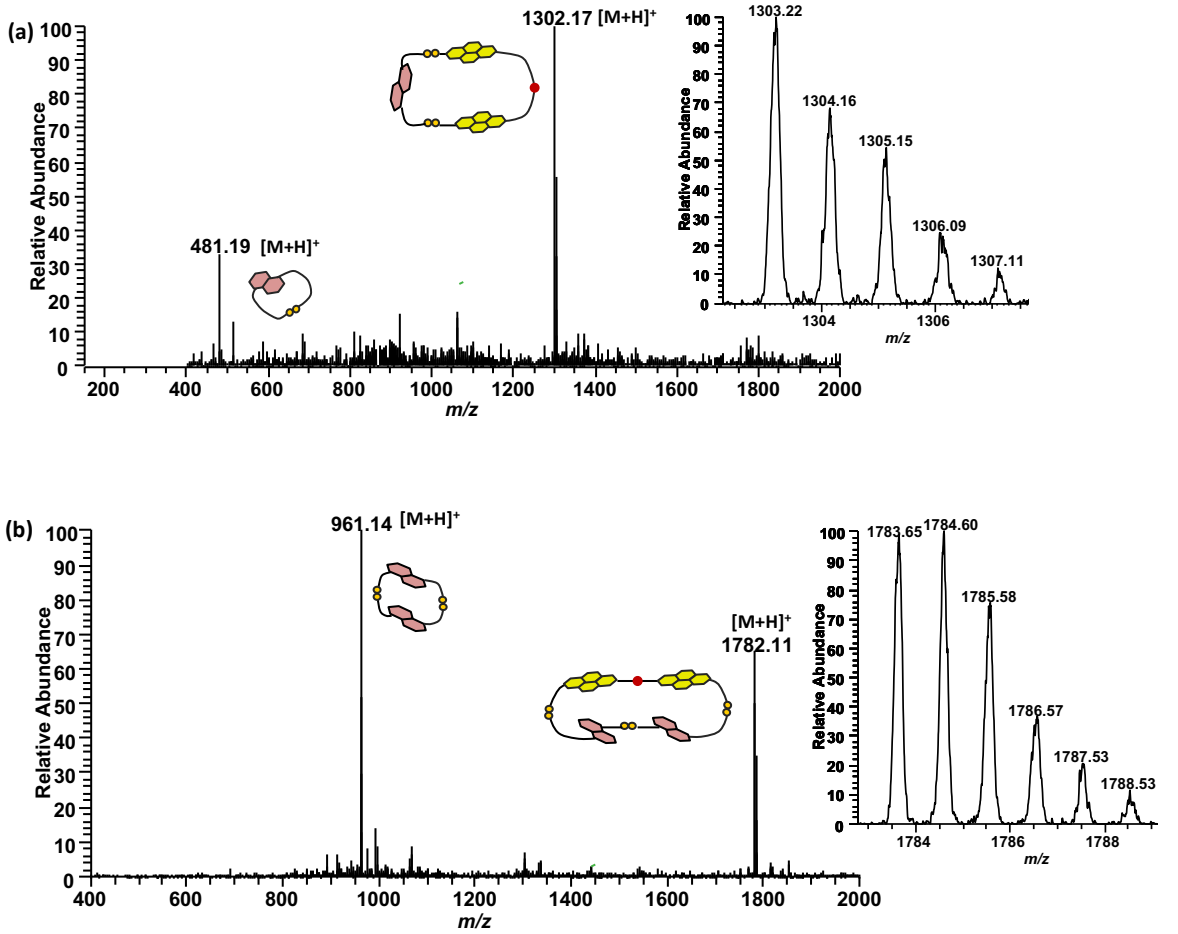

Figure 2-26. ESI-MS (+*ve*) spectra of (a) heterodimer **[A1b-D1S]** (as singly charged cation) and the cyclic monomer **[D1S]**, (b) heterotrimer **[A1b-D1S$_2$]** (as singly charged cation) and the cyclic dimer **[D1S]$_2$**. The expansion of parent molecular ions are shown as insert.

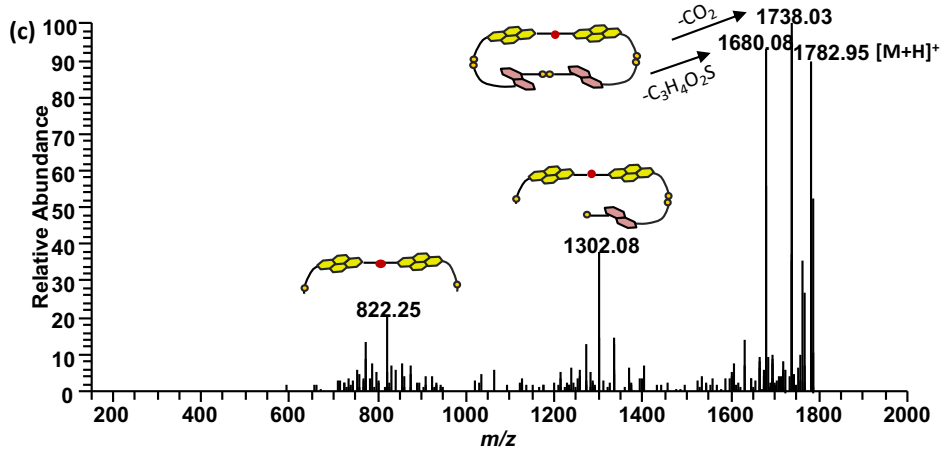

Figure 2-27. MS/MS fragmentation spectra of **[A1b-D1S$_2$]**.

2.10 D-A DCL of A1b with D2S: Identification of the first DADA [2]catenane: Cat1

The LC-MS analysis of D-A DCL of **A1b** with **D2S** reveals that the fully oxidised library contains a [2]catenane along with a series of macrocycles. The formation of heterodimer **[A1b-D2S]** has significantly increased in the presence of 1 M $NaNO_3$, and the concentration of heterotrimer **[A1b-D2S$_2$]** has decreased by 31% (Figure 2-28).

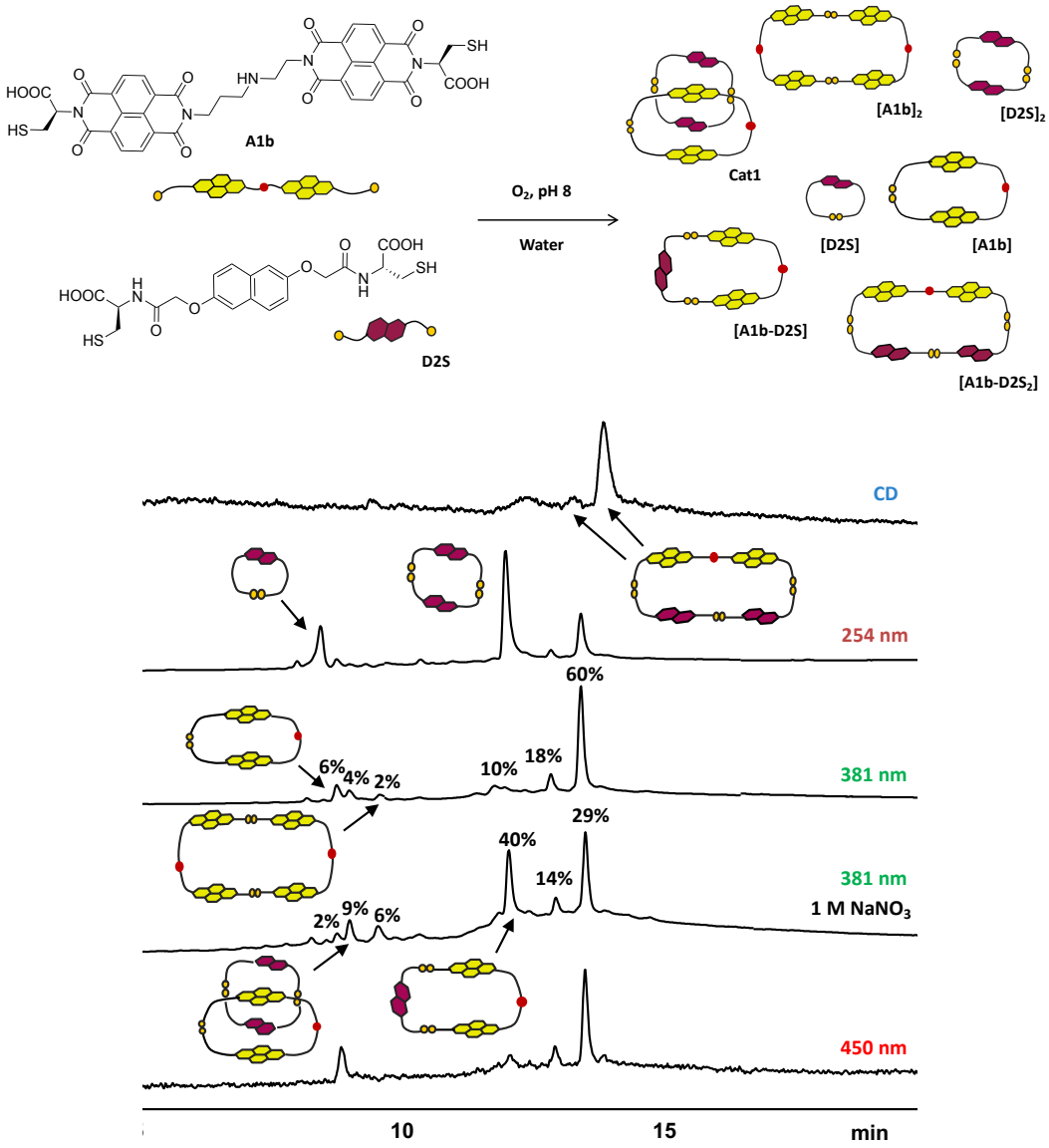

Figure 2-28. The HPLC analysis of **A1b** and **D2S** DCL (1:2 molar ratio, 5 mM total concentration). Estimated yield is indicated above the corresponding peaks.

The MS and MS/MS data confirmed that a small amount of a new species (9% in presence of $NaNO_3$), at a surprisingly low retention time, 8.9 min is a [2]catenane. However, its isomeric form is still obtained – the macrocycle – in much higher yield (up to 60%).

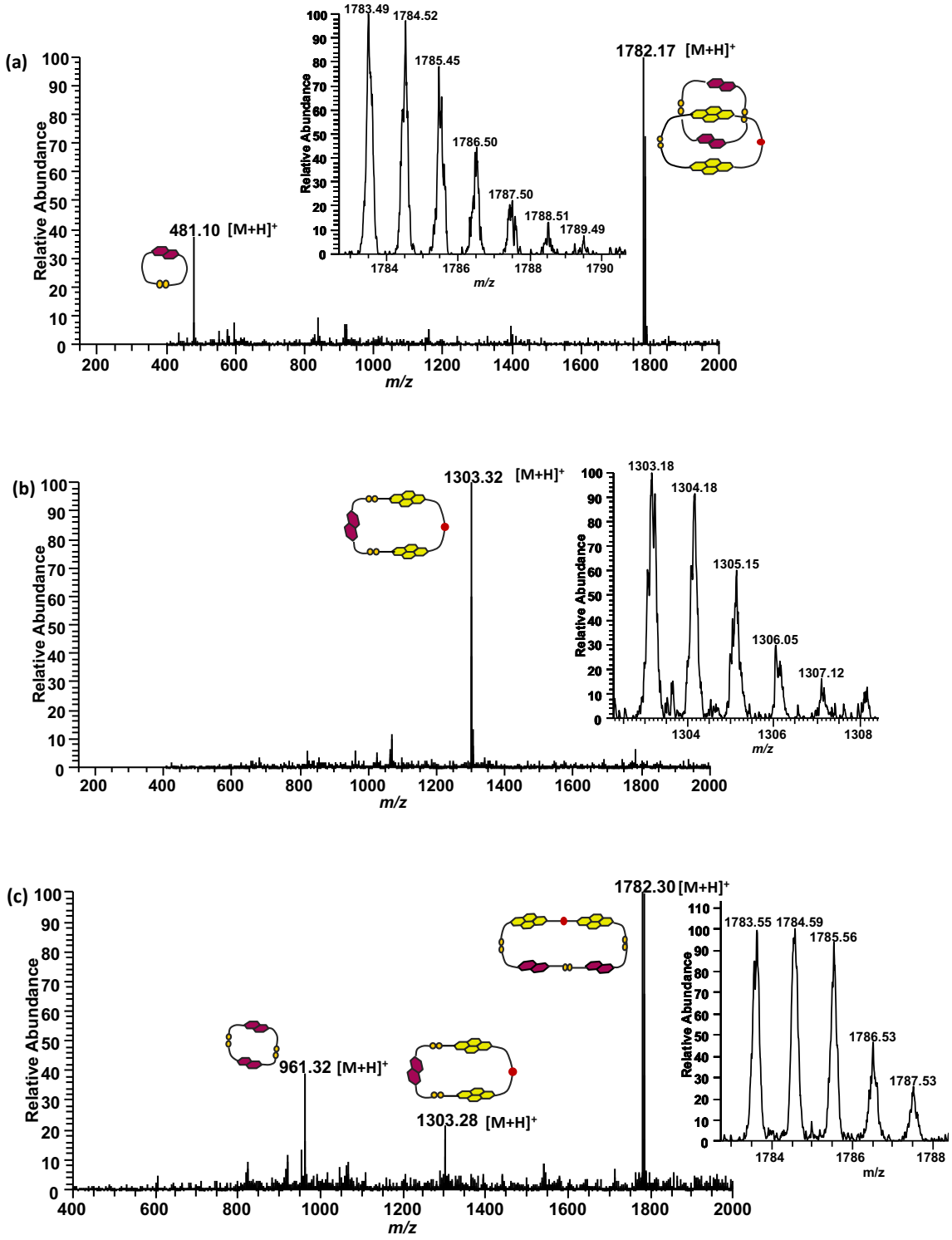

Figure 2-29. ESI-MS (+*ve*) spectra of (a) **Cat1** and **[D2S]** (as singly charged cation), (b) heterodimer **[A1b-D2S]** (as singly charged cation), (c) heterotrimer **[A1b-D2S$_2$]** (as singly charged cation) and **[D2S]$_2$** (as singly charged cation). The expansions of parent molecular ions are shown as inserts.

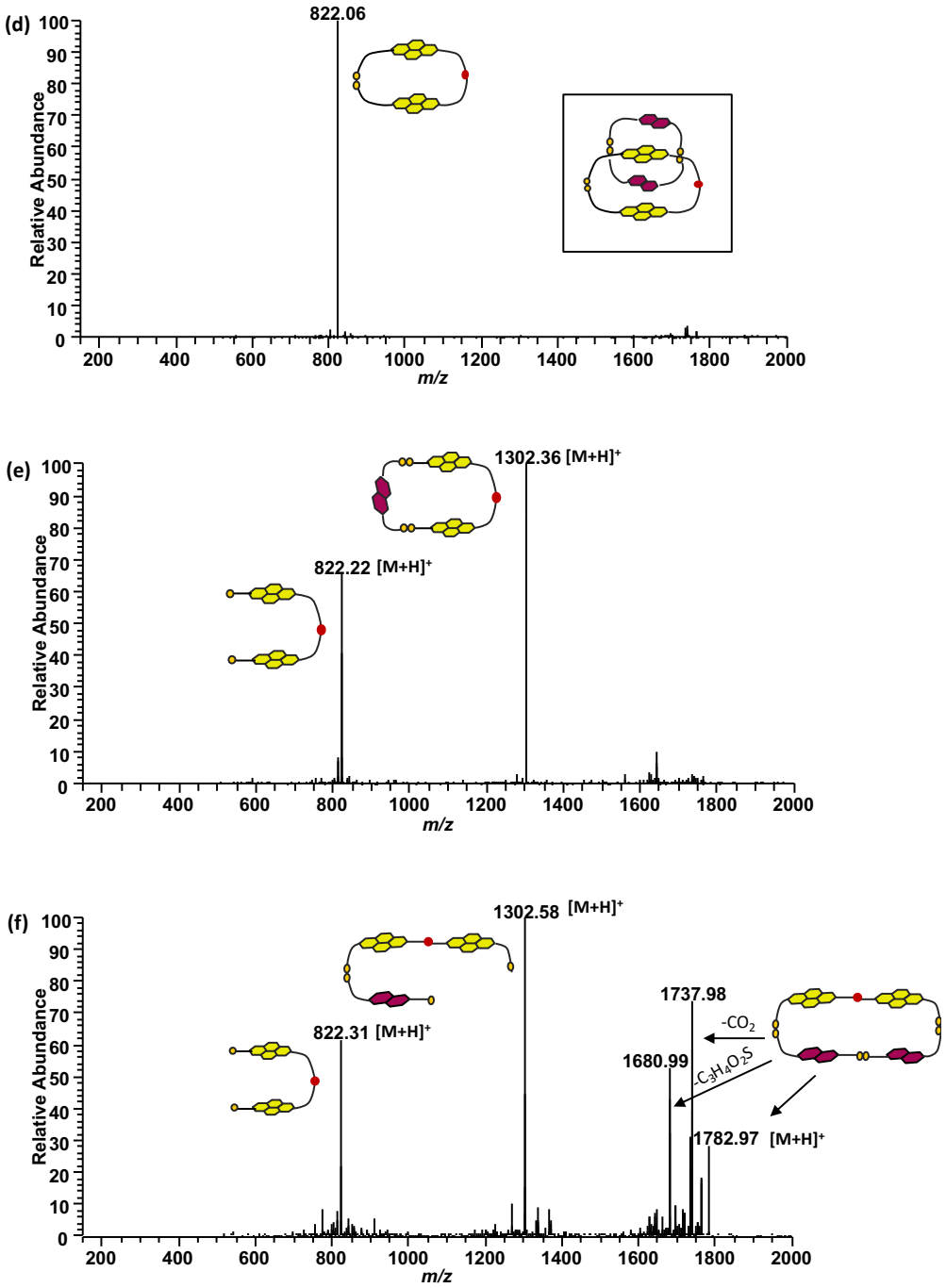

Figure 2-30. MS/MS fragmentation spectra of (d) **Cat1,** (e) **[A1b-D2S]**, and (f) **[A1b-D2S$_2$]**.

The fragmentation pattern for the [2]catenane, **Cat1,** is characteristic for a [2]catenane, with the loss of **D2S** dimer producing the intermediate of **A1b** monomer. Due to its low yield, the further characterisation of **Cat1** was not possible. The DCL in presence of 1 M $NaNO_3$ improved the yield of **Cat1** only by 5%.

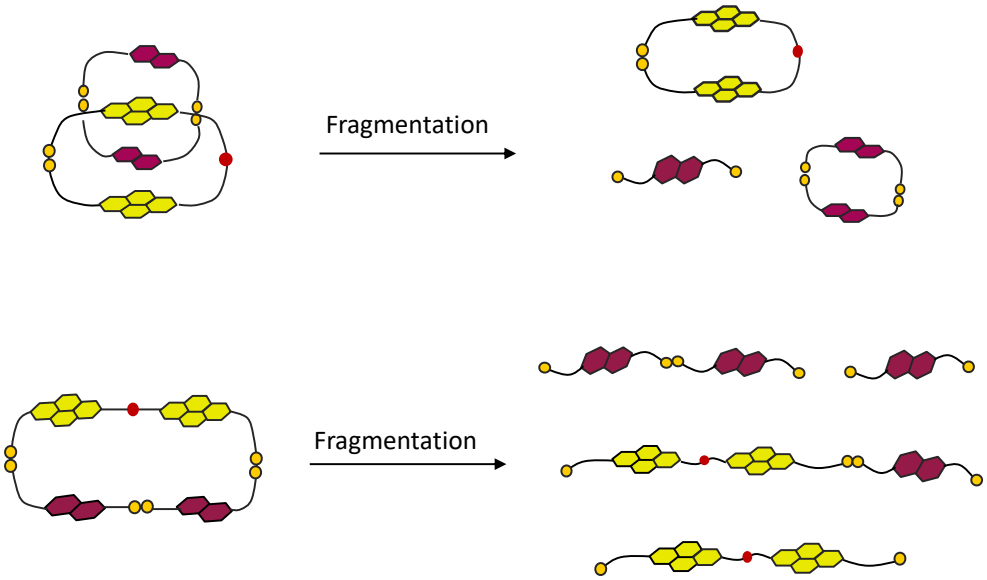

Figure 2-31. The theoretical MS/MS fragmentation of **Cat1** and **[A1b-D2S$_2$]** heterotrimer.

In Figure 2-31, the fragmentation pattern for a macrocycle is compared to a [2]catenane. A macrocycle fragments into more species than an isomeric [2]catenane due to its structure, i.e. fragments containing both donor and acceptor building blocks can be observed. This is not the case for the MS/MS fragmentation of **Cat1** where only separate donor or acceptor fragments can be observed. The experimental data matches the theoretical fragmentation of a [2]catenane which provides evidence for its formation.

2.11 D-A DCL of A1b Acceptor and D1L Donor: Cat2

A new D-A DCL consisting of **A1b** and **D1L** was set up. The analysis has revealed that library consists of a series of macrocycles and a new [2]catenane (**Cat2**). The formation of **[A1b-D1L]** dimer has decreased 9% in the presence of 1 M $NaNO_3$, and the concentration of **[A1b-D1L$_2$]** has increased 19% (Figure 2-32). The formation of **Cat2** does not improve in the presence of $NaNO_3$ salt, and therefore, cannot be isolated and further analysed.

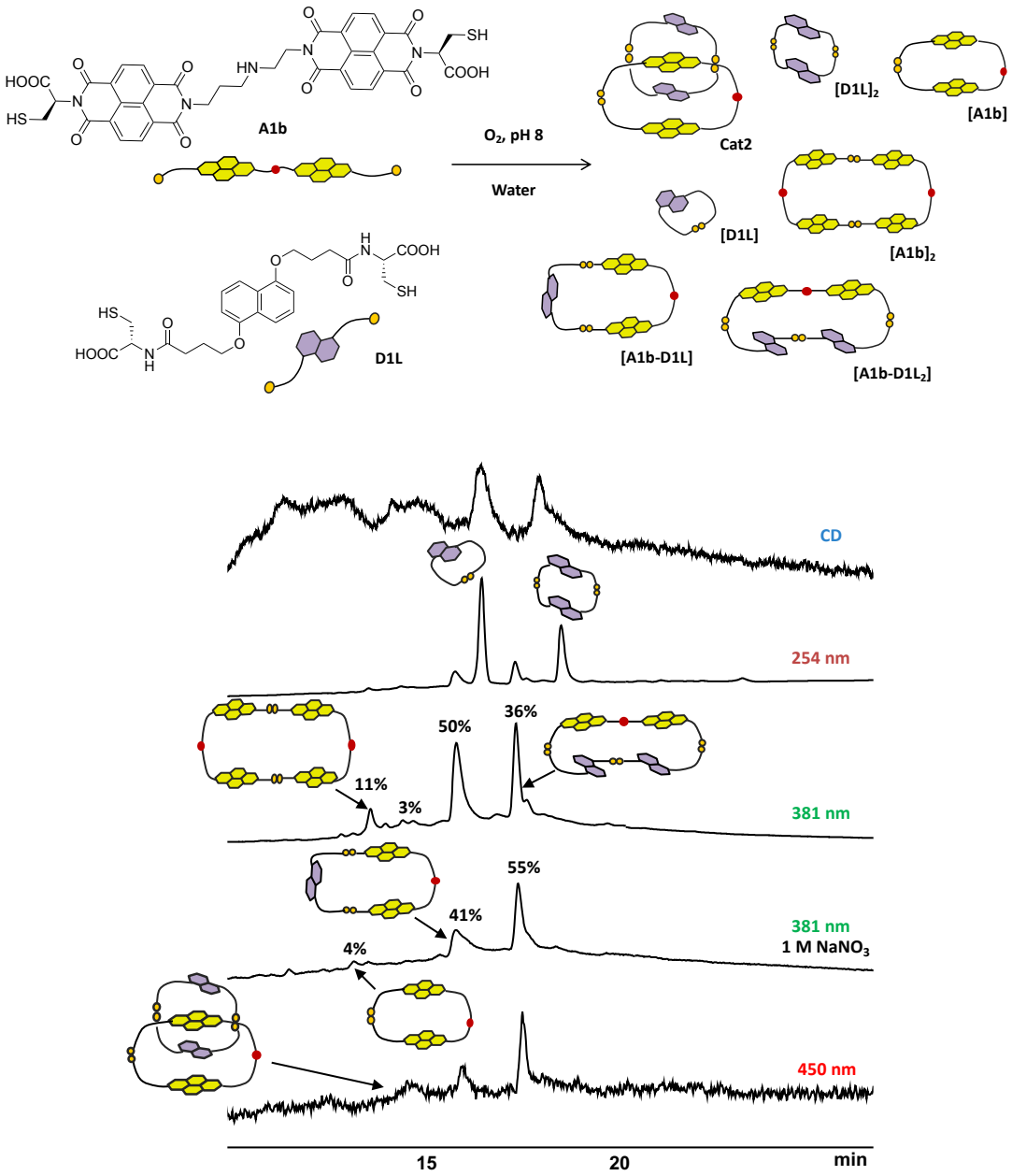

Figure 2-32. The HPLC analysis of **A1b** and **D1L** DCL (1:2 molar ratio, 5 mM total concentration). Estimated yield is indicated above the corresponding peaks.

The MS and MS/MS data confirmed that a trace amount of a [2]catenane at 14.5 min has formed. However, its concentration is very small (3%) and the catenane's isomeric form is still obtained in much higher yield (up to 55% in the presence of 1 M $NaNO_3$).

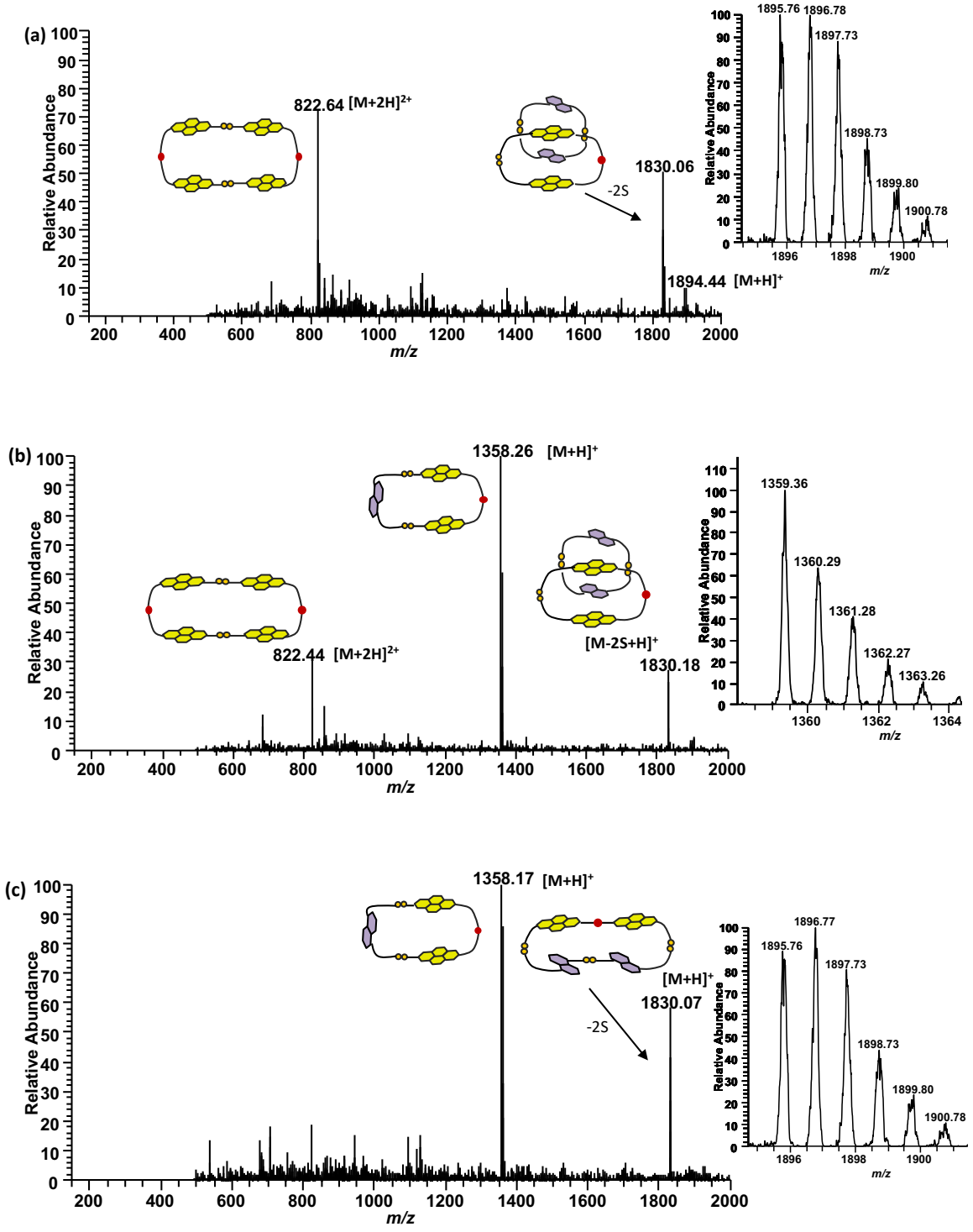

Figure 2-33. ESI-MS (+*ve*) spectra of (a) **Cat2** (as singly charged cation) and **[A1b]** (as doubly charged cation), (b) heterodimer **[A1b-D1L]** (as singly charged cation), (c) heterotrimer **[A1b-D1L$_2$]** (as singly charged cation). The expansions of parent molecular ions are shown as inserts.

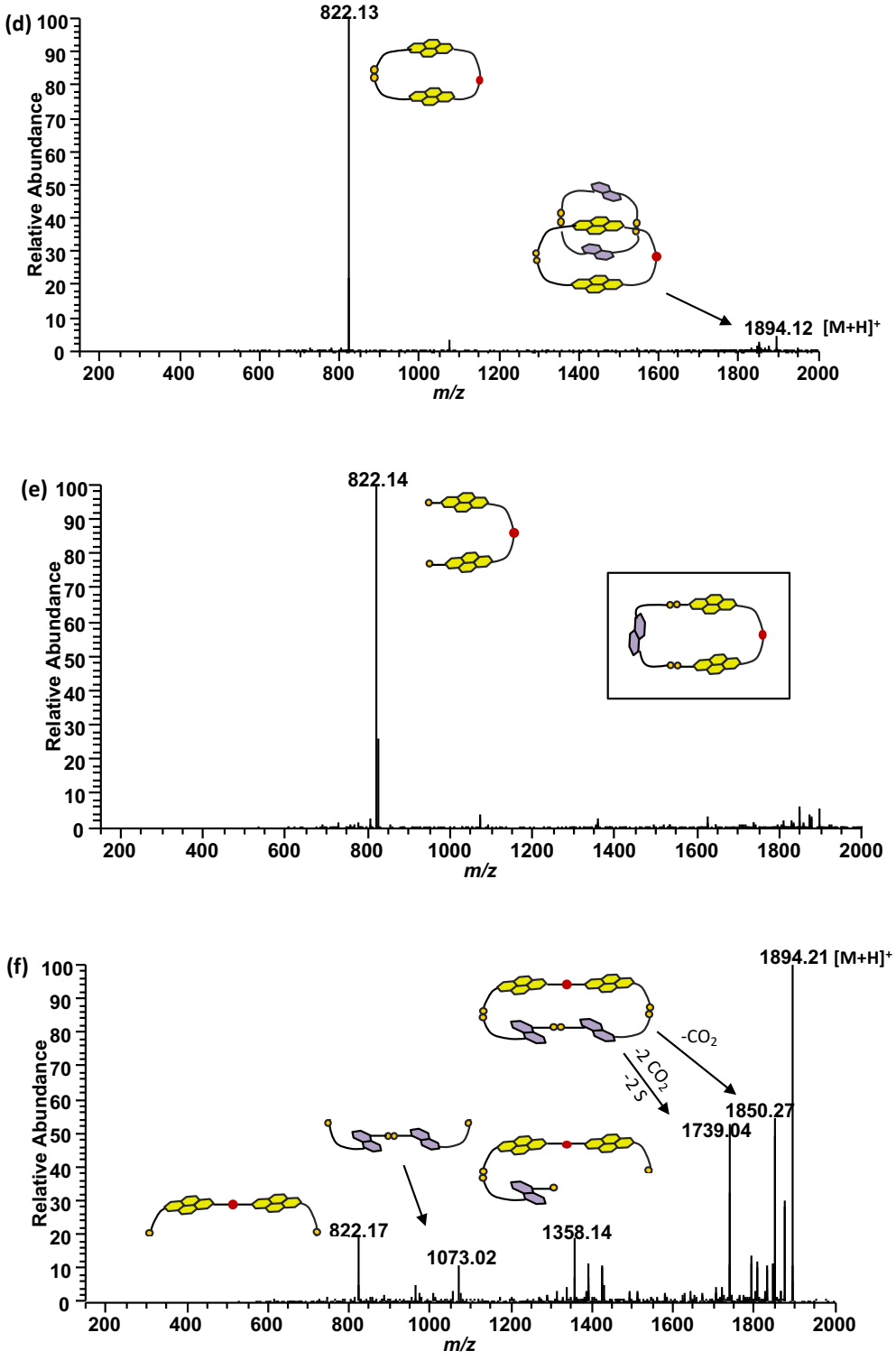

Figure 2-34. MS/MS fragmentation spectra of (d) **Cat2,** (e) **[A1b-D1L]**, and (f) **[A1b-D1L$_2$]**.

2.12 D-A DCL of A1b Acceptor and D2L Donor: Cat3

The last library of **A1b** acceptor employed the **D2L** donor building block. In this library, the [2]catenane forms in the presence of 1 M $NaNO_3$ and its concentration is still too small (6%) to be further characterised.

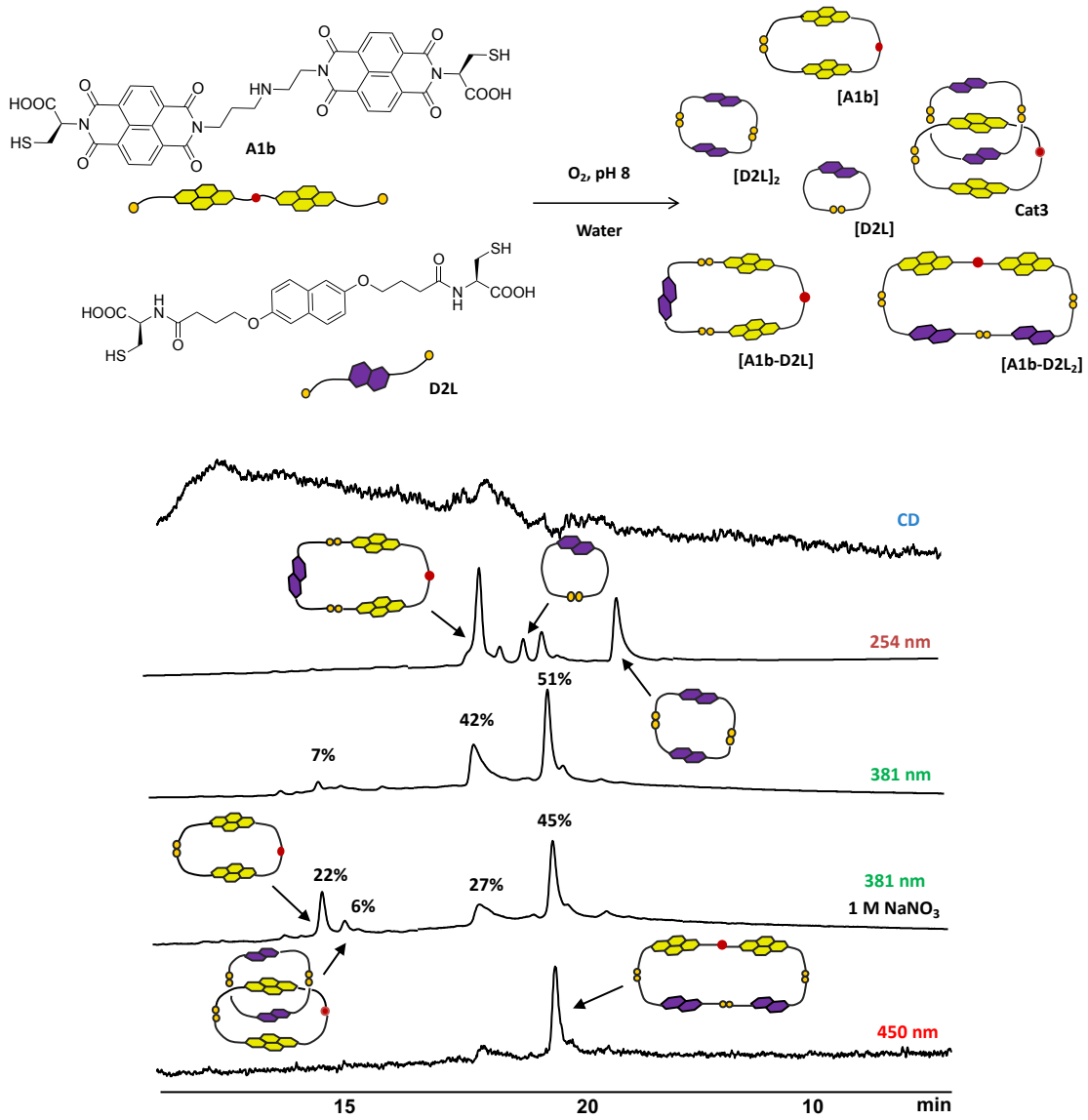

Figure 2-35. The HPLC analysis of **A1b** and **D2L** DCL (1:2 molar ratio, 5 mM total concentration). Estimated yield is indicated above the corresponding peaks.

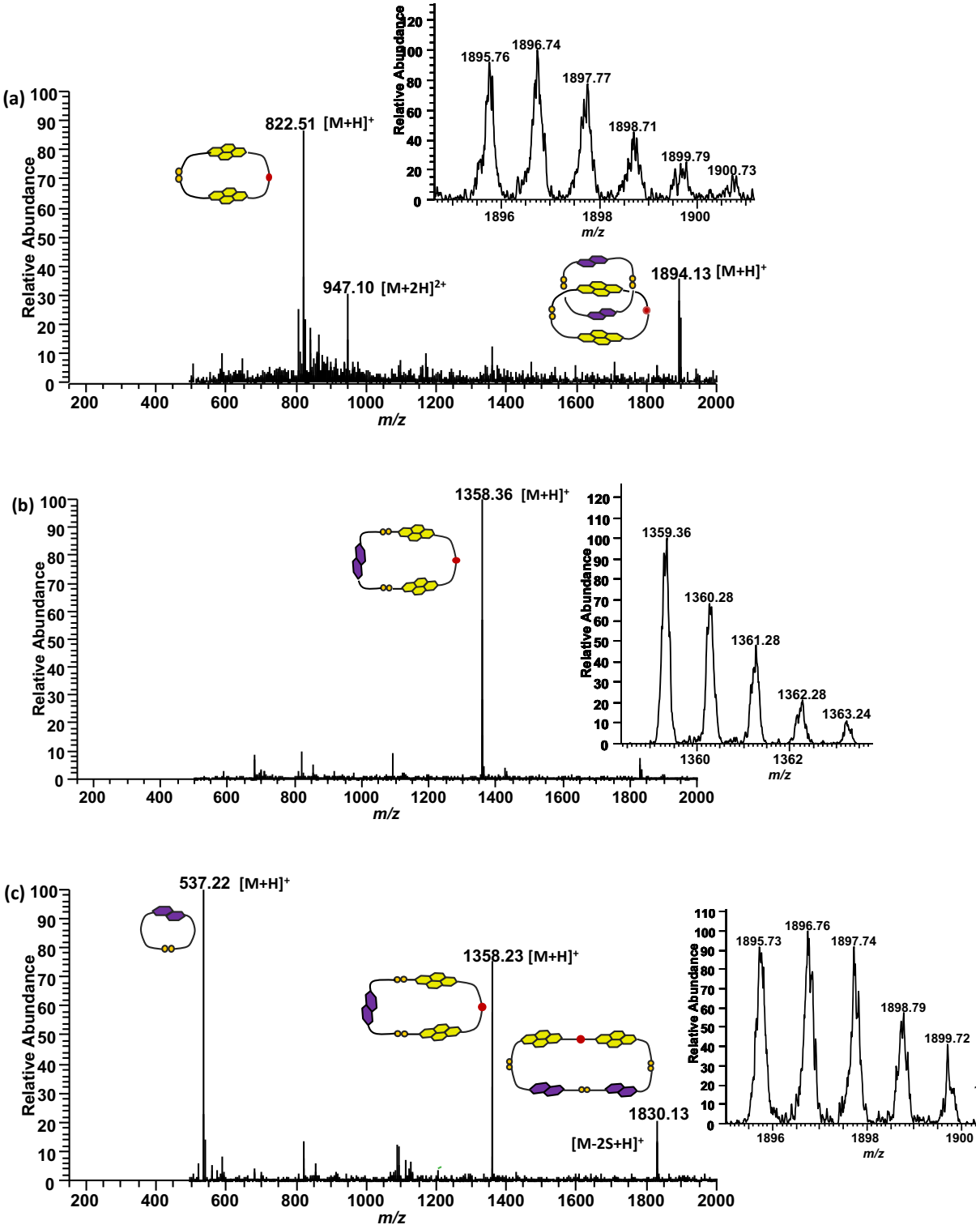

Figure 2-36. ESI-MS (+*ve*) spectra of (a) **Cat3** (as singly charged cation) and **[A1b]** (as singly charged cation), (b) heterodimer **[A1b-D2L]** (as singly charged cation), (c) heterotrimer **[A1b-D2L$_2$]** (as singly charged cation). The expansion of parent molecular ions is shown as inserts.

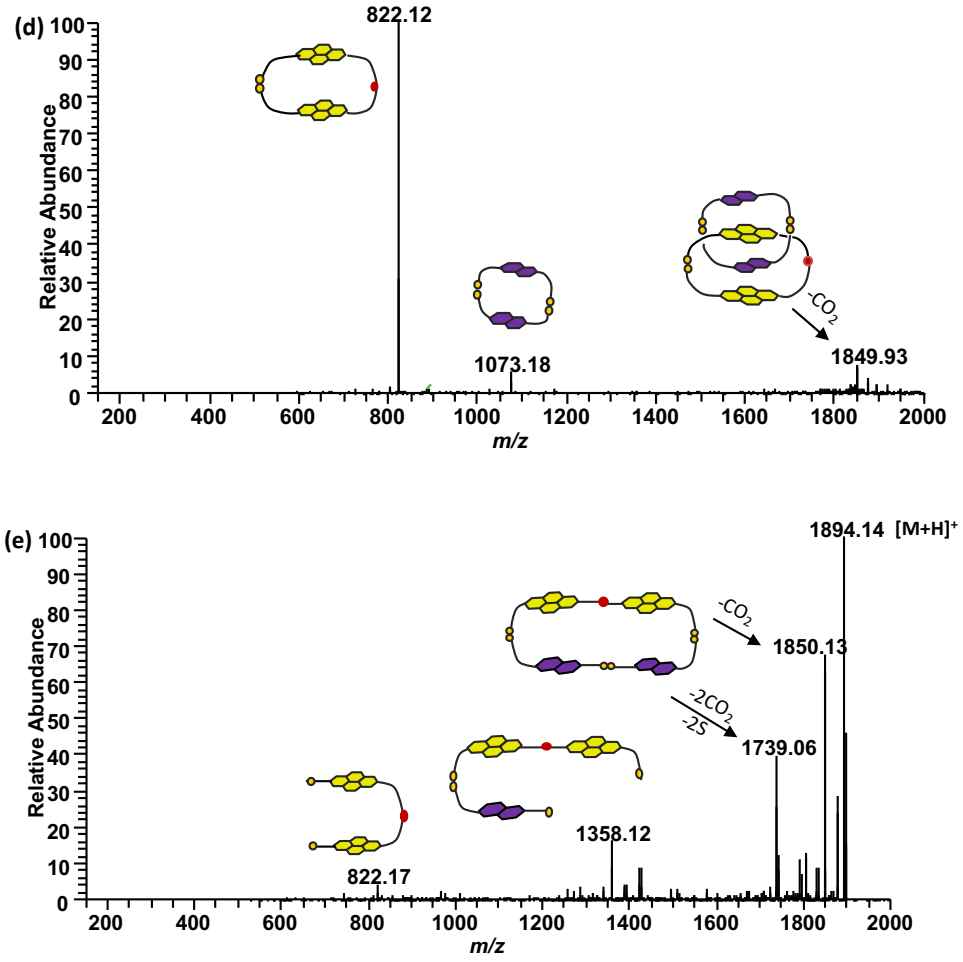

Figure 2-37. MS/MS fragmentation spectra of (d) **Cat3,** and (e) **[A1b-D2L$_2$]**.

The fragmentation pattern for the [2]catenane, **Cat3,** is characteristic for the one expected, with the loss of **D2L** dimer producing the intermediate of **A1b** monomer. The mass and isotopic pattern of **Cat3** is identical to the one obtained for **Cat2**, implying that the two structures are isomeric. This is to be expected as the only difference between the two is the connectivity on the DN dimer.

2.13 DCL of A1c Building Block

A new set of libraries were set up using **A1c** building block. **A1c** incorporates spermidine, a triamine with eight atoms in the linker, thus being longer than the two previous building blocks. The longer polyamine provides increased flexibility to the building block which can lead to the formation of cyclic monomers with larger cavity for fitting another aromatic moiety through. This would favour the π-π stacking and, consequently, the formation of donor-acceptor catenanes.

A disulfide-based DCL was obtained by dissolving the building block **A1c** in water at pH 8.5 (5 mM concentration). The pH was increased by 0.5 units when compared to the previous DCLs due to the low solubility of **A1c** molecule. The library was stirred in capped vial under air for one day before HPLC and LC-MS analyses.

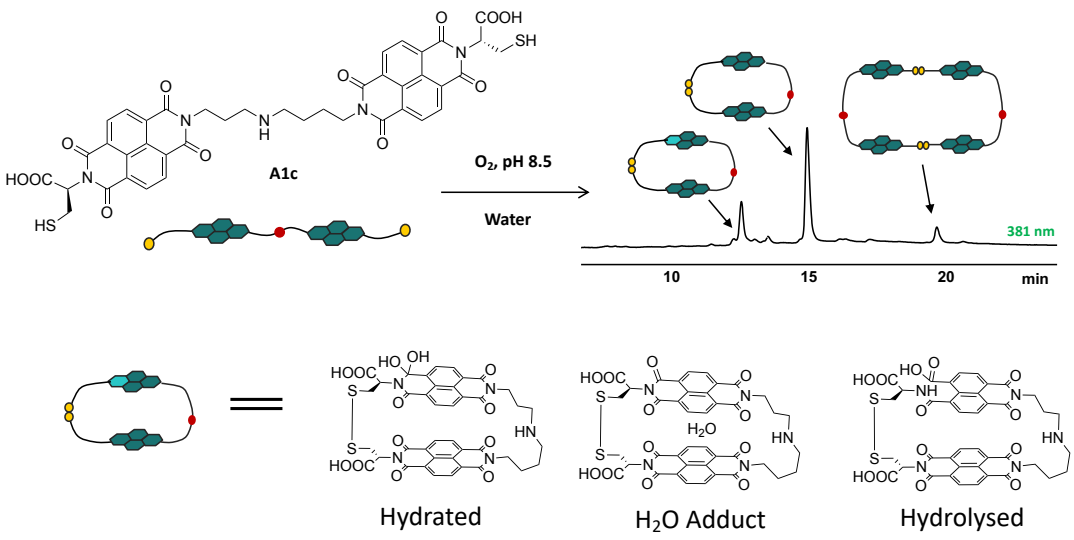

Figure 2-38. The HPLC analysis of **A1c** library in water. Absorbance was recorded at 381nm.

This DCL shows three major components at equilibrium (Figure 2-38). The first peak at 12.7 min corresponds to the hydrated cyclic monomer up to 26% (represented by light green colour on the cartoon representation of the molecule). There are two other possible species (H_2O adduct and hydrolysed specie) with the same molecular weight, however the hydrated and H_2O adduct species are more realistic than the hydrolysed specie due to the reversibility observed in the formation of this molecule.

The peak at 15.1 min is the cyclic monomer of **A1c**, which forms up to 62%. The building blocks with the shorter polyamine (n < 7) form more of the cyclic dimer, while the building blocks with the longer polyamine generate more of the cyclic monomer. In this library, the **A1c** dimer forms only up to 12%.

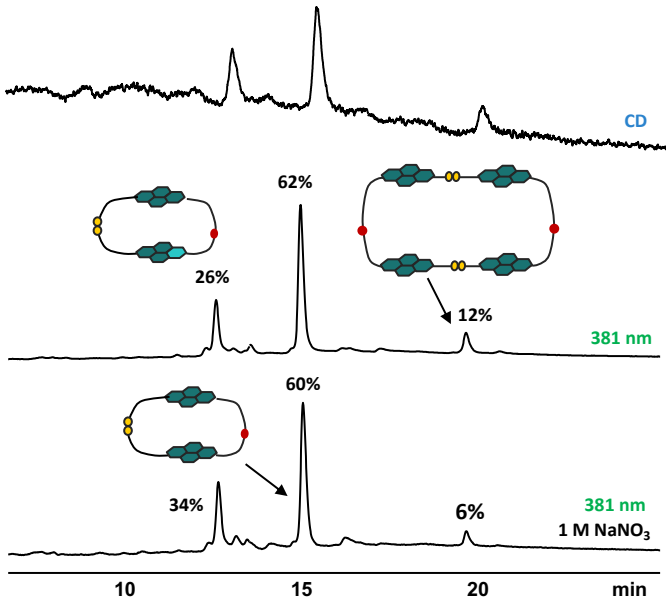

Figure 2-39. The HPLC analysis of **A1c** library in water with and without $NaNO_3$. Absorbance was recorded at 381 nm and CD was also recorded at 381 nm. Estimated yields are indicated above the corresponding peaks.

The concentration of **A1c** cyclic dimer decreased from 12% to 6% upon addition of 1 M $NaNO_3$.

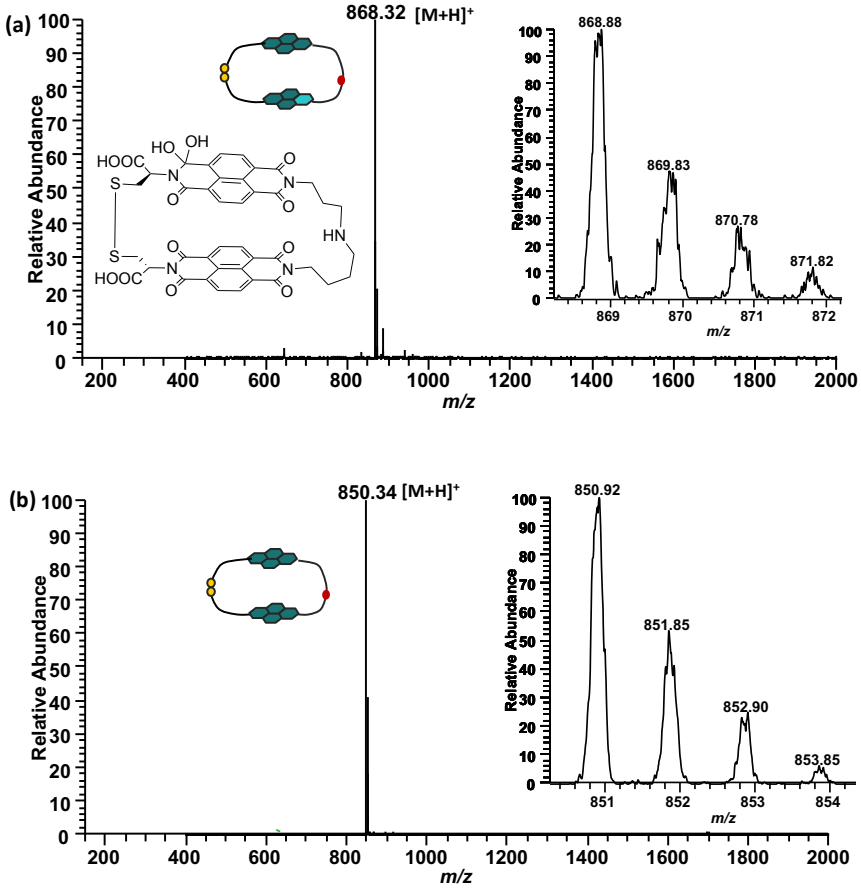

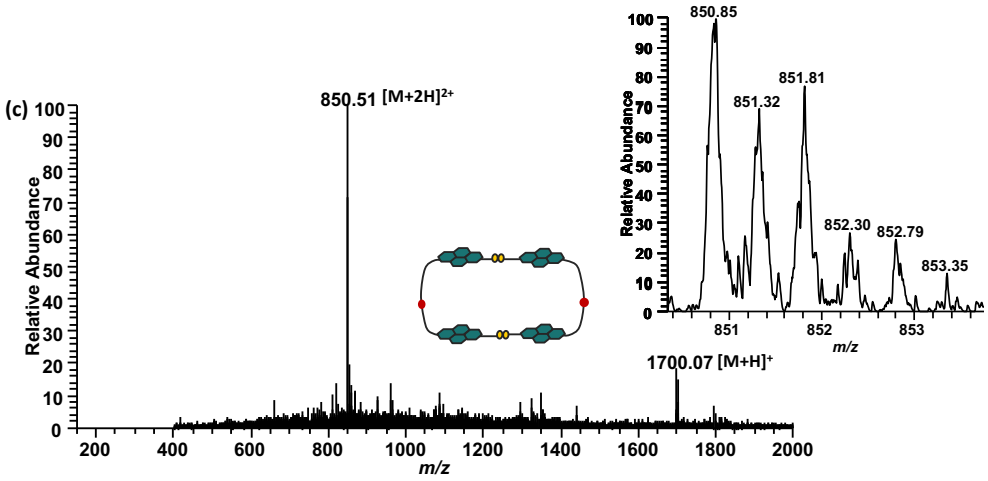

Figure 2-40. ESI-MS (+*ve*) spectra of (a) **A1c** cyclic monomer hydrated on one of the carbonyl groups (as singly charged cation), (b) the cyclic monomer **[A1c]** (as singly charged cation), (c) the cyclic dimer **[A1c]$_2$** (as doubly charged cation). Expansions of molecular ions are shown as inserts.

Previous studies have shown that using a linker where n = 8 has led to the formation of an all-acceptor [2]catenane (Figure 2-41). However, it has been proven that this [2]catenane has not been formed through π-π stacking, but instead through π-σ interactions between the aromatic units of NDI and the alkyl chain. This interaction has overcome the π-π stacking of all acceptor moieties, which is less favourable due to its offset arrangement.

This interaction, π-σ, is not favourable in **A1c**, because of the presence of nitrogen atom in the linker, which in its protonated state makes the interaction with aromatic surfaces less favourable than hydration.

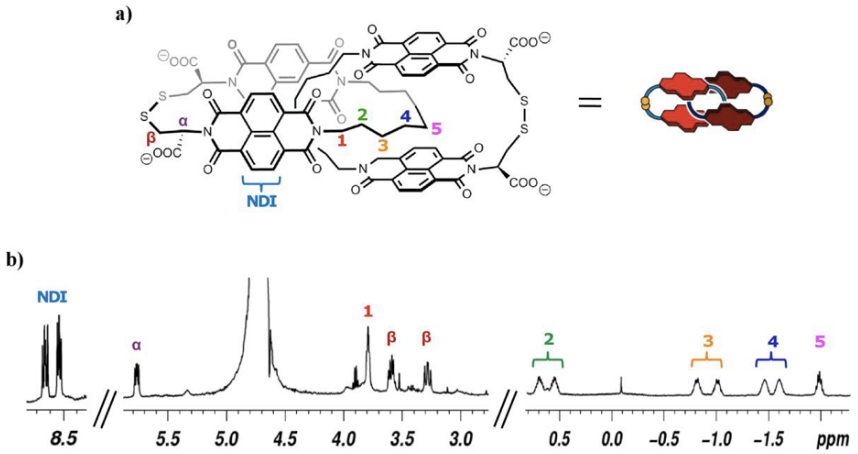

Figure 2-41. (a) Structure of the all-acceptor [2]catenane (b) ^{1}H NMR (500 MHz, 298 K) spectrum of the all-acceptor [2]catenane in D_2O.[126]

2.14 D-A DCL of A1c Acceptor and D1S Donor

The D-A DCL was prepared from the acceptor **A1c** and the rigid donor building block **D1S** in water at pH 8.5. The solution was stirred for one day before it was analysed by HPLC and LC-MS. The HPLC and LC-MS analyses of the libraries have indicated the formation of a [2]catenane, **Cat4**, up to 8% in presence of $NaNO_3$, along with **A1c**, **D1S** dimers, D-A heterotetramer **[A1c-D1S]$_2$**, and heterotrimer **[A1c-D1S$_2$]** (Figure 2-42).

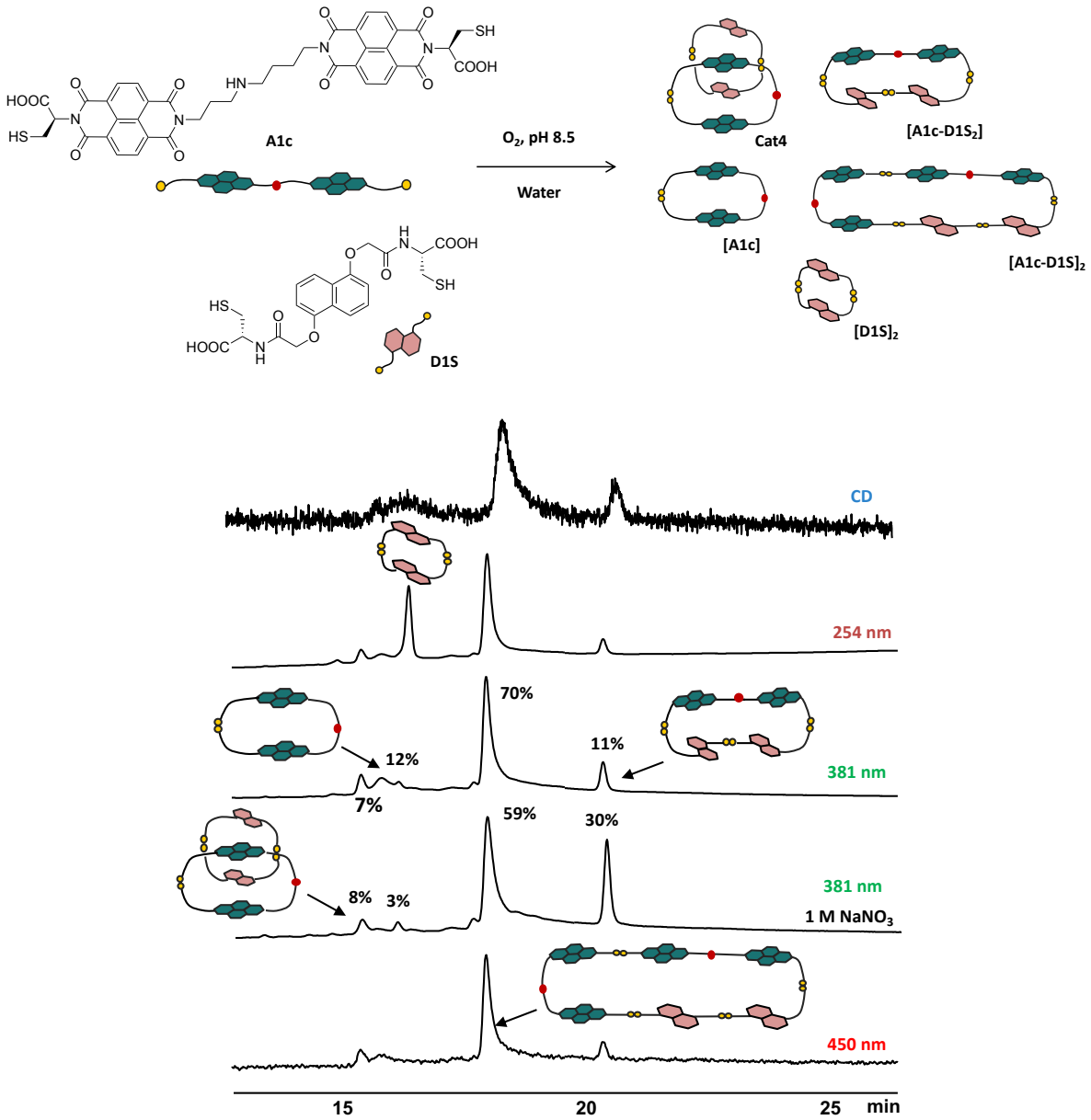

Figure 2-42. The HPLC analysis of **A1c** and **D1S** DCL (1:2 molar ratio, 5 mM total concentration). Estimated yield is indicated above the corresponding peaks.

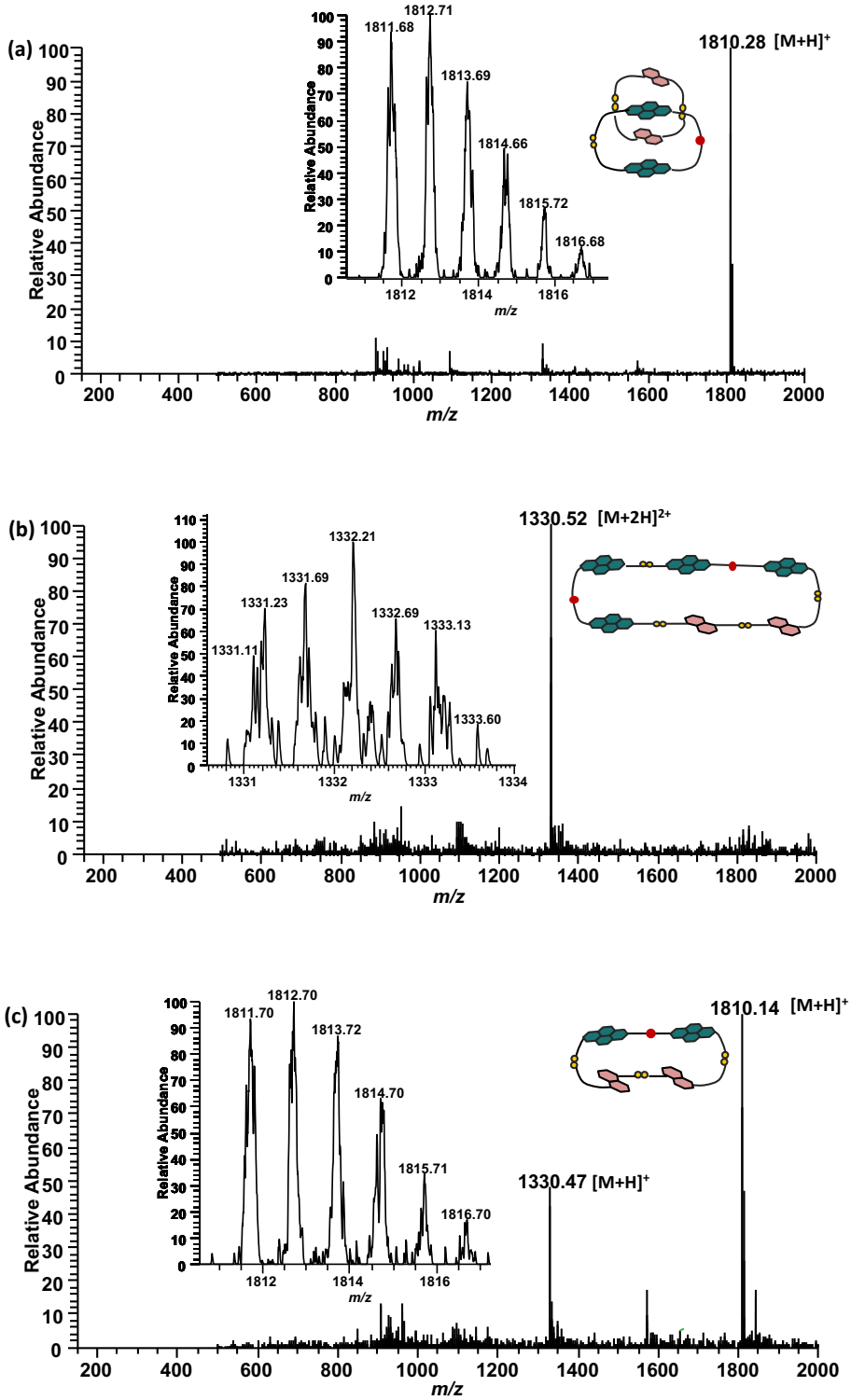

Figure 2-43. ESI-MS (+*ve*) spectra of (a) **Cat4** (as singly charged cation), (b) the heterotetramer **[A1c-D1S]$_2$** (as doubly charged cation), (c) the heterotrimer **[A1c-D1S$_2$]** (as singly charged cation). Expansions of molecular ions are shown as inserts.

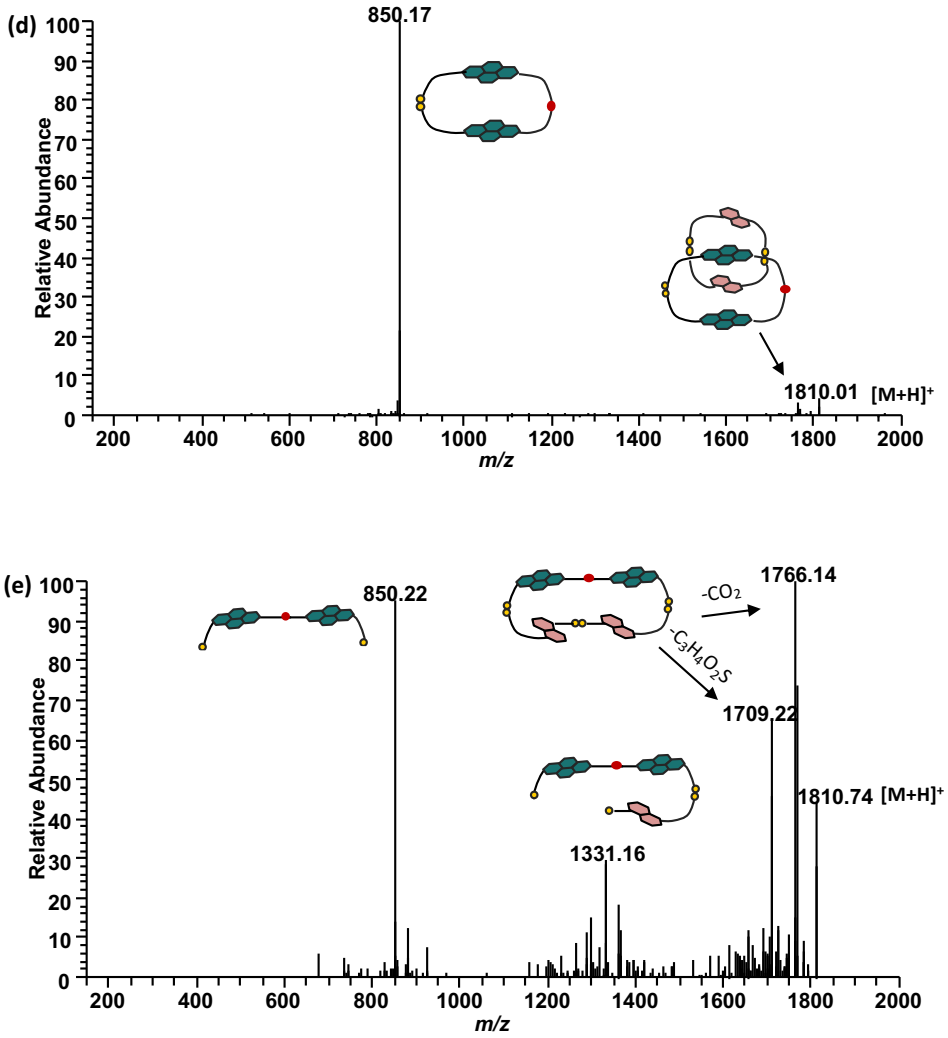

Figure 2-44. MS/MS fragmentation spectra of (d) **Cat4** and (e) and **[A1c-D1S$_2$]**.

As previously discussed, The **D1S** donor building block has a relatively rigid structure, thus limiting the formation of [2]catenane to a very small concentration when compared to the more flexible DN, **D2S**. A new macrocycle has been identified in this library, and that is the DN heterotetramer **[A1c-D1S]$_2$**, which is the major component of the library without salt (70%) at 18.0 min. However, the concentration of **[A1c-D1S]$_2$** decreased to 59% in the presence of 1 M $NaNO_3$ and the concentration of D-A heterotrimer **[A1c-D1S$_2$]** increased 19%. This can be explained by the tighter packing of **[A1c-D1S$_2$]** macrocycle in comparison to **[A1c-D1S]$_2$**.

2.15 D-A DCL of A1c with D2S: Synthesis in high yield of DADA [2]catenane: Cat5

The LC-MS analysis of D-A DCL of **A1c** with **D2S** has revealed that the fully oxidised library contains a surprisingly high yield of a [2]catenane, **Cat5**, up to 92% (containing 92% of **A1c** present in the DCL). The short retention time of **Cat5** along with the strong CD signal have been the first indications that **Cat5** is a topologically complex interlocked molecule.

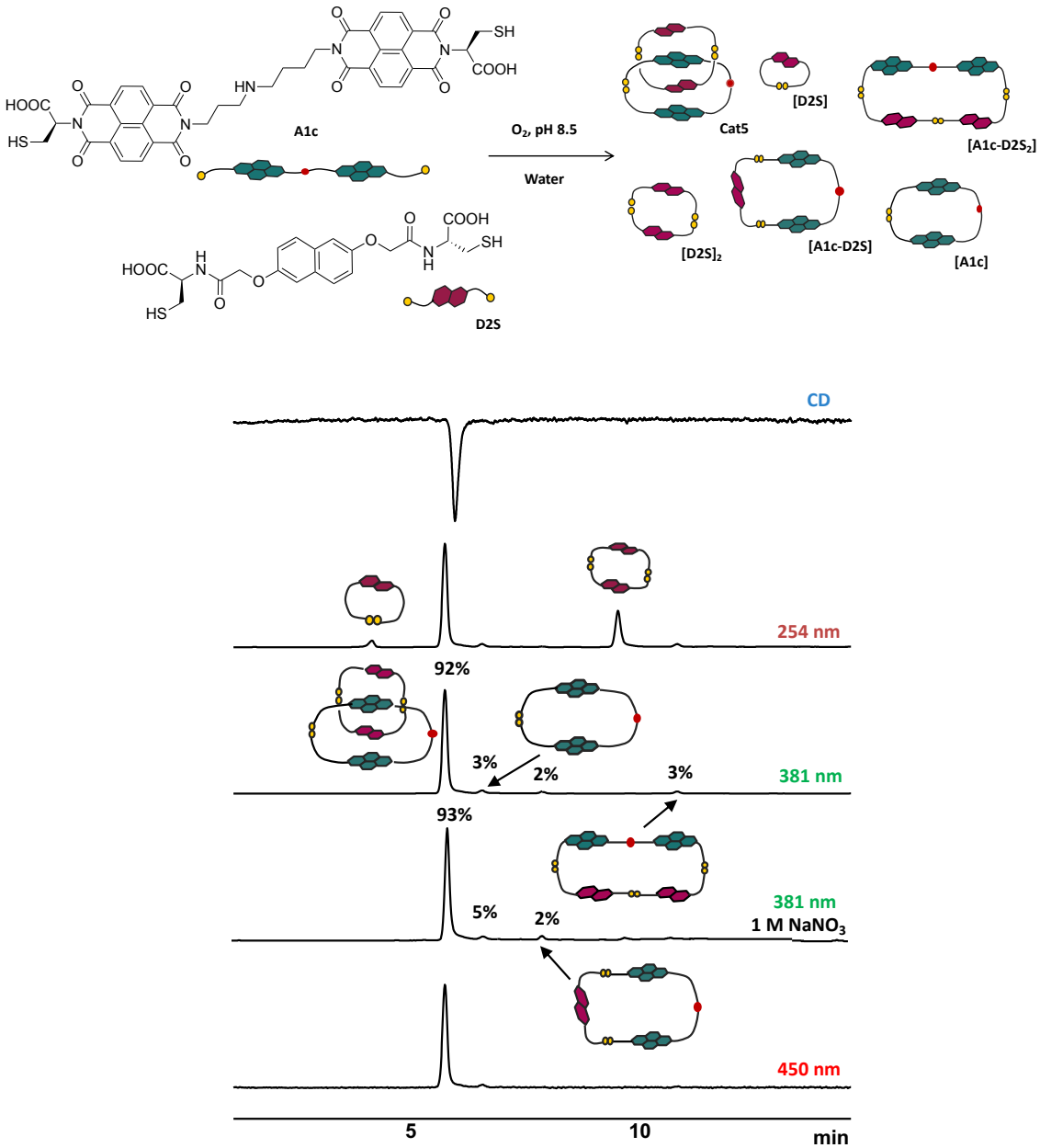

Figure 2-45. The HPLC analysis of **A1c** and **D2S** DCL (1:2 molar ratio, 5 mM total concentration). Estimated yield is indicated above the corresponding peaks.

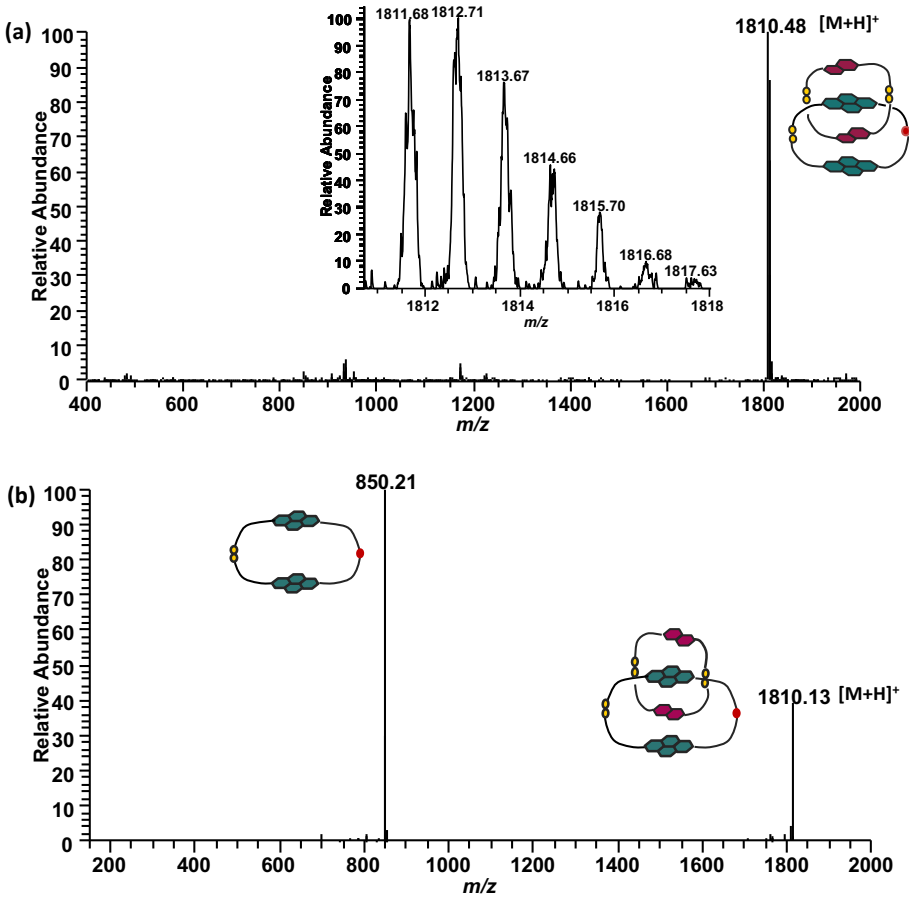

Figure 2-46. (a) Full MS (+*ve*) and (b) MS/MS fragmentation of **Cat5**. Expansions of molecular ion is shown as insert.

The ESI-MS and MS/MS fragmentation patterns are in agreement with the proposed structure of **Cat5**. The results reveal that the **Cat5** is indeed composed of **A1c** cyclic monomer, interlocked with a **D2S** dimer. In this library the subtle difference in geometry of **D2S** when compared to **D1S** leads to the more efficient packing of the aromatic surfaces and formation of the corresponding [2]catenane (93% for **Cat5** *vs.* 8% for **Cat4**). This exceptionally high yield indicates that the **Cat5** structure is the most thermodynamically favoured arrangement of these donor-acceptor building blocks. The efficiency of a DADA catenane formation is linked to the length of the polyamine and the tightness of the acceptor ring as well as the geometry of the DN building block. Heterodimer and heterotrimer D-A are also observed in very small yields (2 and 3% respectively). The formation of **Cat5** in such high yield indicates a combination of optimal donor-acceptor and hydrophobic interactions and their efficient cooperation, leading to this particularly favourable synthesis of a catenane. This catenane has been isolated by preparative HPLC and further characterised.

2.15.1 1D and 2D ^{1}H NMR Characterisation of Cat5

The peak representing **Cat5** was isolated by preparative HPLC and analysed by ^{1}H NMR to prove it is a catenane and not a macrocycle. Isolated yield: 97%, Figure 2-47.

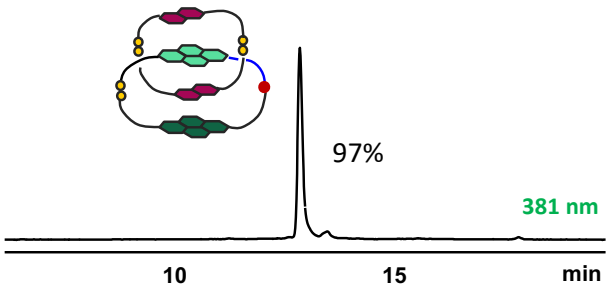

Figure 2-47. Reverse-Phase HPLC result of the isolated **Cat5**. Absorbance was recorded at 381 nm.

The **Cat5** lacks symmetry due to the **A1c** cyclic monomer (the NDIs are chemically inequivalent due to the spermidine linker) and the intrinsic conformational planar chirality of the 2,6-DN in the **[D2S]$_2$** macrocycle.

There are eight possible arrangements of the building blocks in **Cat5** representing four diastereomers (due to the two stereogenic 2,6-DN moieties present in **D2S**), each having two possible co-conformations depending on which NDI is inside the **D2S** cyclic dimer. These structures cannot be separated by achiral reverse-phase HPLC, therefore, the peak at 5.6 min counts for all four isomers.

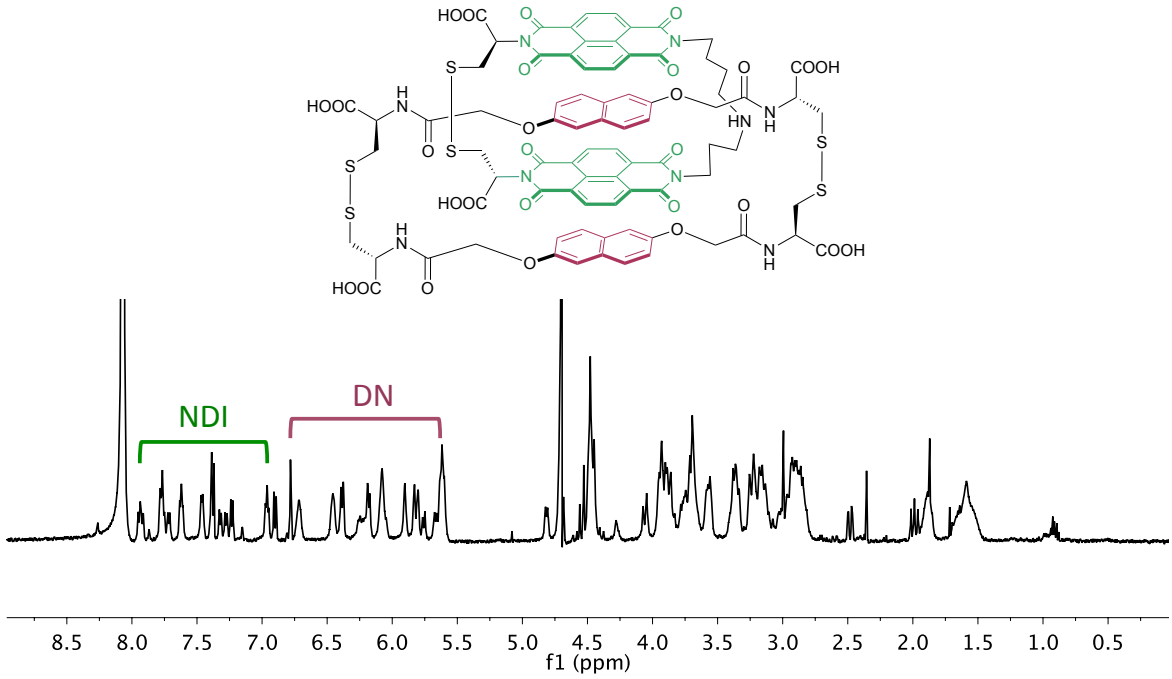

Figure 2-48. ^{1}H NMR full spectrum of the **Cat5** (D_2O, 500 MHz, 308 K). The solvent peak was referenced at 4.74 ppm. The chemical structure of **Cat5** is also shown.

^{1}H NMR spectrum (500 MHz, 298 K, D_2O) shows sharp signals, indicating the rigidity of the system through complex topology of the structure. Typically, macrocycles usually display broad NMR signals due to their flexibility. The complexity of ^{1}H NMR spectrum confirms that **Cat5** is produced as a pair of diastereomers due to the lack of symmetry.

Each conformation has two sets of signals in the acceptor region (6.95 to 7.95 ppm) which have been assigned by correlation spectroscopy (COSY). The signals coming from the inner NDI scaffold are upfield shifted, whereas the outer NDI protons are downfield shifted. A similar pattern across the donor region (5.65 to 6.90 ppm) with two sets of signals for each conformation was observed.

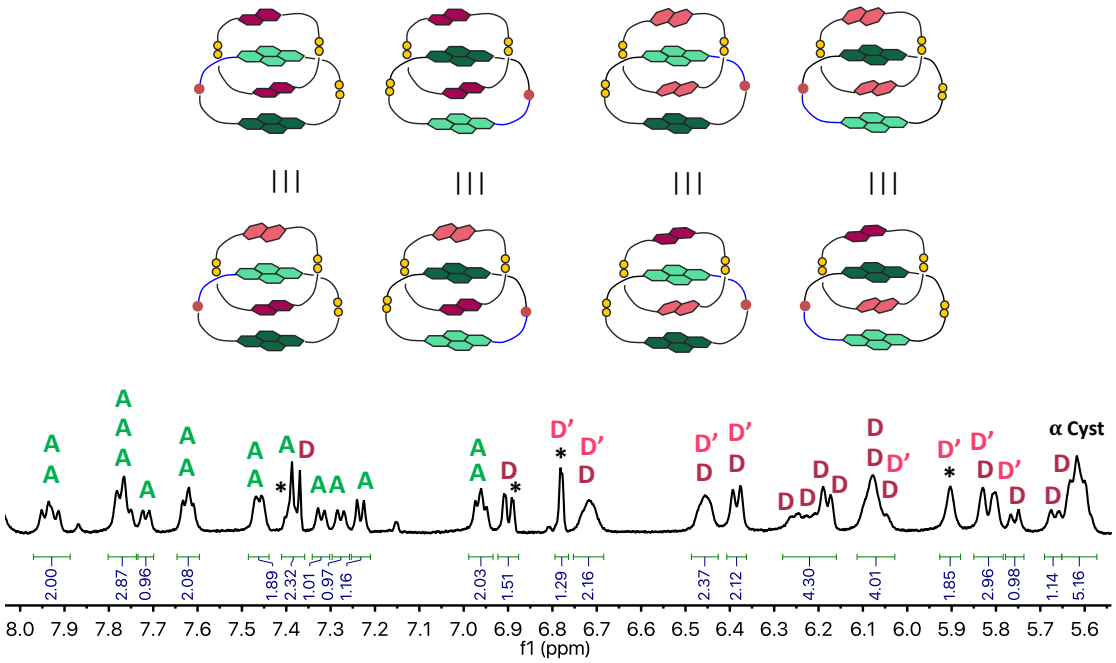

Figure 2-49. Partial ^{1}H NMR spectrum of **Cat5** across 5.5 – 8.0 ppm region in D_2O. The **D'** represents the singlet peak of DN and the * represents impurity.

The ^{1}H NMR spectrum of **Cat5** is consequently extremely complex. However, the analysis of the acceptor, donor and **α**, **β** regions by a combination of the COSY, NOESY and for the first time for these types of catenanes, HSQC spectra (1.90 to 8.00 ppm) have allowed the correlation of the signals corresponding to each of the four isomeric catenanes. The ^{1}H NMR spectrum could be fully rationalised by matching the structures of four [2]catenanes with the acquired COSY and NOESY spectra, allowing the assignment of each proton of the molecule, as labelled in Figures 2-(50-54).

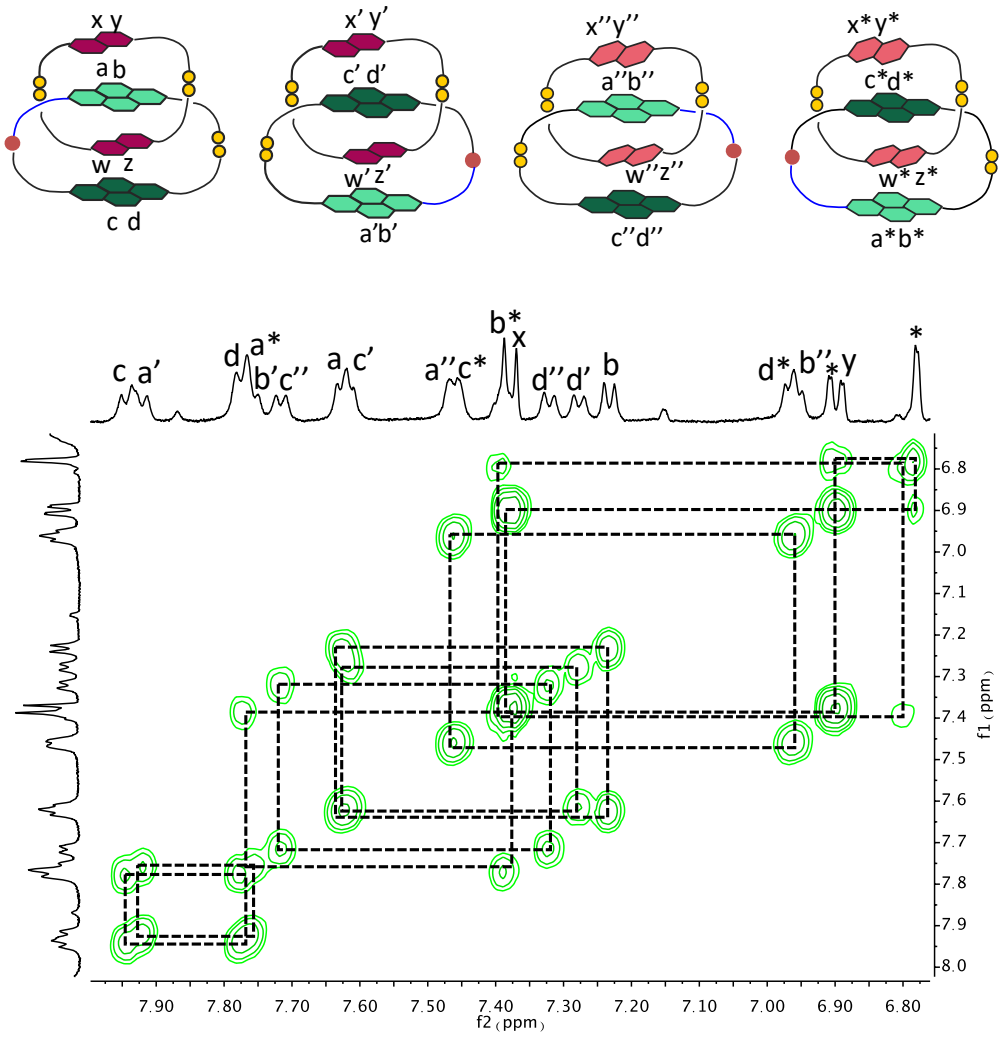

Figure 2-50. Partial COSY spectrum of **Cat5** in the NDI region, between 6.80 and 8.00 ppm (D_2O, 308 K, 500 MHz). The dotted lines highlight peaks connected through chemical exchange. The solvent peak was referenced at 4.74 ppm.

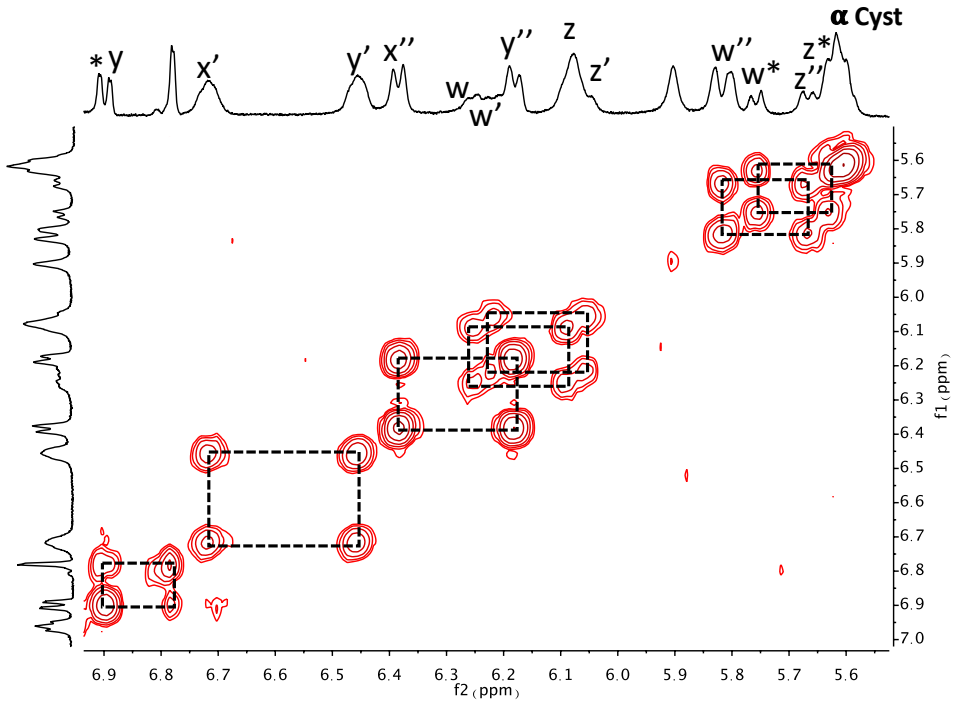

Figure 2-51. Partial COSY spectrum of **Cat5** in the DN region, between 5.50 ppm and 7.00 ppm (D_2O, 308 K, 500 MHz). The dotted lines highlight peaks connected through chemical exchange. The solvent peak was referenced at 4.74 ppm.

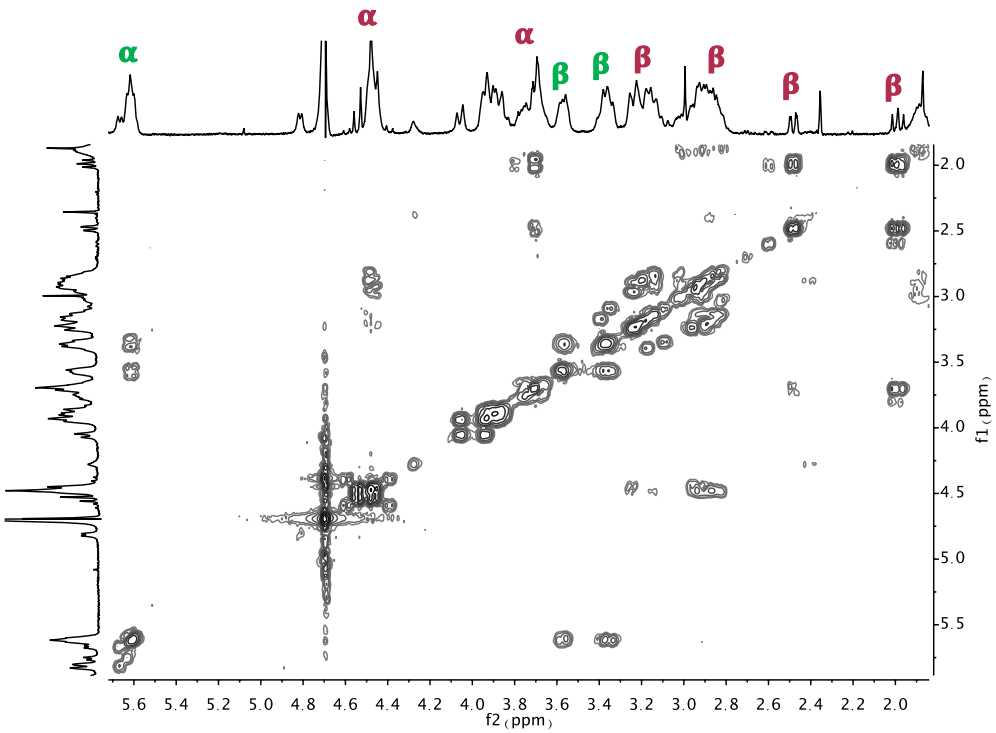

Figure 2-52. Partial COSY spectrum of **Cat5** between 1.90 ppm and 5.70 ppm, showing the region of spermidine chain, cysteine **α** and **β** of NDI and DN. Only the **α** and **β** regions are labelled (D_2O, 308 K, 500 MHz). The dotted lines highlight peaks connected through chemical exchange. The solvent peak was referenced at 4.74 ppm.

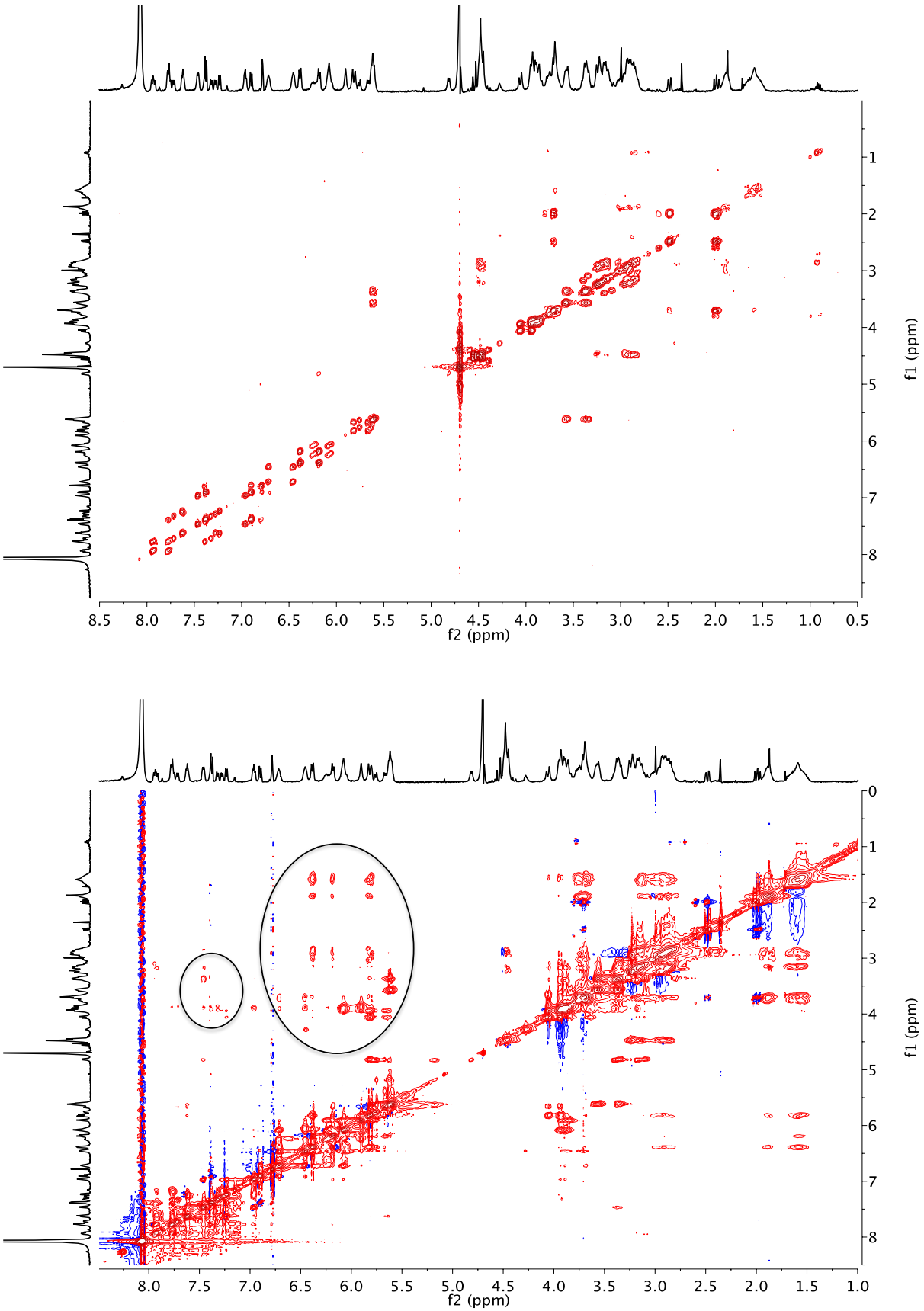

Figure 2-53. Full COSY and NOESY spectrum of **Cat5** (D_2O, 500 MHz, 308 K) the solvent peak was referenced at 4.74 ppm.

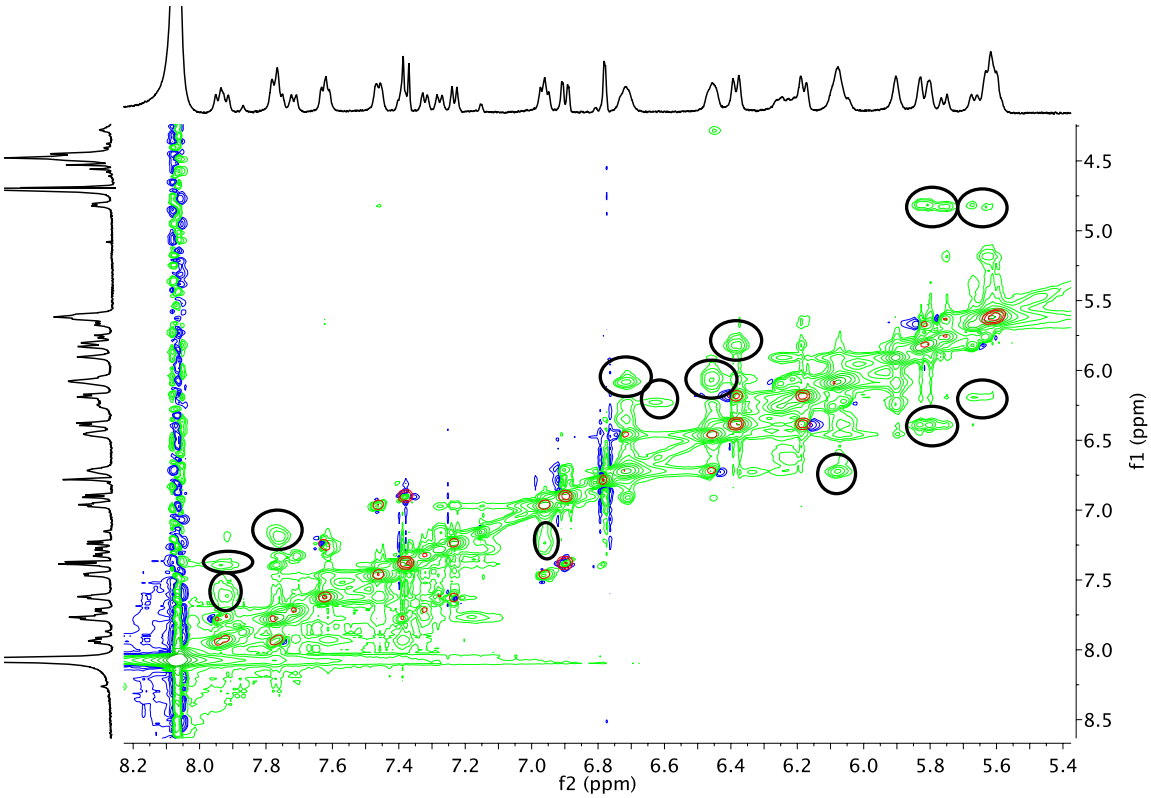

Figure 2-54. Partial NOESY spectrum of **Cat5** across 5.4 – 8.2 ppm region (D_2O, 500 MHz, 308 K) the solvent peak was referenced at 4.74 ppm.

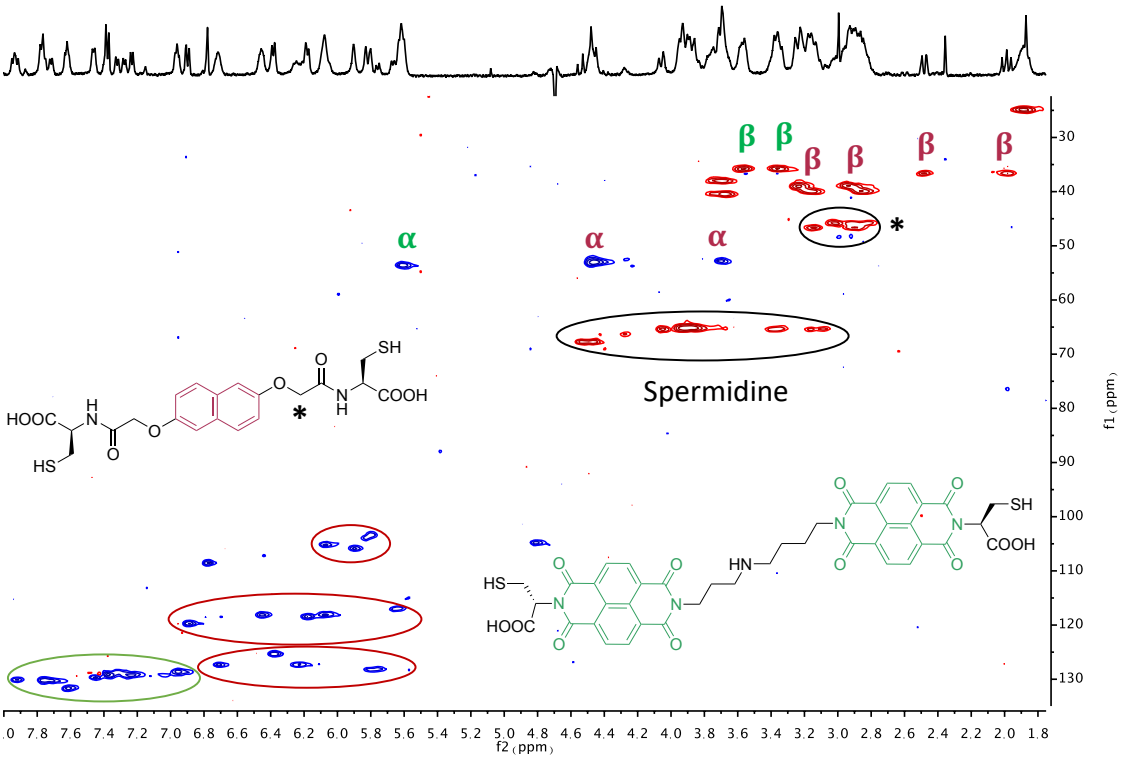

Figure 2-55. Full HSQC spectrum of **Cat5** across 1.8 – 7.9 ppm region (D_2O, 500 MHz, 308 K) the solvent peak was referenced at 4.74 ppm).

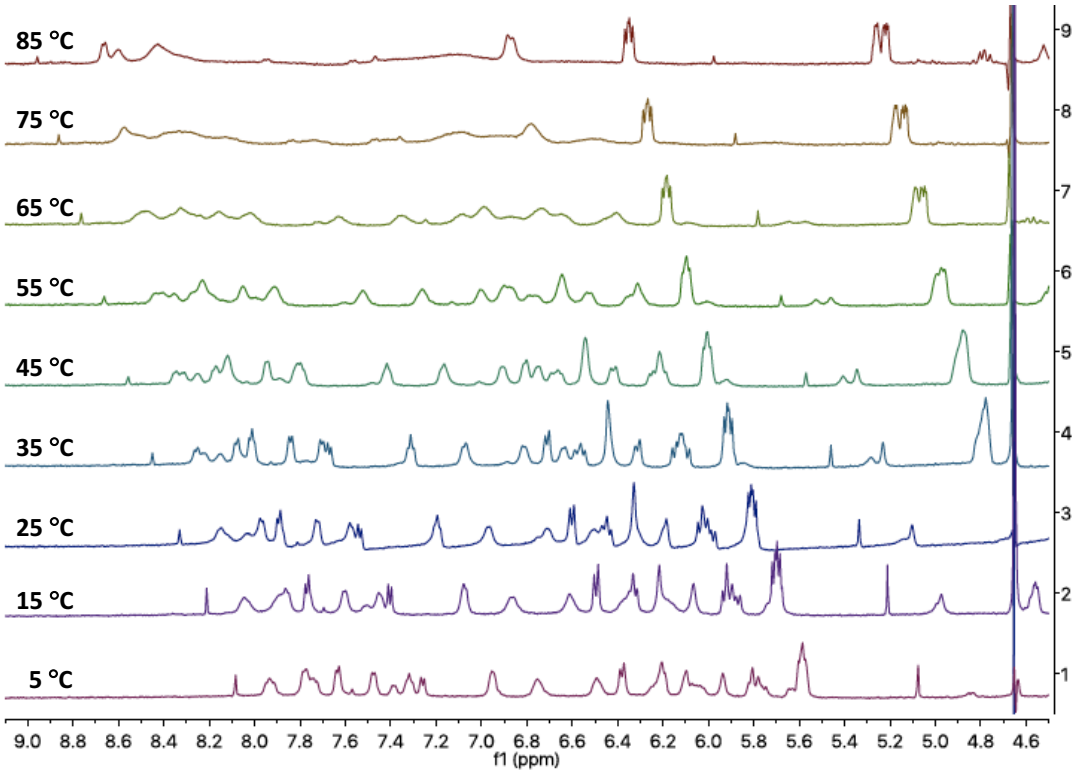

Figure 2-56. ^{1}H NMR spectrum of **Cat5** at various temperatures (D_2O, 500 MHz) the solvent peak was referenced at 4.74 ppm).

The NMR analysis shows very sharp NMR signals in D_2O which indicates the rigidity through complex molecular topology. However, the variable temperature (VT) study on the isolated sample proved that this rigidity can be reduced by increasing the temperature (up to 85 °C). At higher temperatures, the characteristic peaks start to broaden, indicating that the [2]catenane exhibits a dynamic structure. The peak broadening is due to the fast rotation of the rings in the [2]catenane. This further supports the assignment of these spectra to a [2]catenane; if the molecule was a macrocycle, the flexibility in the ring would give very broad NMR signals which would sharpen with an increase in temperature.

2.15.2 UV-Vis and Circular Dichroism (CD) analysis

Circular Dichroism studies the chirality of molecules and these macromolecules can have chirality due to their inter-linkage in addition to intrinsic chirality of any of the components. Generally, [2]catenanes are topologically achiral molecules, but the presence of the cysteine linkers introduces chirality in their structure, and in the case of **Cat5** with unsymmetrical polyamine, the [2]catenane has four diastereomers. The peak that represents **Cat5** with a strong CD signal in the library was isolated by preparative HPLC and studied further by CD. It has also extensively been studied by synchrotron radiation CD where the light source is much more confined, and the beamline has more directionality than that produced by conventional CD instruments, providing a much higher signal-to-noise ratio over a wide wavelength range (170-700 nm). The isolated catenanes were analysed by variable temperature (VT) CD and UV-Vis spectroscopies.

2.15.3 UV-Vis Analysis of Cat5

The UV-Vis absorption spectrum of **Cat5** represents a combination of the DN (220 – 260 nm) and NDI (250 – 400 nm) chromophores as well as a new charge-transfer band between (400 – 550 nm). This is characteristic for a donor-acceptor interaction between these chromophores and is evidenced by the bright red colour of the DCLs.

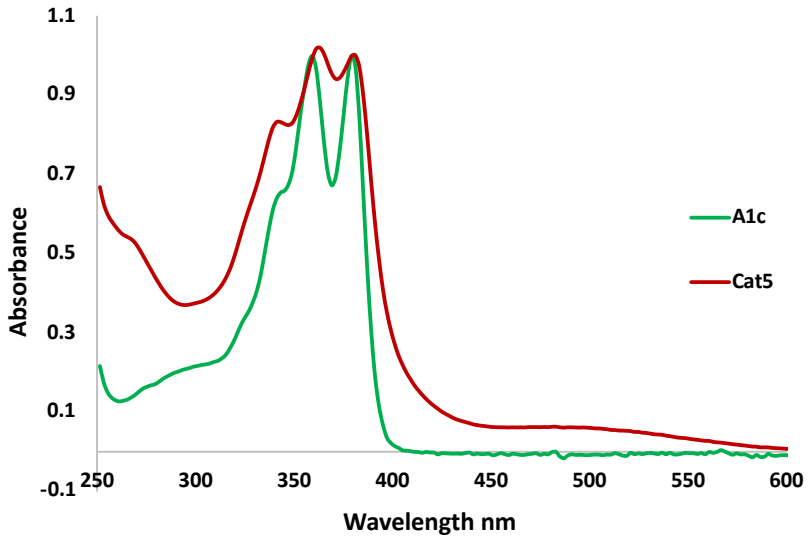

Figure 2-57. Normalised at (379 nm) UV-Vis spectra of **Cat5** and **A1c**.

Figure 2-57 shows the NDI and charge-transfer regions of **Cat5** compared with the cyclic **A1c** monomer. The charge-transfer band is evident in **Cat5** when compared to **A1c**, which reflects the absence of donor in **A1c**.

2.15.4 Circular Dichroism (CD) Analysis of Cat5

The **Cat5** is chiral due to its topology as well as the point chirality from the cysteine and that is proved by the spectra on Figure 2-58. These spectra highlight that the induced CD signal around 400 nm in **Cat5** is orders of magnitude stronger than **A1c** protected and deprotected in acetonitrile.

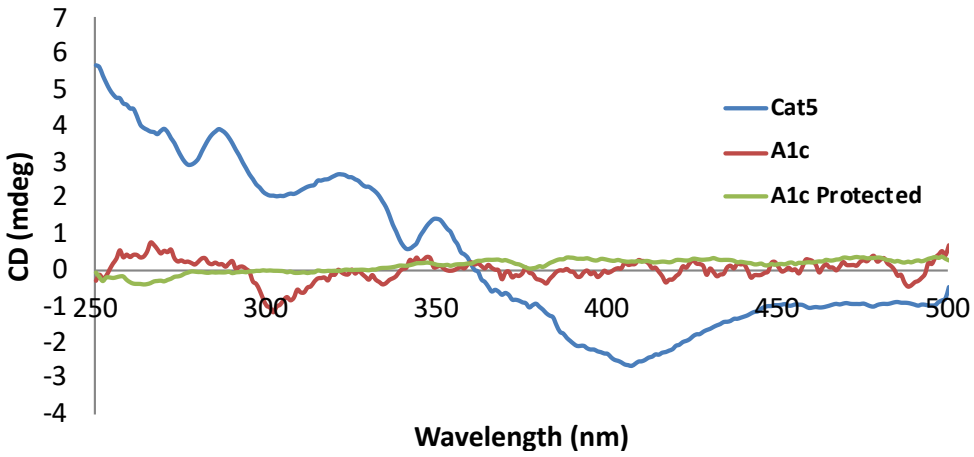

Figure 2-58. The CD spectra of **Cat5** compared to the **A1c** protected and **A1c** deprotected on the thiol moiety. The experiment was done at 23 °C.

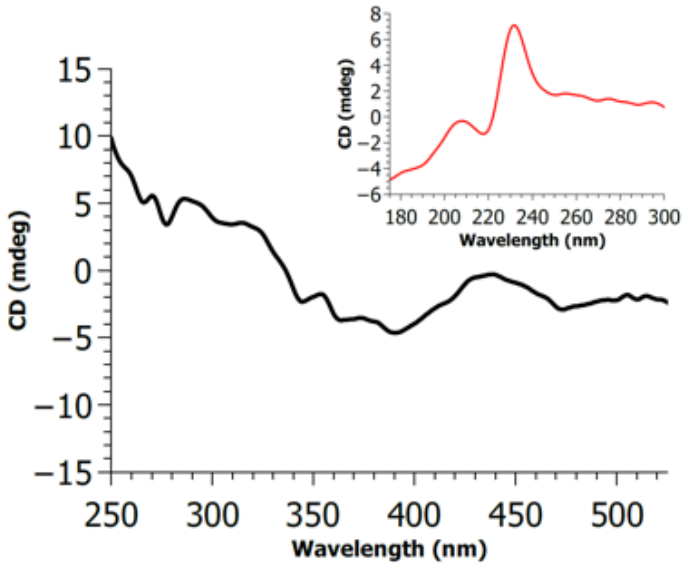

Figure 2-59. The CD spectrum of **Cat5** (250 – 600 nm), recorded in a 10 mm pathlength cuvette. Inset the UV region (175 – 300 nm) recorded in a 1mm pathlength cuvette. The experiment was done at 23 °C.

The CD spectra show negative Cotton effect between (175 – 210 nm) and strong positive Cotton effect between (220 – 245 nm), which is ascribed to the disulfide n→σ* and aromatic π→π* transitions with lower contributions from the amide / imide and carboxylate

chromophores. The NDI chromophore (300 – 400 nm) is in a chiral environment as indicated by a negative Cotton effect (Figure 2-59). This is not surprising as, in the **Cat5**, the DN and NDI moieties are stacked, allowing for both topological and point chirality to be transferred onto these chromophores. The VT experiments (5 – 85 °C) showed only a slight change on CD spectra of the NDI region, confirming the interlocked structure.

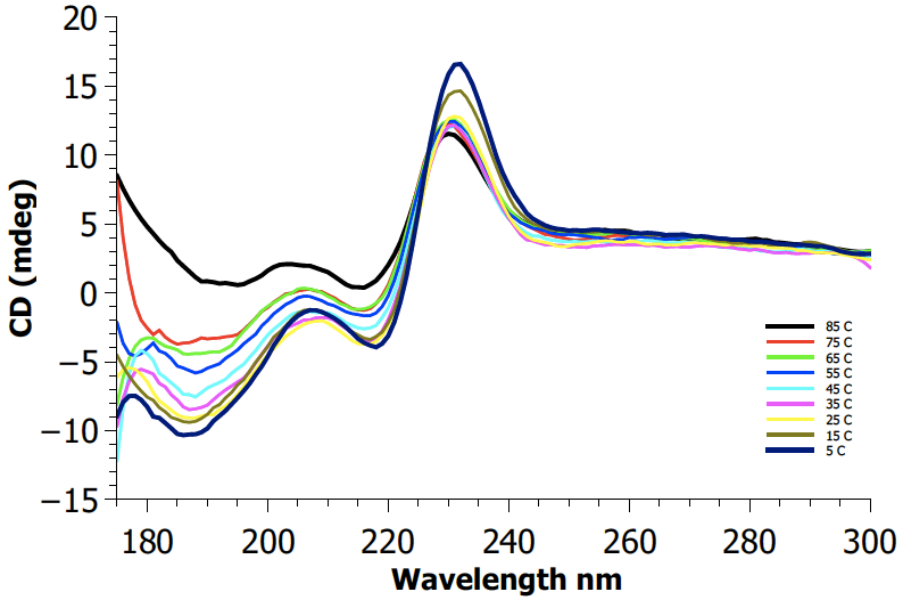

Figure 2-60. Variable temperature CD spectra between 5 – 85 °C of **Cat5** (D_2O, 175 – 300 nm, 1 mm pathlength cuvette).

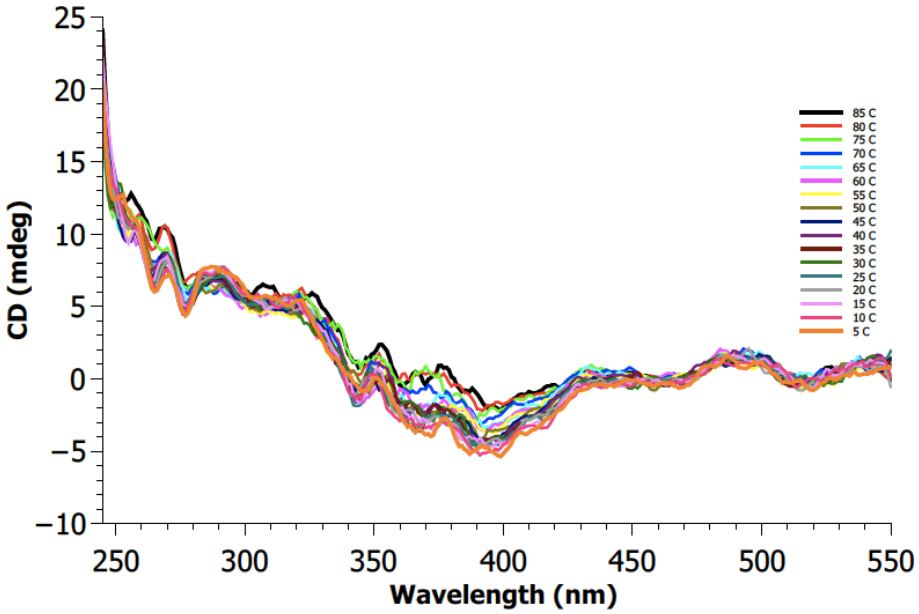

Figure 2-61. Variable temperature CD spectra between 5 – 85 °C of **Cat5** (D_2O, 245 – 550 nm, cuvette pathlength: 10 mm).

The percentage of change illustrates the variation of CD intensity at different temperatures. This study shows that there is more flexibility at higher wavelengths (which corresponds to the NDI region of catenane) than within the cysteine region when the temperature increases, this is due to the fast rotation of the rings which reduces the chirality transfer from cysteines onto the aromatic regions.

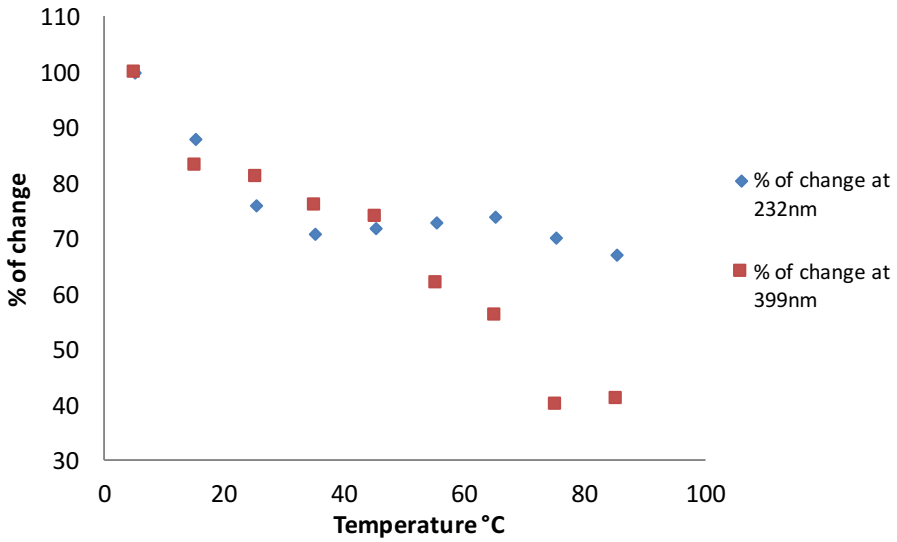

Figure 2-62. The comparison between % of change at two wavelengths (232 and 399 nm) of **Cat5**.

2.15.5 DCL in Large Volume

The library of **A1c** and **D2S** was also made in large volume (60 mL) to compare the library's distribution with the typical 1 mL DCL. The slight erosion in yield is most likely due to an error in relative ratio of the building blocks due to the hygroscopicity of the TFA salt of the **A1c** building block.

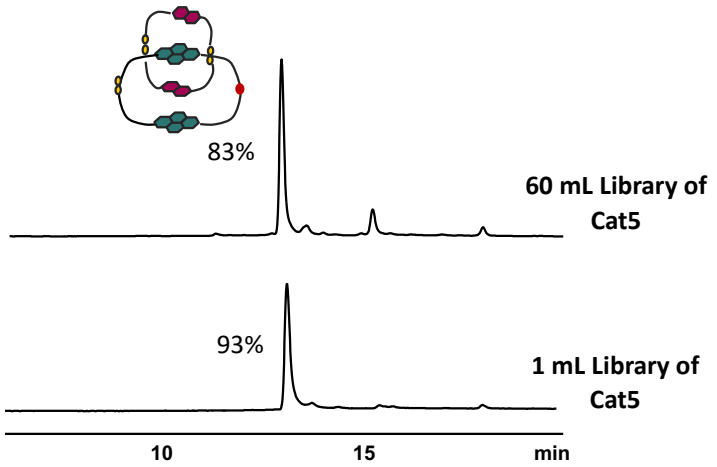

Figure 2-63. The HPLC analysis of **A1c** and **D2S** (1:2 molar ratio, 5mM total concentration, H_2O). Absorbance was recorded at 381 nm.

2.15.6 Separation of Cat5 Diastereomers Using Chiral Chromatography

The separation of diastereomers of **Cat5** by achiral columns has never been possible as they are not built to separate chiral compounds. However, chiral columns provide promising chances in separating such diastereomers. Various columns with different packing were tried in diverse conditions; however, the separation of the diastereomers of **Cat5** was not successful. Figure 2-64 shows the best separation achieved using a Kromasil column, in which acylated *N*,*N*′-diallyl-l-tartardiamide network polymers are covalently bound to silica. The peak representing the four diastereomers only gets broader or shows a shoulder next to the main peak. Table 2-1 displays the different methods tried to separate the diastereomers, most of which have not been successful.

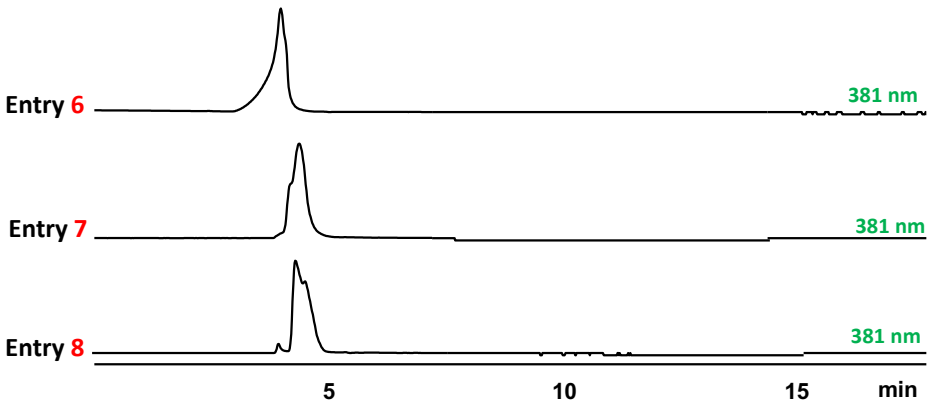

Figure 2-64. The HPLC analysis of **Cat5** using chiral column for separation of diastereomers. Column used for the separation was Kromasil 100-5Chi-TBB (25 x 0.46 cm dimension, 10 µm). Absorbance was recorded at 381 nm.

Table 2.1. Different methods used for separation of **Cat5** diastereomers using the same column as in Figure 2-64.

Entry	Solvent	Temp °C	Gradient/Isocratic	Flow rate
1	60% CH_3CN : 40% H_2O	38	Isocratic	1 ml/min
2	100% CH_3CN	38	Isocratic	1 ml/min
3	100% CH_3CN	38	Isocratic	0.5 ml/min
4	80% CH_3CN : 20% H_2O	15	Isocratic	0.5 ml/min
5	60% CH_3CN : 40% H_2O	15	Isocratic	0.5 ml/min
6	80% CH_3CN : 20% H_2O + 0.1% FA	15	Isocratic	0.5 ml/min
7	70% CH_3CN : 30% H_2O + 0.1% FA	15	Isocratic	0.5 ml/min
8	60% CH_3CN : 40% H_2O + 0.1% FA	15	Gradient	0.5 ml/min
9	80 - 60% CH_3CN + 0.1% FA	15	Isocratic	0.5 ml/min
10	70% CH_3CN : 30% H_2O + 0.1% FA	10	Isocratic	0.5 ml/min
11	50% CH_3CN : 50% H_2O + 0.1% FA	10	Isocratic	0.5 ml/min
12	80 - 70% CH_3CN + 0.1% FA	10	Gradient	0.5 ml/min
13	70% CH_3CN : 30% H_2O + 0.1% FA	10	Isocratic	0.25 ml/min

2.15.7 The Effect of Chirality on Formation of [2]Catenane

Replacement of cysteine chirality from L to D on the NDI molecule has led to a library with a similar distribution, the only difference being a slight change in the retention time of **Cat5*** to **Cat5** catenanes. This is expected as the two catenanes only differ in point chirality of two atoms but have the same topology.

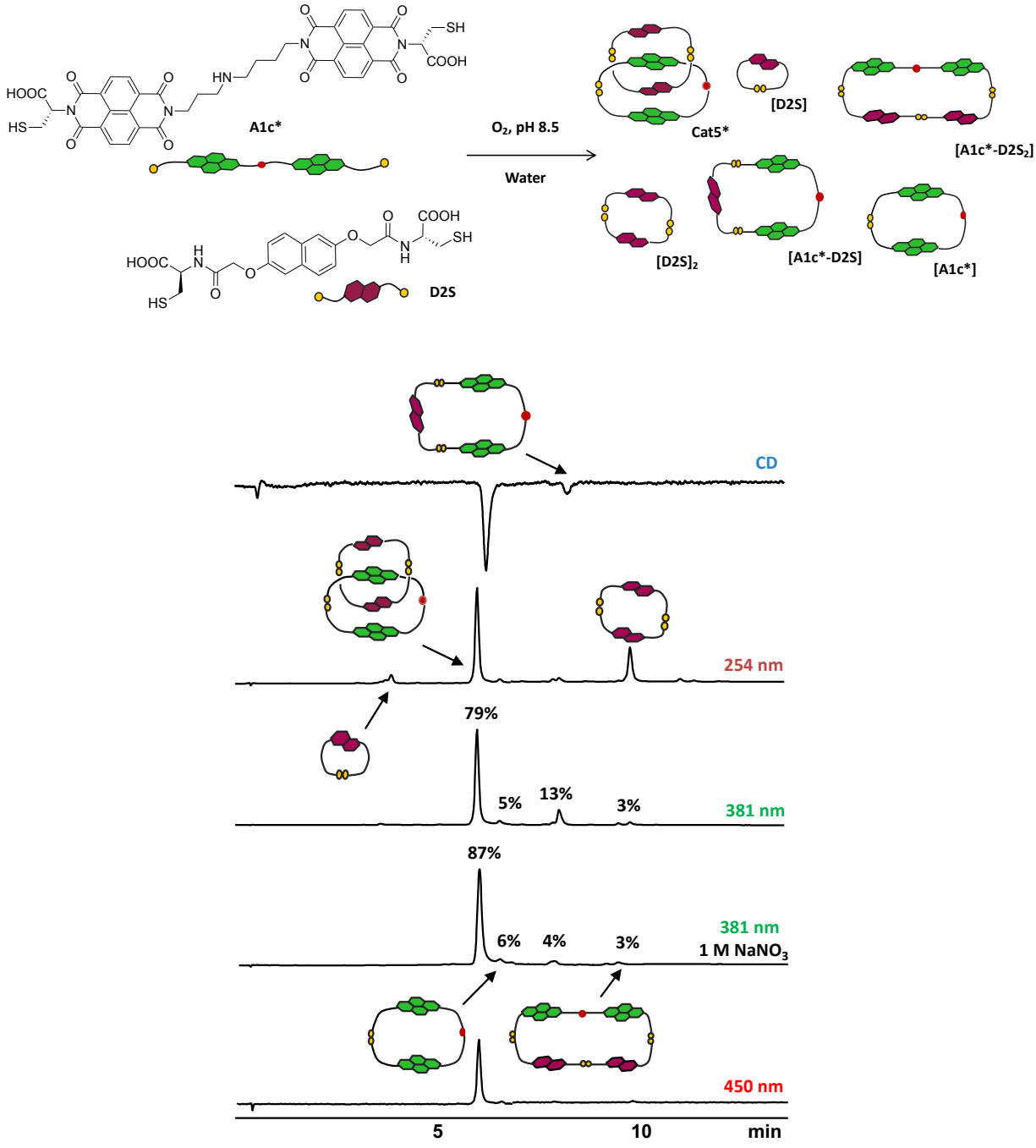

Figure 2-65. The HPLC analysis of **A1c*** and **D2S** (1:2 molar ratio, 5 mM total concentration).

The yield of **Cat5*** is 87% in presence of $NaNO_3$, based on HPLC peaks integration, which is slightly lower than that of **Cat5** (93%). This is possibly indicating a less efficient packing of **A1c*** with two **D2S** building blocks.

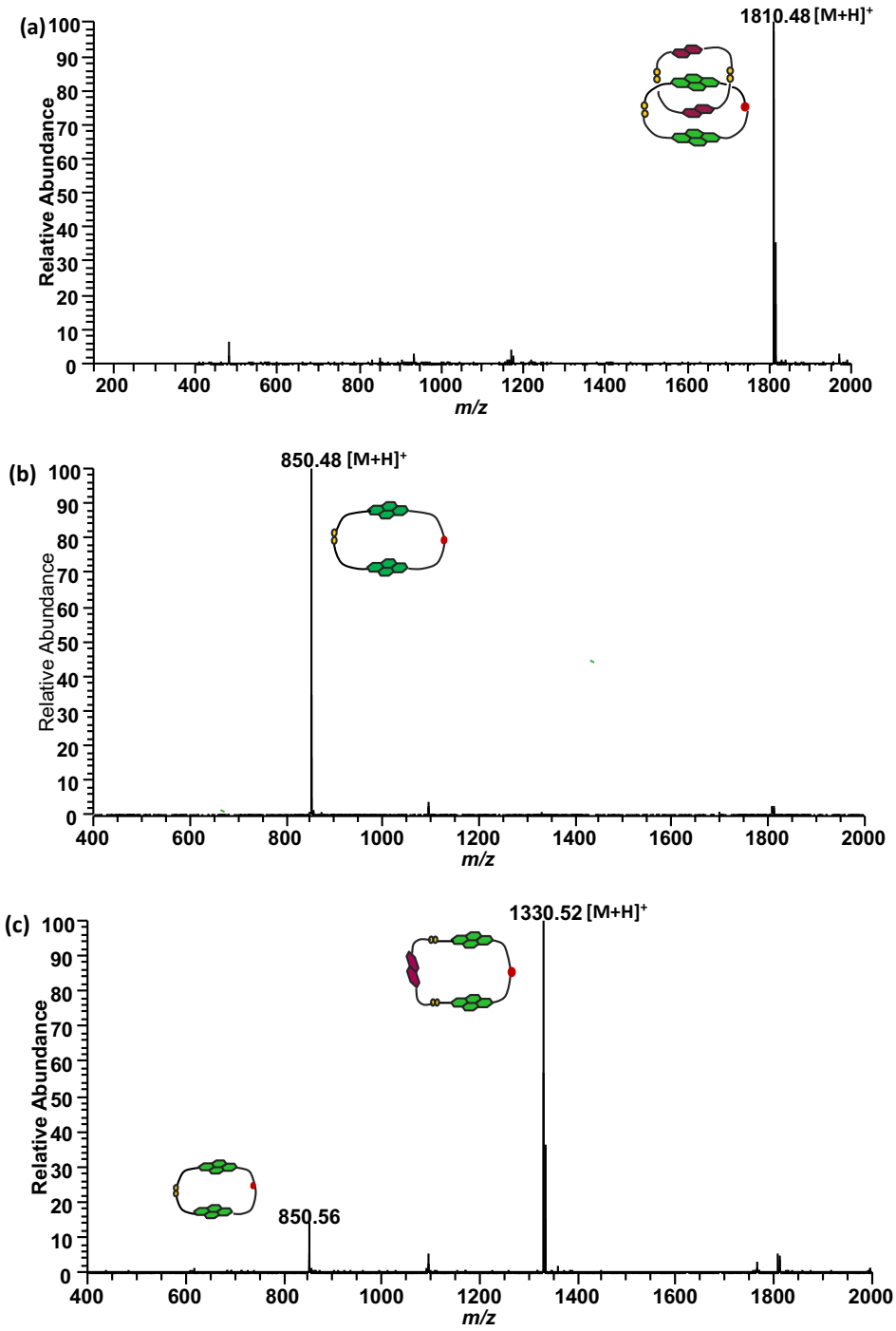

Figure 2-66. ESI-MS (+*ve*) spectra of (a) **Cat*** (singly charged cation), (b) **[A1c*]** cyclic monomer (as singly charged cation) and (c) heterodimer **[A1c*-D2S]** (as singly charged cation).

The HPLC traces of the two libraries containing **Cat5** and **Cat5*** were overlapped to compare the retention time for their peaks.

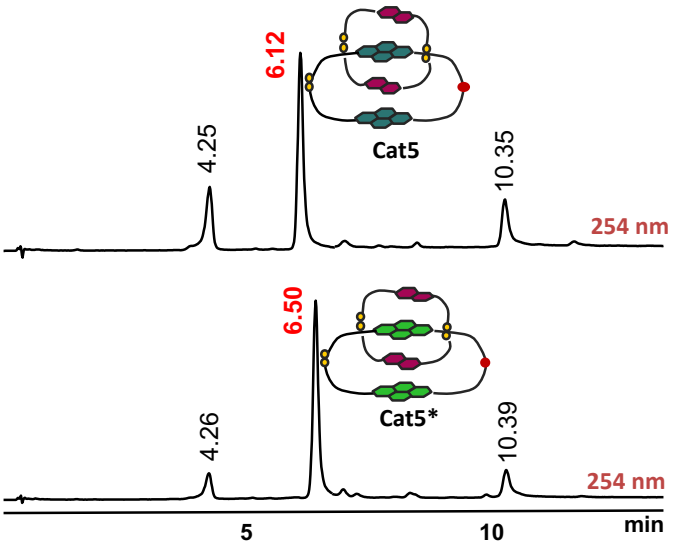

Figure 2-67. The comparison between the HPLC traces of **Cat5** and **Cat5*** at 254 nm.

As it is shown in Figure 2-67, the retention times of the peaks representing the [2]catenanes differ by 0.4 mins, whereas the retention time for peaks representing the **D2S** cyclic monomer and dimer stay almost the same. The peaks that correspond to the formation of **[D2S]** and **$[D2S]_2$** can be used as an internal reference in both HPLC chromatograms, thus observing the change in the catenanes' retention times.

2.15.8 Kinetic Study of Cat5* Formation

The kinetic study for the formation of **Cat5*** was performed on a DCL containing **A1c*** and **D2S** in 1:2 molar ratio (absorbance was recorded at 254 nm for DN and 381 nm for NDI, Figures 2-68 and 2-69).

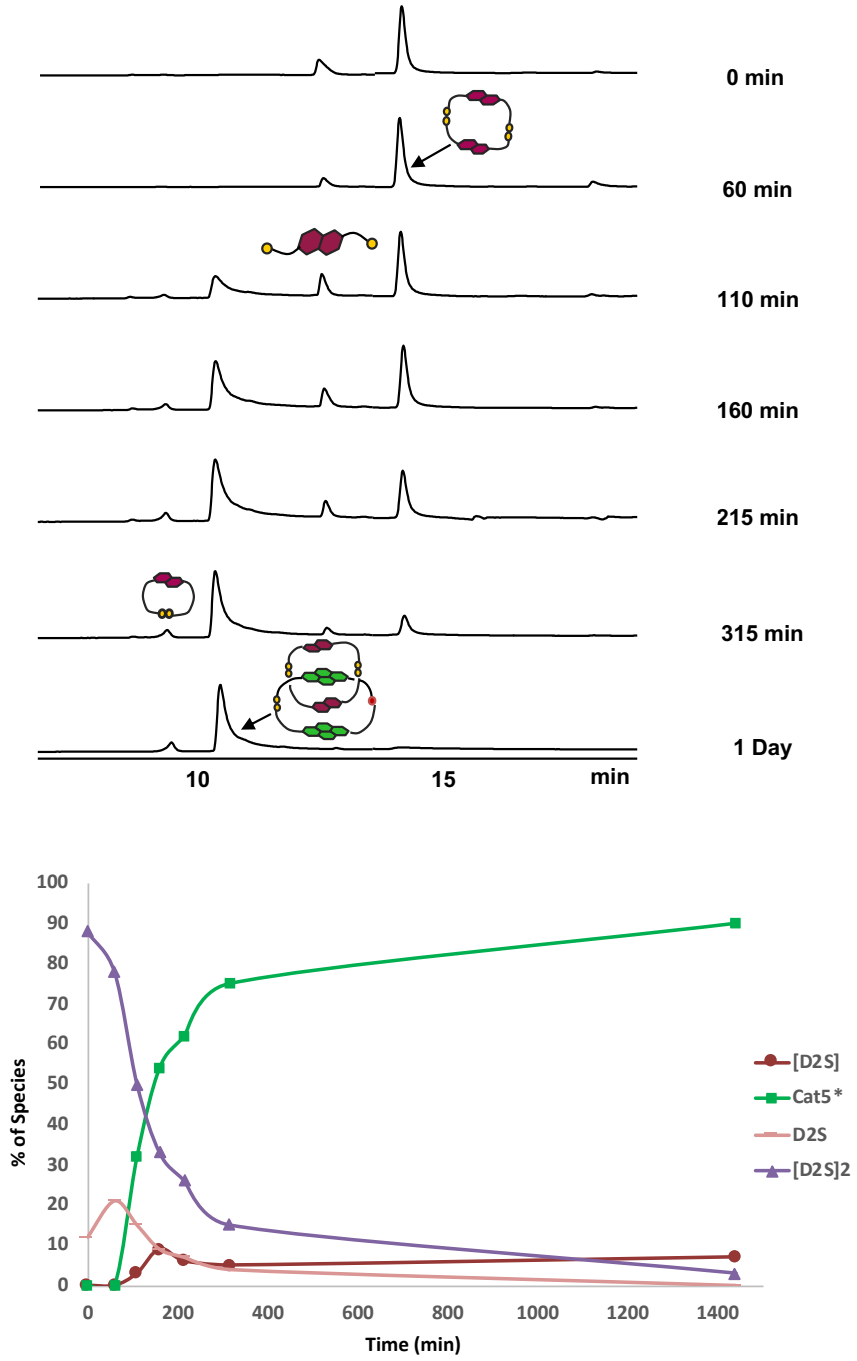

Figure 2-68. Kinetic study showing the formation of **Cat5*** over time. Absorbance was monitored at 254 nm.

The presence of linear intermediates and macrocyclic species of **D2S** and **[D2S]** at the start of library is expected as the oxidation of DN is a fast process. These species ultimately recombine to fall into the thermodynamic sink that represents the [2]catenane, **Cat5***.

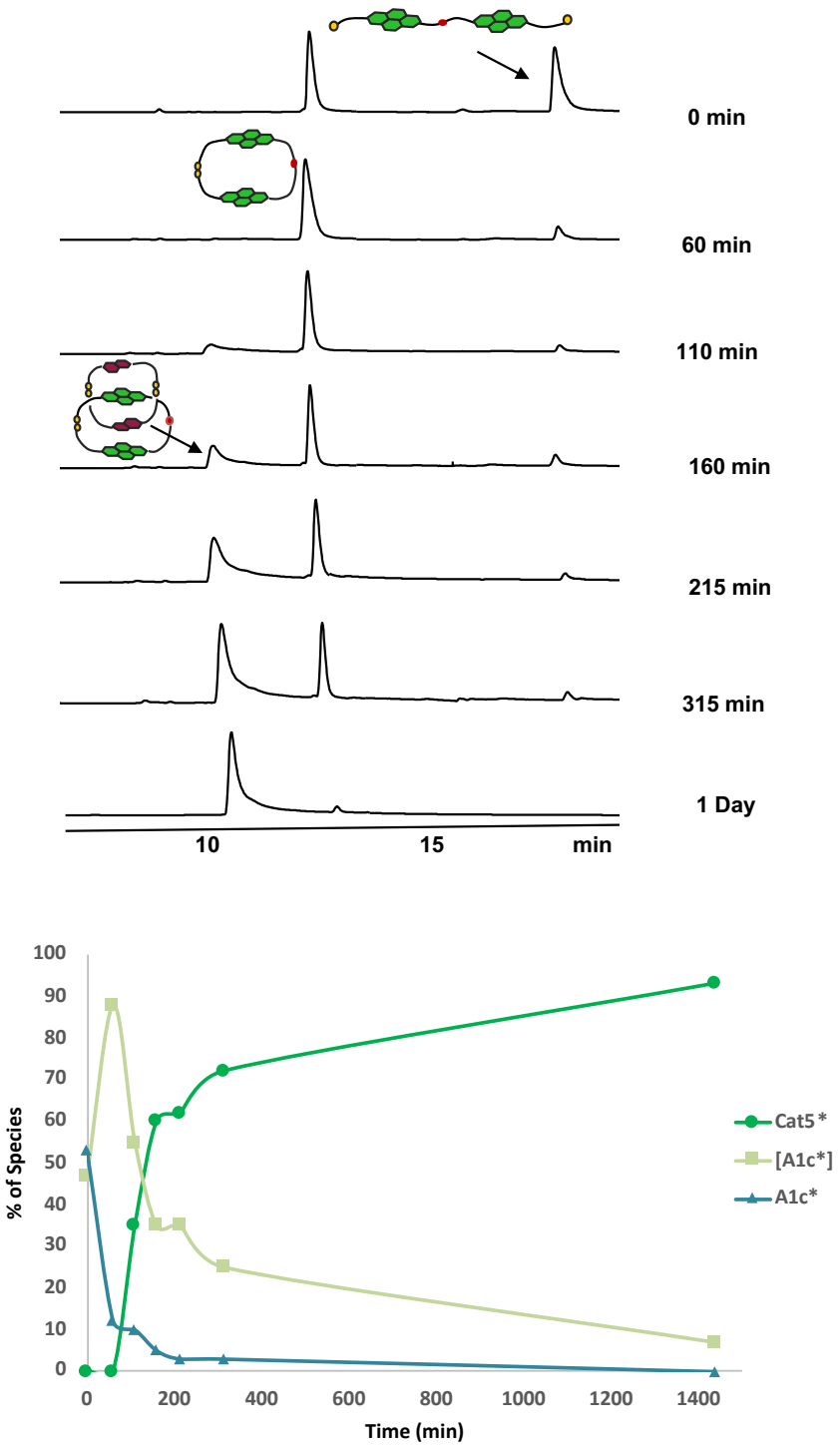

Figure 2-69. Kinetic study showing the formation of **Cat5*** over time. Absorbance was monitored at 381 nm.

The presence of intermediates and macrocyclic species (**A1c*** and **[A1c*]**) at the start of library is observed, which ultimately fall into the thermodynamic sink that leads to formation of **Cat5***. This observation clearly shows that the disulfide exchange stops few hours after oxidation: the catenane is progressively formed within the library until it reaches a steady state, corresponding to the full oxidation of the thiols.

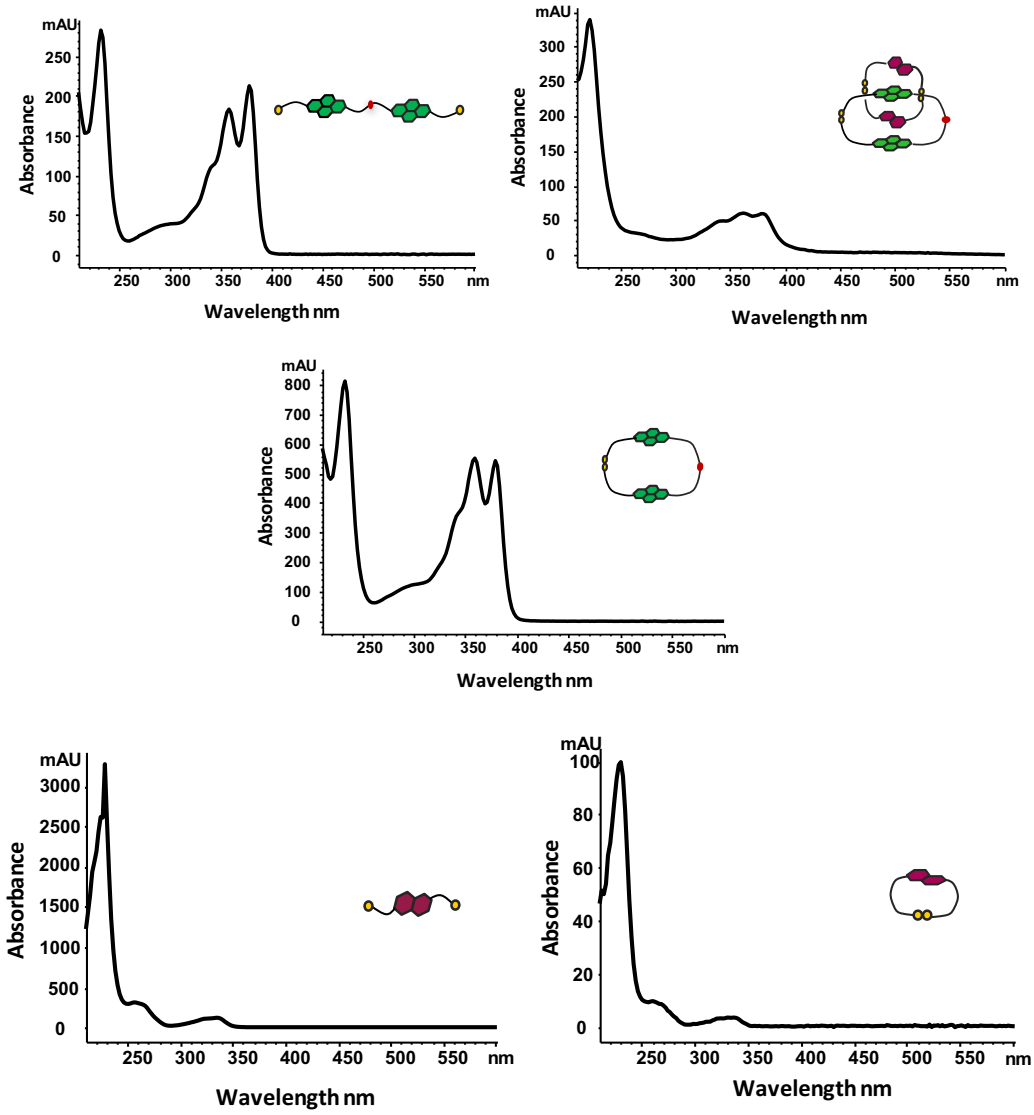

Figure 2-70. The UV-Vis spectrum of **A1c*-D2S** library in H_2O showing the absorbance trace of each peak corresponding to each structure.

2.15.9 CD Analysis of Cat5*

The CD spectrum of the [2]catenane containing the D-NDI building block is more defined in the DN / NDI region of the spectrum (Figure 2-71 inset). This can be related to a particular arrangement of the aromatic units with respect to the chiral centre as imposed by the electrostatic repulsions of the carboxylate units in the NDI and DN rings. This arrangement is more flexible in the L-NDI series as indicated by the weaker and less defined CD spectrum.

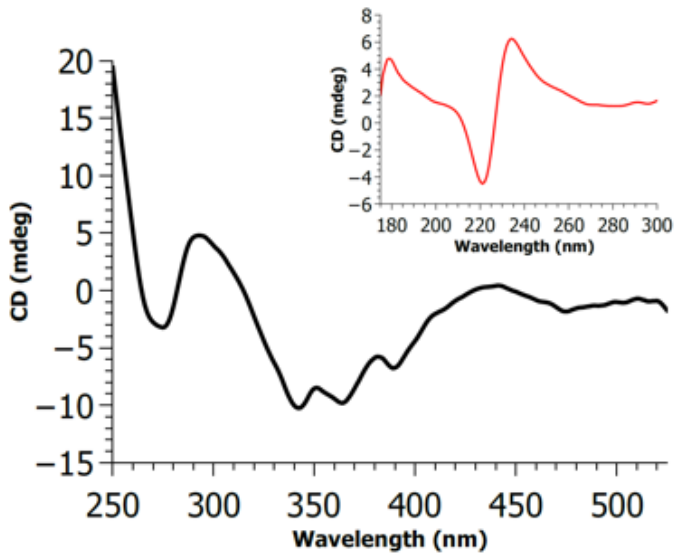

Figure 2-71. The CD spectrum of **Cat5*** (250 – 600 nm), recorded in a 10 mm pathlength cuvette; Inset the UV region (175 – 300 nm), recorded in a 1 mm pathlength cuvette. The experiment was done at 23 °C.

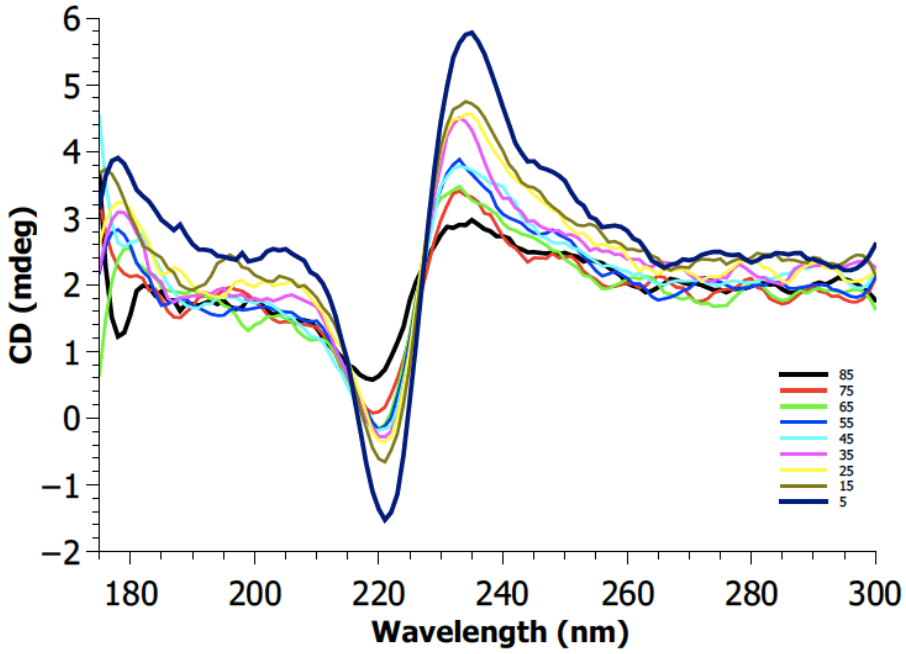

Figure 2-72. Variable temperature CD spectra between 5 – 85 °C of **Cat5*** (D_2O, 175 – 300 nm, 1 mm pathlength cuvette).

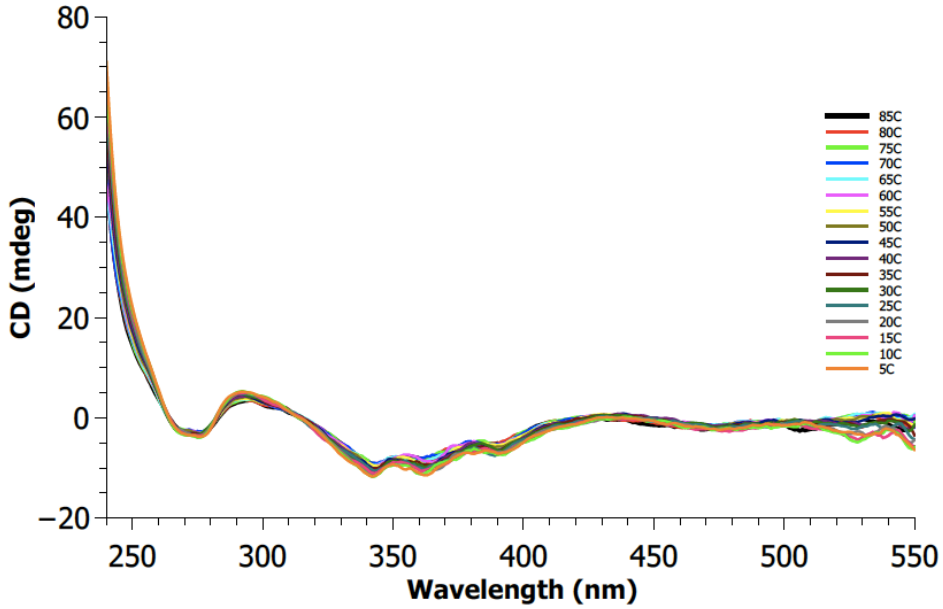

Figure 2-73. Variable temperature CD spectra between 5 – 85 °C of **Cat5*** (D_2O, 245 – 550 nm, 10 mm pathlength cuvette).

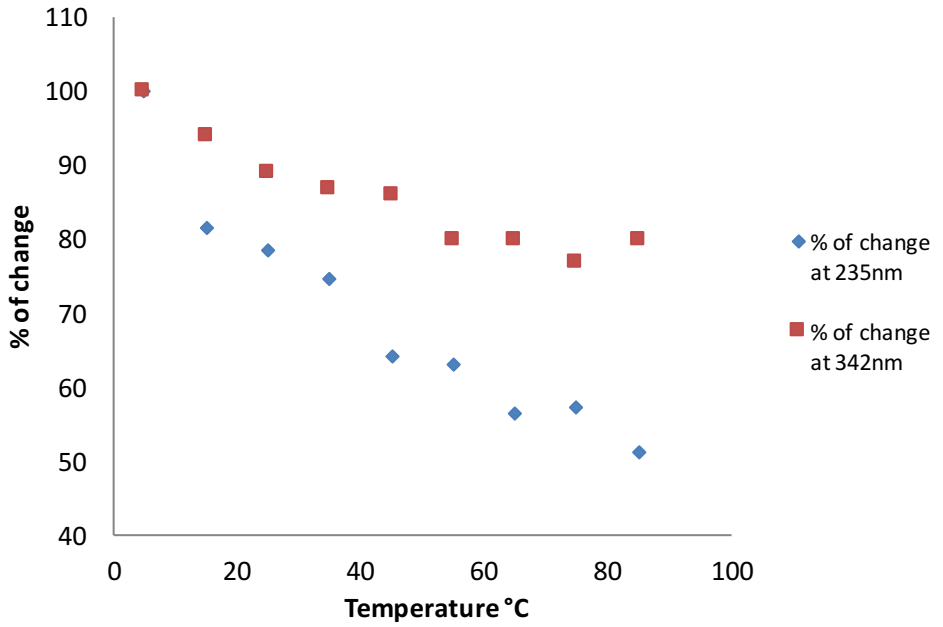

Figure 2-74. The comparison between % of change in two wavelengths (235 and 342 nm) of **Cat5***. This catenane, unlike **Cat5**, displays more flexibility across the cysteine region, and therefore the % of change is greater at lower wavelength.

2.15.10 Synthesis of Cat5 and Cat5* in different conditions

The variation of **A1c** and **A1c*** with **D2S** building blocks ratio has led to the formation of new molecules such as different macrocycles and their identification by HPLC analysis and MS spectra.

As the ratio of two building blocks change from 2:1 to 1:1 (NDI : DN), the formation of **Cat5** and **Cat5*** starts to reduce and instead the formation of heterodimer, heterotrimer and other macrocycles is favoured.

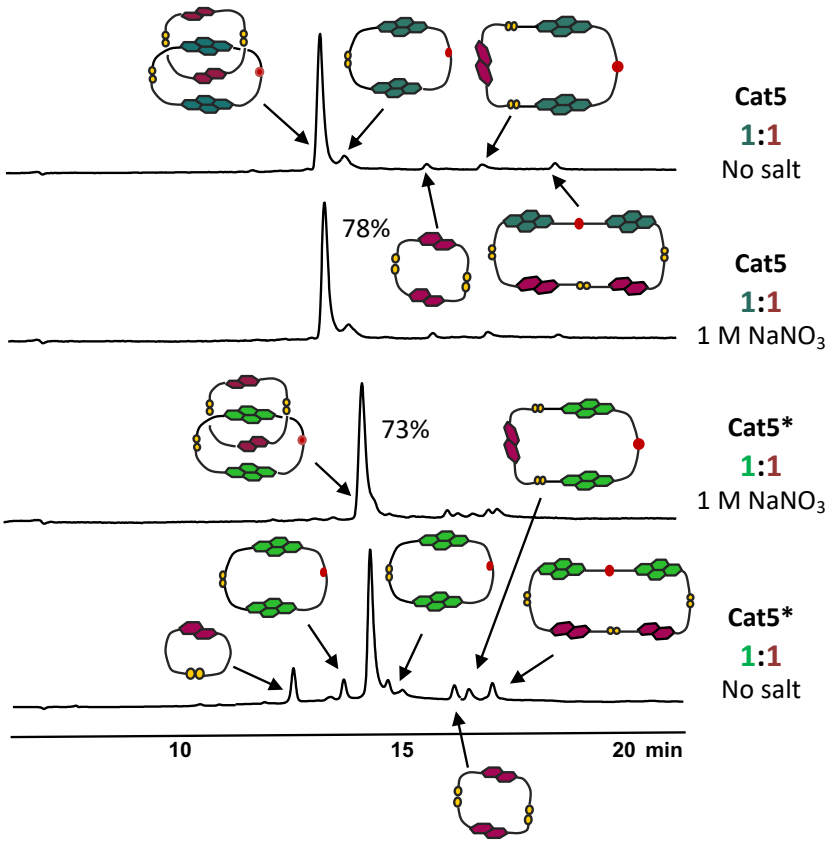

Figure 2-75. The **Cat5** and **Cat5*** catenanes form up to 78 and 73%, respectively, in libraries with 1:1 ratio of the two building blocks. Absorbance was recorded at 254 nm. Identification of new macrocycles was observed.

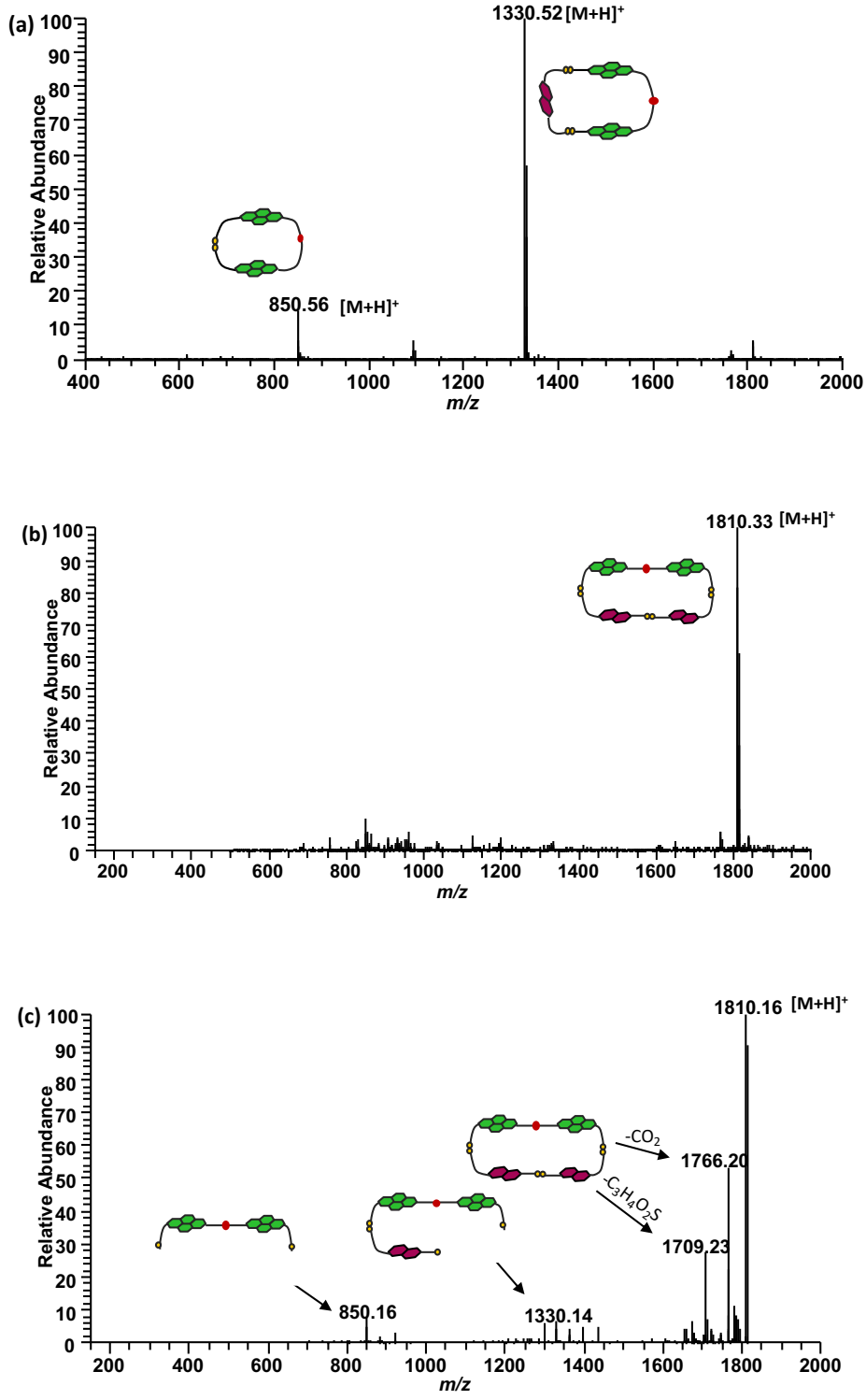

Figure 2-76. ESI-MS (+*ve*) spectra of (a) **[A1c*]** and **[A1c*-D2S]** (as singly charged cation), (b) **Cat5*** (as singly charged cation) and (c) the MS/MS fragmentation spectra of **[A1c*-D1S$_2$]**.

2.15.11 Effect of Tetrabutylamonium Nitrate on Formation of Catenane

It has been proven from previous studies that the addition of salts such as $NaNO_3$ can amplify the formation [2]catenanes by increasing the polarity of the solvent's system. However, addition of templates such as tetrabutylammonium nitrate, Bu_4NNO_3, can have a negative effect on formation of interlocked structures, namely the [2]catenanes because Bu_4N^+ can solvate the NDI surface, and therefore, leads to a different library distribution, amplifying the cyclic **D2S** and cyclic **A1c*** at the expense of the [2]catenane (Figure 2-77).

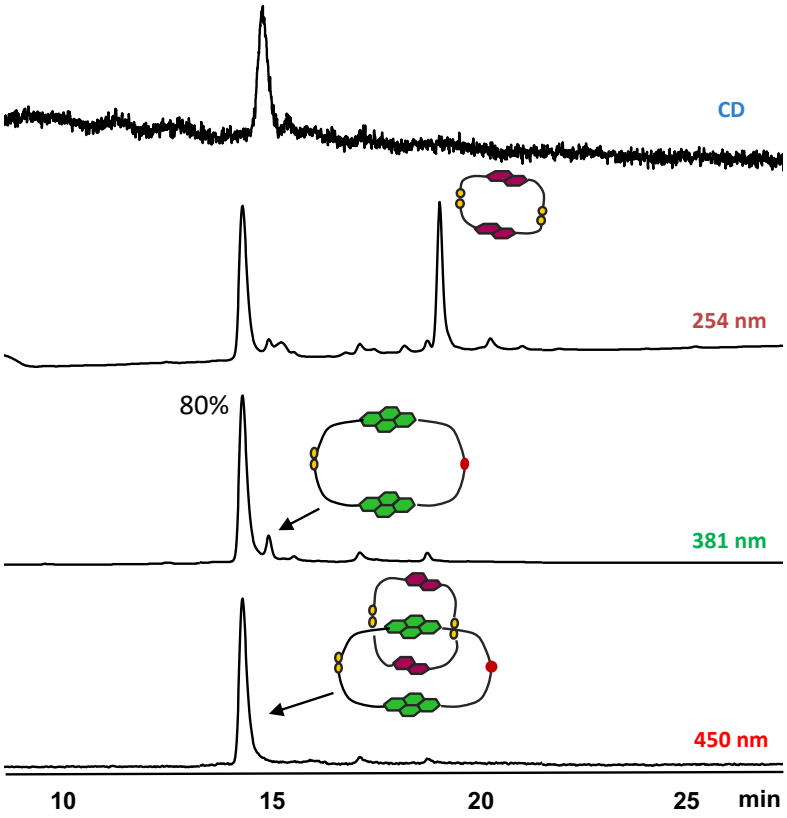

Figure 2-77. Effect of Bu_4NNO_3 salt on the library's distribution (5 mM, H_2O, 1 M Bu_4NNO_3 salt, pH 8.5).

In the library with Bu_4NNO_3 salt, Bu_4N^+ competes with the NDI to fit into the DN dimer and reduces the formation of [2]catenane. However, the library with Bu_4NNO_3 still forms the [2]catenane up to 80%, which illustrates the affinity of NDI for DN and how this overcomes the Bu_4NNO_3 effect.

2.15.12 Effect of Polarity of solvent on Formation of Catenane

In order to provide a comprehensive study about the effect of solvent polarity on formation of [2]catenanes (**Cat5** and **Cat5***), the libraries were set-up in a lower polarity solvent (acetonitrile:water 1:1 ratio). The results from HPLC show that the addition of acetonitrile reduces both the polarity of solvent and the percentage yield of the catenane (Figure 2-78).

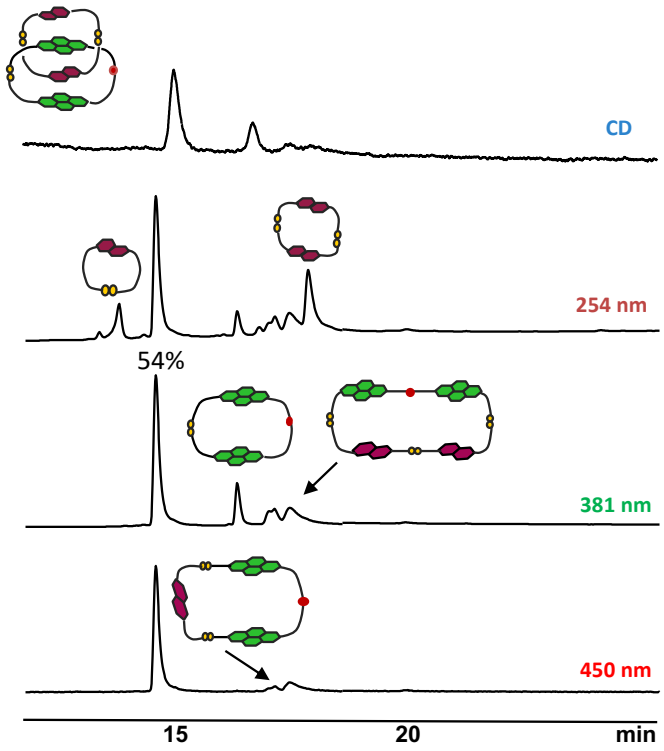

Figure 2-78. Effect of acetonitrile-water mixture (1:1) on the library distribution after 24hr stirring at room temperature (5 mM, H_2O, pH 8.5).

Figure 2-79 demonstrates the formation of **Cat5*** over time in water : acetonitrile solvent mixture. At the beginning of the library there is no sign of the [2]catenane and even after 215 min, when usually the libraries in water have already formed the catenane, there is a very small percentage of **Cat5*** present. The slow formation of [2]catenane is normal as the less polar solvent is stabilising the macrocycles and slows the formation of tighter structures (by decreasing the hydrophobic effect).

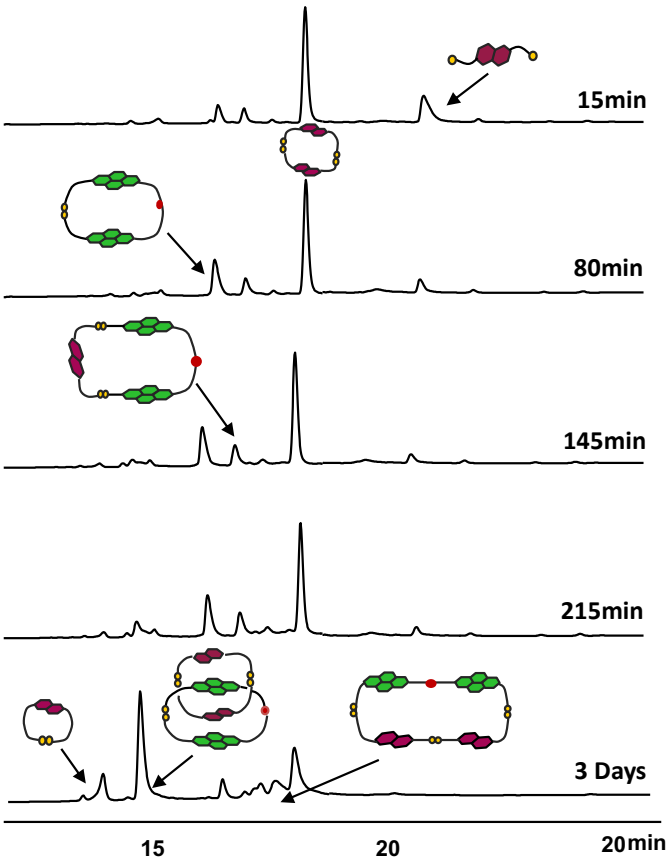

Figure 2-79. The kinetic study showing the gradual process of **Cat5*** formation over time. The kinetic of **Cat5*** formation is slower in acetonitrile-water than only in water. Absorbance was monitored at 254 nm.

2.16 Identification of a New [2]Catenane Using Different Donor Building Block

Since **A1c** and **A1c*** acceptor building blocks have showed promising results towards synthesising [2]catenanes in very high yields, their interaction with a different donor building block was also examined. The new donor building block (**BDT**) has a benzodithiophene core, which acts as the electron rich moiety and consists of two cysteines on each sides of the molecule that allows for the disulfide exchange and provides solubility. This molecule was synthesised by Tiberiu M. Gianga in the Pantoș' group.

A D-A DCL of **A1c*** and **BDT** (benzodithiophene) was set up in water, pH 8.5, and stirred for one day prior to analysis. The LC-MS analysis has revealed that the fully oxidised library contains a [2]catenane in a very high yield of 90% (**Cat-BDT***).

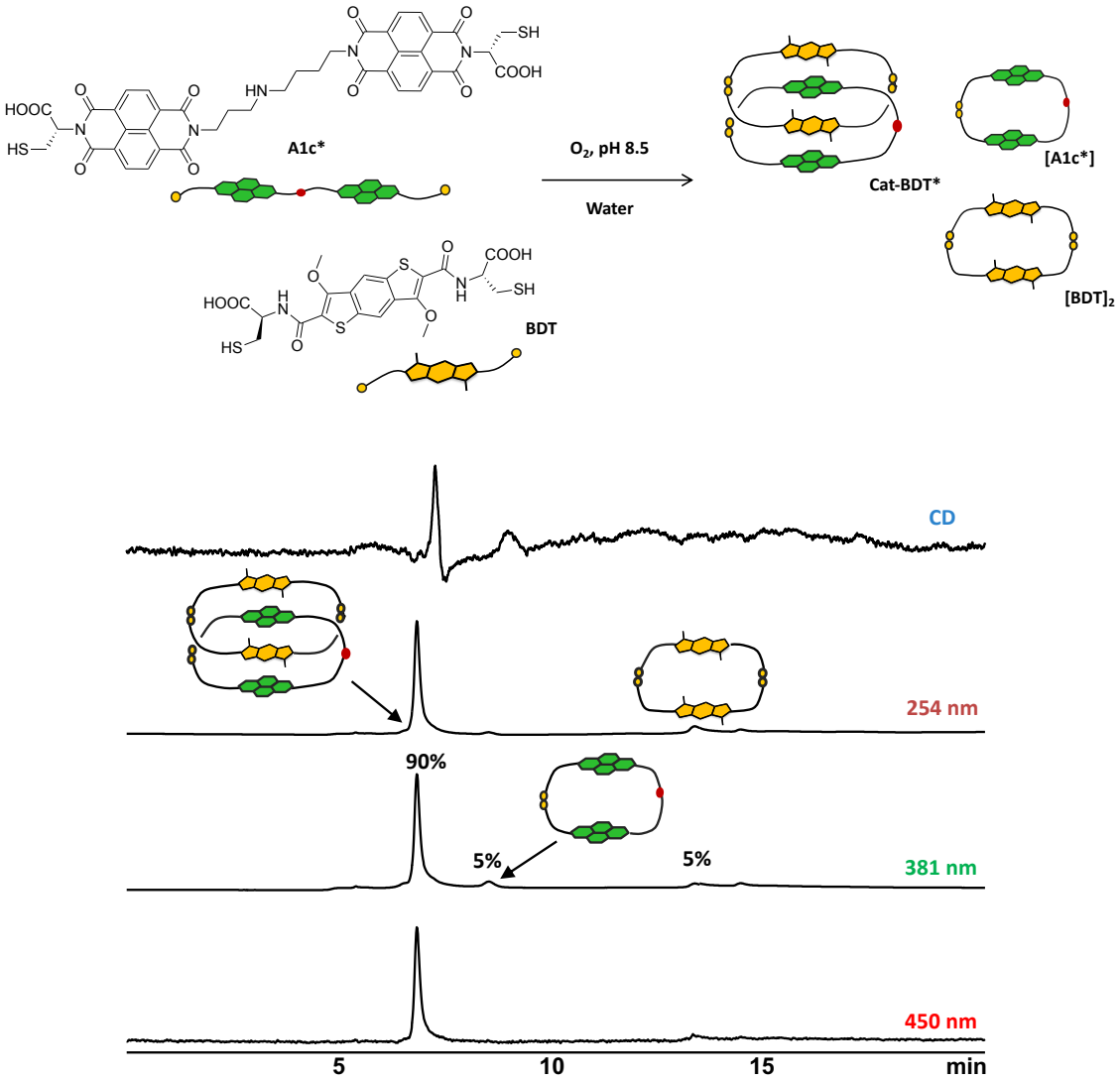

Figure 2-80. The HPLC analysis of **A1c*** and **BDT** (1:2 molar ratio, 5 mM total concentration).

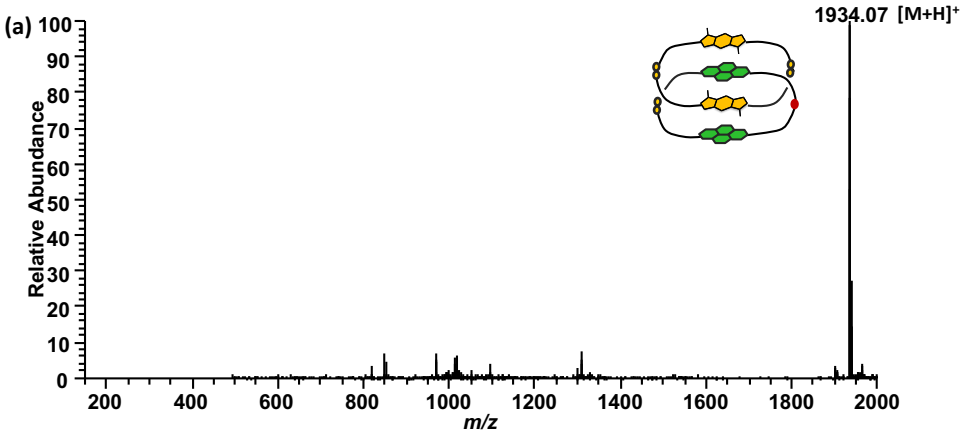

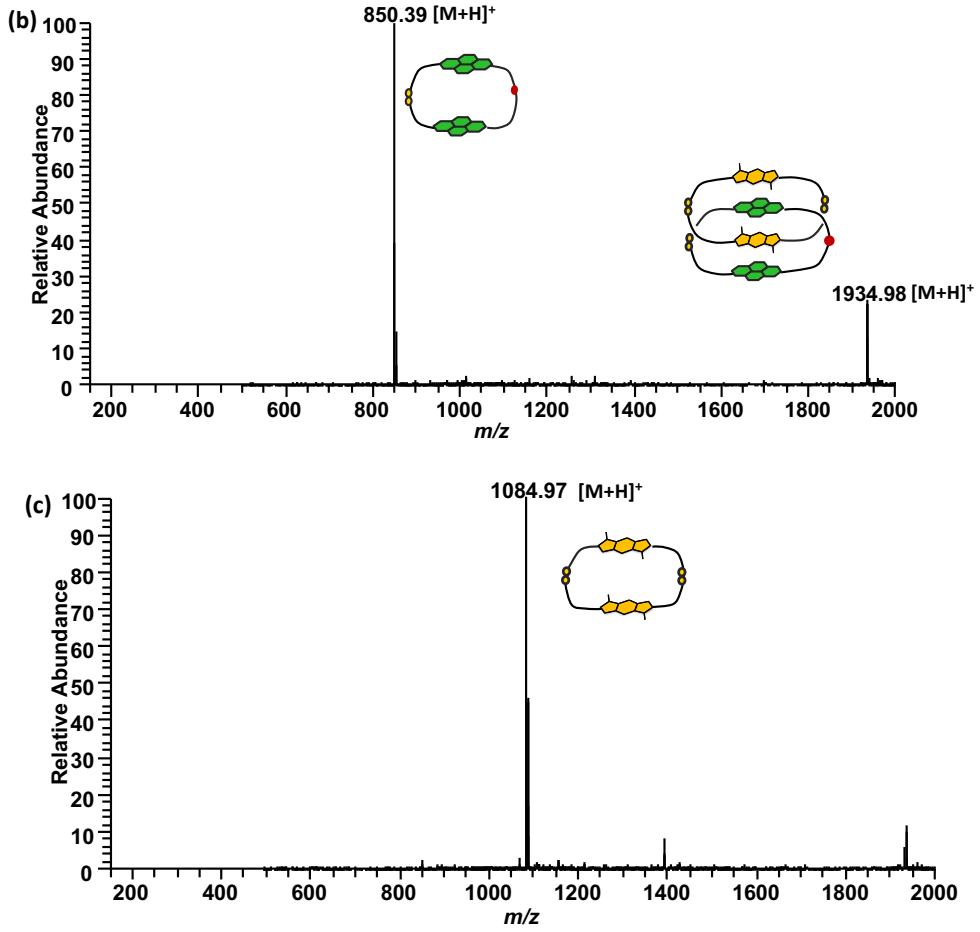

Figure 2-81. ESI-MS (+*ve*) spectra of (a) **Cat-BDT*** (as singly charged cation), (b) the **[A1c*]** (as singly charged cation) and (c) the **[BDT]**$_2$ dimer (as singly charged cation).

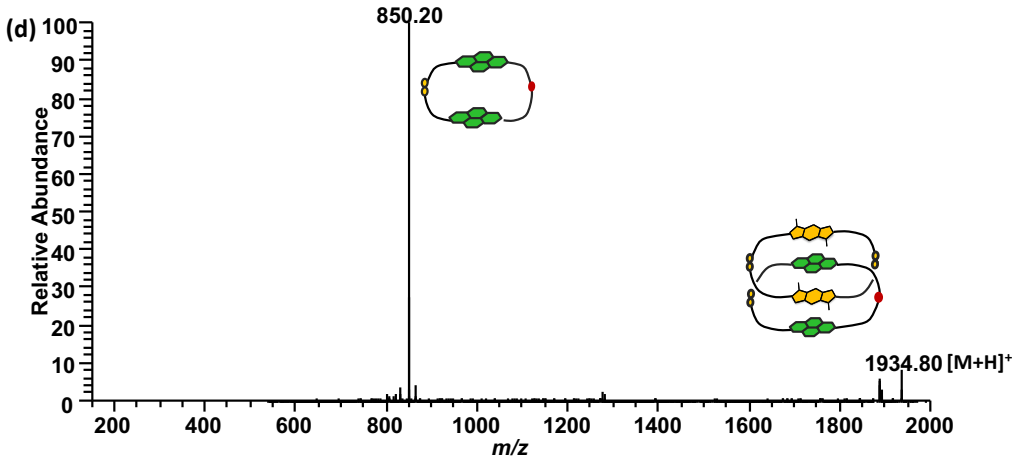

Figure 2-82. MS/MS fragmentation spectra of (d) **Cat-DBT***.

These results have indicated that, by changing the donor building block from **D2S** to **BDT**, the [2]catenane is still formed in a remarkable high yield.

2.16.1 NMR Characterisation of Cat-BDT*

The peak represents the [2]catenane was not isolated by preparative HPLC because it already contained 90% of the **Cat-BDT***. The library was directly subjected to NMR studies and analysed by ^{1}H, COSY and NOESY NMR spectroscopy.

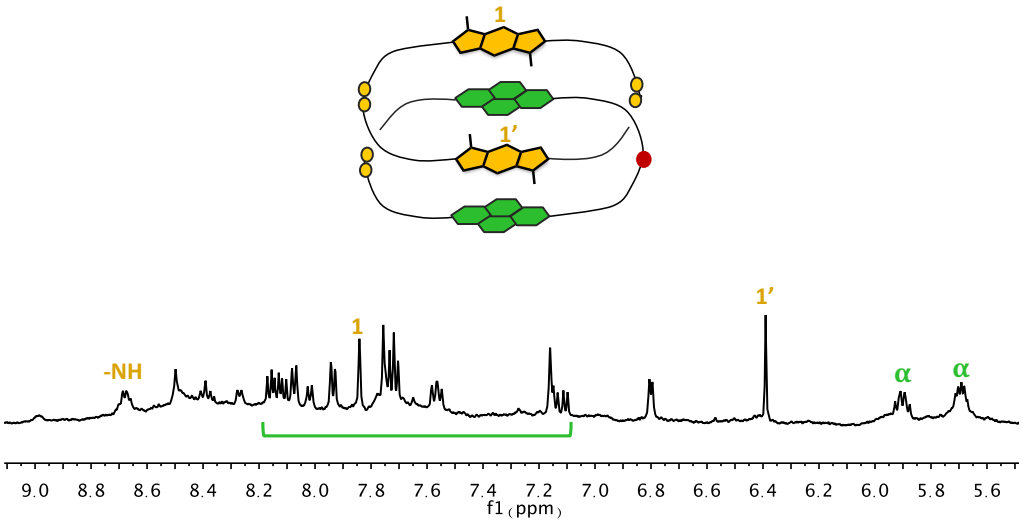

Figure 2-83. Partial ^{1}H NMR spectrum of the **Cat-BDT*** in D_2O (500 MHz, 296 K). The solvent peak was referenced at 4.74 ppm.

This catenane similar to **Cat5** and **Cat5***, has four diastereomers, therefore, a very complex spectrum has been expected. The analysis of the acceptor, donor and **α**, **β** regions by combination of the ^{1}H, COSY, NOESY has allowed the correlation of the signals corresponding to each of the four isomeric catenanes.

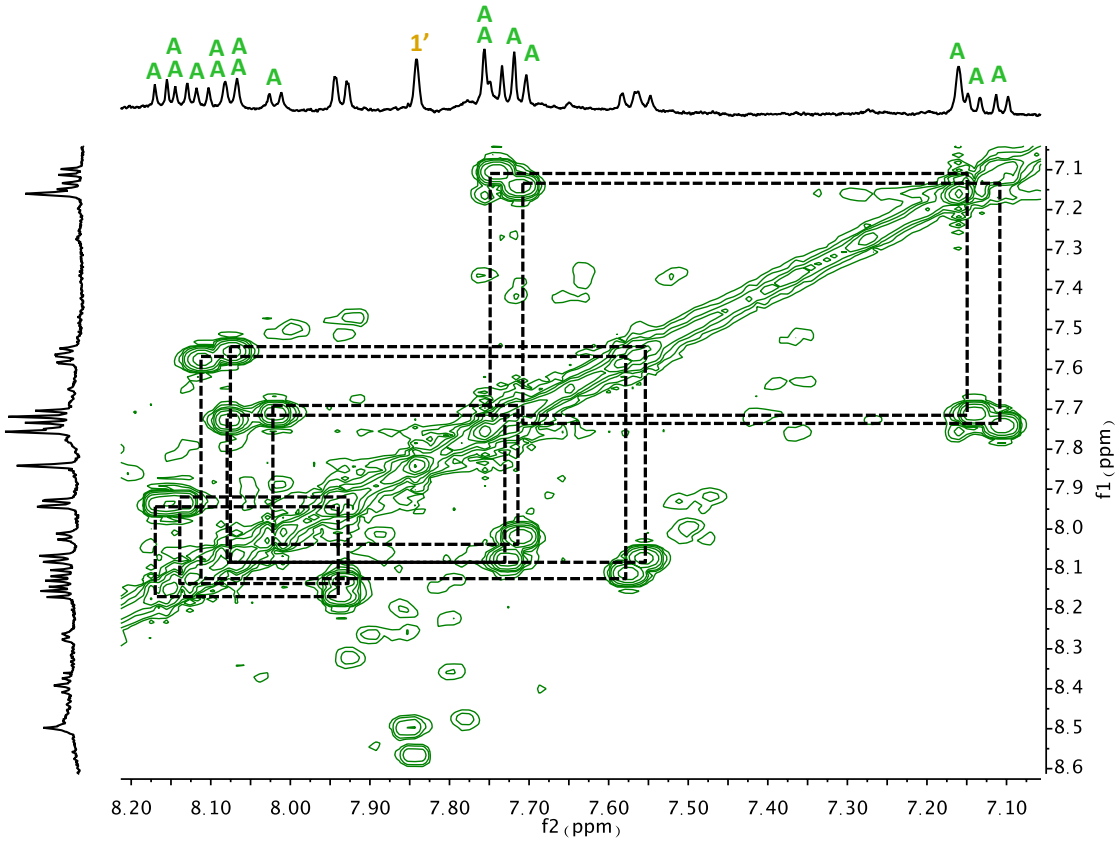

Figure 2-84. Partial COSY spectrum of **Cat-BDT*** in the NDI region between 7.00 and 8.20 ppm (D_2O, 500 MHz, 296 K). The dotted lines highlight peaks connected through chemical exchange. The solvent peak was referenced at 4.74 ppm.

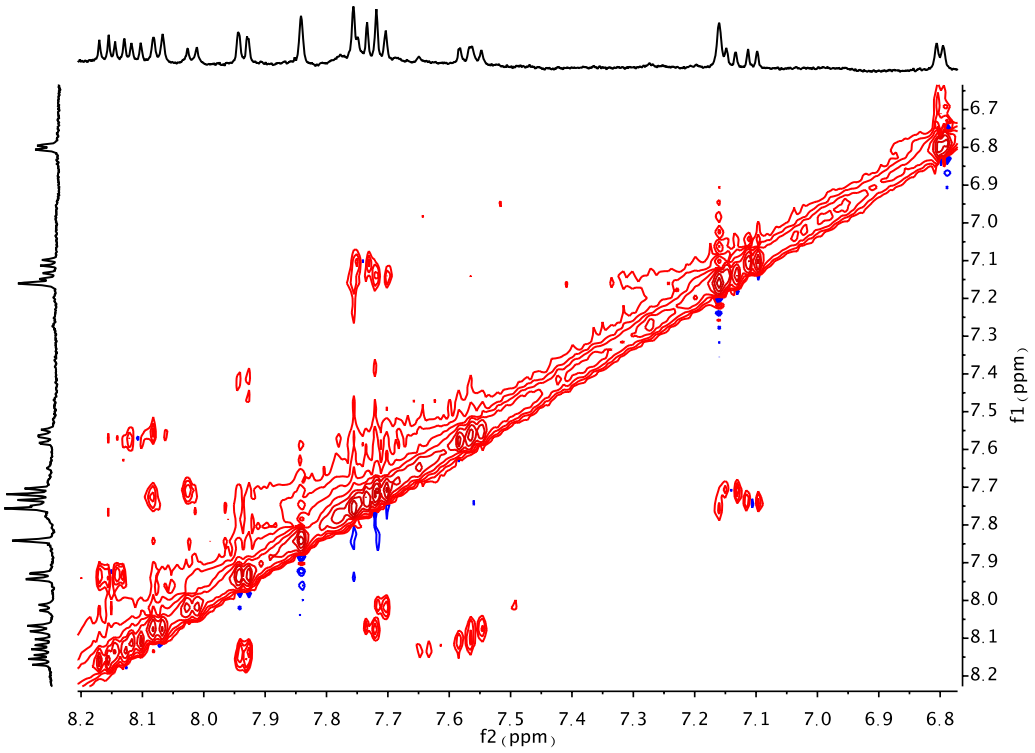

Figure 2-85. Partial NOESY spectrum of **Cat-BDT*** across 6.75 – 8.20 ppm region (D_2O, 500 MHz, 296 K) the solvent peak was referenced at 4.74 ppm.

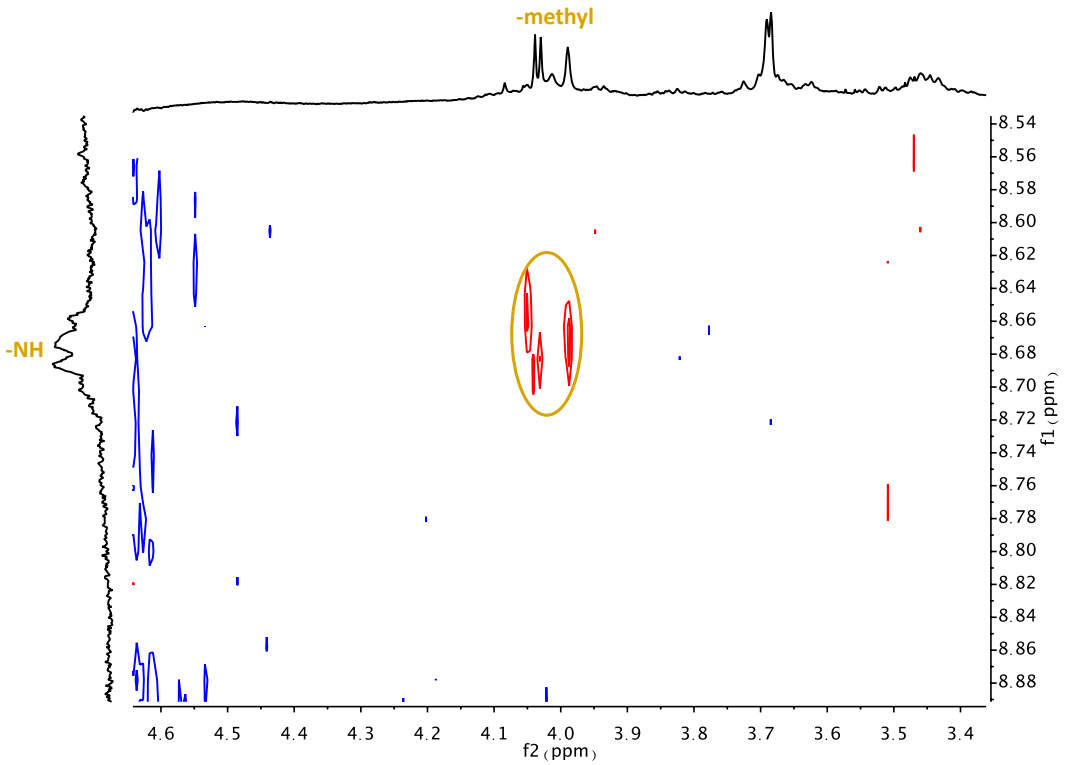

Figure 2-86. Partial NOESY spectrum of **Cat-BDT*** shows the correlation between the methyl and -NH on the **BDT** (D_2O, 500 MHz, 296 K), the solvent peak was referenced at 4.74 ppm.

2.17 DCL of A1c Acceptor and D1L Donor: Cat6

The LC-MS analysis of D-A DCL of **A1c** with **D1L** has revealed that the fully oxidised library contains the classical DADA catenane in 52% (**Cat6**) along with a series of macrocycles (Figure 2-87).

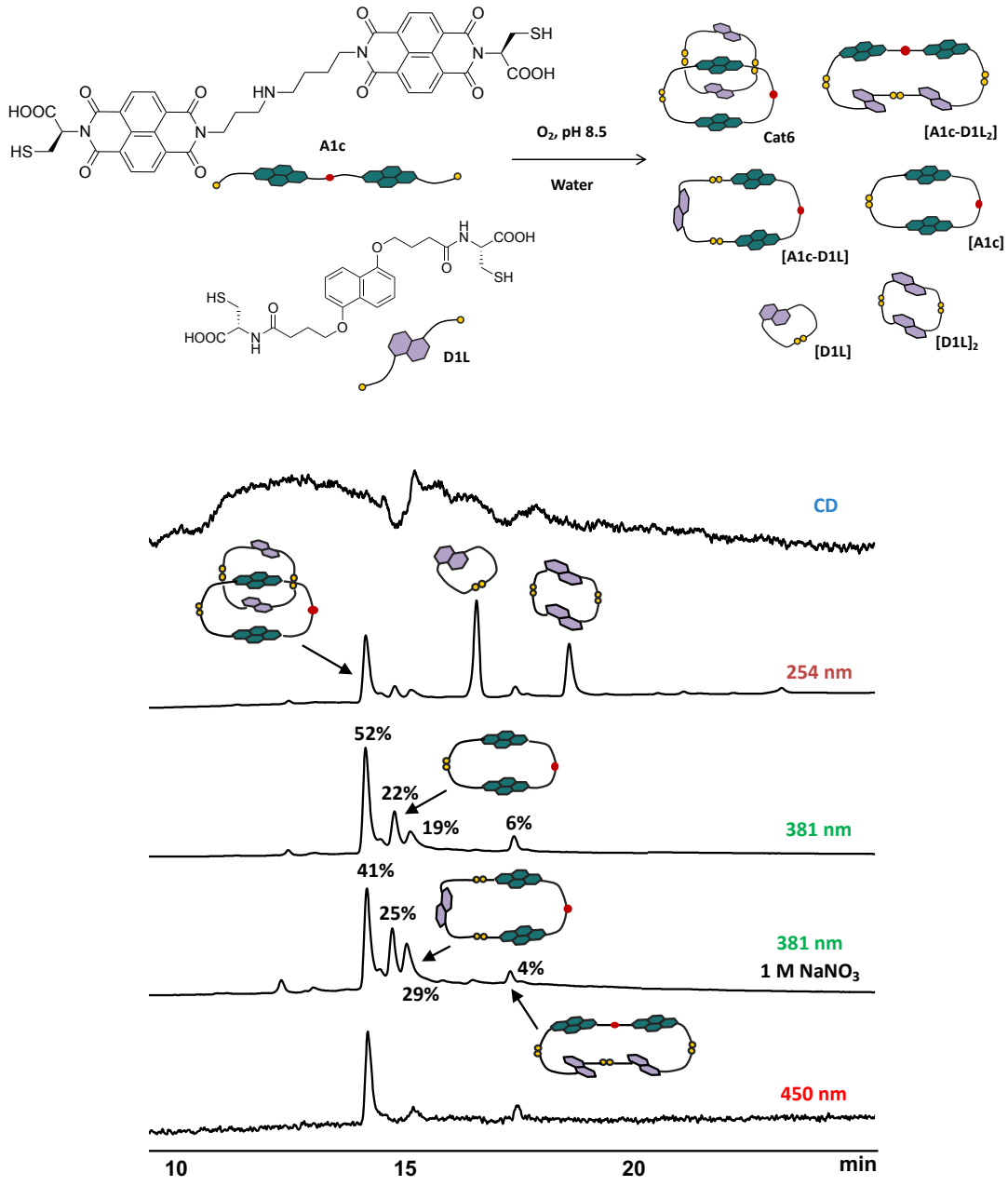

Figure 2-87. The HPLC analysis of D-A DCL of **A1c** and **D1L** (1:2 molar ratio, 5mM total concentration). Estimated yield is indicated above the corresponding peaks.

The concentration of **Cat6** decreases upon addition of $NaNO_3$ (by 11%) at the expense of heterodimer **[A1c-D1L]**, which increases by 10%. This means the packing in **[A1c-D1L]** is

much tighter and the arrangement of the aromatic moieties is better in terms of their contact with the solvent than in **Cat6**. Thus, another possible arrangement for **[A1c-D1S]** to minimise its surface area and form a very tight packing is shown in Figure 2-88. This arrangement is achievable with the longer and more flexible DN (the longer arms make the DN more flexible and allow for the folding inside the A1c cavity).

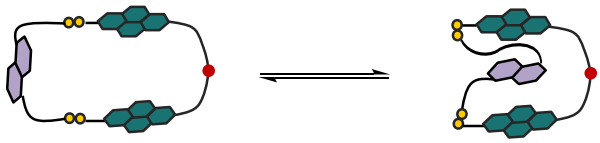

Figure 2-88. The two possible arrangements in **[A1c-D1L]**.

In ESI-MS analysis, the mass for some of the molecules is observed to overlap and this is due to the partial co-elution with the neighbouring molecules.

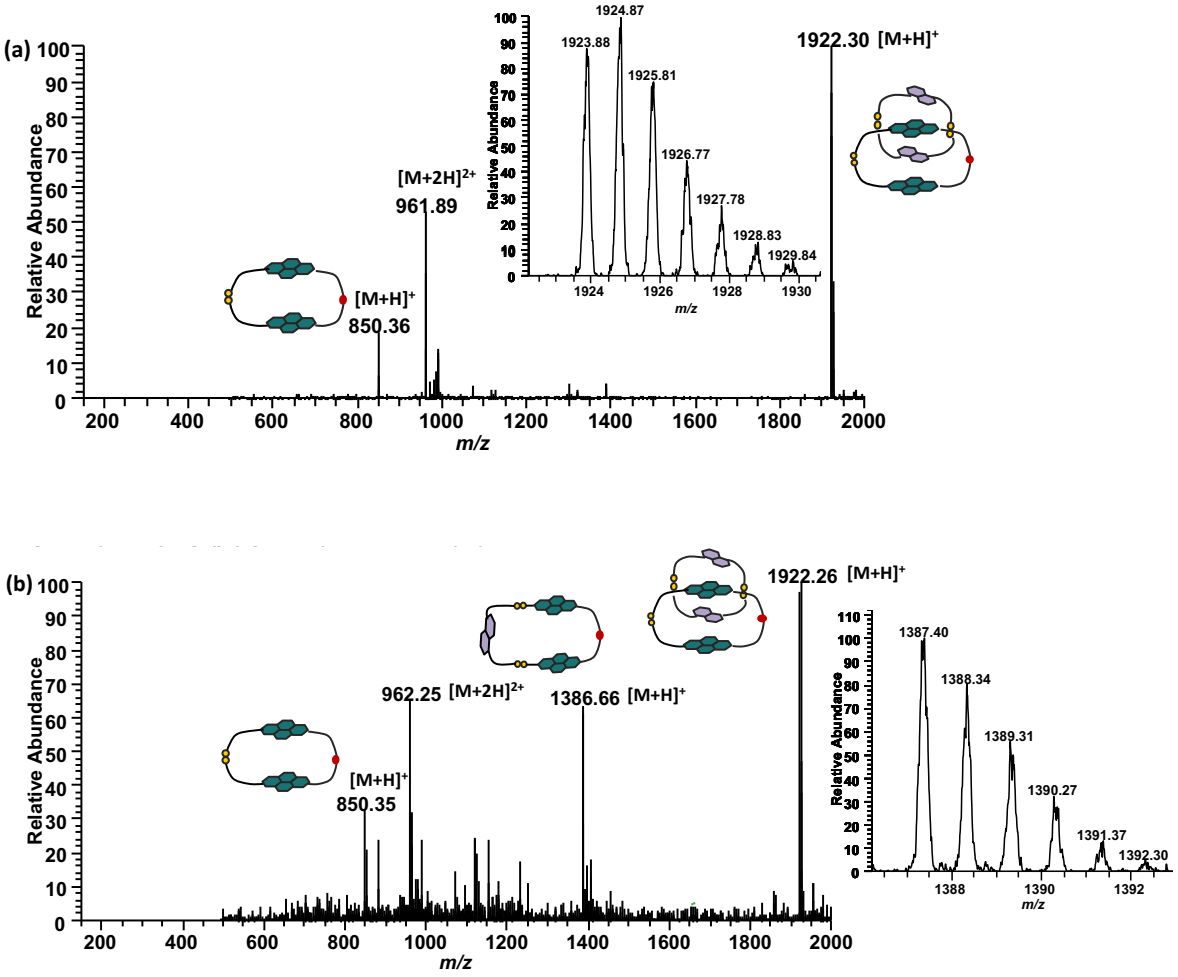

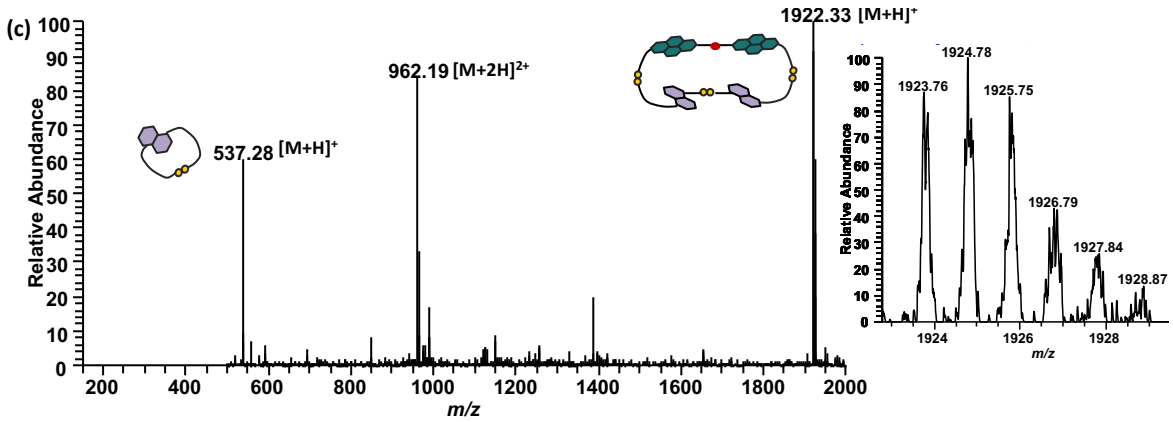

Figure 2-89. ESI-MS (+*ve*) spectra of (a) **Cat6** (as singly charged cation), (b) the heterodimer **[A1c-D1L]** (as singly charged cation), (c) the heterotrimer **[A1c-D1L$_2$]** (singly charged cation). The expansion of parent molecular ions is shown as inserts.

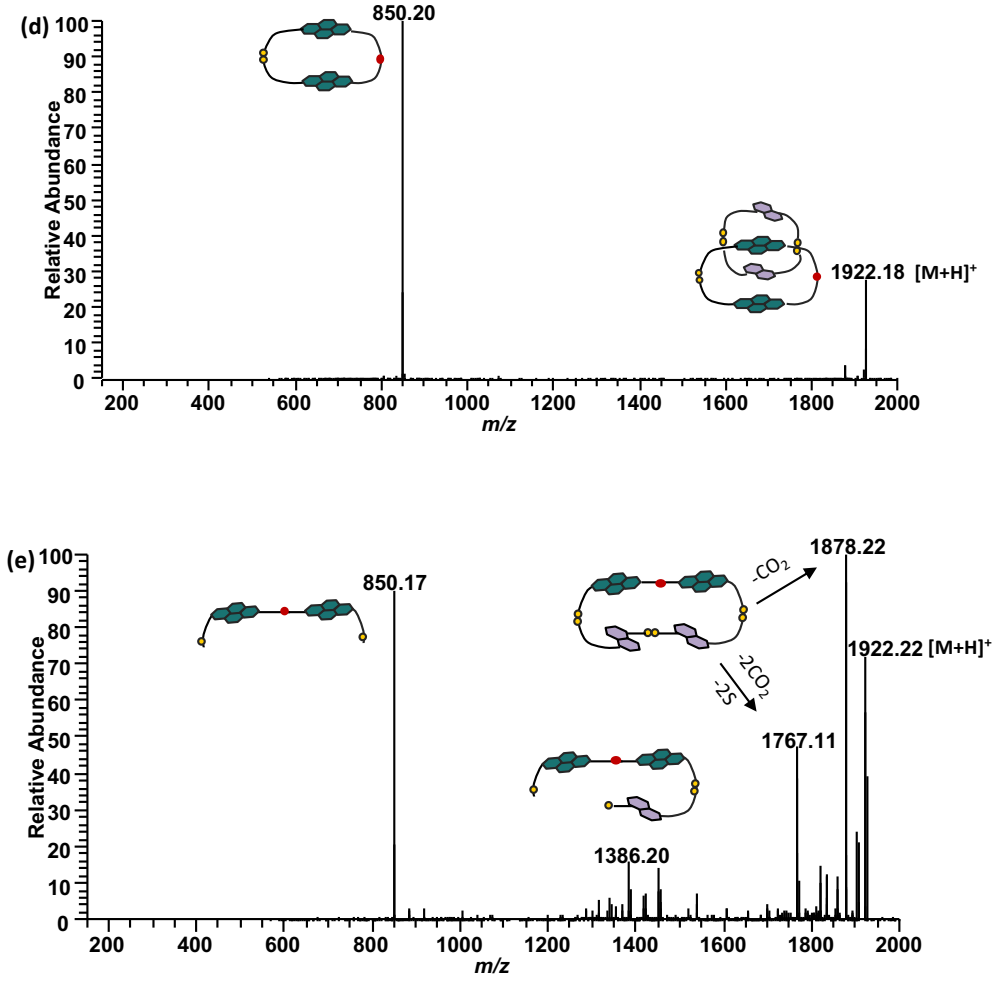

Figure 2-90. MS/MS fragmentation spectra of (d) **Cat6** and (e) heterotrimer **[A1c-D1L$_2$]**.

2.18 D-A DCL of A1c Acceptor and D2L Donor: Cat7

The LC-MS analysis of D-A DCL of **A1c** with **D2L** has indicated that the fully oxidised library also contains the classical DADA catenane in 58% (**Cat7**) along with a series of macrocycles (Figure 2-91). This library has similar distribution to the one with **D1L**, and the effect of $NaNO_3$ is the same for both libraries, where the catenane's concentration decreases in favour of the heterodimer. The concentration of **Cat7** slightly decreases, while the concentration of **[A1c-D2L]** increases (from 58 to 51% for **Cat7** and from 28 to 32% for **[A1c-D2L]**).

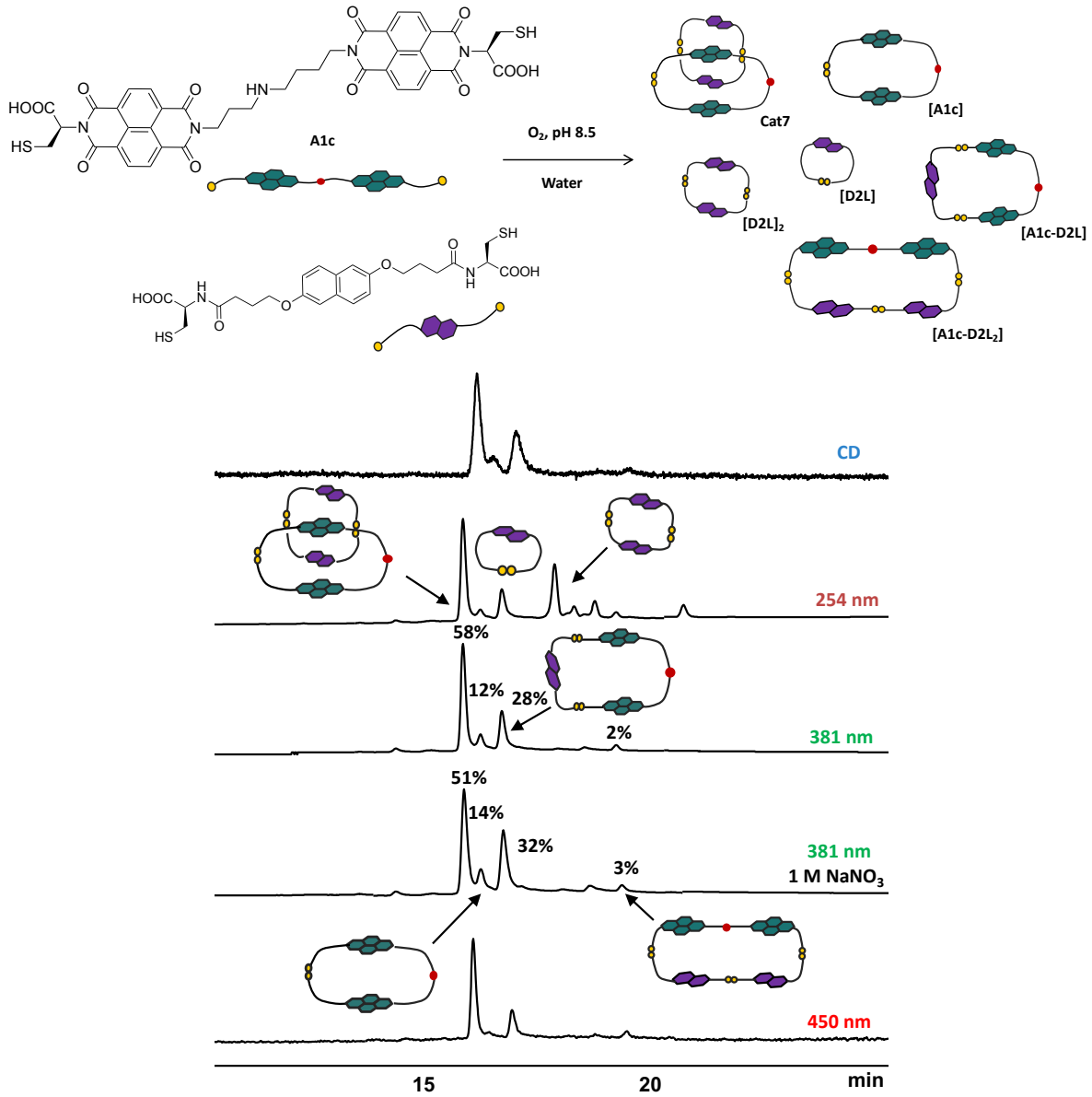

Figure 2-91. The HPLC analysis of D-A DCL of **A1c** and **D2L** (1:2 molar ratio, 5 mM total concentration). Estimated yield is indicated above the corresponding peaks.

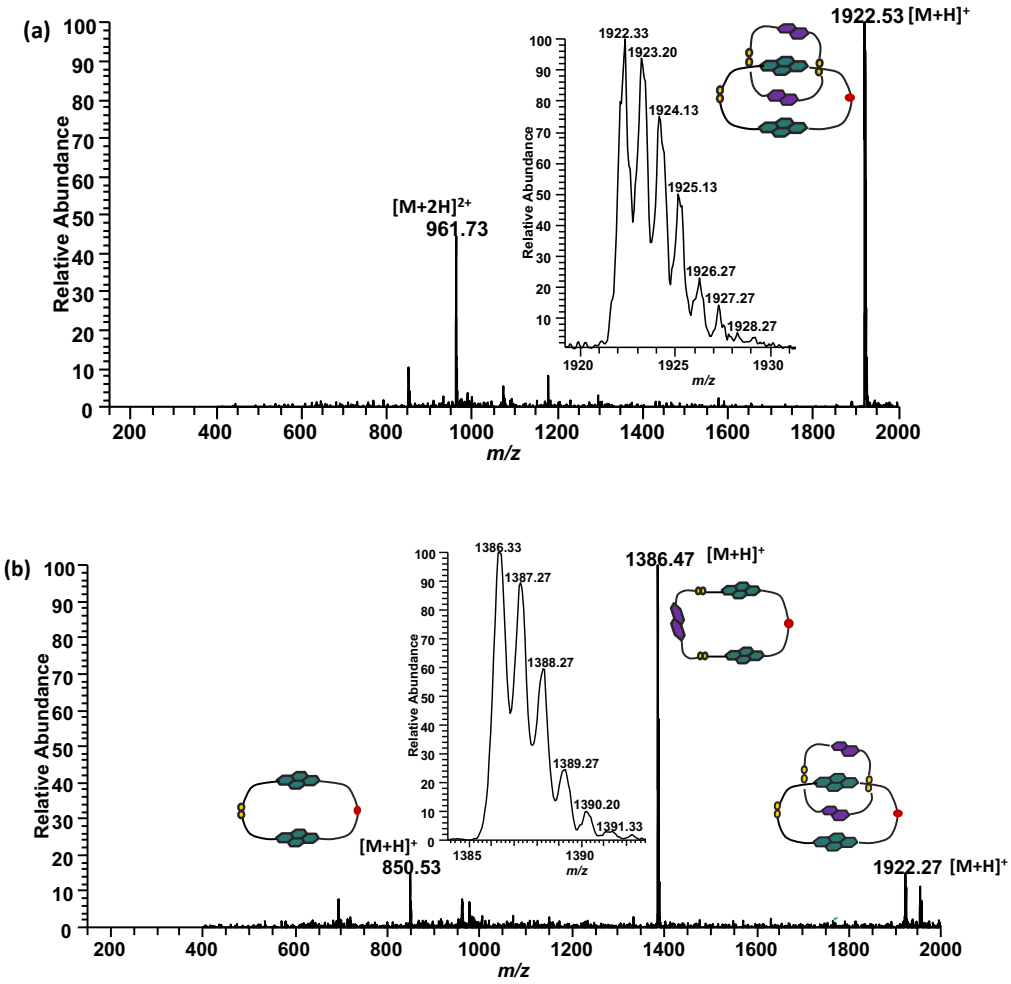

Figure 2-92. ESI-MS (+*ve*) spectra of (a) **Cat7** (as singly charged cation) and (b) the heterodimer **[A1c-D2L]** (as singly charged cation). The expansions of parent molecular ions are shown as inserts.

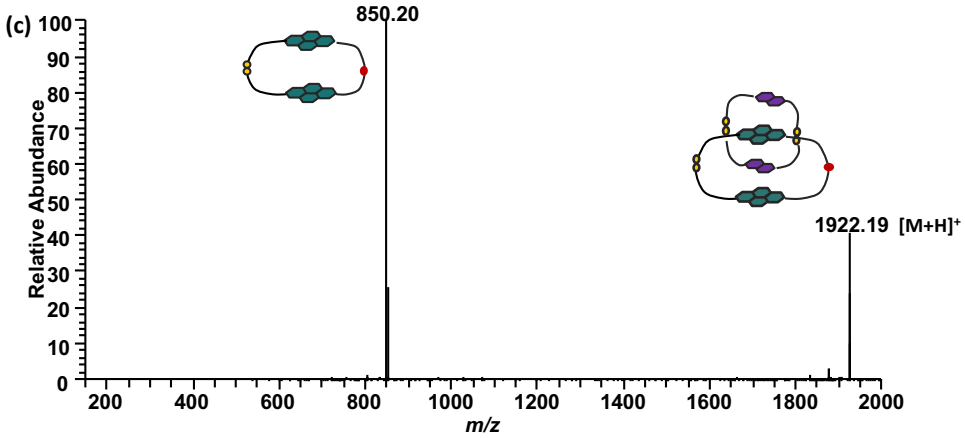

Figure 2-93. MS/MS fragmentation spectra of **Cat7**.

2.19 Conclusion

In conclusion, the **D2S**, **D1L** and **D2L** building blocks make stable dimers [-D-D-], which is an important intermediate for the formation of DADA [2]catenanes. **D1S,** however, has not been the best donor candidate for the formation of [2]catenanes, as the catenane yield obtained with each acceptor (**A1b** and **A1c**) was low.

The formation of the [2]catenanes in these libraries strongly depends on the length of the linker connecting the two NDI molecules. As shown in Figure 2-94, **A1a** can only make macrocycles when using different DN building blocks with no sign of catenation; the formation of the [2]catenane starts to increase by using longer linkers (**A1b** and **A1c**). In the case of **A1b**, the proportion of [2]catenane in DCLs is not very high, but when the polyamine with eight atoms in the linker (spermidine) is used, the catenane is formed in much greater yield (up to 93%). The **A1c** acceptor has formed catenanes in the highest yield compare to other two acceptor molecules (**A1a** and **A1b**), and it shows how the efficiency of the DADA catenane formation is linked to the size of the cyclic acceptor ring. The HPLC, MS, NMR, UV and CD results all confirm the formation of **Cat5**, and we learned that even by changing the chirality of cysteine for **A1c**, a similar library with an identical distribution is formed, and that the catenane (**Cat5***) is assembled equally efficiently.

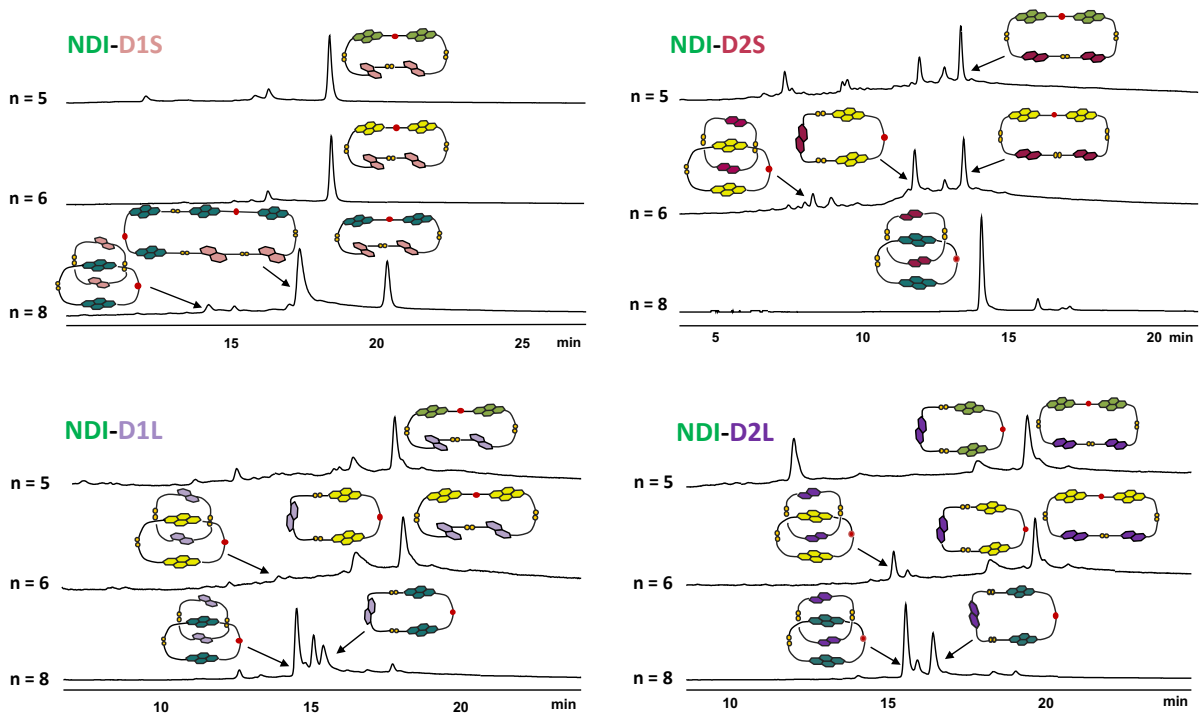

Figure 2-94. HPLC chromatograms comparison of **A1a**, **A1b** and **A1c** acceptors with **D1S**, **D2S**, **D1L** and **D2L** donors. Absorbance was recorded at 381 nm.

As shown in Figure 2-94, the formation of a catenane when using the 1,5-DN (**D1S**) donor is limited compared to **D1L**. For example, **A1b** acceptor does not form a catenane with **D1S**, but the reverse is true when **D1L** donor is used in the DCL. Similar behavior was observed for **A1c** that formed the catenane with **D1S** in low concentration; better yield was achieved for the analogous species containing **D1L**. This shows that a slightly longer chain on the donor building block makes the DN dimer more flexible and its cavity more suitable to fit an NDI moiety. The opposite is true when the 2,6-DNs are used as donor building blocks; the catenanes assemble in better yield with **D2S** than **D2L**, indicating that the overall donor ring size is influenced not only by the cysteine-terminated linkers, but also by the geometry of the DN.

The use of $NaNO_3$ to increase the polarity of the system also has interesting impact on our libraries. Previous studies have showed that the increase of the system's polarity favours the formation of interlocked molecules. This is due to the solvophobic effect and the way the aromatic scaffolds remove themselves from the interaction with the solvating environment, thus forming a more compact structure. In some of our library, especially the ones with **D1L** and **D2L**, a lower percentage of the catenane and more of the macrocycles (either their isomer or the heterodimer) is obtained when increasing the polarity of the DCL. This means that those macrocycles have better packing than the catenane, *i.e.,* the interaction of aromatic moieties with the solvent is minimised. All the libraries discussed in this chapter are red-coloured aqueous solutions, which indicates the presence of charge-transfer interactions between the complementary aromatic units, although not all libraries form catenanes or other interlocked molecules. This suggests that, for those libraries forming only macrocycles, there are charge-transfer interactions between the aromatic units (the macrocycle rings could be very tight and lead to this charge-transfer or, for the larger species, they can fold in a way that the NDI and DN cores are in close proximity).

In this chapter, we learned that the length of the linker connecting two NDIs is very important,as it drives the formation of either interlocked molecules or macrocycles. The nitrogen atom in the linker has increased the flexibility of cyclic monomers or dimers (bringing the aromatics in close proximity). Therefore, this does not allow the DN to thread inside the cavity and form interlocked molecules such as [2] or [3]catenanes. Also, the nitrogen in the linker prevents the formation of all acceptor [2]catenanes because in its protonated state it makes the interaction with aromatic surfaces less favourable that the hydration of the positive charge.

Chapter 3

3.1 NDI-based Building Blocks in This Chapter: A2a, A2b and A2c

The building blocks described in this chapter are dumb-bell NDI-based molecules with two nitrogen atoms in their linker. These three molecules have longer polyamine-based linkers when comparing to the three building blocks discussed in Chapter 2, with the shortest building block being **A2a** with eight atoms in the linker and longest **A2b** containing ten atoms in the linker. **A2a** has the same number of atoms (n = 8) as **A1c**, which produced a [2]catenane up to 93%, so here we can investigate the effect of replacing a carbon atom with a nitrogen atom on the library's distribution.

A2a and **A2b** both have two carbon atoms between the nitrogen atoms, whereas **A2c** has three carbon atoms between its two nitrogen atoms. This, along with the length of the linker, will affect the flexibility of molecule and therefore, the library's distribution.

The two nitrogen atoms in the linker make the molecules poorly soluble in water. Thus, the libraries of building blocks by themselves form poorly water-soluble cyclic monomers, making their analysis difficult.

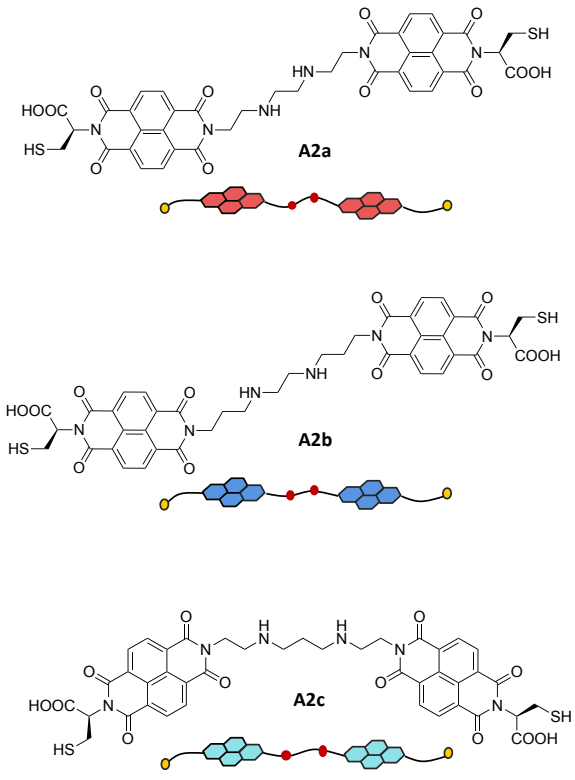

Figure 3-1. The three NDI-based molecules used in this chapter (**A2a**, **A2b** and **A2c**).

3.2 DCL of A2a-Dithiol Acceptor

The DCL of **A2a** acceptor was generated by dissolution of the building block in water (5 mM concentration) and the pH was adjusted to 8.5 using an aqueous solution of 100 mM NaOH. The library was stirred for one day under air in capped vial to allow full oxidation of the thiols.

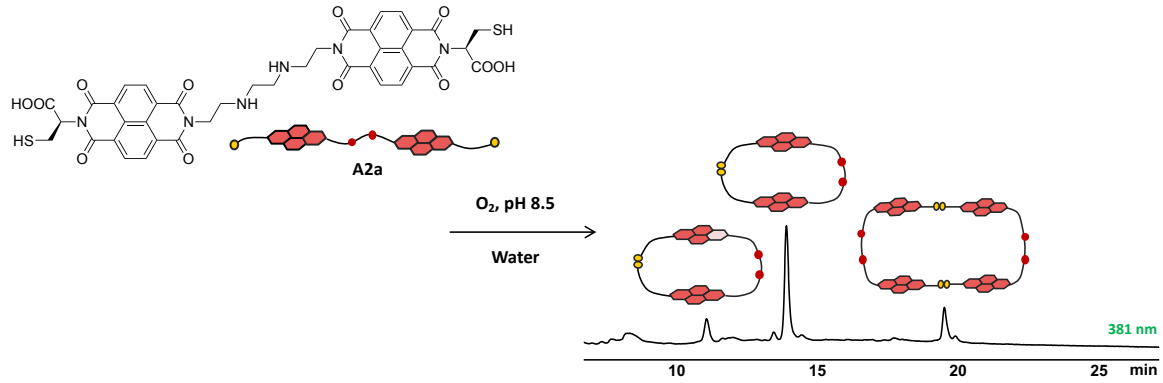

Figure 3-2. The HPLC analysis of **A2a** library in water. Absorbance was recorded at 381 nm.

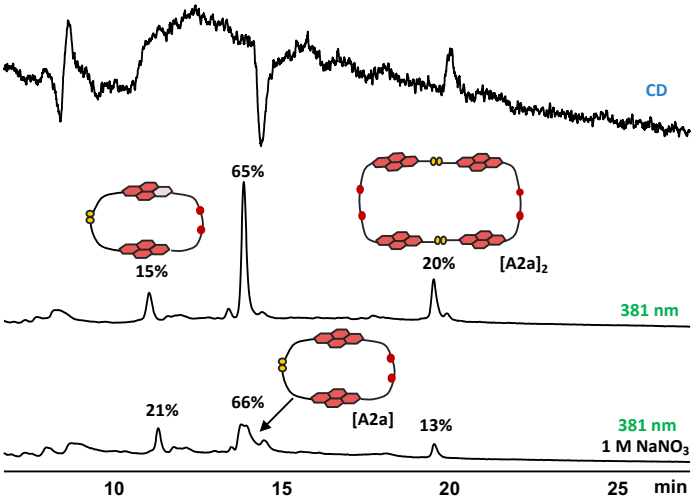

Figure 3-3. The HPLC analysis of **A2a** library in water with and without 1 M $NaNO_3$. Absorbance was recorded at 381 nm and CD was also recorded at 381 nm. Estimated yields are indicated above the corresponding peaks.

The DCL of **A2a** building block by itself shows three major components at equilibrium. The first peak at 11.4 min corresponds to the hydrated cyclic monomer formed up to 21% (represented by light pink colour on the cartoon representation of the molecule). The peak at 14.0 min is the cyclic monomer of **A2a**, which forms up to 66%. The building blocks with longer polyamine chains produce more of the cyclic monomer rather than dimers. The dimer **[A2a]$_2$** forms up to 20% in the library without $NaNO_3$ and in the library with $NaNO_3$, its

concentration reduces to 13% due to hydrophobic effect. In the HPLC chromatogram of the library containing $NaNO_3$, the peaks have low intensity, which is due to the low solubility of building block in water and possibly the formation of the cyclic monomer, which is the main component in this library. The cyclic monomer has a compact structure and tends to precipitate from the solution (further details provided in Chapter 2), therefore making the samples laborious to study as the solutions have to be filtered before analysing them by HPLC or MS.

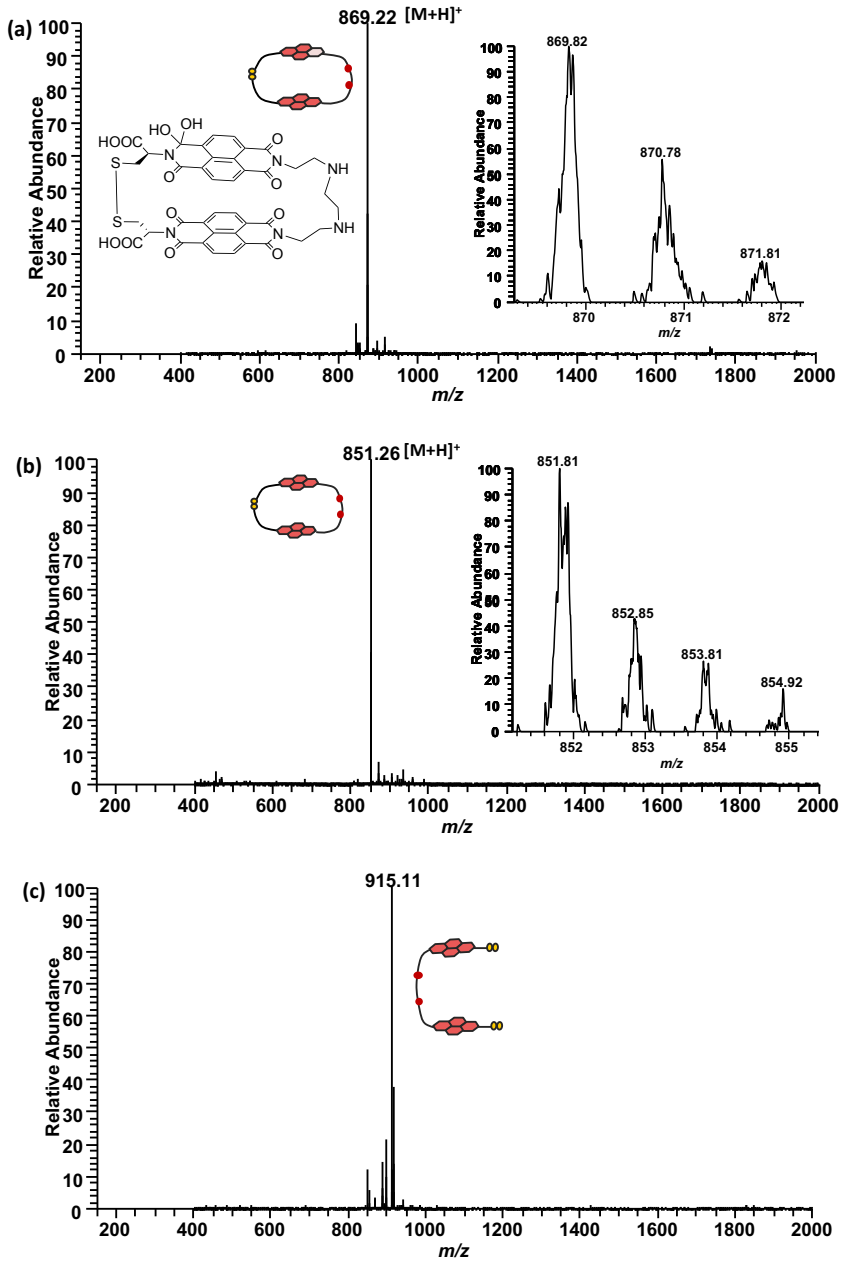

Figure 3-4. ESI-MS (+*ve*) spectra of (a) **A2a** cyclic monomer hydrated on one of the carbonyl groups (as singly charged cation), (b) **[A2a]** (as singly charged cation) and (c) **[A2a]$_2$** fragmented (as doubly charged cation). Expansions of molecular ion are shown as inserts.

3.3 D-A DCL of A2a Acceptor and D1S Donor

The D-A DCL was prepared from the acceptor **A2a** and the short, rigid donor building block **D1S** in water at pH 8.5. The solution was stirred for one day before analysing it by HPLC and LC-MS. Although different ionisation methods and techniques have been involved, MS could not ionise all the species present in the DCL. Therefore, the assignment of the molecules shown above each peak is based on MS and / or DAD data along as well as drawing from the behaviour observed for similar molecules.

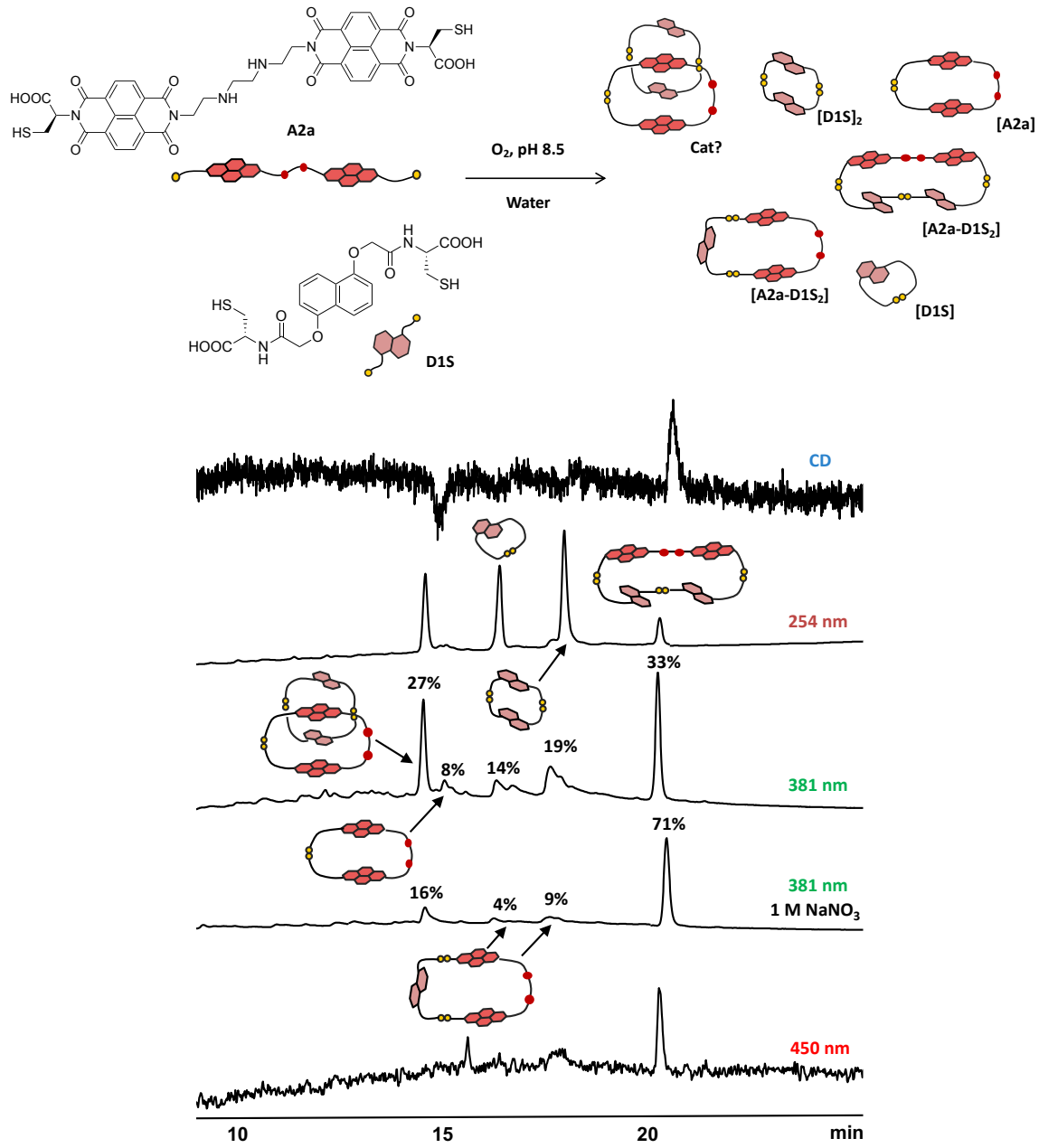

Figure 3-5. The HPLC analysis of D-A DCL of **A2a** and **D1S** (1:2 molar ratio, 5 mM total concentration). Estimated yields are indicated above the corresponding peaks.

3.4 D-A DCL of A2a Acceptor and D2S Donor: Discovering Two New DADA [2]catenanes: Cat8 and Cat9

The LC-MS analysis of D-A DCL of **A2a** with **D2S** has revealed that the fully oxidised library contains two catenanes: one in high yield (88%, **Cat8**), and a new [2]catenane (**Cat9**) in very small yield, 5%, in the presence of $NaNO_3$.

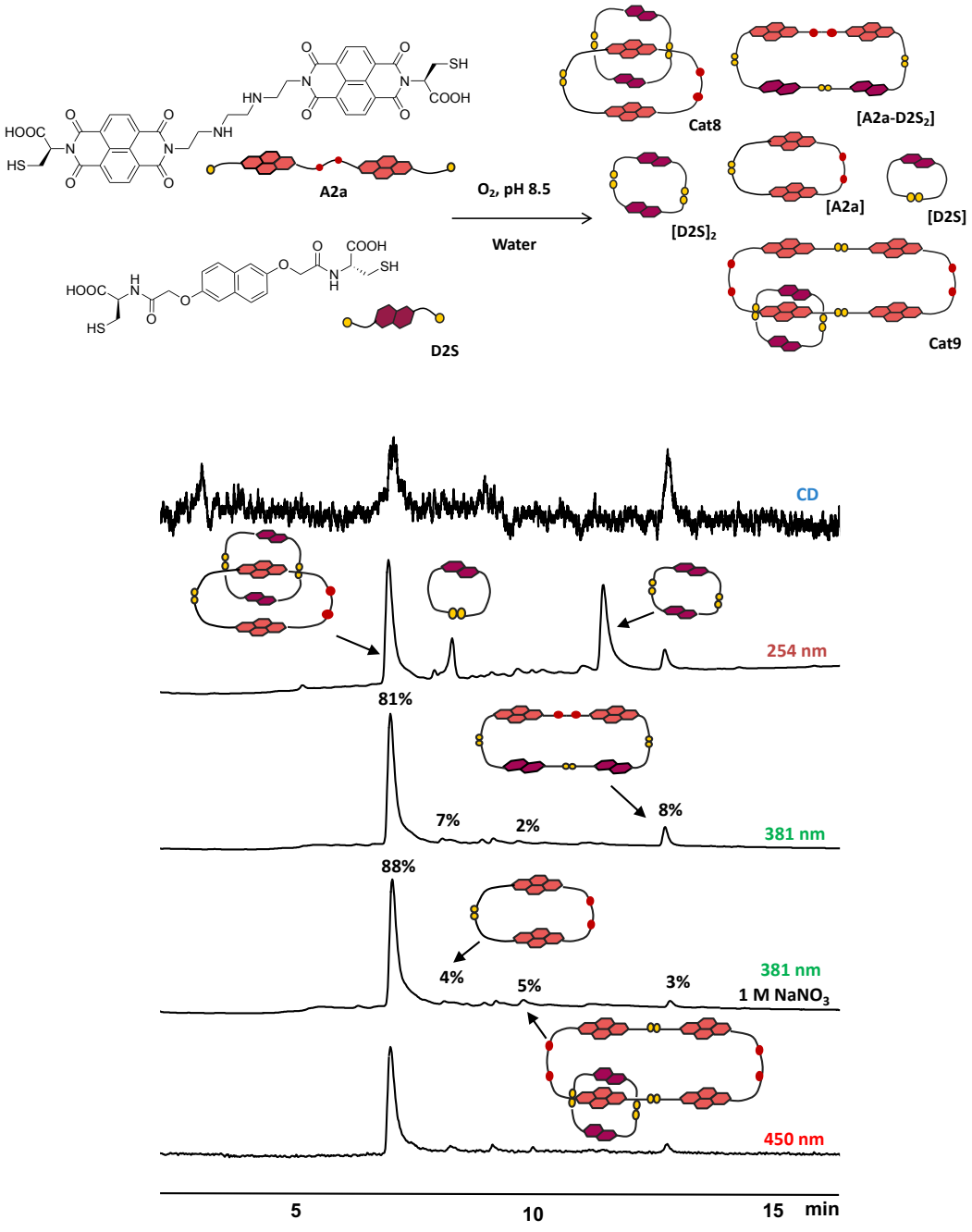

Figure 3-6. The HPLC analysis of D-A DCL of **A2a** and **D2S** (1:2 molar ratio, 5 mM total concentration). Estimated yields are indicated above the corresponding peaks.

The short retention time of **Cat8** along with the strong CD signal have been the first indications that **Cat8** is a topologically complex interlocked molecule.

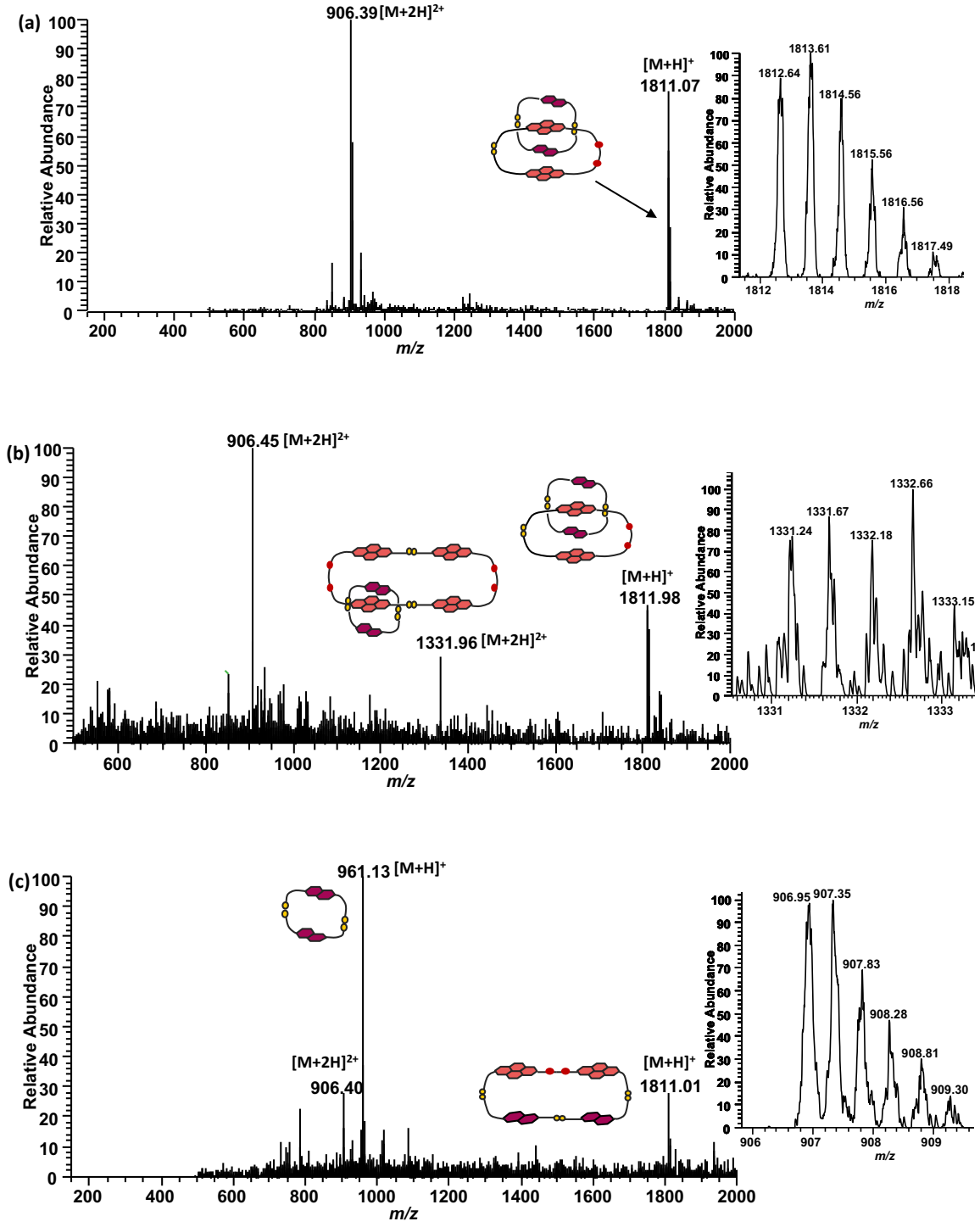

Figure 3-7. ESI-MS (*+ve*) spectra of (a) **Cat8** (as singly charged cation), (b) **Cat9** (as doubly charged cation) and (c) heterotrimer **[A2a-D2S$_2$]** (as singly and doubly charged cation). The expansion of parent molecular ions is shown as inserts.

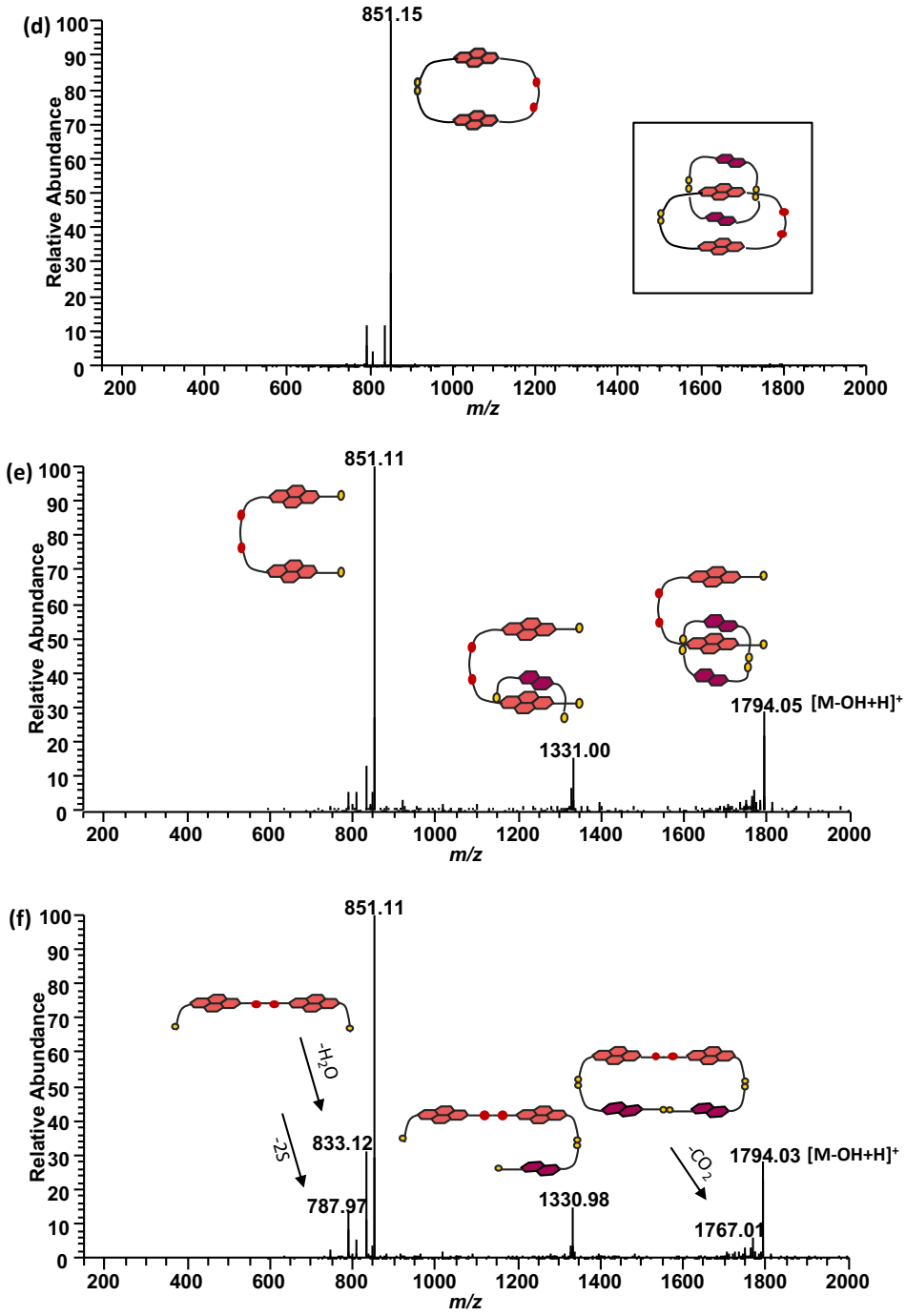

Figure 3-8. MS/MS fragmentation spectra of (d) **Cat8** and (e) **Cat9** and (f) heterotrimer **[A2a-D2S$_2$]**.

The MS and MS/MS fragmentation pattern confirm the formation of a new [2]catenane, **Cat9**, where a **D2S** dimer is interlocked with an **A2a** cyclic dimer. However, the concentration of this new [2]catenane is insignificant (< 5%), which makes its isolation and further analysis laborious. The smaller [2]catenane, **Cat8**, was isolated by preparative HPLC (purity of isolated **Cat8**: 96%) and further analysed by CD (the analysis by NMR was not perfomed because the structure can be fully confirmed based on HPLC and MS analyses).

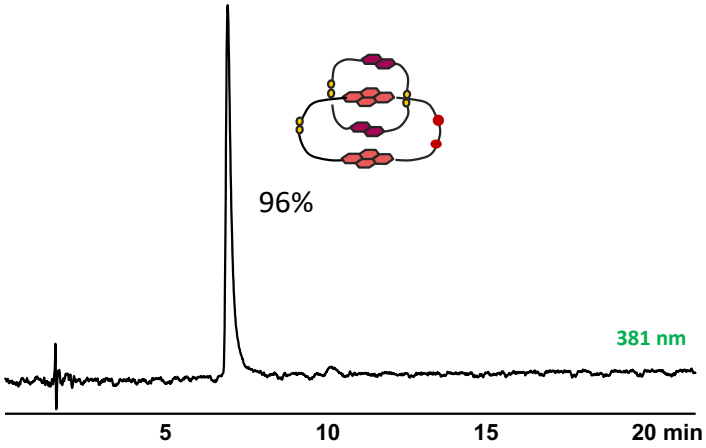

Figure 3-9. Reverse-Phase HPLC result of the isolated **Cat8**. Absorbance was recorded at 381 nm.

3.4.1 Circular Dichroism (CD) analysis

The CD spectrum shows negative Cotton effect around (220 nm) and positive Cotton effect around (240 nm) which is ascribed to the disulfide n→σ* and aromatic π→π* transitions with lower contributions from the amide/ imide and carboxylate chromophores.

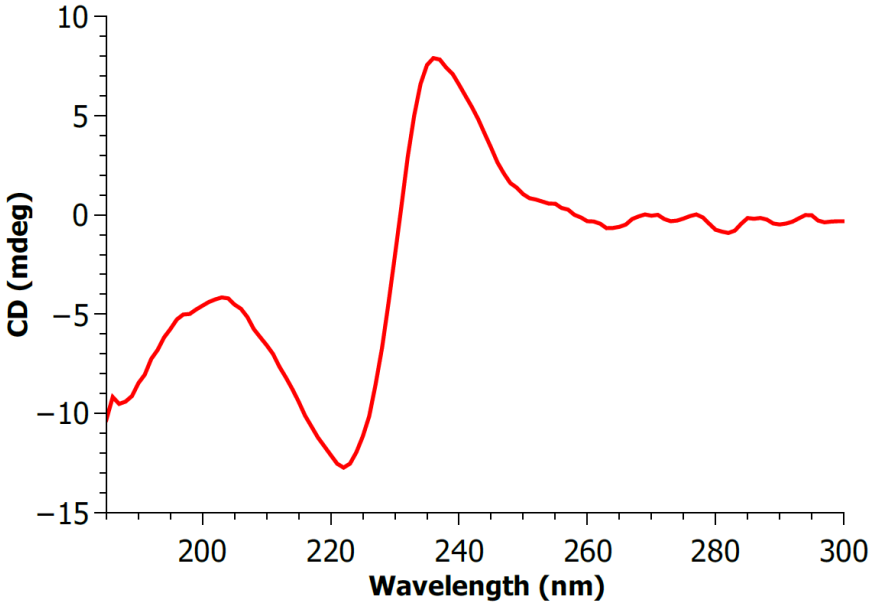

Figure 3-10. The CD spectrum of **Cat8** in (D_2O, 185 – 300 nm), recorded in a 1 mm pathlength cuvette.

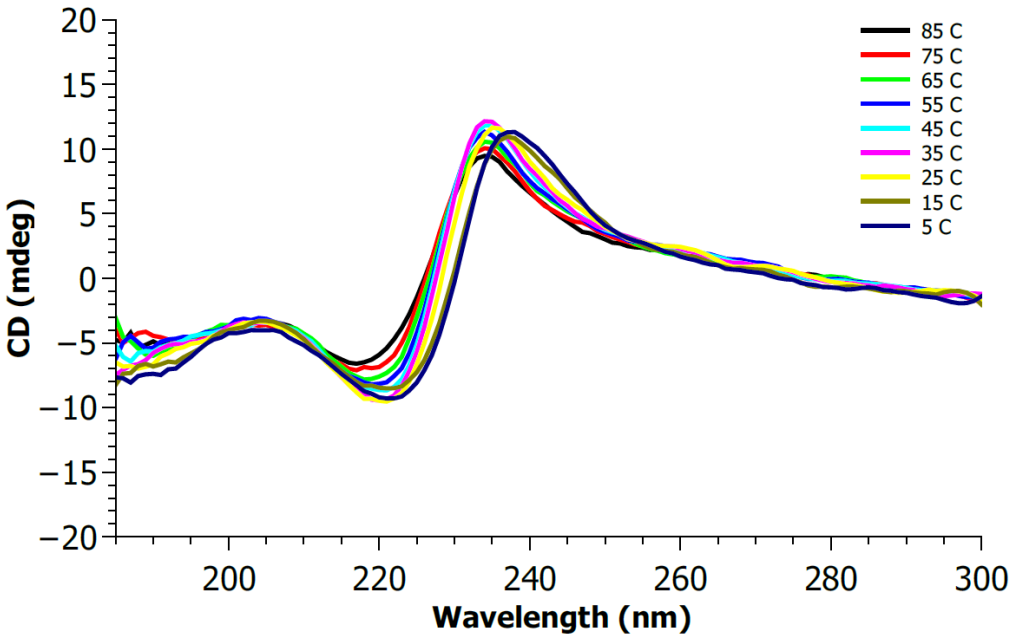

Figure 3-11. Variable temperature CD spectra from 5 to 85 °C of **Cat8** (D_2O, 185 – 300 nm, 1 mm pathlength cuvette).

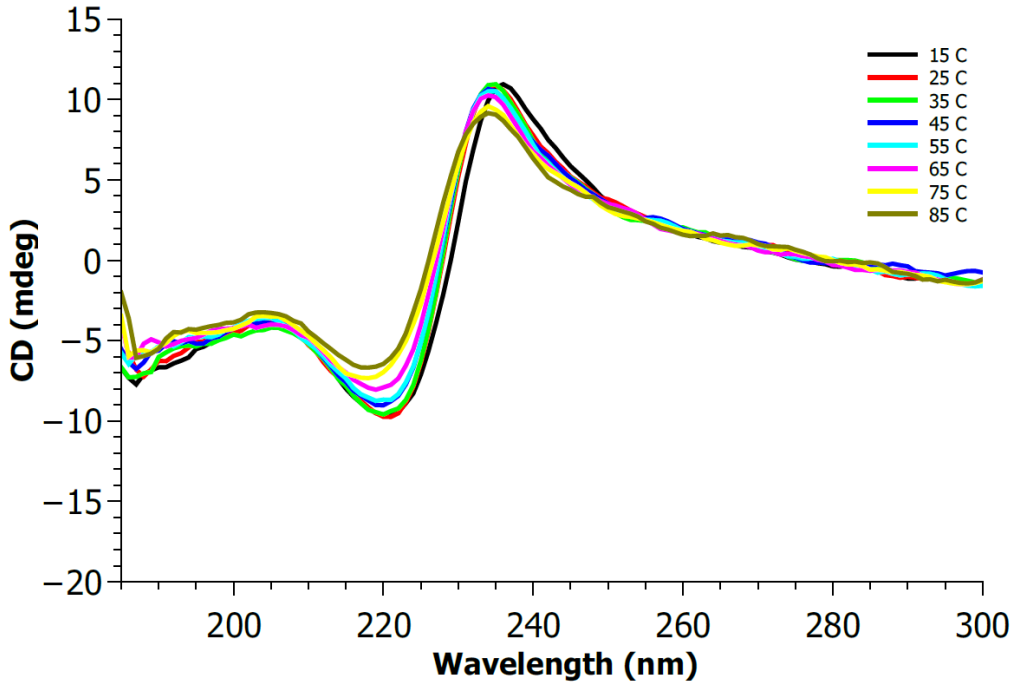

Figure 3-12. Variable temperature CD spectra from 85 to 15 °C of **Cat8** (D_2O, 185 – 300 nm, 1 mm pathlength cuvette).

Both CD VT experiments (5 – 85 °C) and (85 – 15 °C) showed minor change of the disulfide n→σ* and aromatic π→π* transitions regions, confirming the interlocked structure.

3.5 D-A DCL of A2a Acceptor and D1L Donor: Cat10

The LC-MS analysis of D-A DCL of **A2a** with **D1L** has showed that the fully oxidised library contains the classical DADA catenane in 52% (**Cat10**) along with a series of macrocycles. The concentration of **Cat10** decreases 7% with the addition of $NaNO_3$, while the concentration of its isomer **[A2a-D1L$_2$]** increases by 4%.

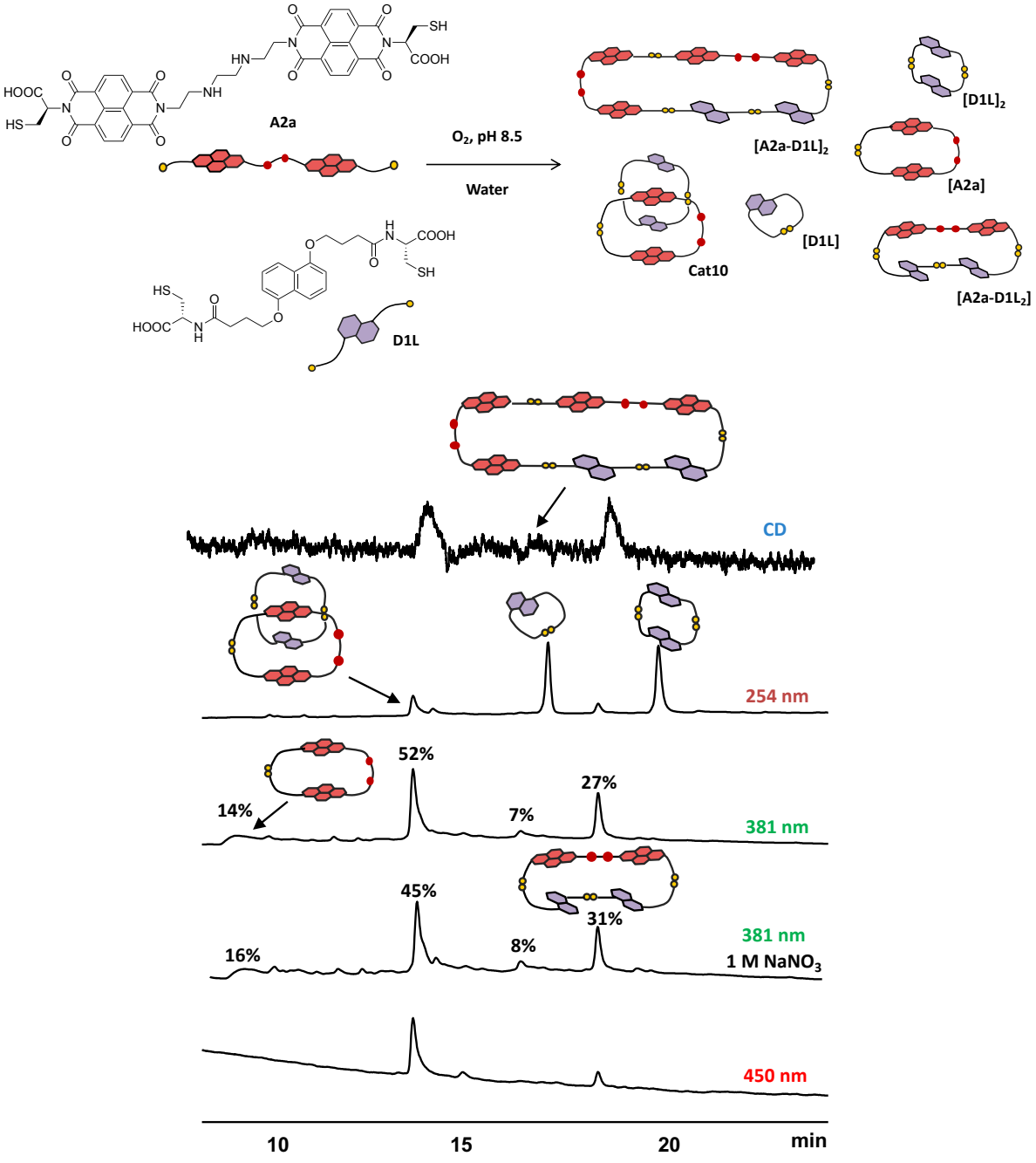

Figure 3-13. The HPLC analysis of D-A DCL of **A2a** and **D1L** (1:2 molar ratio, 5 mM total concentration).

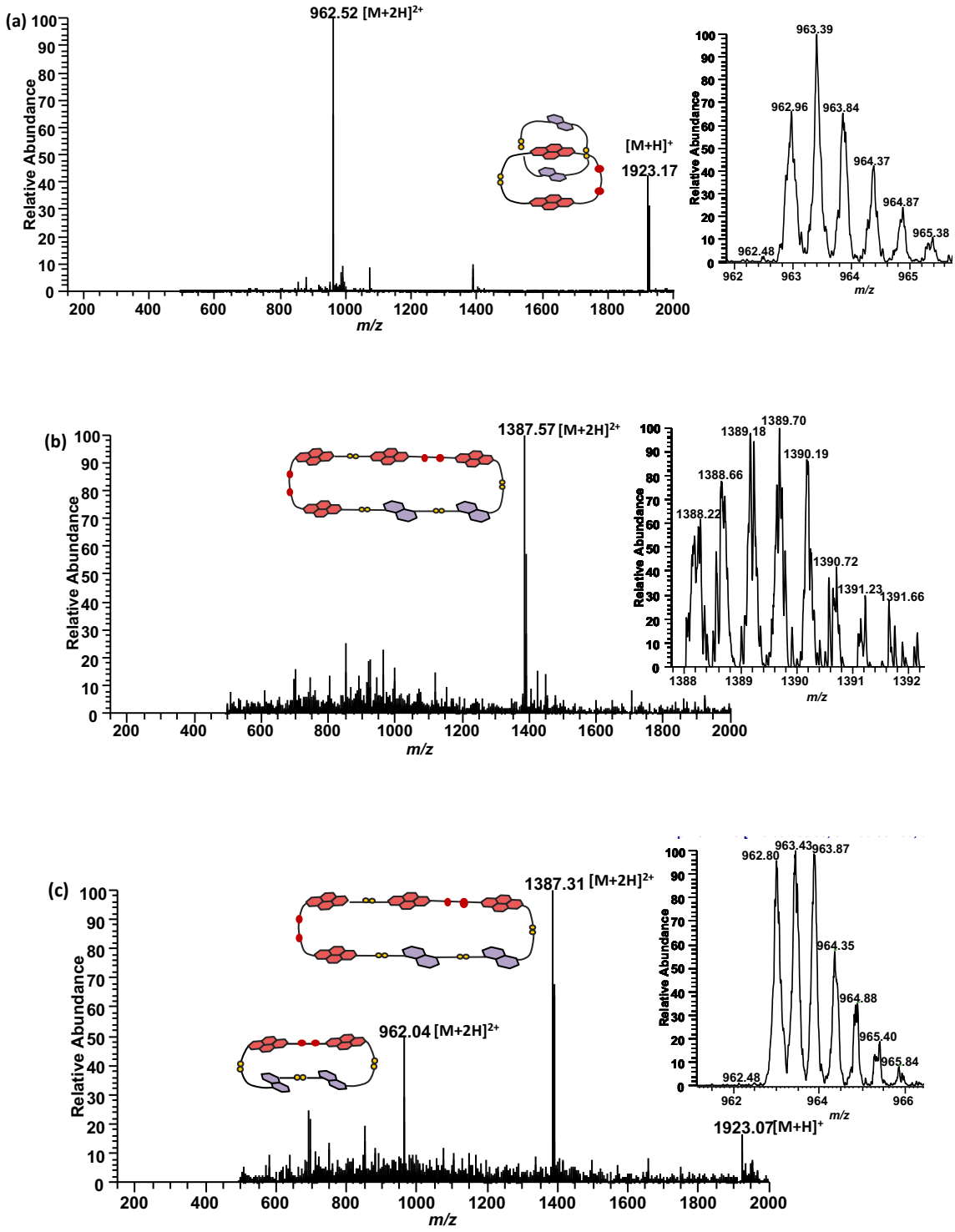

Figure 3-14. ESI-MS (+*ve*) spectra of (a) **Cat10** (as singly and doubly charged cation), (b) the heterotetramer **[A2a-D1L]$_2$** (as doubly charged cation) and (c) the heterotrimer **[A2a-D1L$_2$]** (doubly charged cation). The expansions of parent molecular ions are shown as inserts.

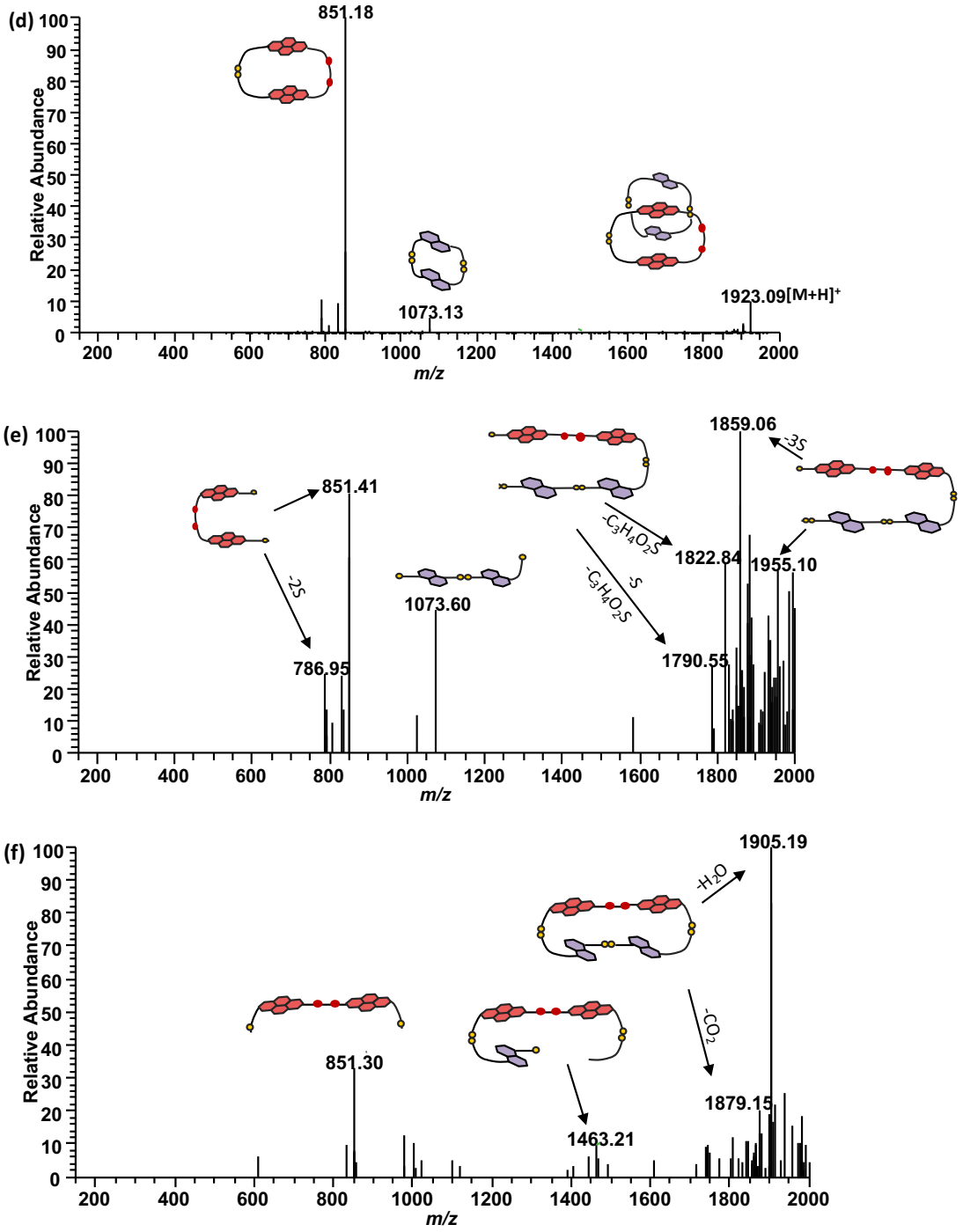

Figure 3-15. MS/MS fragmentation spectra of (d) **Cat10**, (e) heterotetramer **[A2a-D1L]$_2$** and (f) heterotrimer **[A2a-D1L$_2$]**.

The HPLC and MS analyses confirm the formation of **Cat10** as well as of other macrocycles present in this library.

3.6 DCL of A2a Acceptor and D2L Donor: Discovering two new DADA [2]catenane: Cat11 and Cat12

The LC-MS analysis of D-A DCL of **A2a** with **D2L** has revealed that the fully oxidised library contains two catenanes: one in a relatively good yield (59%, **Cat11**), and another [2]catenane (**Cat12**) in lower yield, 18%. The library with $NaNO_3$ has displayed almost the same distribution as the one without the salt.

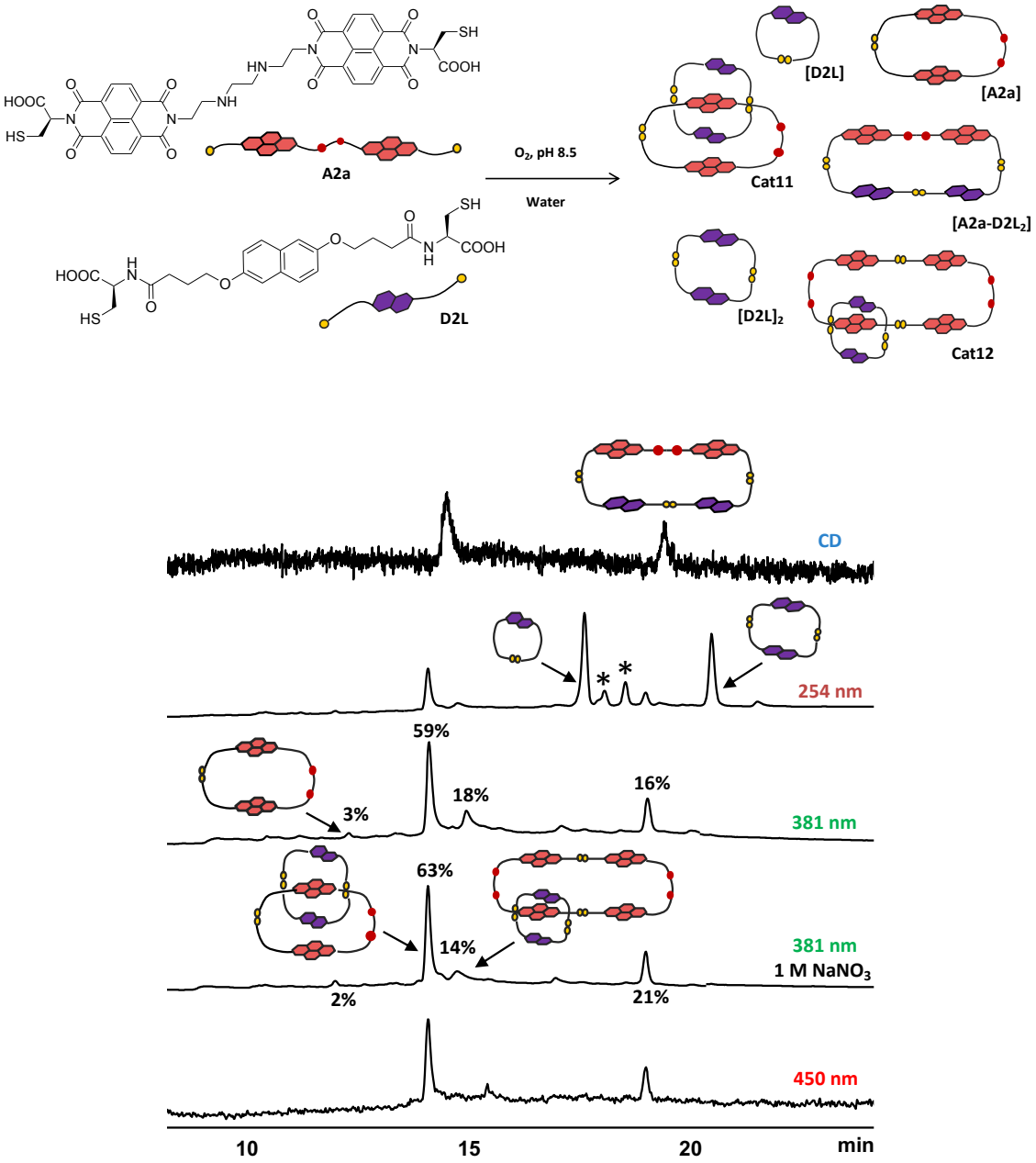

Figure 3-16. The HPLC analysis of D-A DCL of **A2a** and **D2L** (1:2 molar ratio, 5 mM total concentration). The * represent **D2L** impurity.

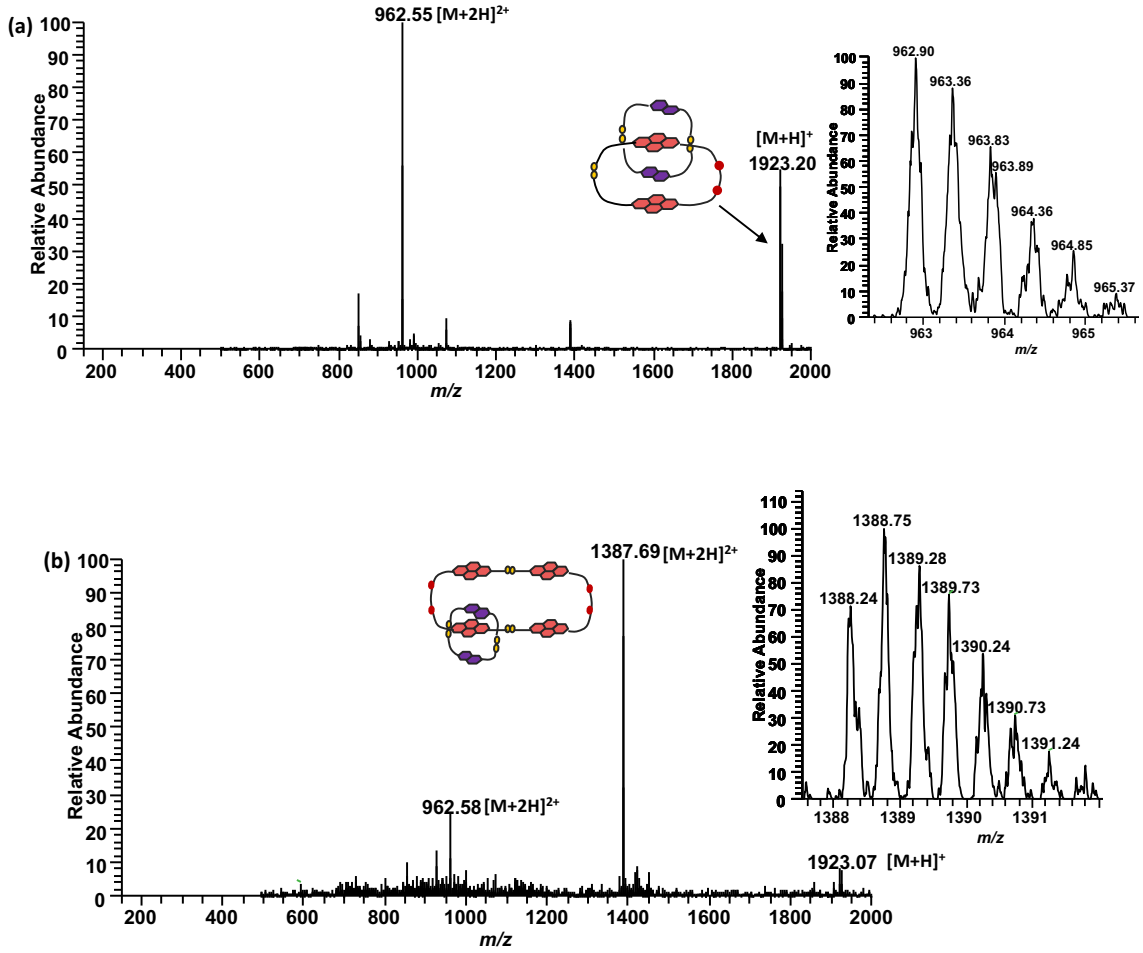

Figure 3-17. ESI-MS (+*ve*) spectra of (a) **Cat11** (as singly and doubly charged cation) and (b) **Cat12** (as doubly charged cation). The expansions of parent molecular ions are shown as inserts.

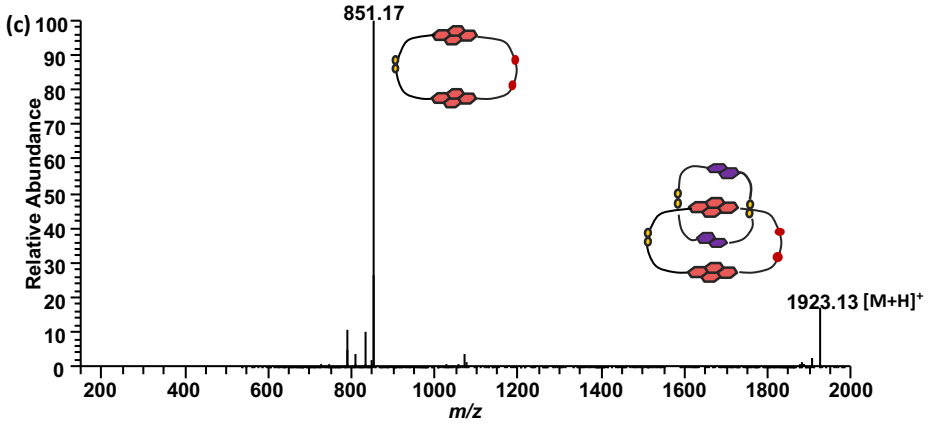

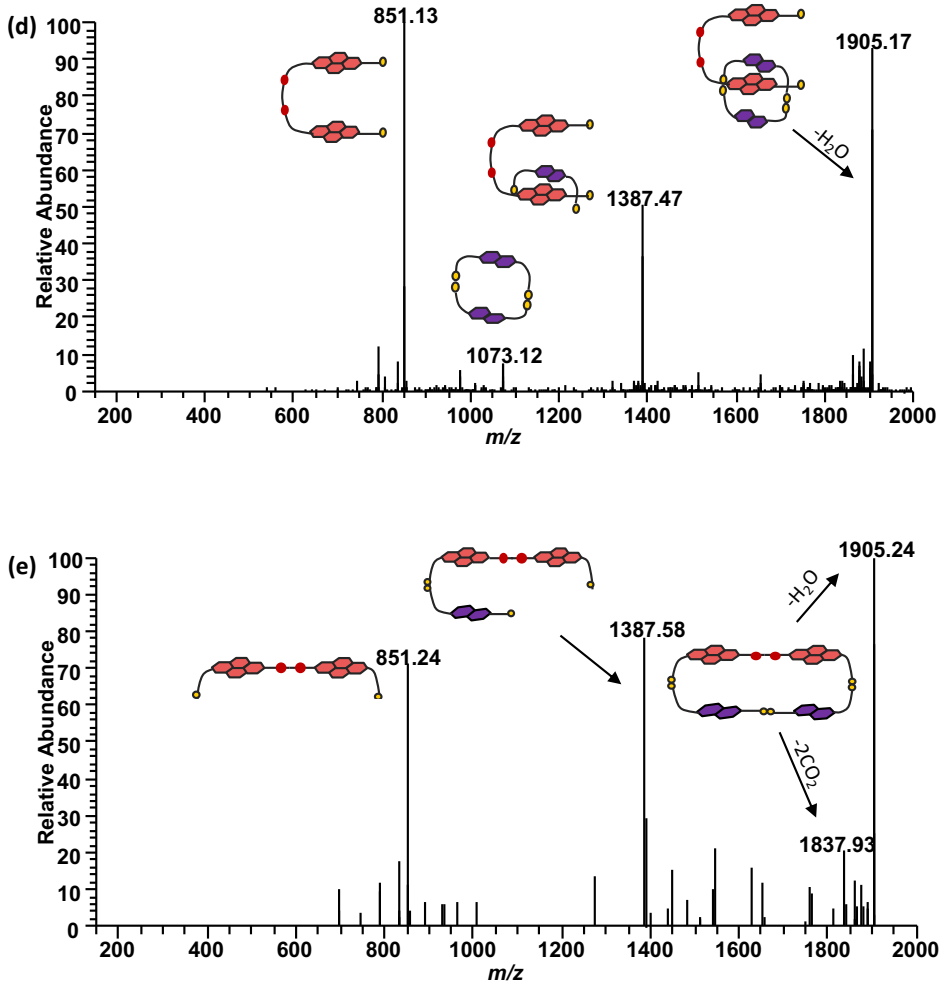

Figure 3-18. MS/MS fragmentation spectra of (c) **Cat11**, (d) **Cat12**, and (e) **[A1a-D2L$_2$]**.

When comparing the libraries of **A2a** with different DN building blocks, the formation of classical DADA [2]catenane from cyclic **A2a** and cyclic DN dimer was observed as the common feature. However, the libraries with 2,6-DN have showed more potential to produce new [2]catenanes consisting of a **A2a** cyclic dimer interlocked with a cyclic DN dimer. Despite their relatively low concentrations (8% with **D2S**) and (18% with **D2L**), their formation is remarkable. Comparing these libraries with the **A1c**-based DCLs (also eight atoms in the linker), it has been observed that, by replacing one carbon atom with a nitrogen atom, the library is more diverse, and the formation of other complex molecules has been promoted.

3.7 DCL of A2b Building Block

A new set of libraries were set up using **A2b** building block. The DCL of **A2b** was generated by dissolution of the building block in water (5 mM concentration) and the pH was adjusted to 8.5 using an aqueous solution of 100 mM NaOH. Two libraries were set up, one with $NaNO_3$ and one without, and stirred for one day under air in capped vials to allow full oxidation of the thiols.

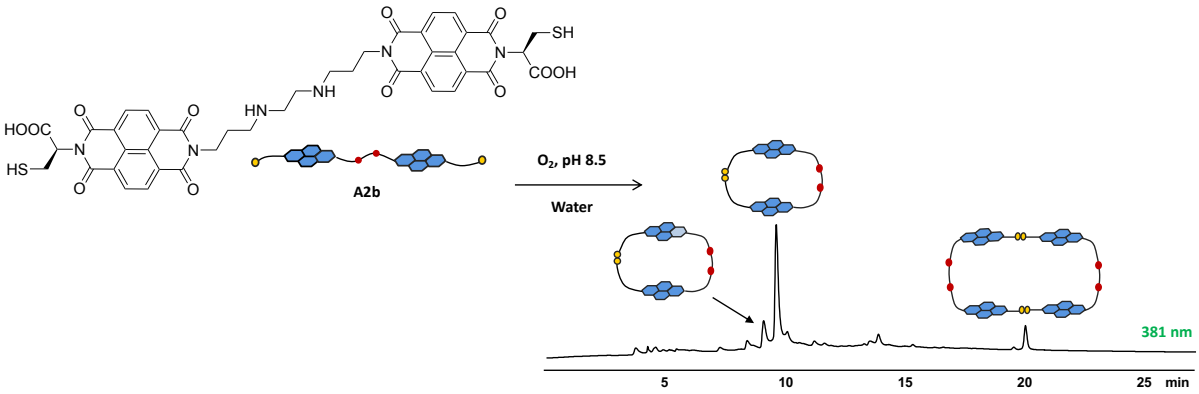

Figure 3-19. The HPLC analysis of **A2b** library in water. Absorbance was recorded at 381 nm.

Three major components were at equilibrium in this library: **A2b** cyclic monomer hydrated on one of the carbonyl groups, cyclic monomer and cyclic dimer.

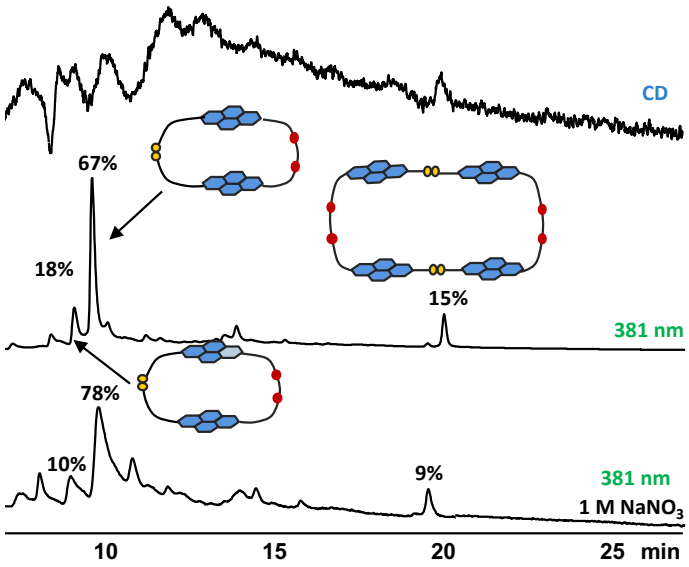

Figure 3-20. The HPLC analysis of **A2b** library in water with and without 1 M $NaNO_3$. Absorbance was recorded at 381 nm.

This building block (**A2b**), as in the case of the previous one (**A2a**), has a poor solubility in water and the formation of cyclic monomer as the major component in the library favours its

precipitation. This leads to the loss of some product (through filtration) and very low resolution by HPLC. The addition of $NaNO_3$ increases the concentration of **[A2b]** to 11% yet it reduces the concentration of **[A2b]$_2$** by 6%.

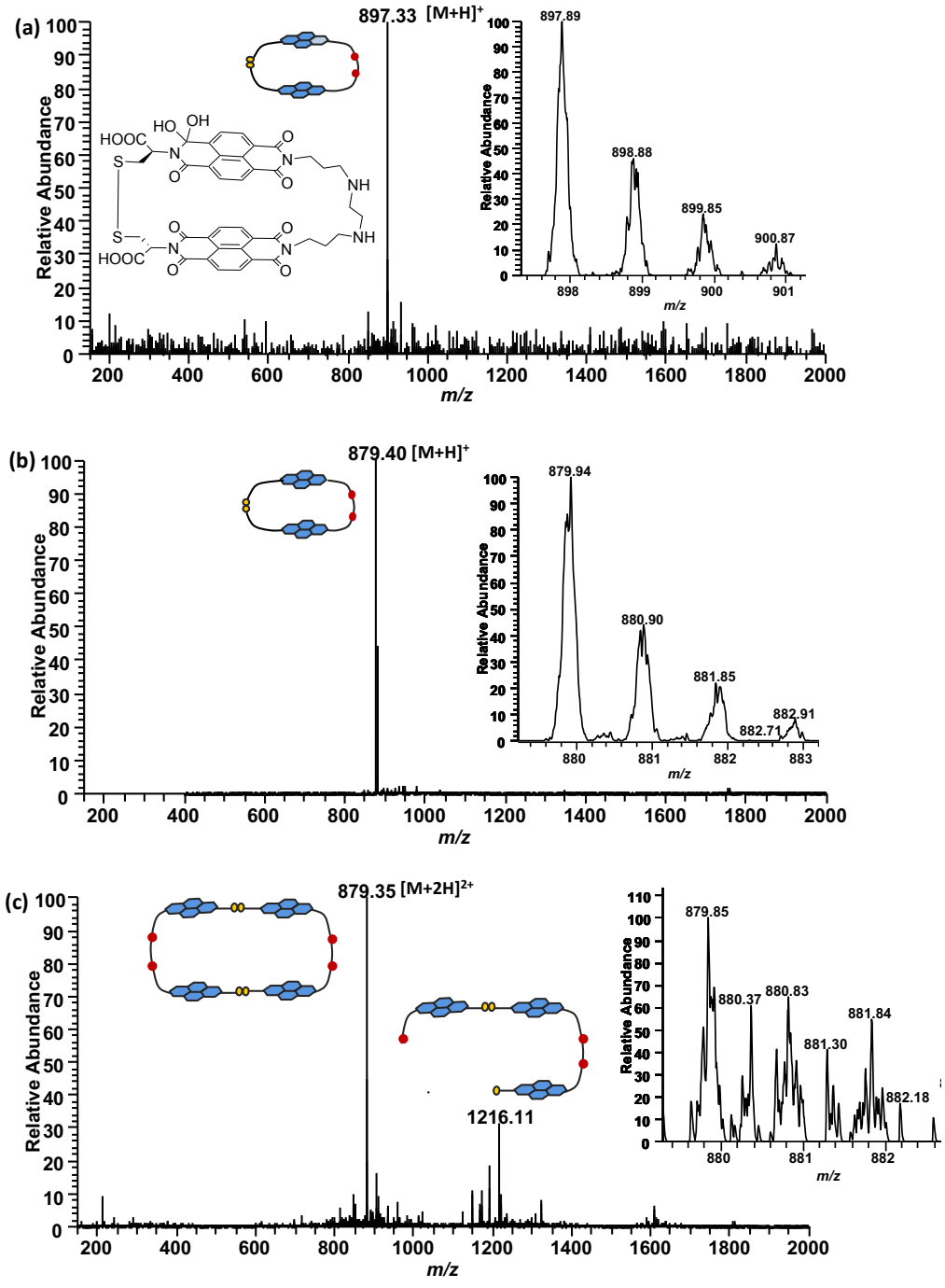

Figure 3-21. ESI-MS (*+ve*) spectra of (a) **A2b** cyclic monomer hydrated on one of the carbonyl groups (as singly charged cation), (b) **[A2b]** cyclic monomer (as singly charged cation) and (c) **[A2b]$_2$** cyclic dimer (as doubly charged cation). Expansions of molecular ions are shown as inserts.

3.8 DCL of A2b Acceptor and D1S Donor: Cat13

The D-A DCL was prepared from the acceptor **A2b** and the rigid donor building block **D1S** in water at pH 8.5. The solution was stirred for one day before it was analysed by HPLC and LCMS.

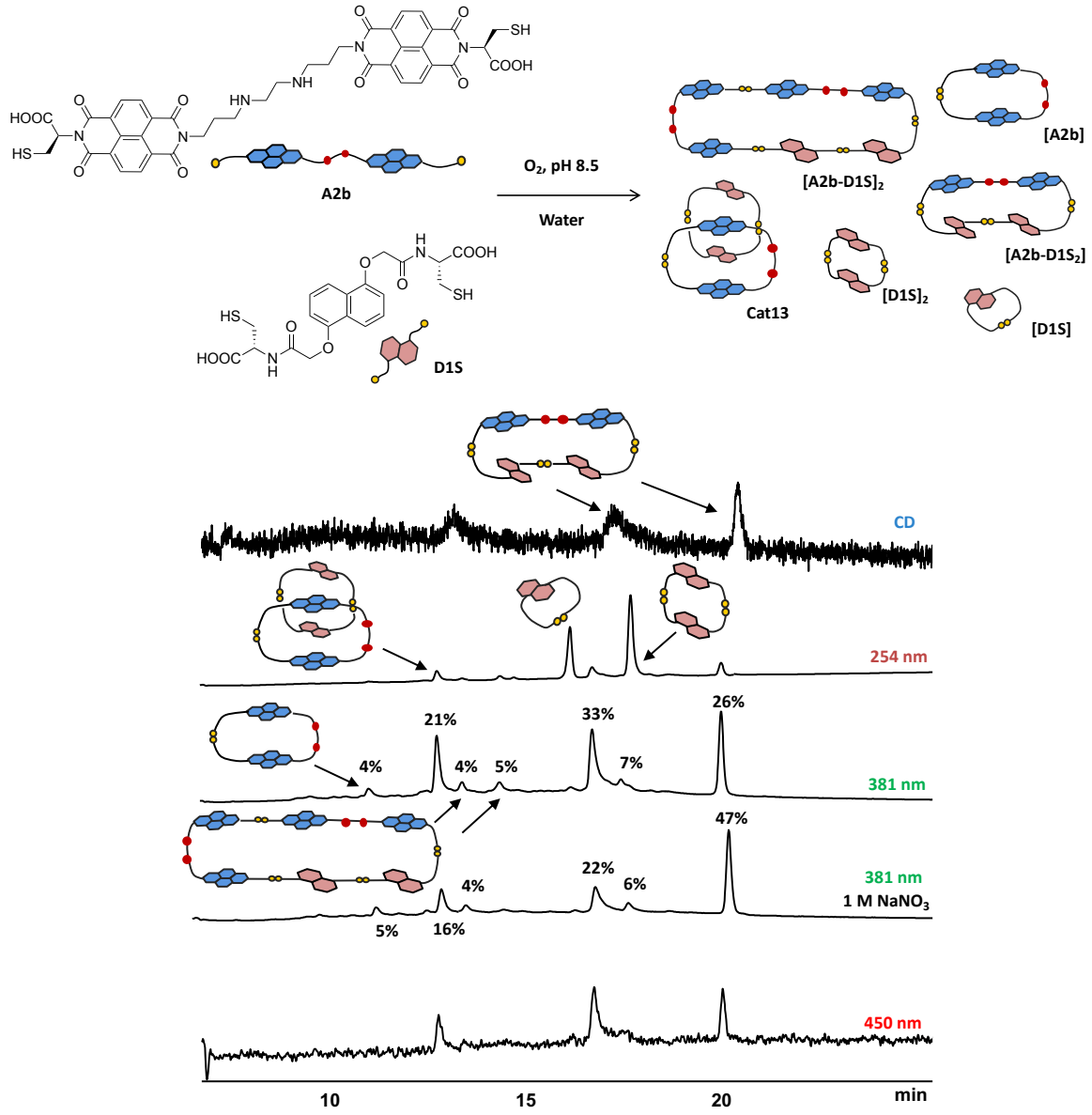

Figure 3-22. The HPLC analysis of D-A DCL of **A2b** and **D1S** (1:2 molar ratio, 5 mM total concentration).

The library at equilibrium consists of several macrocycles and a [2]catenane (**Cat13**). The **Cat13** forms up to 21% yield in the library without salt; however, this concentration decreases to 16% in the presence of $NaNO_3$. This mismatch related to the theory described in the previous chapter that an increase in system's polarity amplifies the tighter structure (which usually refers to interlocked molecules, *e.g.,* catenanes) could mean that the **[A2b-D1S$_2$]** has a much tighter

packing than the [2]catenane. This is possible with the 1,5-DNs (**D1S** and **D1L**), as the rigid structure of **D1S** dimer interlocked with the cyclic **A2b** is likely to be thermodynamically less favourable than its macrocycle isomer. The **[A2b-D1S$_2$]** concentration increases 21% in the library with $NaNO_3$. There are two peaks representing the heterotrimer **[A2b-D1S$_2$]** and have the same *m/z* value, isotopic pattern, and fragmentation behaviour in MS. This can be due to the different, yet stable conformations of the trimer, which slowly interconvert and could be separated by the conditions used in the HPLC analysis.

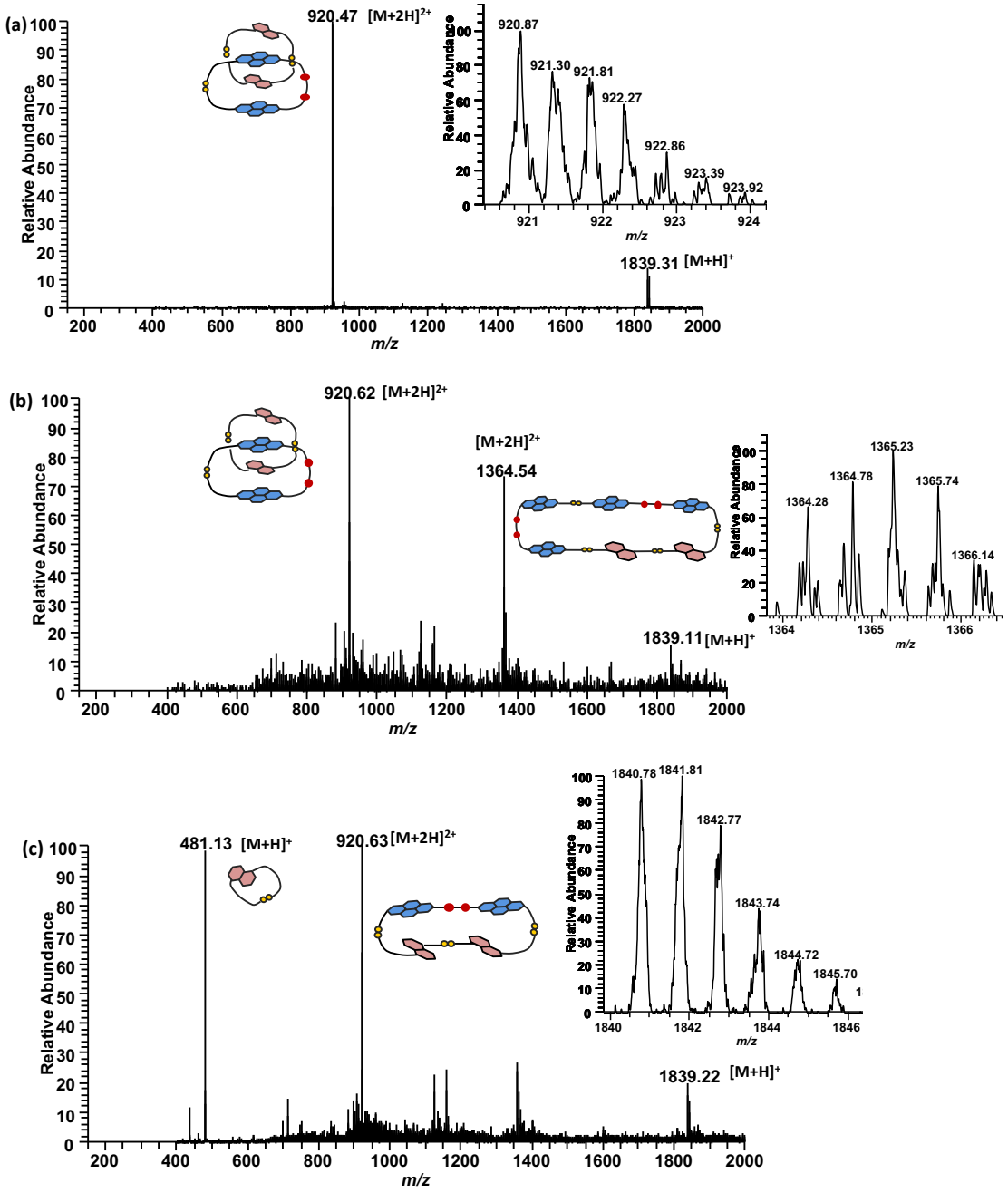

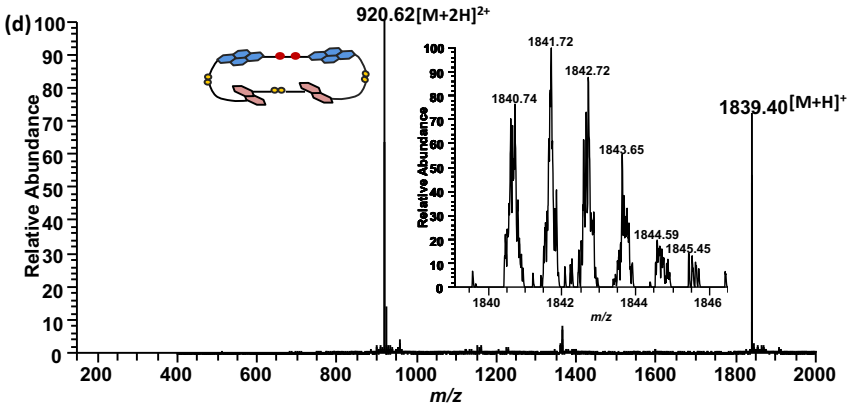

Figure 3-23. ESI-MS (+*ve*) spectra of (a) **Cat13** (as singly and doubly charged cation), (b) the heterotetramer **[A2b-D1S]$_2$** (as doubly charged cation), (c) and (d) both show the heterotrimer **[A2b-D1S$_2$]** (as singly and doubly charged cations). The expansions of parent molecular ions are shown as inserts.

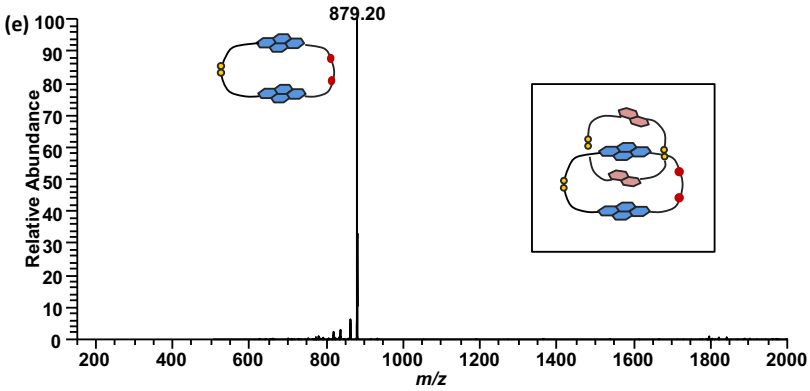

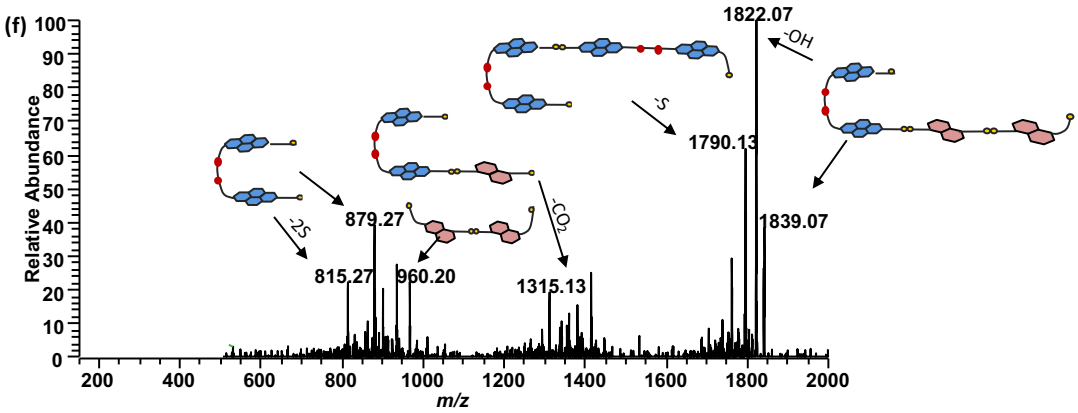

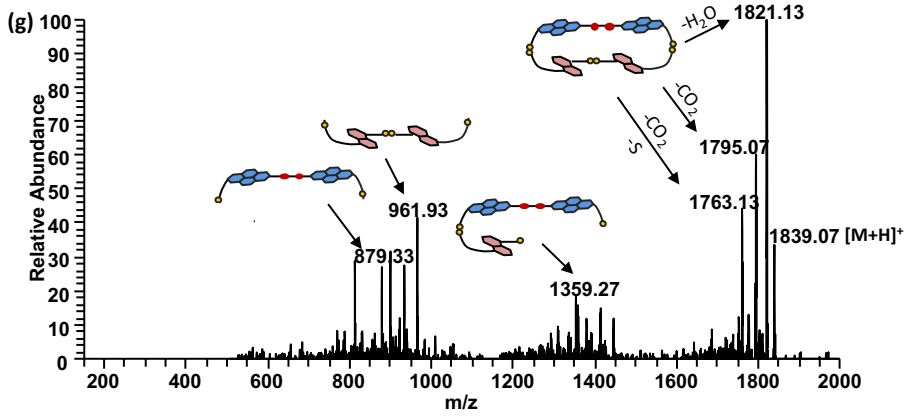

Figure 3-24. MS/MS fragmentation spectra of (e) **Cat13**, (f) **[A2b-D1S]$_2$** and (g) **[A2b-D1S$_2$]**.

3.9 DCL of A2b Acceptor and D2S Donor: Cat14

The LC-MS analysis of D-A DCL of **A2b** with **D2S** revealed that the fully oxidised library contains the [2]catenane (**Cat14**) in 71% (containing 71% of **A2b** present in the DCL). This library forms four major components that have been assigned by HPLC and MS. The small peak at 8.1 min shows a peak at charge-transfer band (450 nm) and it shows chirality on CD, however it does not ionise well by all the different techniques on MS and it only shows the presence of **[A2b]**.

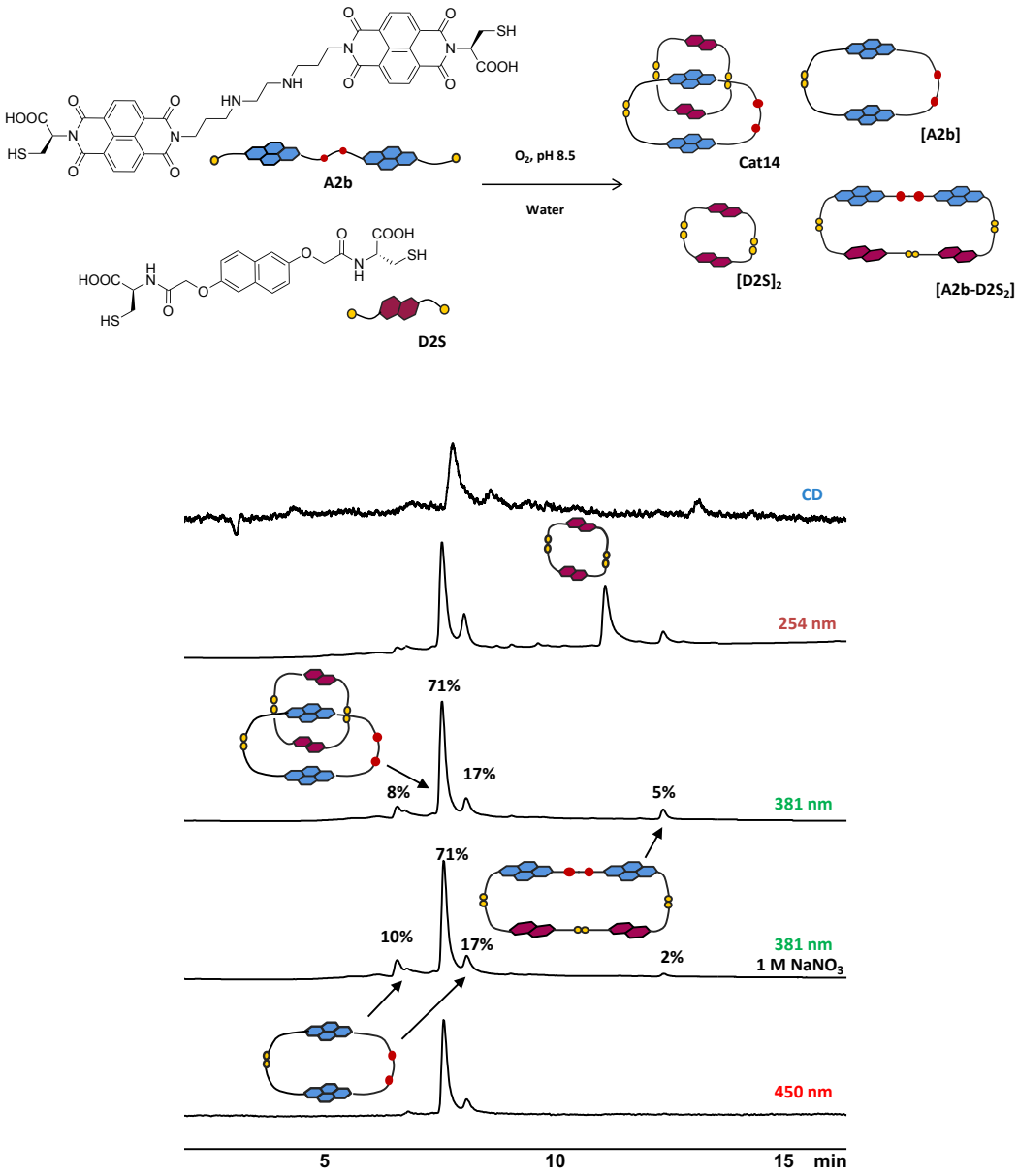

Figure 3-25. The HPLC analysis of D-A DCL of **A2b** and **D2S** (1:2 molar ratio, 5 mM total concentration).

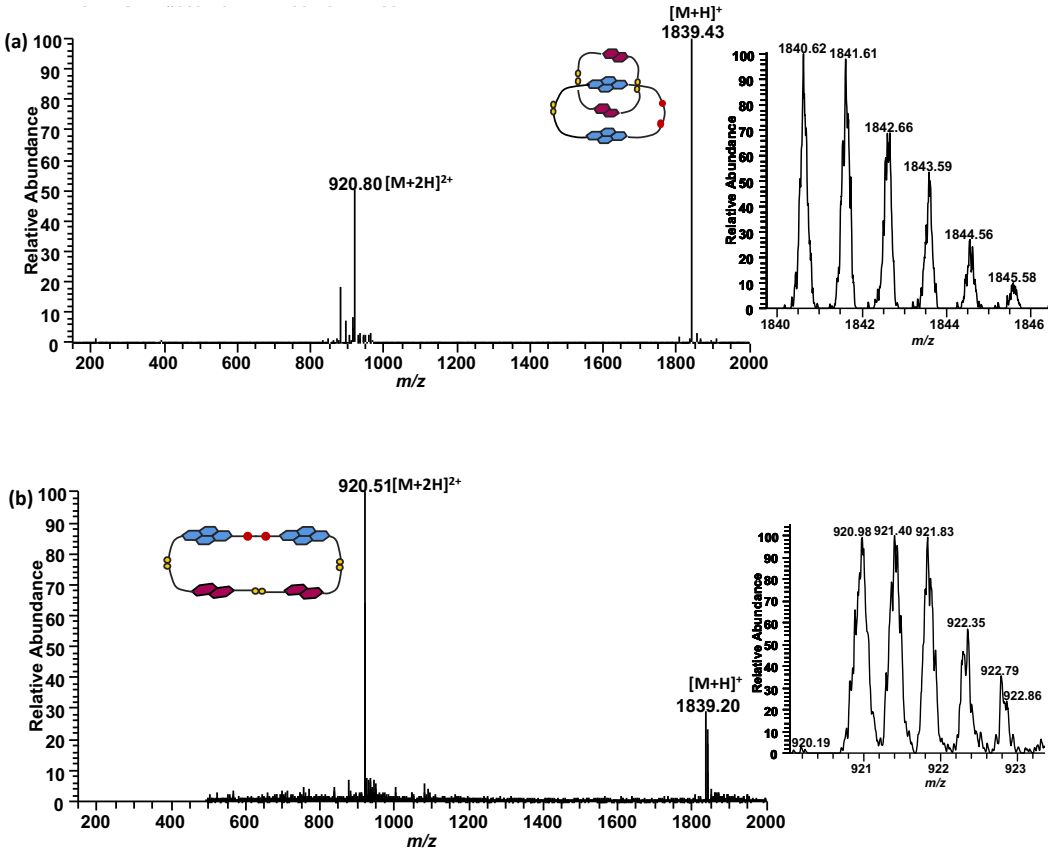

Figure 3-26. ESI-MS (*+ve*) spectra of (a) **Cat14** (as singly and doubly charged cation) and (b) **[A2b-D2S$_2$]** (as singly and doubly charged cation). The expansions of parent molecular ions are shown as inserts.

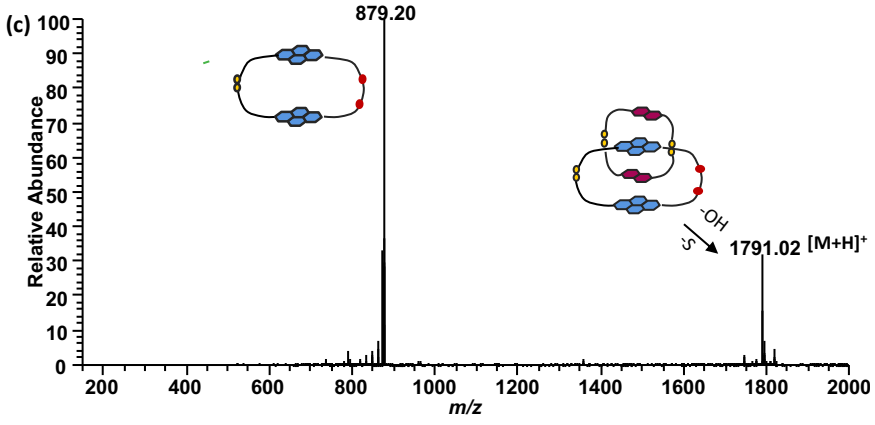

Figure 3-27. The MS/MS fragmentation of (c) **Cat14**.

The [2]catenane (**Cat14**) was isolated by preparative HPLC (purity of isolated **Cat14**: 89%) and further analysed by CD.

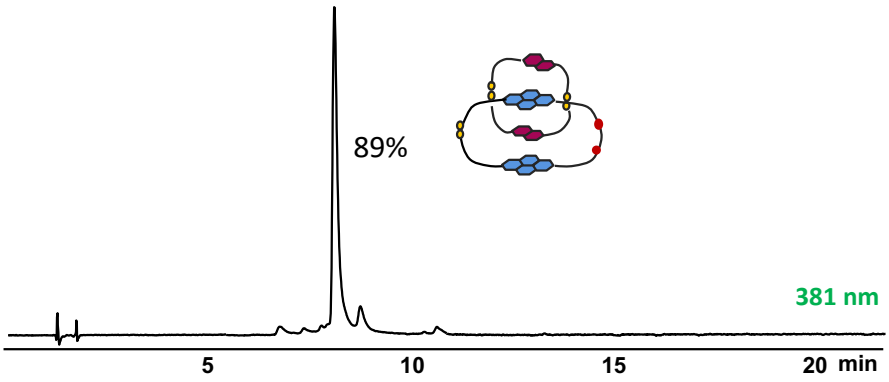

Figure 3-28. Reverse-Phase HPLC result of the isolated **Cat14**. Absorbance was recorded at 381 nm.

3.9.1 Circular Dichroism (CD) analysis

The CD spectrum shows a strong negative Cotton effect between (185 – 220 nm) and strong positive Cotton effect between (220 – 240 nm), which is ascribed to the disulfide n→σ* and aromatic π→π* transitions with lower contributions from the amide / imide and carboxylate chromophores.

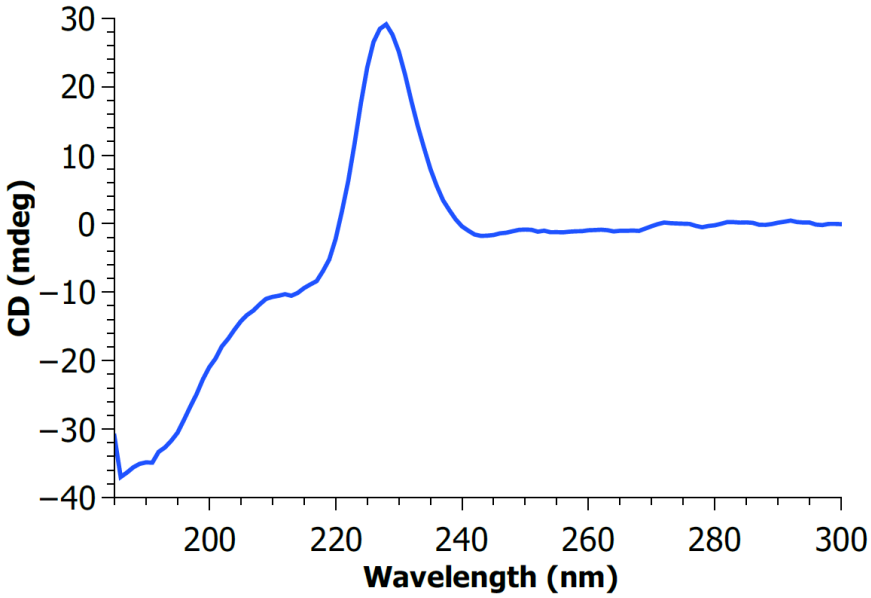

Figure 3-29. The CD spectrum of **Cat14** in (D_2O, 185 — 300 nm), recorded in a 1 mm pathlength cuvette.

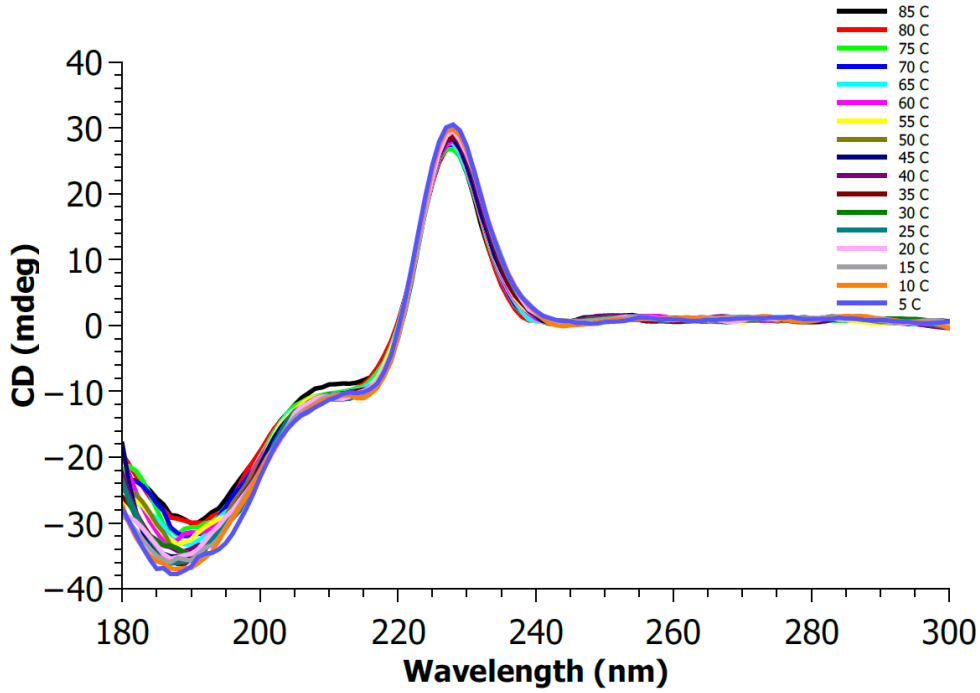

Figure 3-30. Variable temperature CD spectra from 5 to 85 °C of **Cat14** (D_2O, 185 – 300 nm, 1 mm pathlength cuvette).

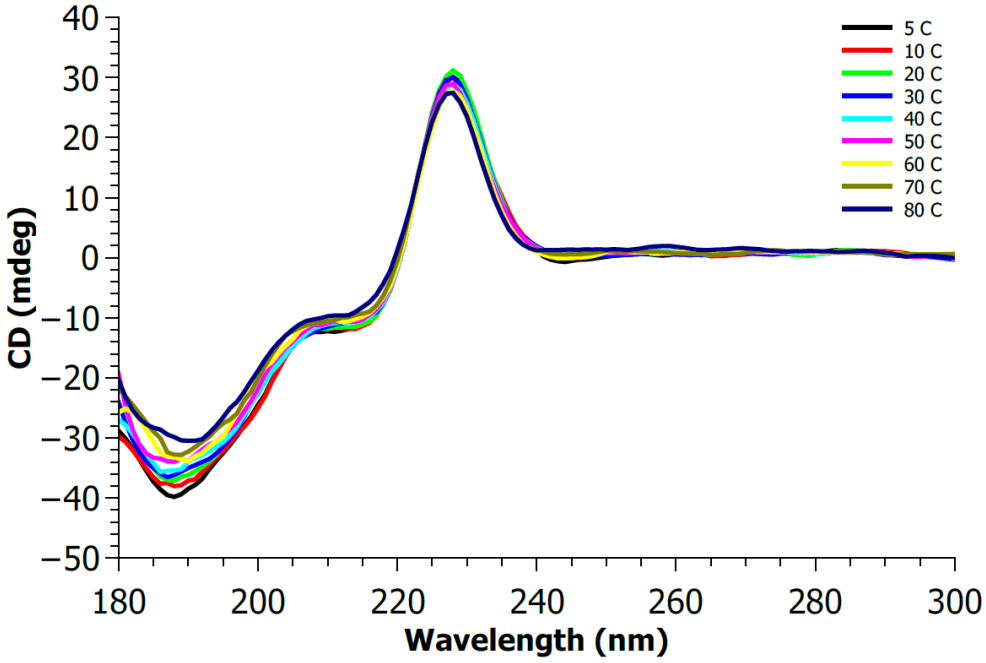

Figure 3-31. Variable temperature CD spectra from 85 to 15 °C of **Cat14** (D_2O, 185 – 300 nm, 1 mm pathlength cuvette).

The CD VT experiment suggests a rigid structure due to hardly any change in the disulfide $n\rightarrow\sigma^*$ and $\pi\rightarrow\pi^*$ transitions region, confirming the interlocked structure.

3.10 DCL of A2b Acceptor and D1L Donor: Cat15

The D-A DCL was prepared from the acceptor **A2b** and the rigid donor building block **D1L** in water at pH 8.5. The solution was stirred for one day before it was analysed by HPLC and LC-MS. This library forms a new [2]catenane (**Cat15**) up to 53% in the presence of 1 M $NaNO_3$, along with a series of macrocycles. The diversity of library is not significantly affected by addition of salt. The formation of heterotrimer **[A2b-D1L$_2$]** is reduced by 12% in favour of **Cat15**, **[A2b-D1L]** and **[A2b]** in the presence of $NaNO_3$.

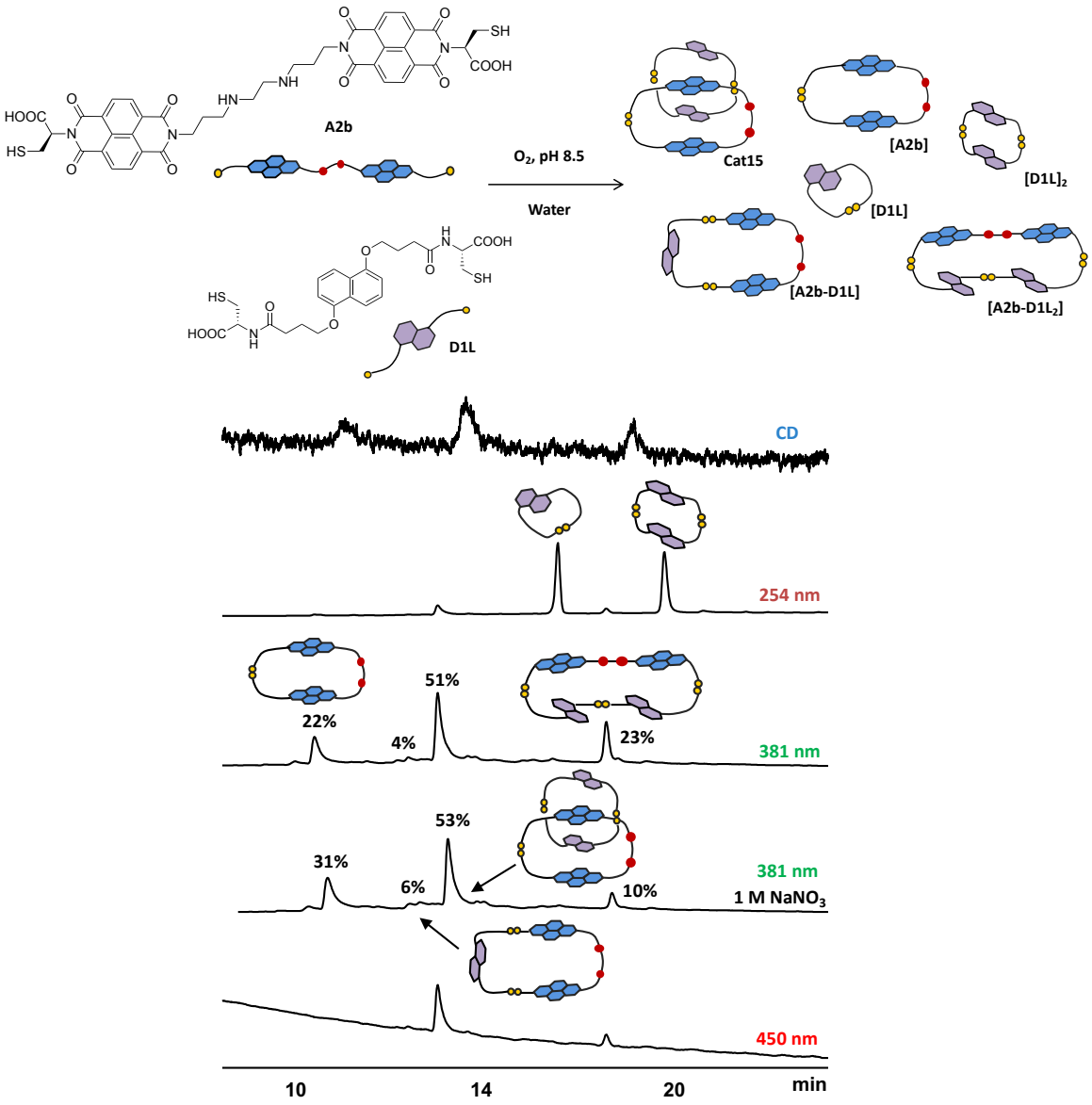

Figure 3-32. The HPLC analysis of D-A DCL of **A2b** and **D1L** (1:2 molar ratio, 5 mM total concentration).

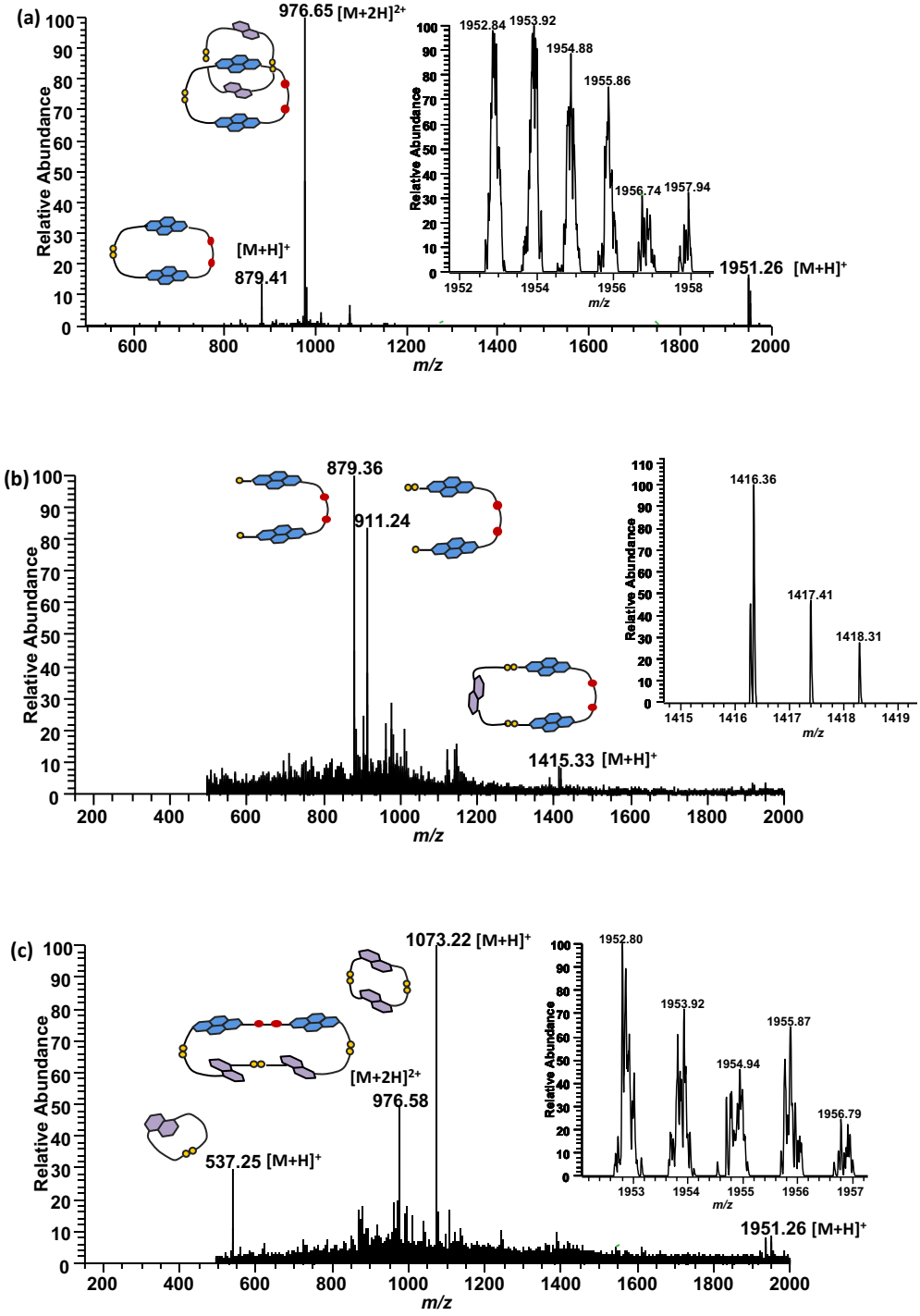

Figure 3-33. ESI-MS (+*ve*) spectra of (a) **Cat15** (as singly and doubly charged cation), (b) the heterodimer **[A2b-D1L]** (as singly charged cation) and (c) the heterotrimer **[A2b-D1L$_2$]** (as singly and doubly charged cation). The expansion of parent molecular ions is shown as inserts.

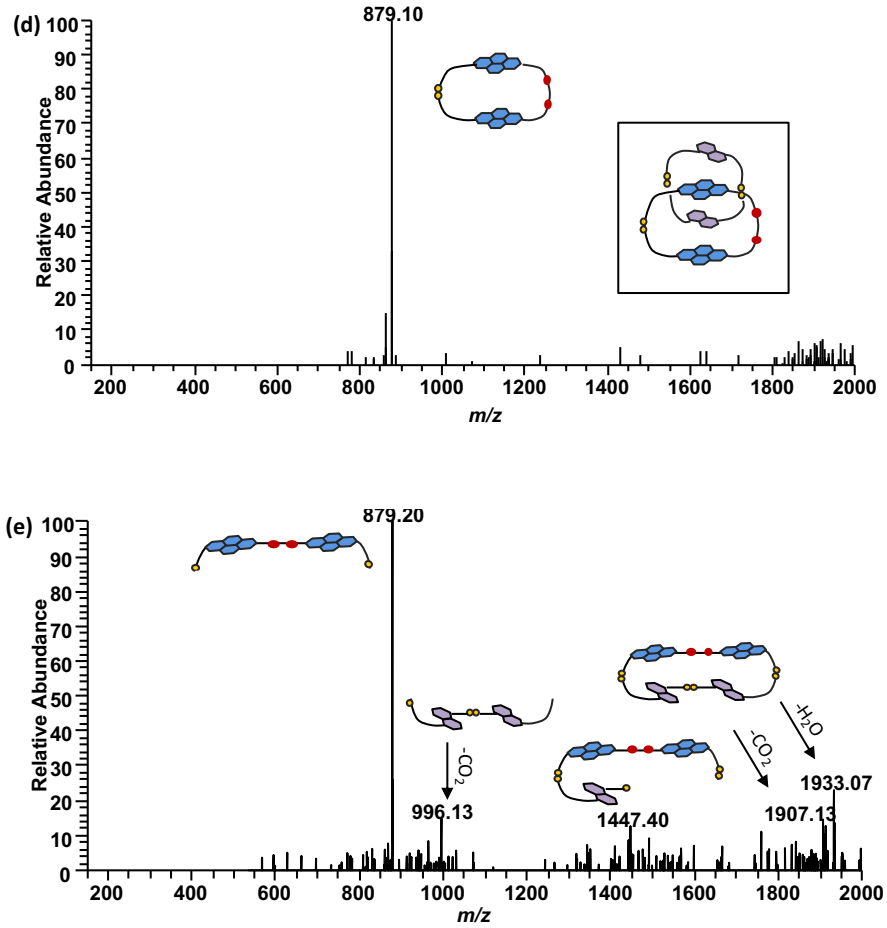

Figure 3-34. MS/MS fragmentation of (d) **Cat15** and (e) heterotrimer **[A2b-D1L$_2$]**.

3.11 DCL of A2b Acceptor and D2L Donor: Cat16

The LC-MS analysis of D-A DCL of **A2b** with **D2L** has revealed that the fully oxidised library contains a [2]catenane in 63% (**Cat16**). The library with $NaNO_3$ has showed the same distribution, yet with slightly different yields.

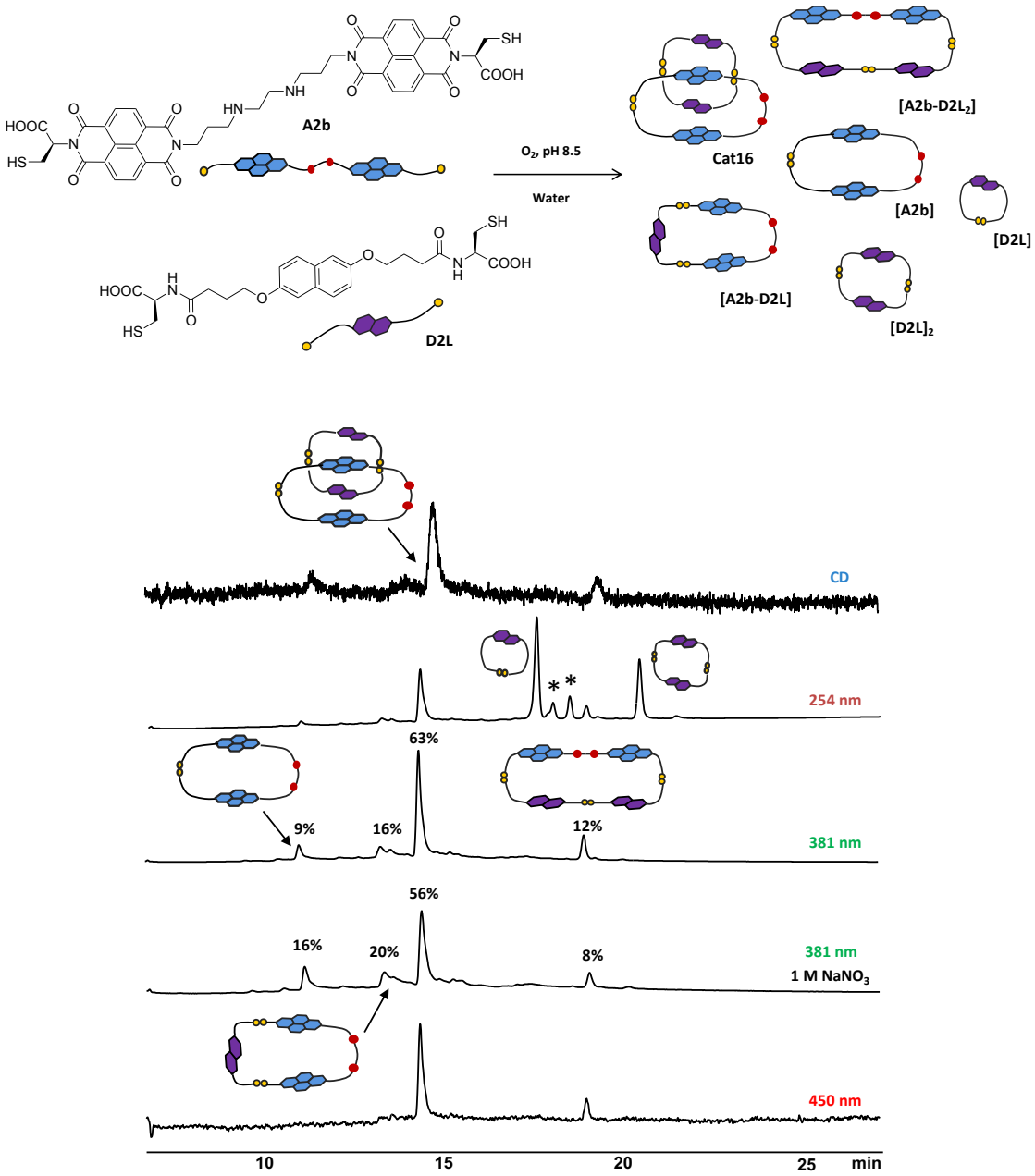

Figure 3-35. The HPLC analysis of D-A DCL of **A2b** and **D2L** (1:2 molar ratio, 5 mM total concentration). The * represents impurity in DN building block.

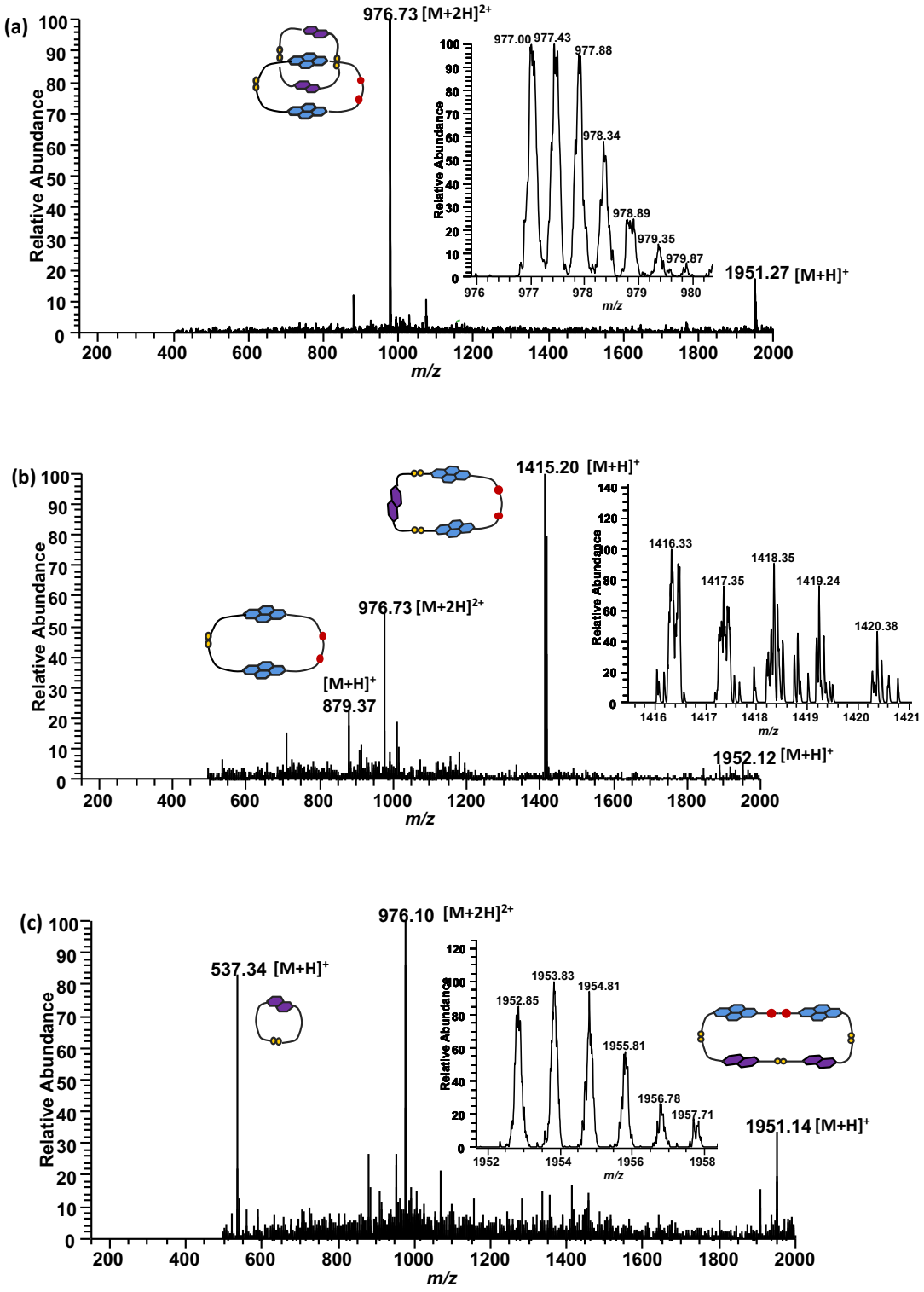

Figure 3-36. ESI-MS (+*ve*) spectra of (a) **Cat16** (as singly and doubly charged cation), (b) heterodimer **[A2b-D2L]** (as singly charged cation), (c) heterotrimer **[A2b-D2L$_2$]** (as singly and doubly charged cation). The expansion of parent molecular ions is shown as inserts.

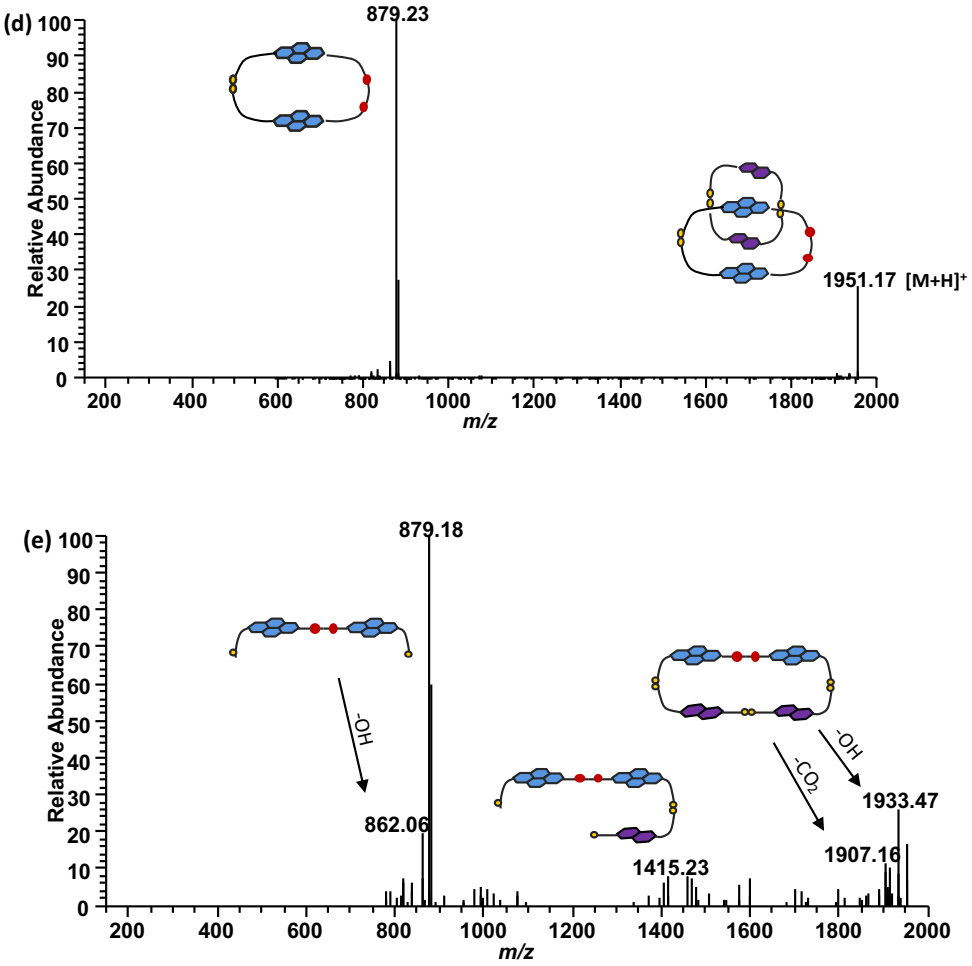

Figure 3-37. MS/MS fragmentation of (d) **Cat16** and (e) heterotrimer **[A2b-D2L$_2$]**.

3.12 DCL of A2c Building Block

The DCL of **A2c** was generated by dissolution of the building block in water (5 mM concentration) and the pH was adjusted to 8.5 using an aqueous solution of 100 mM NaOH. Two libraries were set up, one with $NaNO_3$ and one without, and stirred for one day under air in capped vials to allow full oxidation of the thiols.

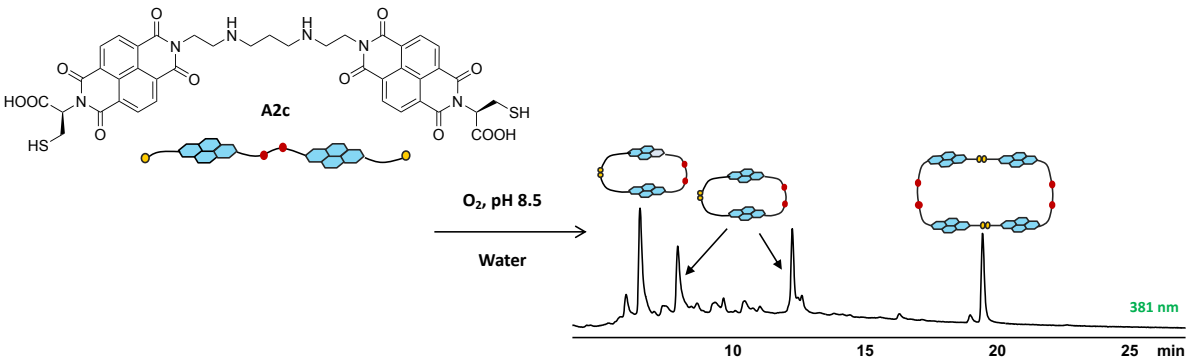

Figure 3-38. The HPLC analysis of **A2c** library in water. Absorbance was recorded at 381 nm.

Three major components were at equilibrium in this library: **A2c** cyclic monomer hydrated on one of the carbonyl groups, cyclic monomer **[A2c]** and cyclic dimer **[A2c]$_2$**.

The library does not ionise very well, and the assignment of **[A2c]$_2$** is based on MS and DAD analyses and comparisons with the behaviour of similar libraries.

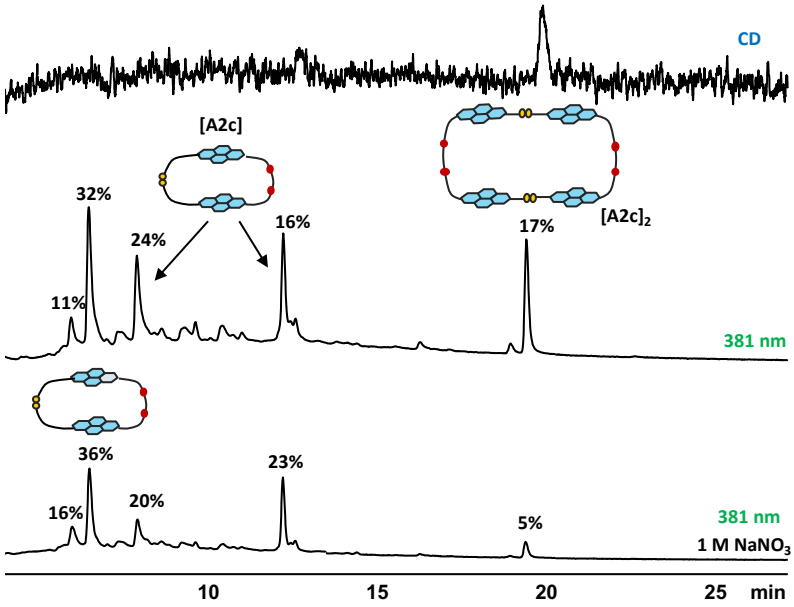

Figure 3-39. The HPLC analysis of **A2c** library in water with and without 1 M $NaNO_3$. Absorbance was recorded at 381 nm.

This building block also has poor solubility in water, and the formation of cyclic monomer as the major component in the library leads to its precipitation. The addition of $NaNO_3$ increases the concentration of **[A2c]** yet reduces the concentration of **[A2c]$_2$**.

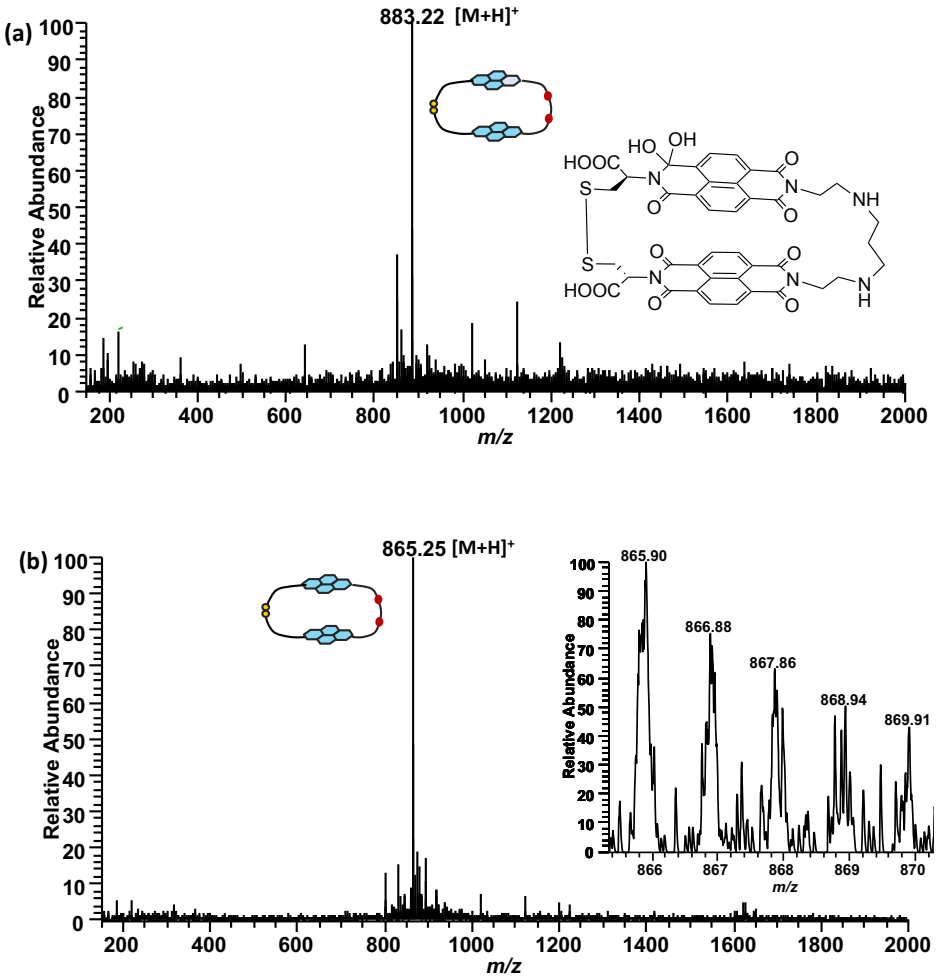

Figure 3-40. ESI-MS (+*ve*) spectra of (a) **A2c** cyclic monomer hydrated and (b) cyclic monomer **[A2c]**.

3.13 DCL of A2c Acceptor and D1S Donor: Cat17

The D-A DCL of **A2c** and **D1S** was prepared in water at pH 8.5. The solution was stirred for one day before it was analysed by HPLC and LC-MS. The LC-MS analysis has revealed that the fully oxidised library contains a series of macrocycles as well as a [2]catenane **Cat17**, in 20% yield (which reduces to 12% in the presence of $NaNO_3$).

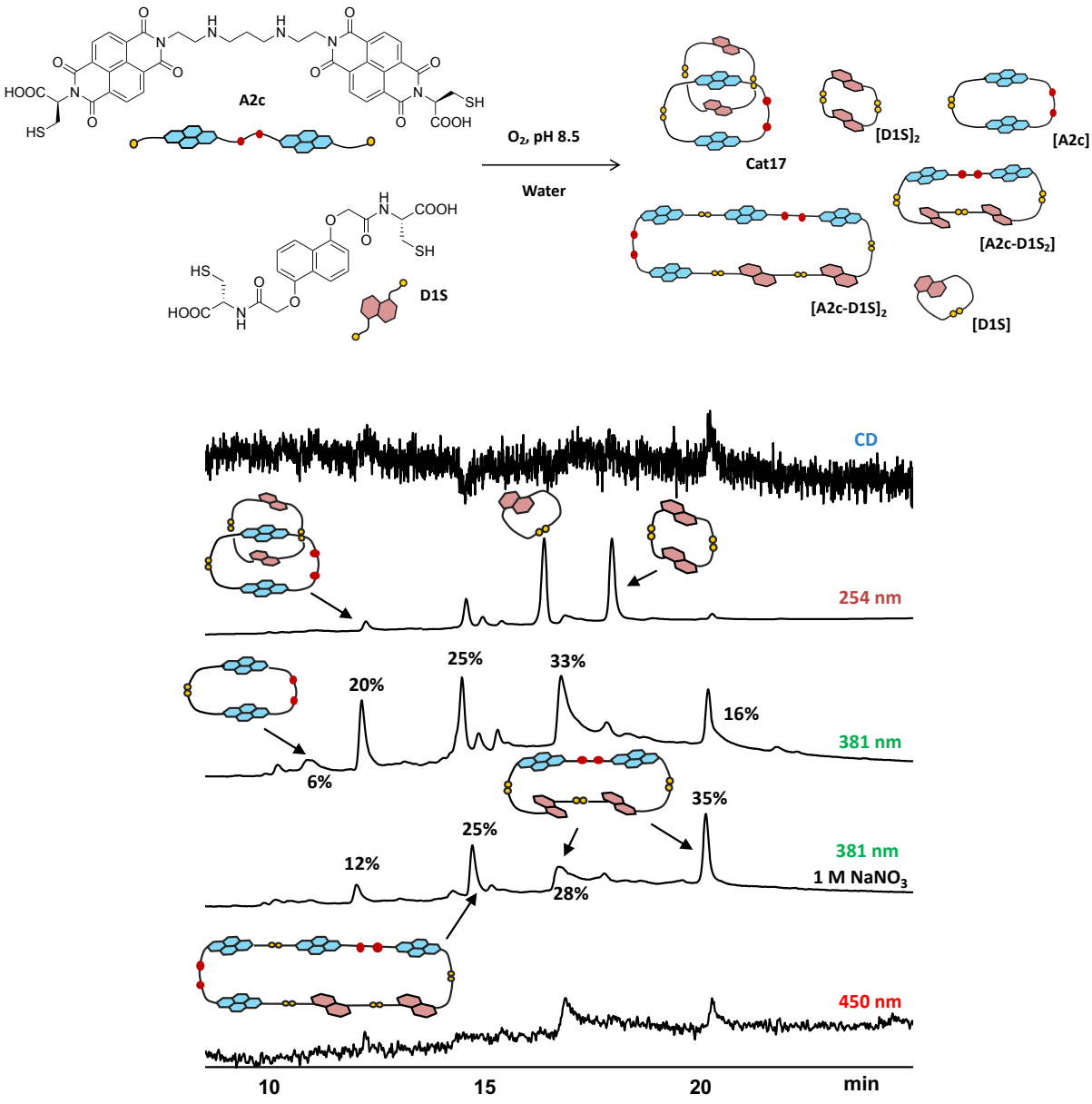

Figure 3-41. The HPLC analysis of D-A DCL of **A2c** and **D1S** (1:2 molar ratio, 5 mM total concentration).

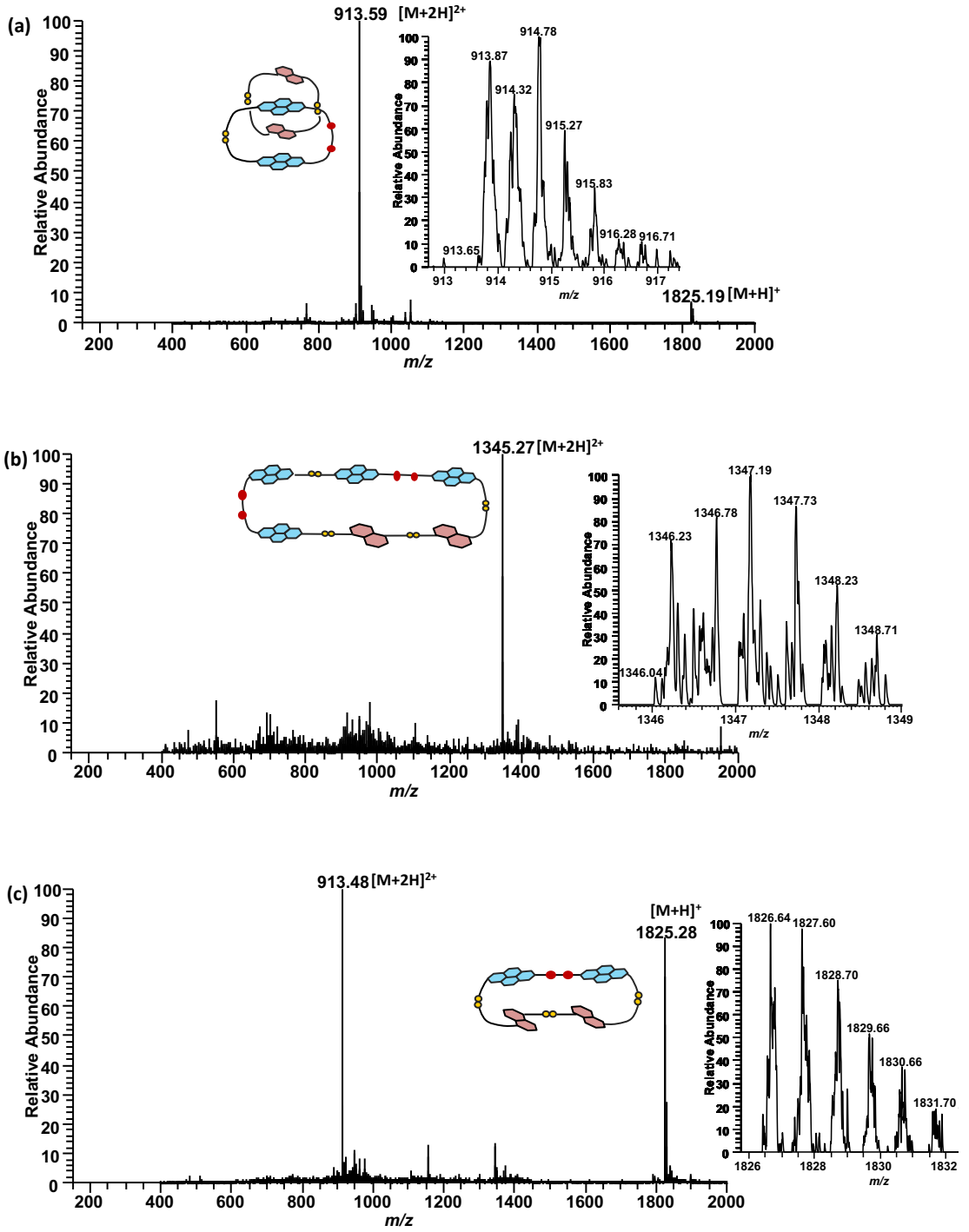

Figure 3-42. ESI-MS (+*ve*) spectra of (a) **Cat17** (as doubly charged cation), (b) heterotetramer **[A2c-D1S]$_2$** (as doubly charged cation), and (c) heterotrimer **[A2c-D1S$_2$]** (as singly and doubly charged cation). The expansion of parent molecular ions is shown as inserts.

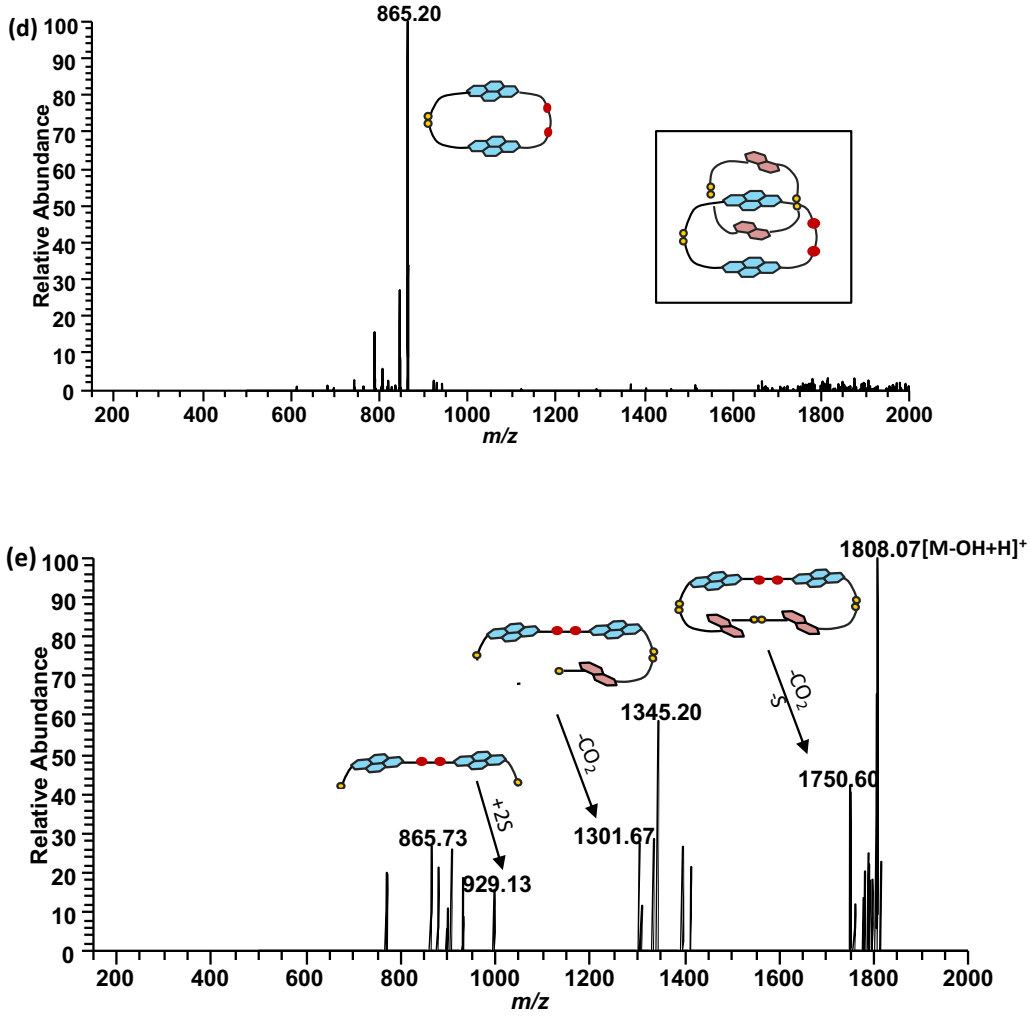

Figure 3-43. MS/MS fragmentation of (d) **Cat17** and (e) heterotrimer **[A2c-D1S$_2$]**.

3.14 DCL of A2c Acceptor and D2S Donor: Cat18

The LC-MS analysis of D-A DCL of **A2c** with **D2S** has showed that the fully oxidised library contains a series of macrocycles in insignificant yields and a new [2]catenane, **Cat18**, in high yield (88%). The fast elution of **Cat18** along with strong CD signal and the sharp peak at 450 nm are in agreement with the assignment of an interlocked molecule for this species.

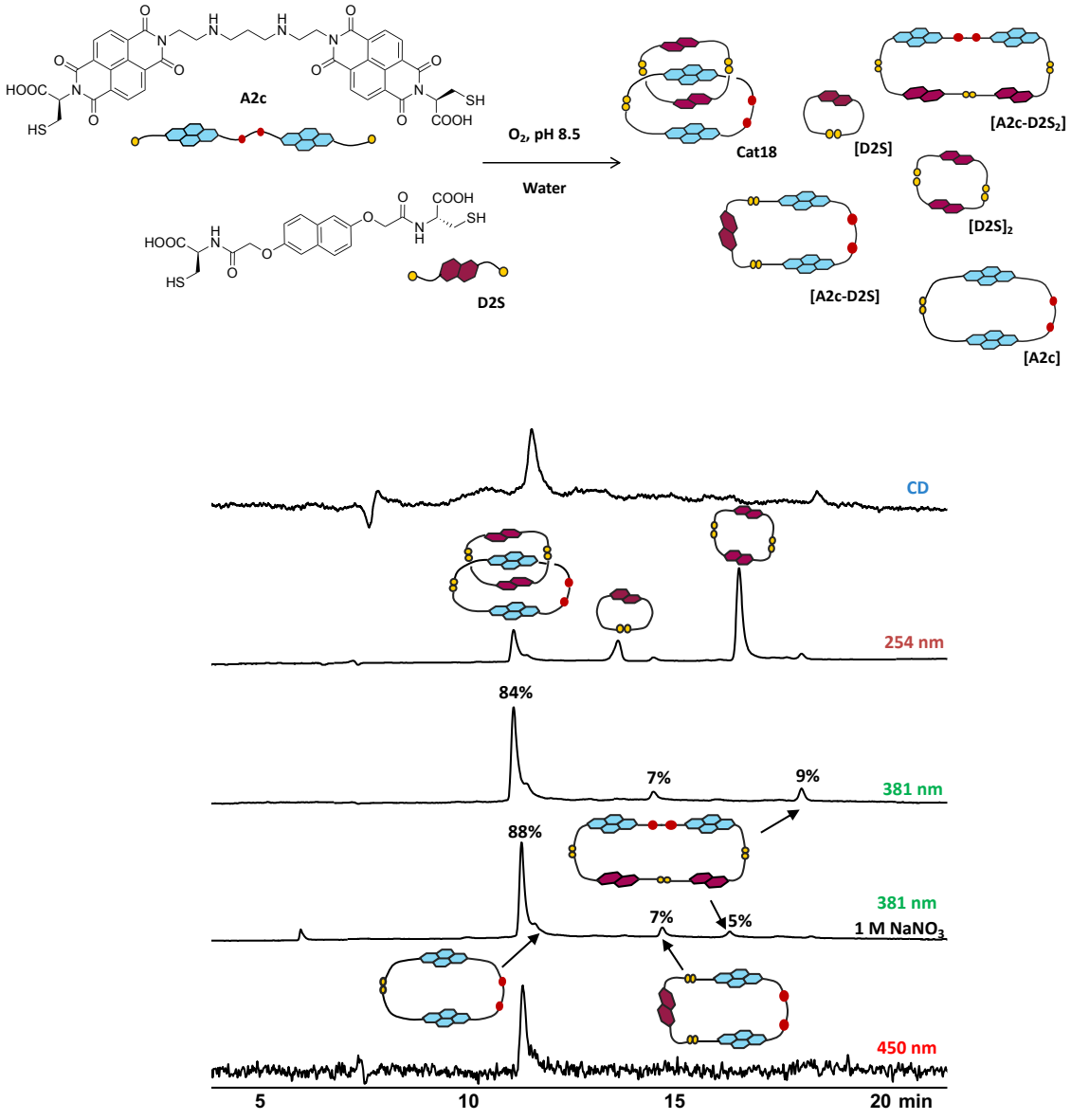

Figure 3-44. The HPLC analysis of D-A DCL of **A2c** and **D2S** (1:2 molar ratio, 5 mM total concentration, H_2O).

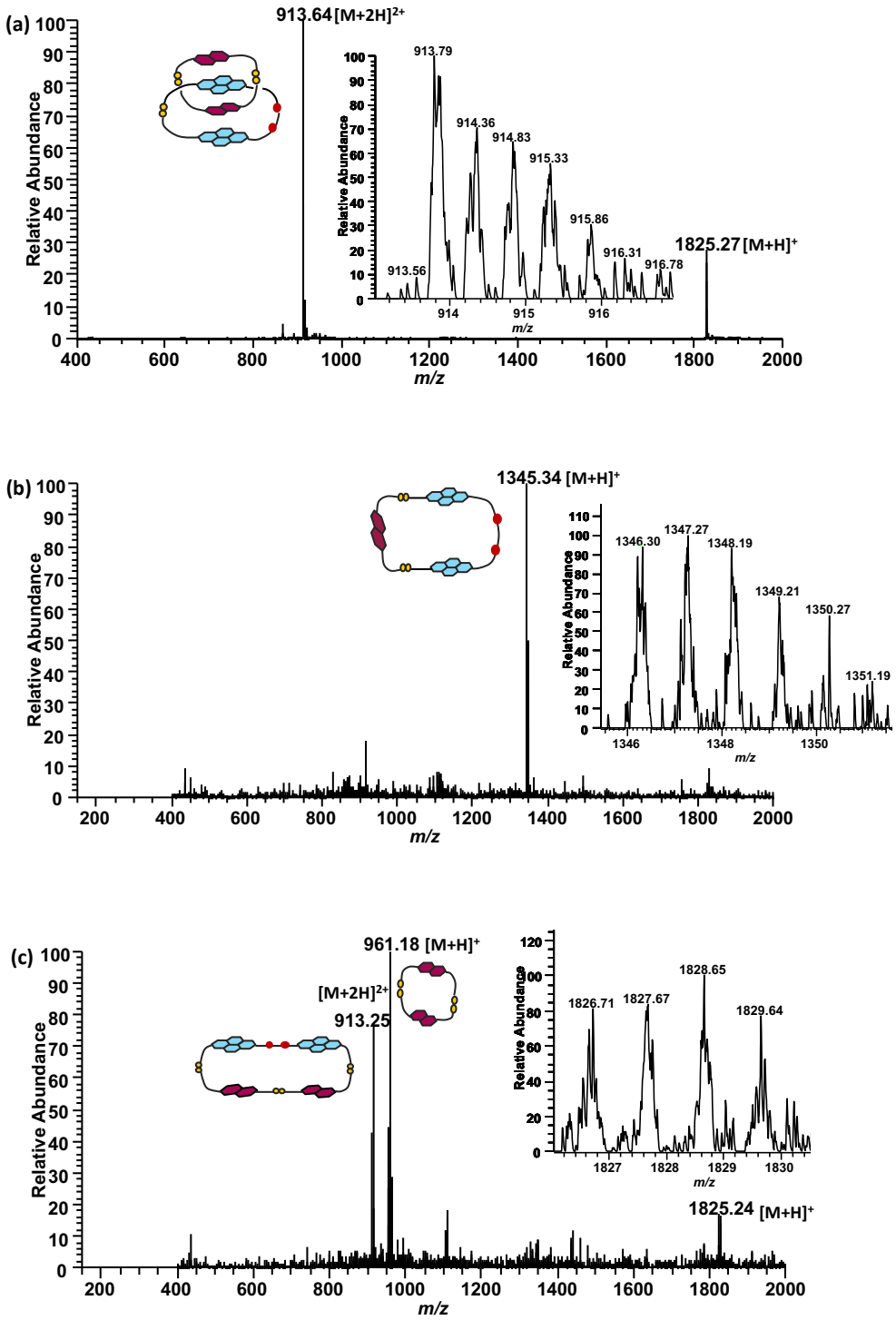

Figure 3-45. ESI-MS (+*ve*) spectra of (a) **Cat18** (as singly and doubly charged cation), (b) the heterodimer **[A2c-D2S]** (as singly charged cation), (c) the heterotrimer **[A2c-D2S$_2$]** (singly and doubly charged cation) and the **[D2S]$_2$** (as singly charged cation). The expansion of parent molecular ions is shown as inserts.

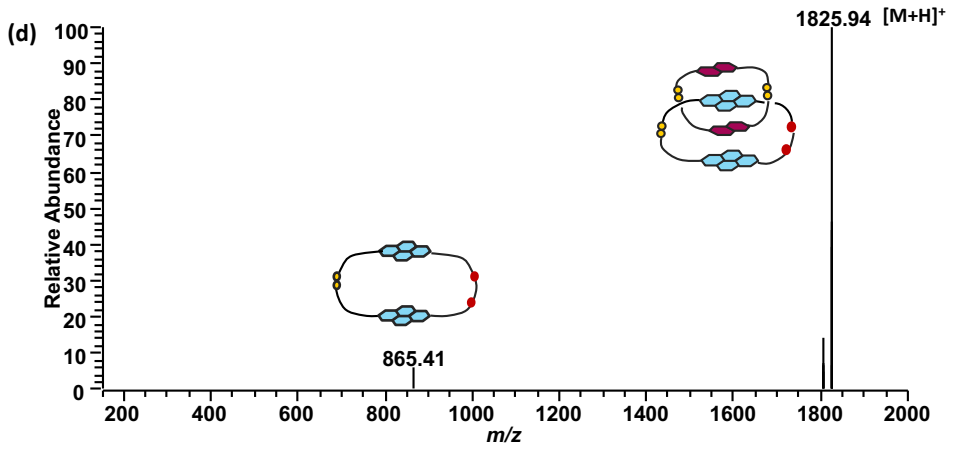

Figure 3-46. MS/MS fragmentation spectra of (d) **Cat18**.

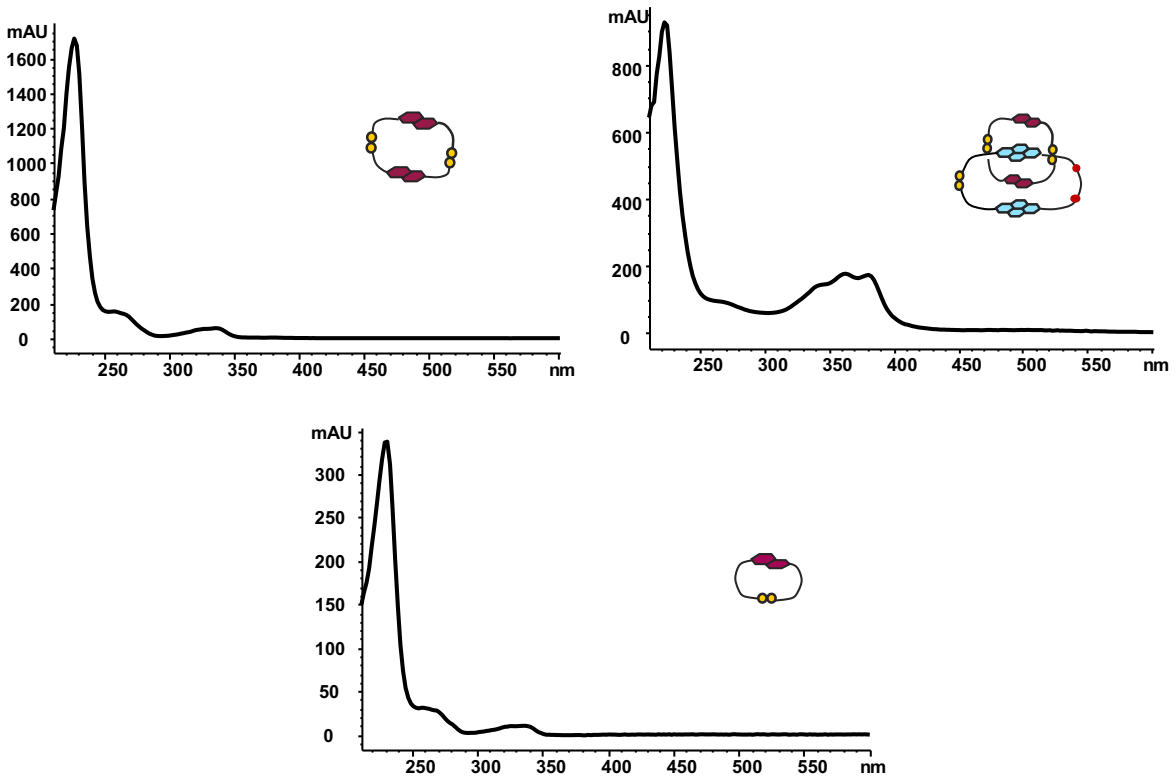

Figure 3-47. The UV-Vis spectrum of **A2c-D2S** library shows the UV of each peak and its corresponding structure (5 mM concentration, H_2O).

3.14.1 1D and 2D ^{1}H NMR Analysis

The 2-aminoethyl-1,3-propanediamine is a symmetrical polyamine, and therefore, **Cat18** can only have two diastereomers. This makes the NMR analysis easier when compared to **Cat5** (with four diastereomers).

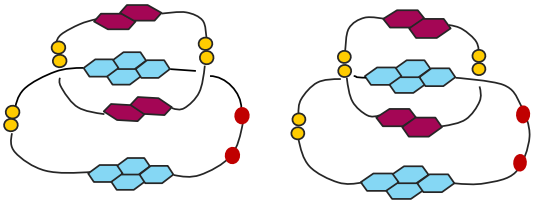

Figure 3-48. The possible diastereomers of **Cat18**.

To further study this species, **Cat18** was isolated by preparative HPLC (purity of isolated **Cat18**: 92%, Figure 3-49) and analysed by NMR and CD.

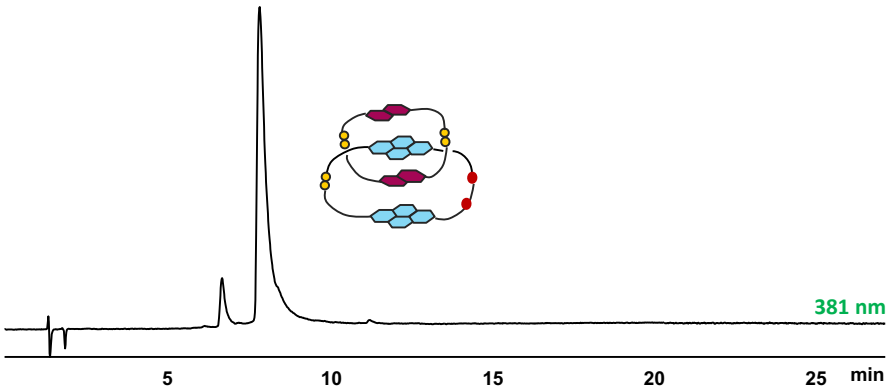

Figure 3-49. Reverse-Phase HPLC result of the isolated **Cat18**. Absorbance was recorded 381 nm.

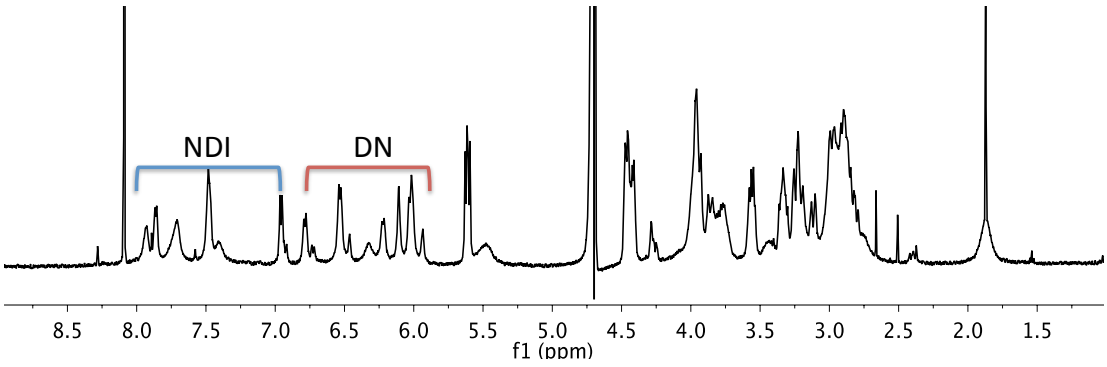

Figure 3-50. ^{1}H NMR full spectrum of **Cat18** (D_2O, 500 MHz). The solvent peak was referenced at 4.74 ppm.

The catenated nature of **Cat18** was confirmed by NMR spectroscopy. The aromatic region of the ^{1}H NMR spectrum displays the peaks corresponding to two diastereomers, which have the characteristic upfield shifts for the stacked NDI and DN moieties (7.93 – 6.95 ppm for NDI and 6.85 – 5.91 ppm for DN; Figure 3-51). The ^{1}H NMR spectrum indicates that one of the two diastereomers is more conformationally flexible as indicated by the broad signals associated to the structure (depicted with * in Figure 3-51). This can be explained by the longer linker in between the NDI cores in **Cat18** when compared to **Cat5**.

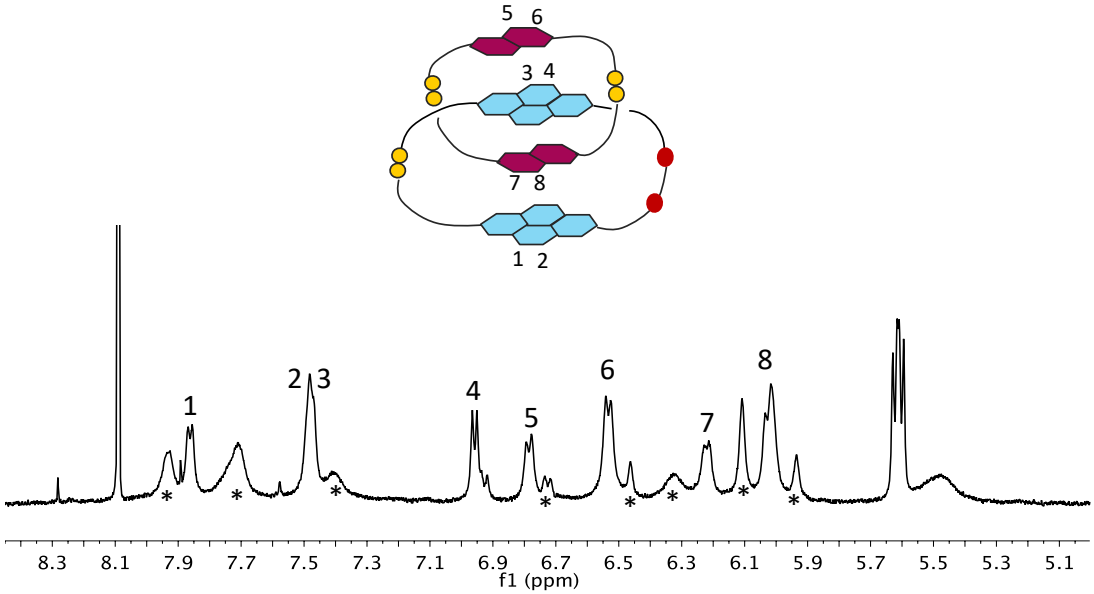

Figure 3-51. ^{1}H NMR spectrum of **Cat19** (D_2O, 500 MHz, 298 K) from 5.0 – 8.4 ppm. The solvent peak was referenced at 4.74 ppm.

The ^{1}H NMR spectrum of **Cat18** is consequently simpler than what we have observed for **Cat5**, as there are only two catenanes formed. However, the COSY analysis of the donor and acceptor regions shows weak correlations and so, not all the peaks could be identified (represented by *).

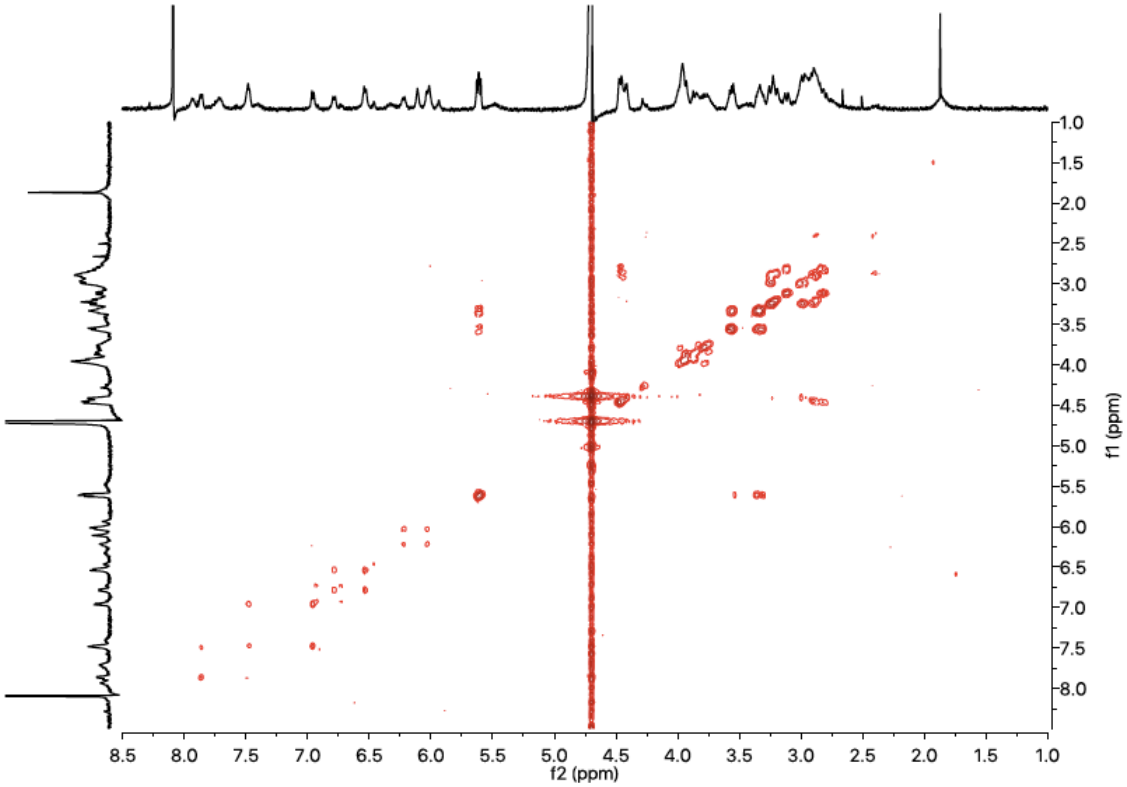

Figure 3-52. Full COSY spectrum of **Cat18** (D_2O, 500 MHz, 298 K). The solvent peak was referenced at 4.74 ppm.

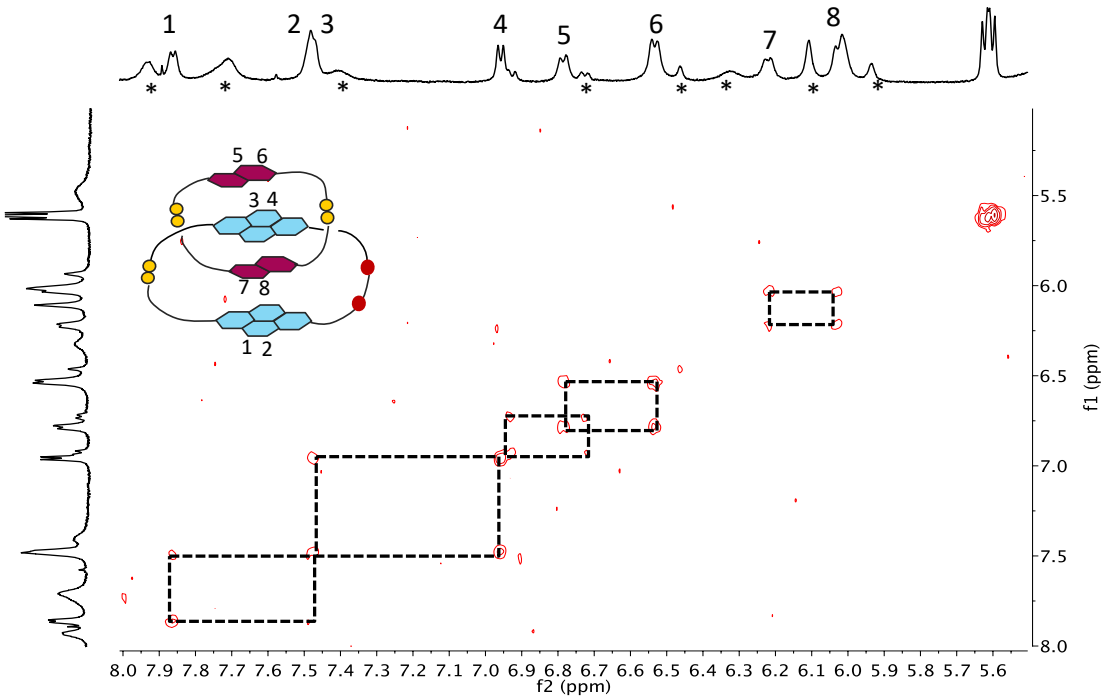

Figure 3-53. Partial COSY spectrum of **Cat18** (between 5.5 – 8.0 ppm, D_2O, 500 MHz, 298 K). The solvent peak was referenced at 4.74 ppm.

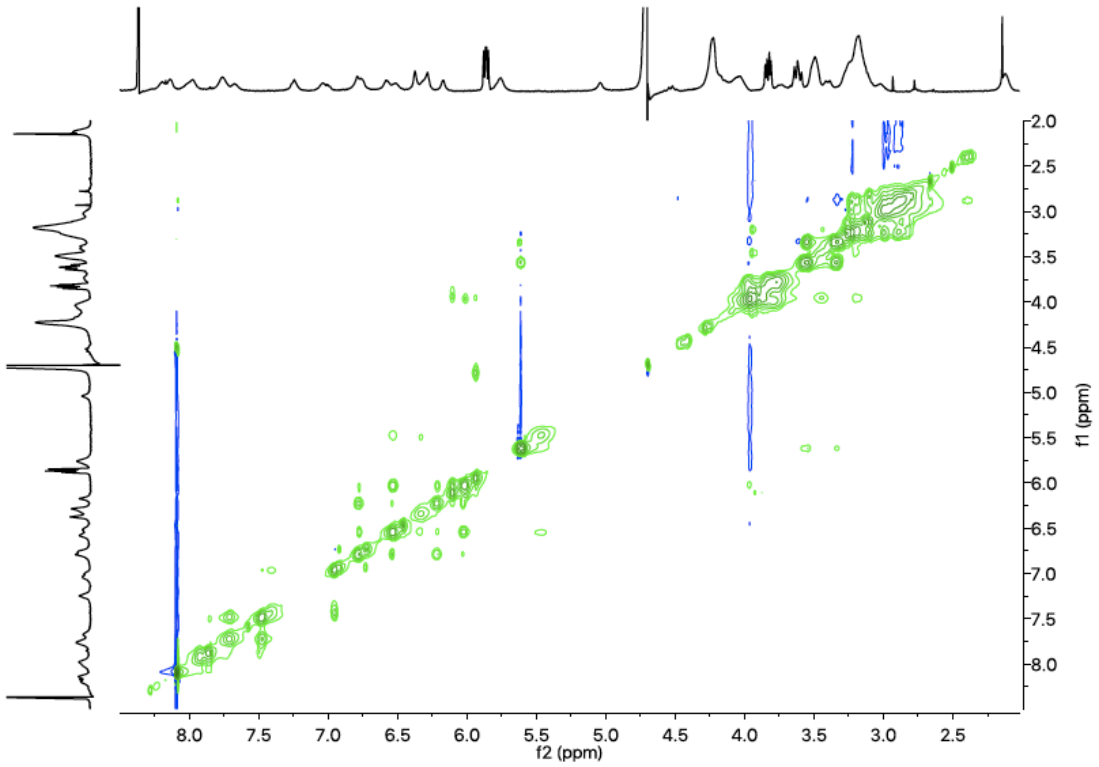

Figure 3-54. Full NOESY spectrum of **Cat18** (D_2O, 500 MHz, 298 K). The solvent peak was referenced at 4.74 ppm.

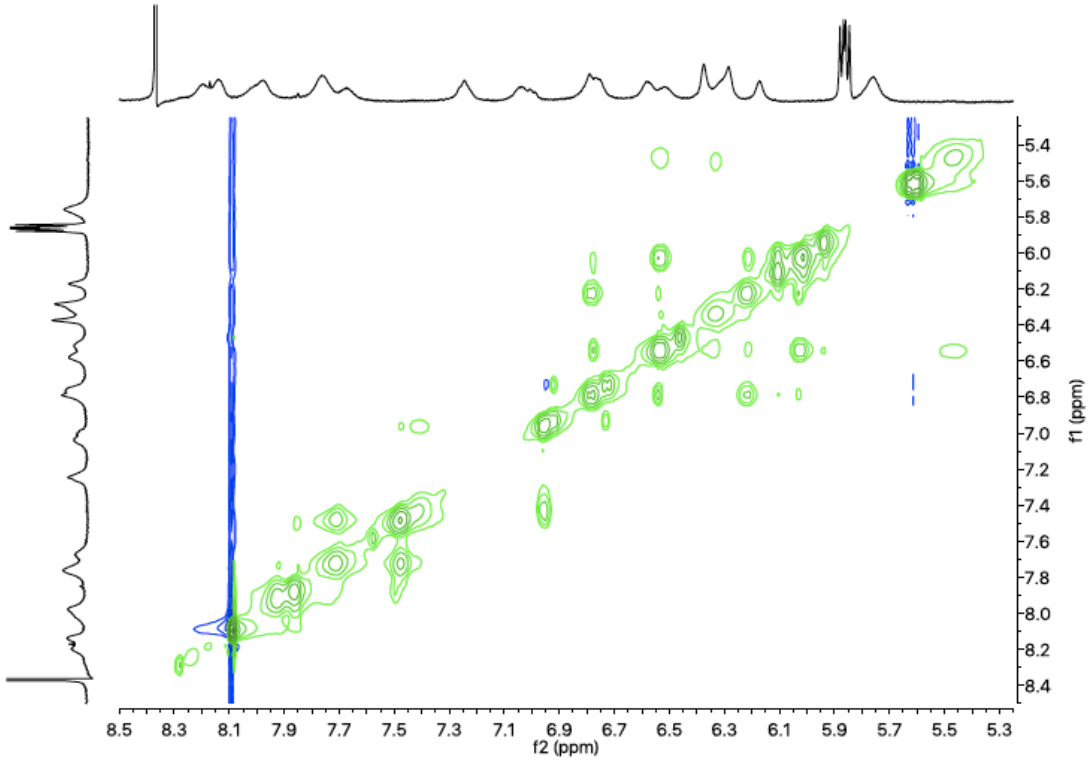

Figure 3-55. Partial NOESY spectrum of **Cat18** (from 5.2 – 8.50 ppm, D_2O, 500 MHz, 298 K). The solvent peak was referenced at 4.74 ppm.

3.14.2 Circular Dichroism (CD) Analysis

The isolated catenane (**Cat18**) was analysed by variable temperature (VT) UV-Vis and CD spectroscopy studies. The CD spectra show a negative Cotton effect between (175 – 200 nm) and strong positive Cotton effect between (220 – 250 nm), which is ascribed to the disulfide n→σ* and aromatic π→π* transitions with lower contributions from the amide / imide and carboxylate chromophores. The NDI chromophore (300 – 400 nm) is in a chiral environment as indicated by a negative Cotton effect (Figure 3-56).

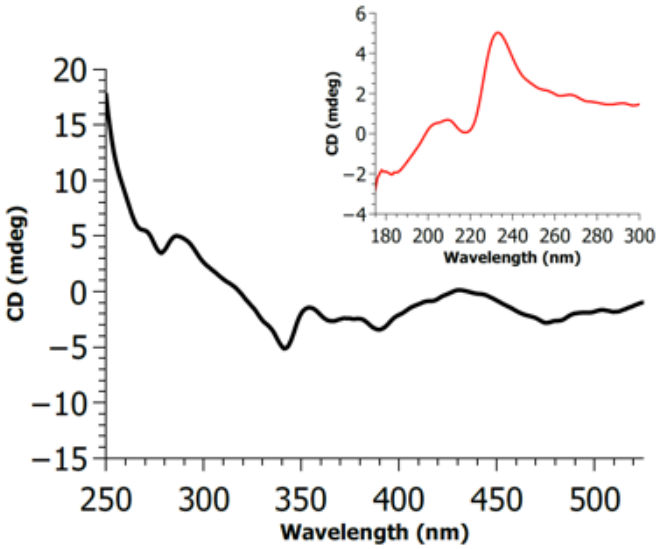

Figure 3-56. The CD spectrum of **Cat18** (250 – 600 nm) recorded in a 10mm pathlength cuvette. Inset: the UV region (175 – 300 nm) recorded in a 1 mm pathlength cuvette. The experiment was done at 23 °C.

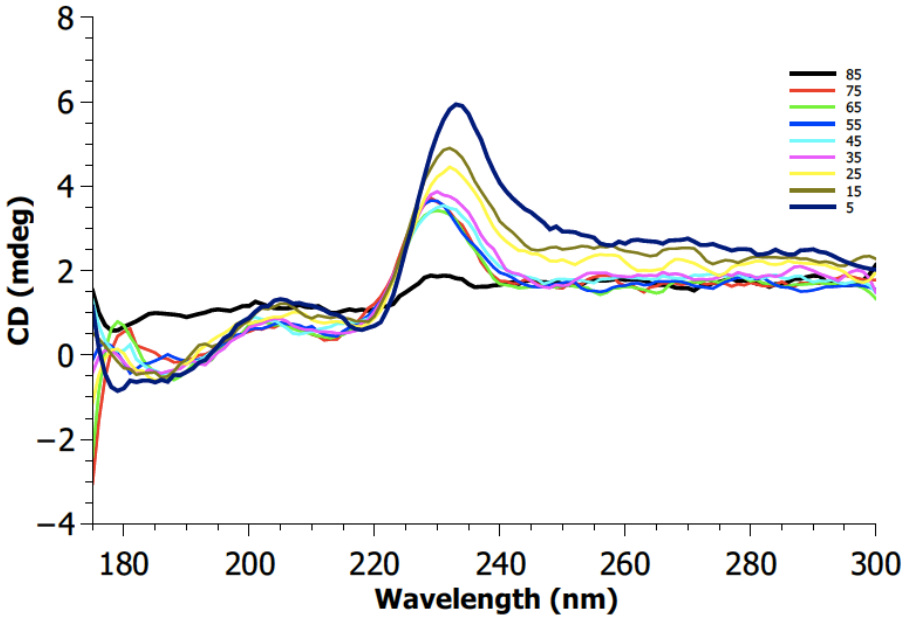

Figure 3-57. Variable temperature CD spectra of **Cat18** from 5 – 85 °C (D_2O, 175 – 300 nm, 1 mm pathlength cuvette).

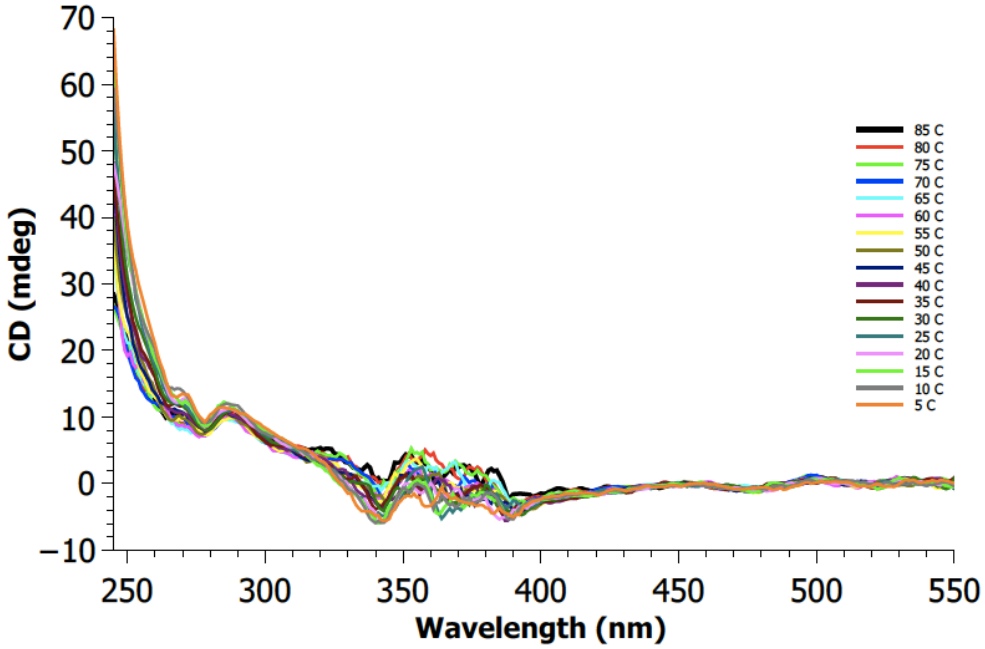

Figure 3-58. Variable temperature CD spectra of **Cat18** from 5 – 85 °C (D_2O, 245 – 550 nm, 10 mm pathlength cuvette).

The VT experiments (5 – 85 °C) showed only a slight change on CD spectra of the NDI region, confirming the interlocked structure.

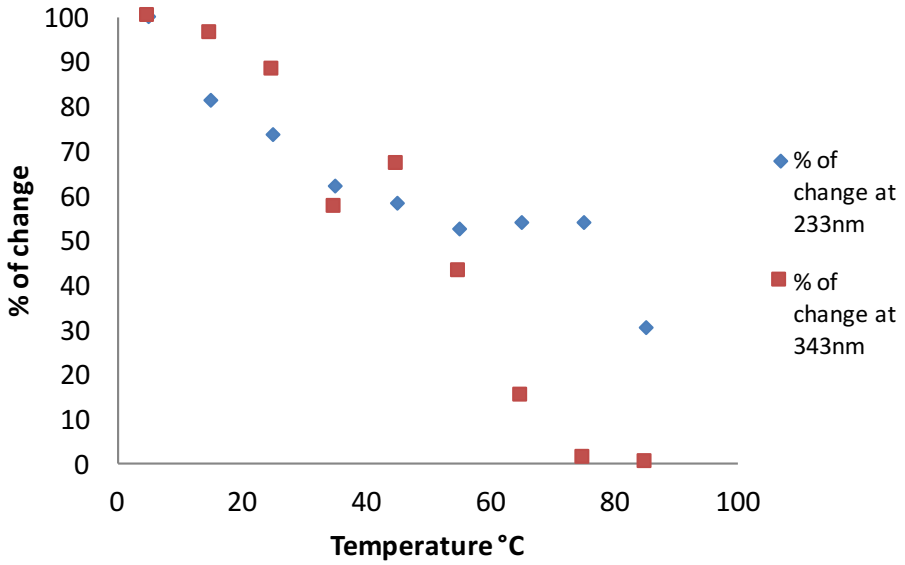

Figure 3-59. The comparison between % of change for **Cat18** at two wavelengths (233 and 343 nm). This catenane is more flexible in the NDI region (higher wavelength – 343 nm) than in the cysteine region.

3.14.3 The Effect of Chirality on Catenane Formation

Changing the point chirality of the **A2c** building block from L to D on the cysteine groups, does not significantly affect the DCL's distribution, with **Cat18*** being formed in 87% in comparison to 88% yield for **Cat18**.

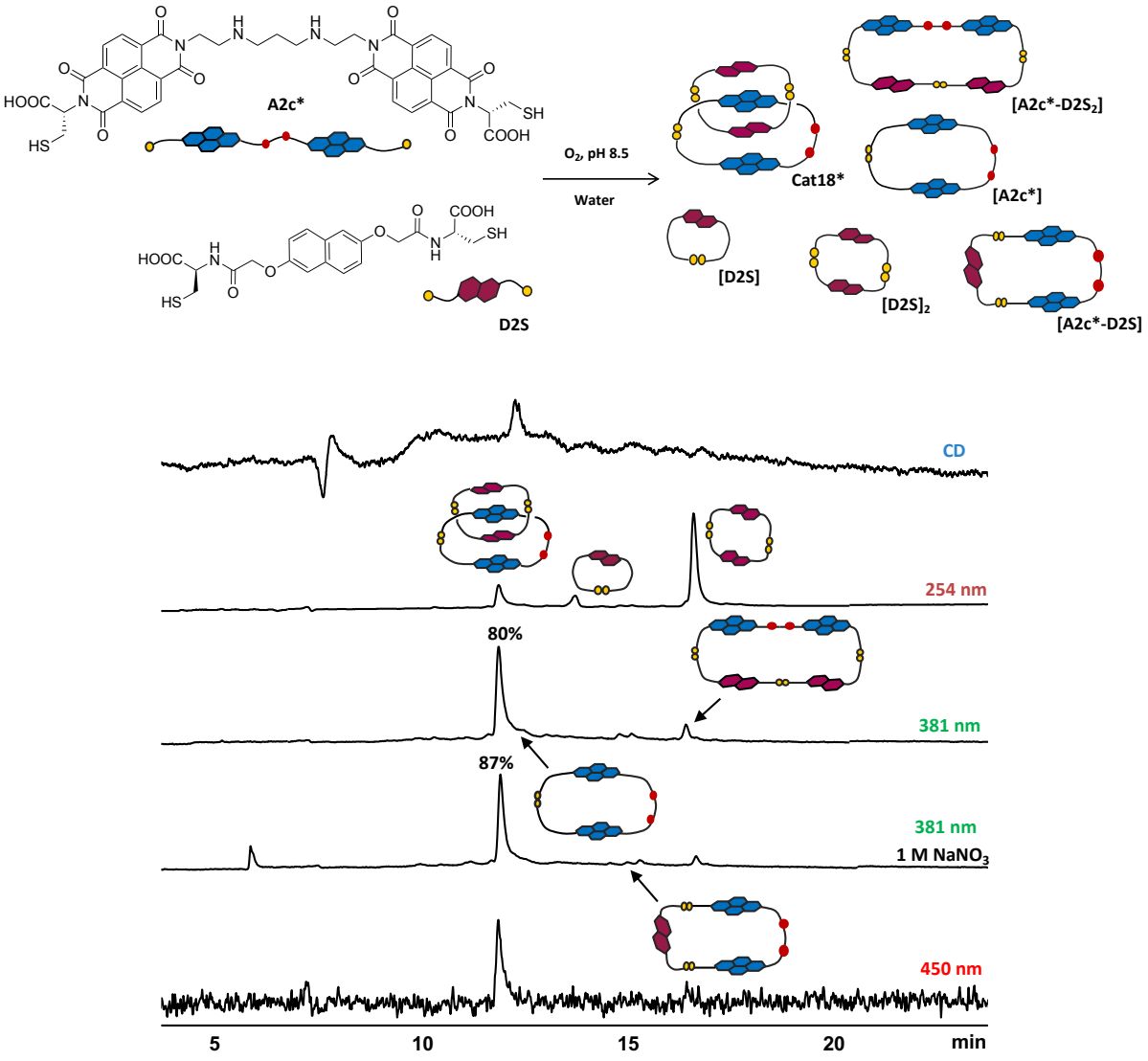

Figure 3-60. The HPLC analysis of D-A DCL of **A2c*** and **D2S** (1:2 molar ratio, 5 mM total concentration, H_2O).

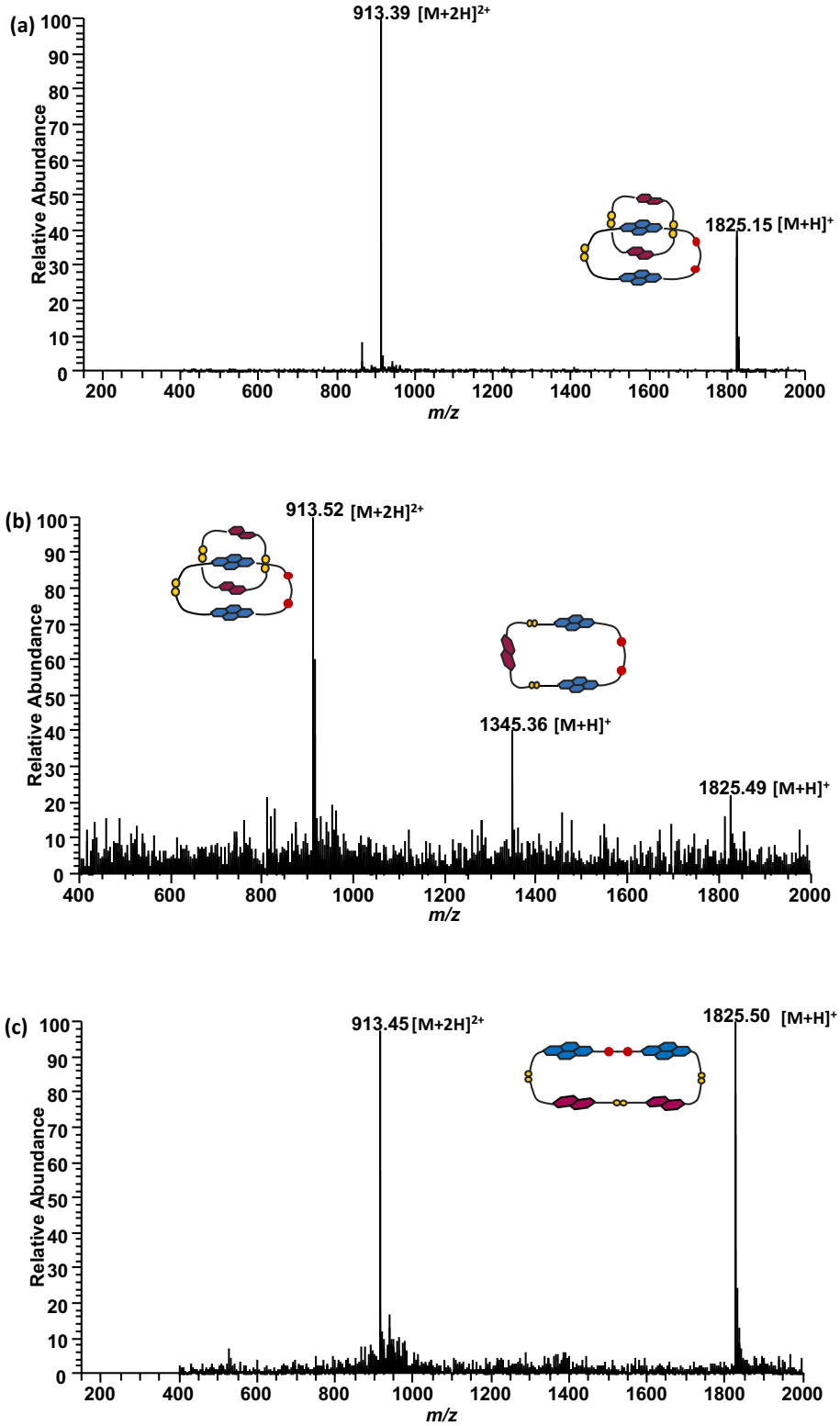

Figure 3-61. ESI-MS (+*ve*) spectra of (a) **Cat18*** (as singly and doubly charged cation), (b) the heterodimer **[A2c*-D2S]** (as singly charged cation) and (c) the heterotrimer **[A2c*-D2S$_2$]** (as singly and doubly charged cation) and the **[D2S]$_2$** (singly charged cation).

3.14.4 Kinetic Study for formation of Cat18*

The kinetic study shows the formation of **Cat18*** over time. The number of intermediates and macrocyclic species is higher at the initial point of the library, and it starts decreasing to three species as the library reaches equilibrium.

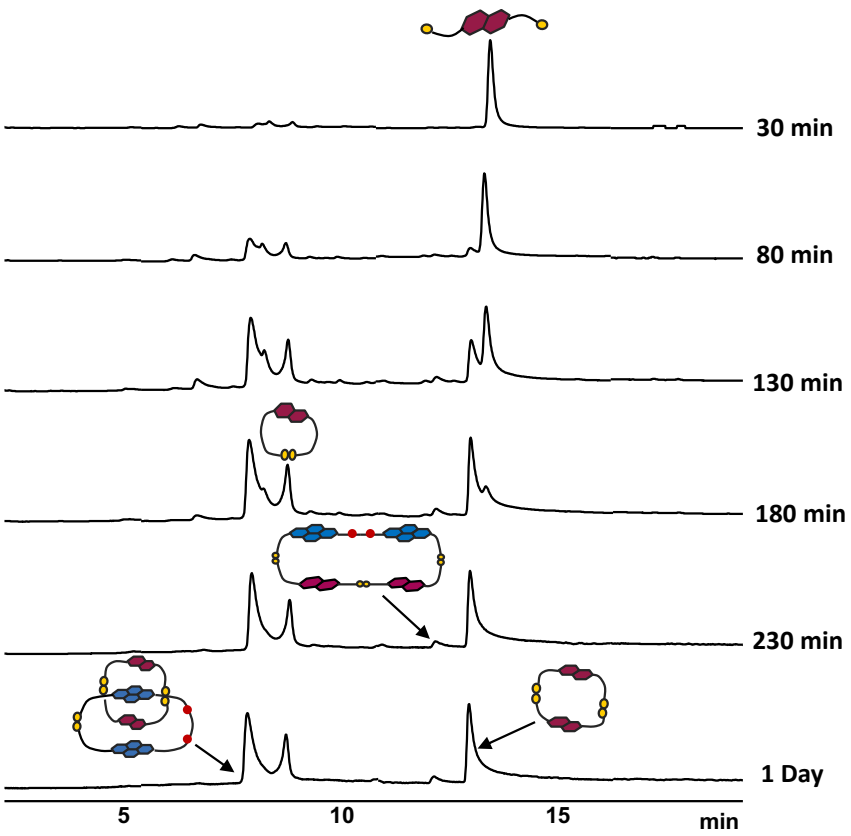

Figure 3-62. Kinetic study showing the formation of **Cat18*** over time. The absorbance was recorded at 254 nm.

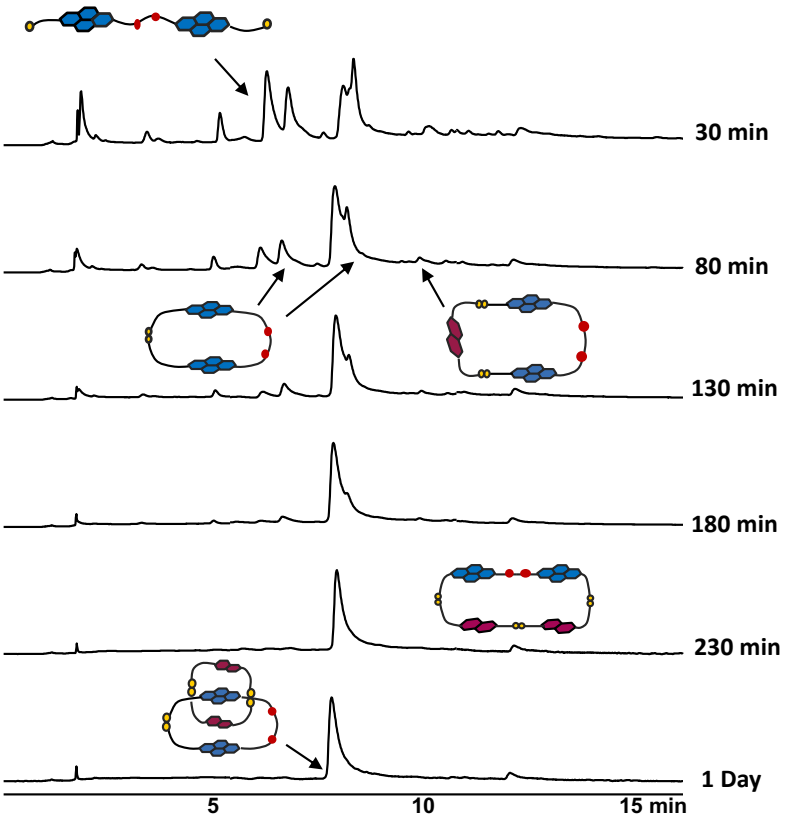

Figure 3-63. Kinetic study showing the formation of **Cat18*** over time. The absorbance was recorded at 381 nm.

The HPLC traces of the two libraries containing **Cat18** and **Cat18*** were overlapped to compare the retention times of their peaks.

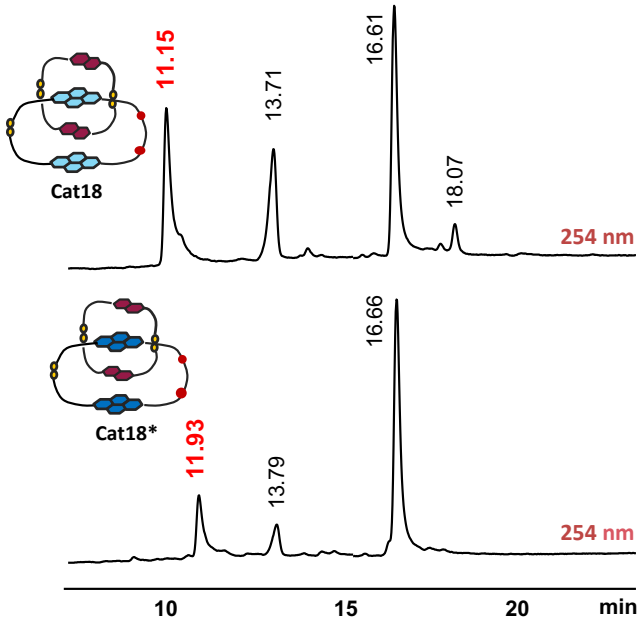

Figure 3-64. The comparison between the HPLC traces of **Cat18** and **Cat18*** (same condition and column).

As with the **Cat5** / **Cat5*** pair, the inversion of chirality on the acceptor cysteine has a slight influence on the retention times of the isomeric **Cat18** / **Cat18*** [2]catenanes, which elute at 11.15 and 11.93 min, respectively, under identical HPLC conditions. The peaks that correspond to the formation of **[D2S]** and **[D2S]$_2$** can be used as an internal reference in both HPLC chromatograms, thus observing the change in the catenanes' retention time.

3.14.5 Circular Dichroism (CD) analysis

The CD spectra show negative Cotton effect between (175 – 220 nm) and a positive Cotton effect between (220 – 250 nm), which is ascribed to the disulfide n→σ* and aromatic π→π* transitions with lower contributions from the amide / imide and carboxylate chromophores. The NDI chromophore (300 – 400 nm) is in a chiral environment as indicated by a negative Cotton effect (Figure 3-65).

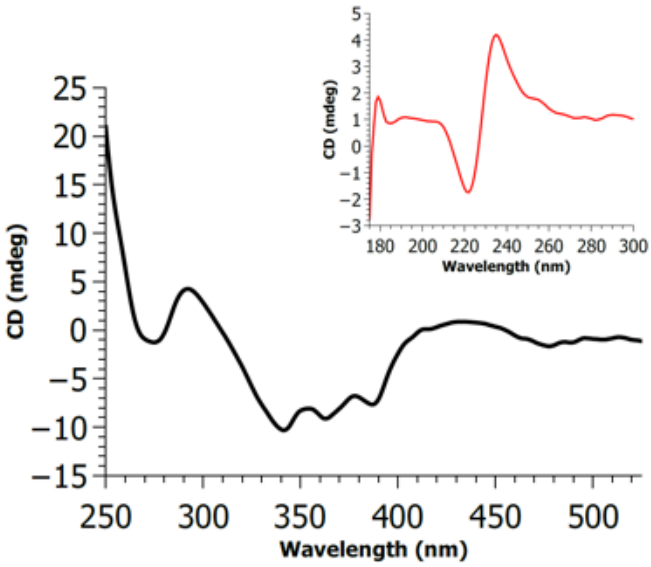

Figure 3-65. The CD spectrum of **Cat18** (250 — 600 nm), recorded in a 10 mm pathlength cuvette; Inset the UV region (175 — 300 nm), recorded in a 1 mm pathlength cuvette.

The VT experiments (5 – 85 °C) displayed only a slight change on CD spectra of the NDI region, confirming the interlocked structure.

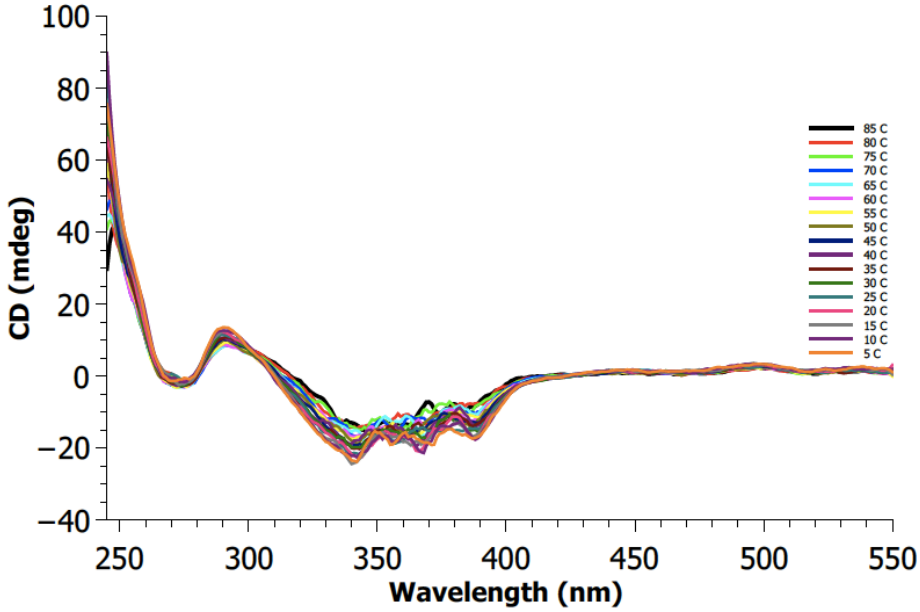

Figure 3-66. Variable temperature CD spectra between 5 – 85 °C of **Cat18*** (D_2O, 245 – 550 nm, 10 mm pathlength cuvette).

3.15 D-A DCL of A2c Acceptor and D1L Donor: Cat19

The LC-MS analysis of D-A DCL of **A2c** with **D1L** has revealed that the fully oxidised library contains a [2]catenane, **Cat19**, in 51% along with a series of macrocycles. The concentration of **Cat19** decreases 17% with the addition of $NaNO_3$, while the concentration of **[A2c-D1L]$_2$** increases 10%. The concentration of **[A2c-D1L$_2$]** maintains almost the same regardless the addition or lack of salt.

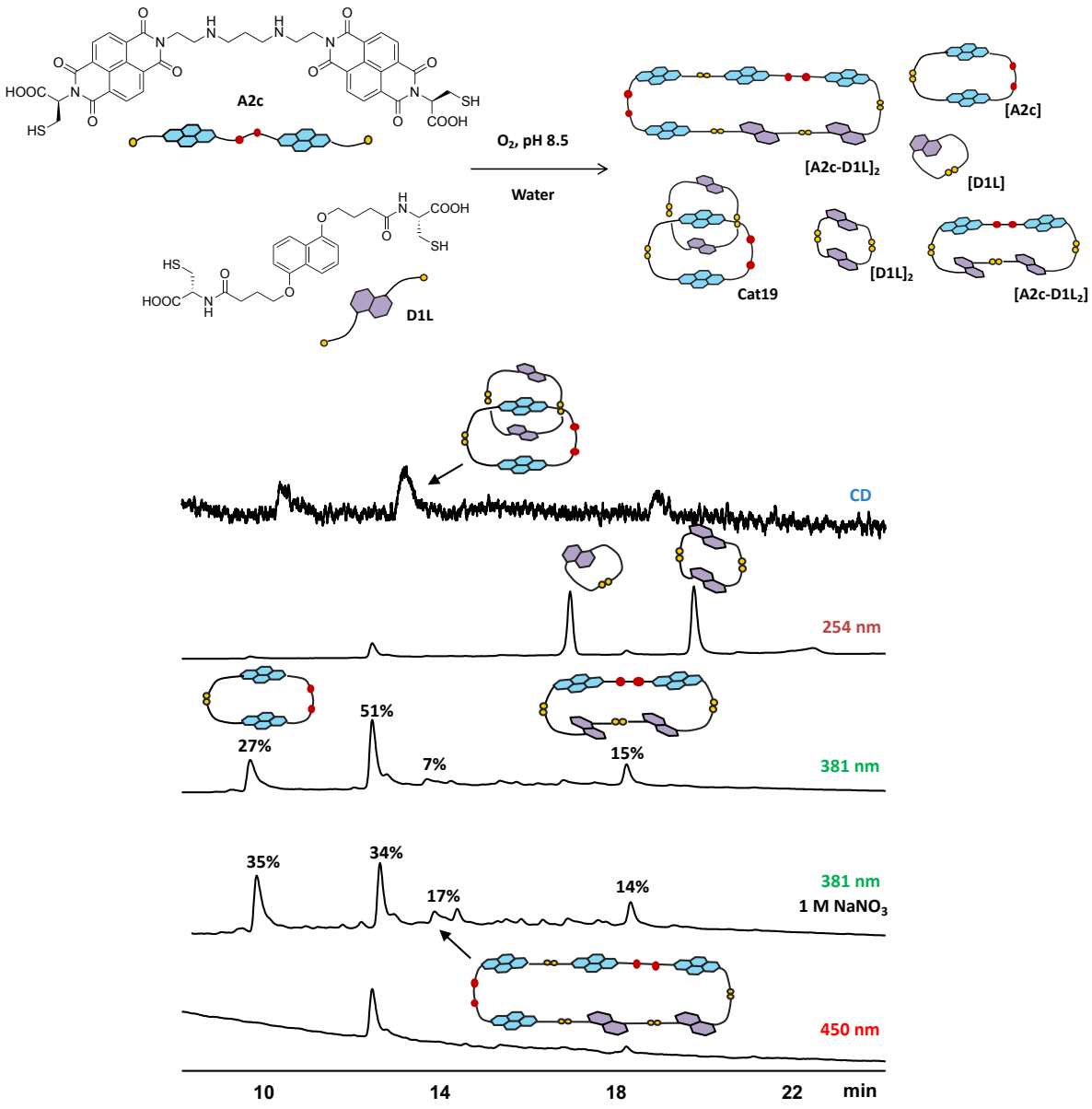

Figure 3-67. The HPLC analysis of D-A DCL of **A2c** and **D1L** (1:2 molar ratio, 5 mM total concentration).

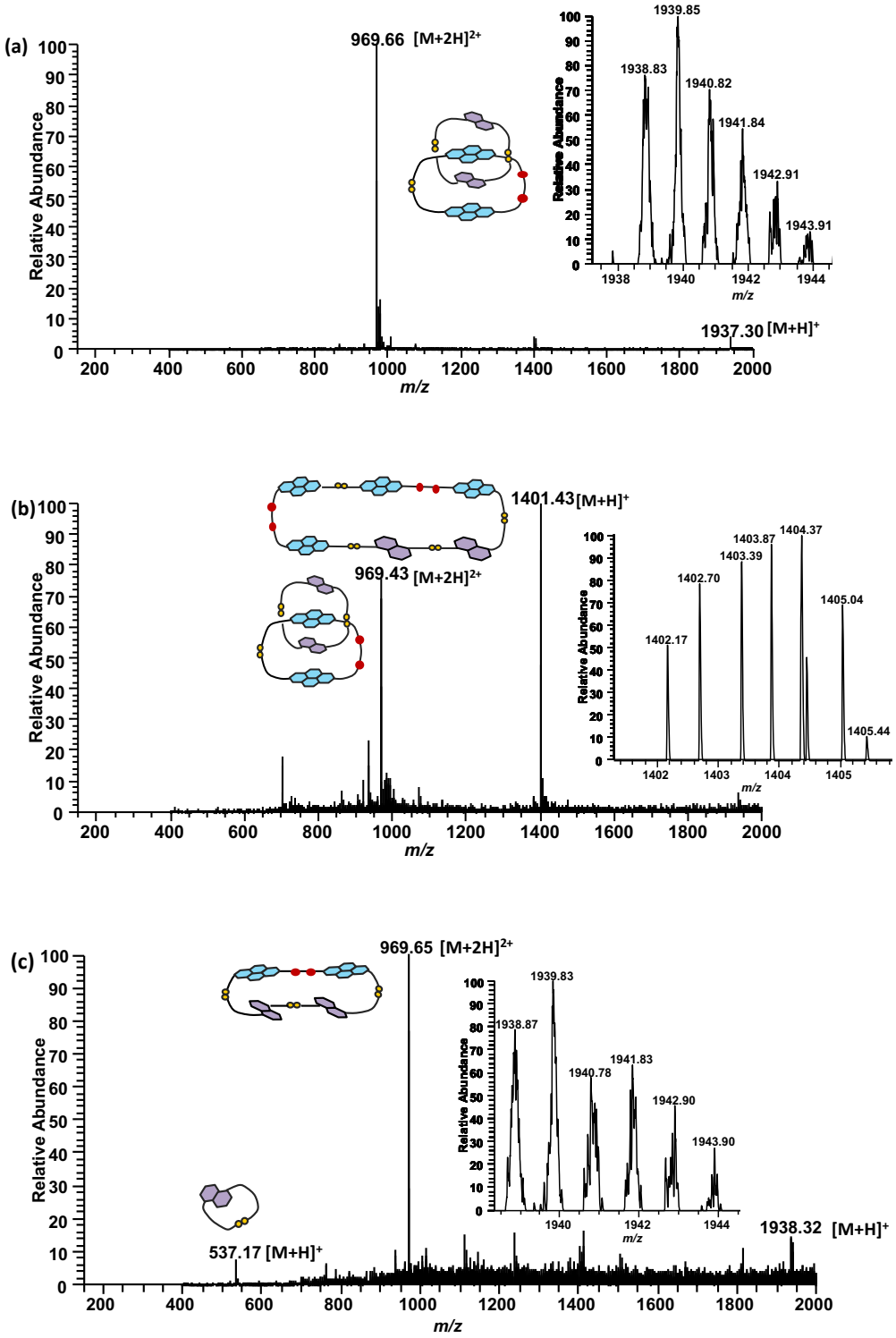

Figure 3-68. ESI-MS (+*ve*) spectra of (a) **Cat19** (as singly and doubly charged cation), (b) the heterotetramer **[A2c-D1L]$_2$** (as doubly charged cation) and (c) the heterotrimer **[A2c-D1L$_2$]**. The expansion of parent molecular ions are shown as inserts.

3.16 DCL of A2c Acceptor and D2L Donor: Cat20

The LC-MS analysis of D-A DCL of **A2c** with **D2L** has indicated that the fully oxidised library contains a [2]catenane in a relatively good yield of 72% (**Cat20**) with a series of macrocycles. The library with $NaNO_3$ showed the same distribution, yet with slightly different yields.

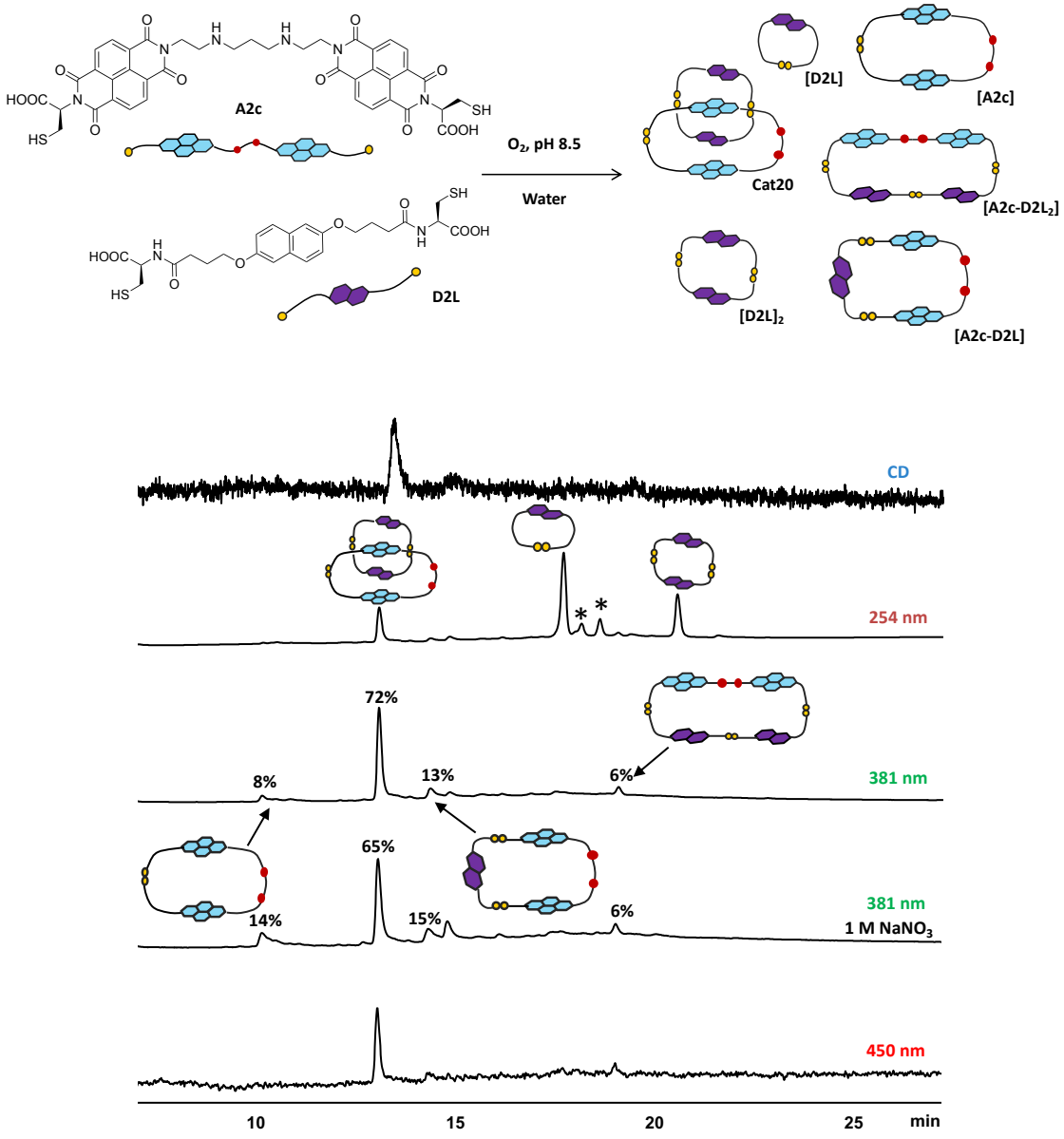

Figure 3-69. The HPLC analysis of D-A DCL of **A2c** and **D2L** (1:2 molar ratio, 5 mM total concentration).

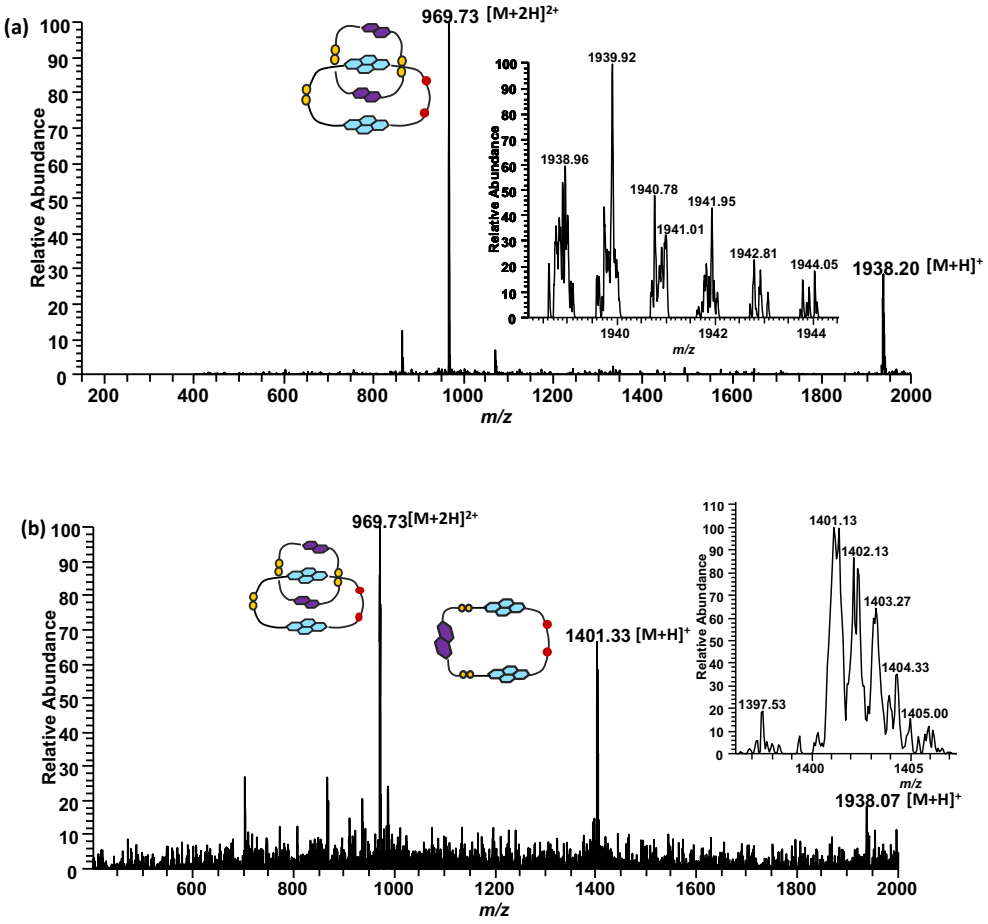

Figure 3-70. ESI-MS (+*ve*) spectra of (a) **Cat20** (as singly and doubly charged cation) and (b) the heterodimer **[A2c-D1L]** (as singly charged cation). The expansion of parent molecular ions are shown as inserts.

3.17 Conclusion

All three acceptor building blocks (**A2a**, **A2b** and **A2c**) have led to catenanes with all the donor building blocks (**D1S**, **D2S**, **D1L** and **D2L**). However, the **D1S** is as expected not the best donor partner for the formation of [2]catenanes, as the yields obtained for each D-A DCL with **D1S** were low.

The results described in this chapter illustrate the importance of the length of the polyamine linker. The employment of the acceptor building blocks with longer polyamine has led to formation of [2]catenanes in a reasonably good yields. In contrast with the molecules used in the previous chapter where only **A1c** with eight atoms in the linker formed [2]catenanes in good yield, all the building blocks described in this chapter have generated catenanes.

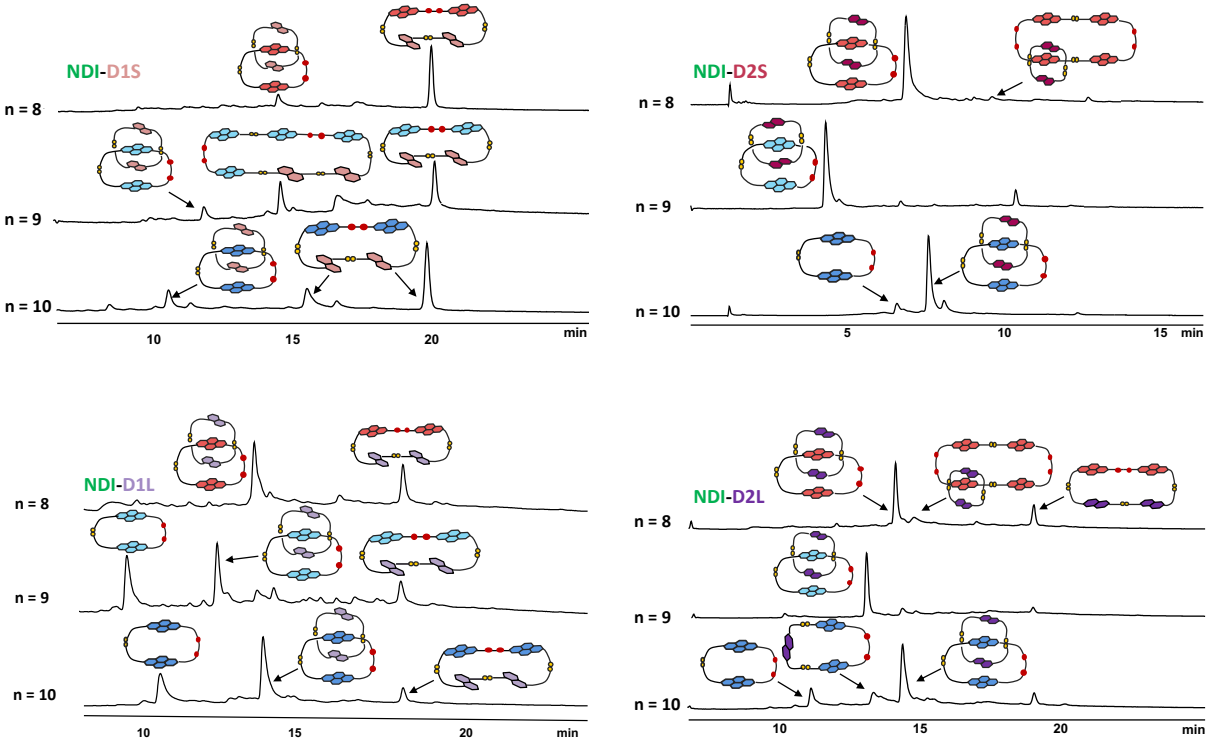

Figure 3-71. HPLC chromatogram of **A2a**, **A2b** and **A2c** acceptors with **D1S**, **D2S**, **D1L** and **D2L** donors. Absorbance was recorded at 381 nm.

The **A2a** acceptor has eight atoms in its linker (same as **A1c**, expect one carbon is replaced by a nitrogen atom) and leads to two types of [2]catenanes with **D2S** and **D2L** donors. The two catenanes include the classical DADA [2]catenane which consist of an NDI cyclic monomer interlocked with a DN dimer, and another [2]catenane with an NDI cyclic dimer interlocked with a DN dimer. The larger [2]catenanes have formed in very small yields and their

concentration did not improve in the presence of $NaNO_3$, thus making the isolation and further analysis difficult.

The acceptors with longer linkers (**A2b** and **A2c**) have also formed catenanes in high yields (88% for **Cat18** and 71% for **Cat12**). The **A2c** acceptor, unlike **A2a** and **A2b** molecules, has three carbon atoms between its two nitrogen atoms. This leads to shorter retention times for the catenanes containing the **A2c** building block compared to **A2a** acceptor molecule, as observed in the HPLC traces. This is potentially associated with the tighter packing in the conformation of this [2]catenane, which makes it elute faster despite its longer linker.

The HPLC, MS, NMR, UV-Vis and CD results all confirm the formation of **Cat18**, and as for **Cat5**, we have learned that even by inverting the chirality of the cysteines on the acceptor, a very similar library with identical distribution is formed.

The use of $NaNO_3$ in some of the libraries (especially the ones with **D1S** and **D1L**) has promoted the formation of heterodimers or heterotrimers rather than catenanes. This is also consistent with the results presented in Chapter 2, whereby non-interlocked species can fold in a more favourable way than the conformationally restricted [2]catenanes.

The **D1L** donor makes catenane in better yield when compared to **D1S**; the opposite effect is observed with **D2S** and **D2L** (the catenane forms in better yield using **D2S** in comparison with **D2L**). This reinforces the previous observations (Chapter 2) regarding the rigidity and geometry of DN in the donor dimer having a significant influence in the assembly of these D-A catenanes.

In this chapter, we learned that the longer the linker connecting the two NDIs is, the more flexible the cyclic monomers become, therefore, the acceptor ring is too large to allow an optimum overlap of the complementary aromatic units. This reduces the formation of [2]catenanes at the expense of other cyclic species, and in some cases the formation of new [2]catenanes has also been observed.

These results are evidence that **A1c** cyclic monomer has the optimum cavity size to fit a DN moiety; **A2a** and **A2c** also have appropriate size cavity to form classical DADA [2]catenanes with **D2S** up to 88% yield in each case.

In all the results discussed, the **D2S** served as ideal donor building block to synthesise [2]catenanes, giving higher yields compare to other DNs.

Chapter 4

This chapter describes new set of libraries with a new NDI dithiol building block (**A3**). This building block is similar to the classic NDI; the only difference between them is the absence of one carboxylic group on **A3**. The core and length of these two building blocks are the same, so it is expected that they behave similarly.

The aim behind synthesis of this new building block was to achieve a more diverse library with DN, where the classical DADA arrangement is not a possible. The reason a DADA [2]catenane cannot form with these building blocks is that the -[A-A]- dimer of **A3** has a very small cavity and cannot fit a DN or any other aromatic moiety inside it. However, DAAD or DADD are two possible arrangements with this building block.

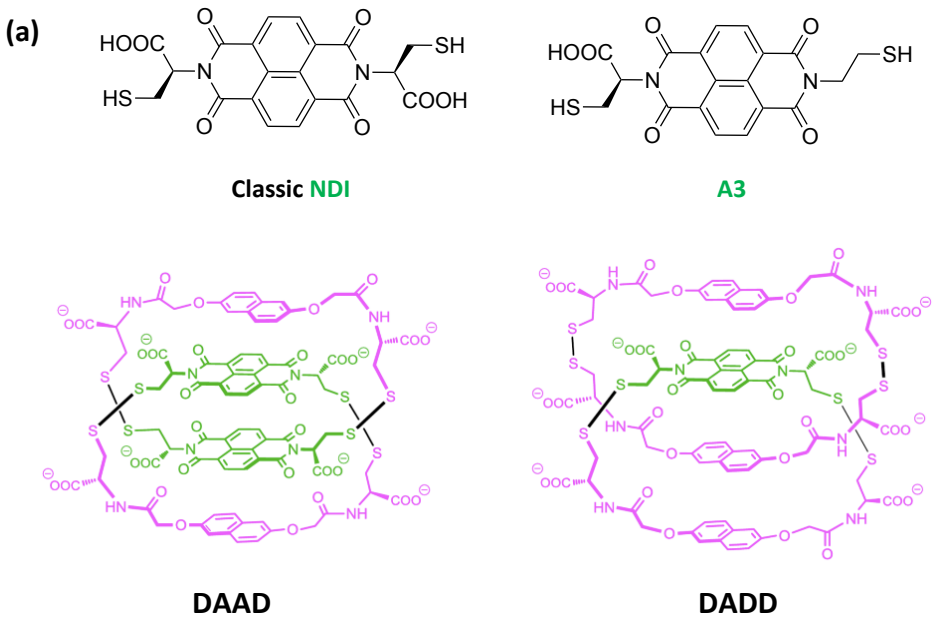

Figure 4-1. (a) The structure of classical NDI and the new building block (**A3**), (b) shows the two [2]catenanes formed from a DCL with the classical NDI and **D2S** building blocks.[119]

4.1 Building Blocks Design

The new acceptor building block (**A3**) is composed of one large hydrophobic, electron-deficient NDI π-system, connected to a trityl-sulfanylethanamine making a new dithiol building block, which unlike all the other building blocks discussed in Chapters 2 and 3, does not have two cysteine moieties.

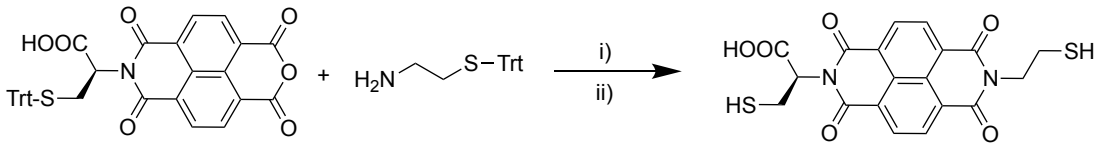

Figure 4-2. The synthetic route towards **A3** acceptor building block (shown as a generic structure, for more detail see experimental section). Reaction conditions: i) Et_3N, DMF, 120°C, μW, 5 min (40% yield); ii) CF_3COOH, Et_3SiH, CH_2Cl_2, 30 min (91% yield).

4.2 D-A DCL of A3 Acceptor and D2S Donor

A D-A DCL was set up using **D2S** as the donor and **A3** as the acceptor building blocks. Figure 4-3 illustrates the expected [2]catenanes and their formation pathway with different arrangements.

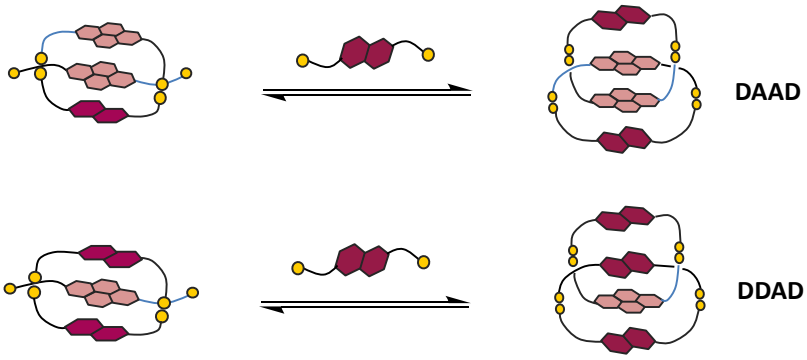

Figure 4-3. Expected [2]catenanes in two different arrangements (**DAAD** and **DDAD**).

The LC-MS analysis of D-A DCL of **A3** with **D2S** has revealed that the fully oxidised library only contains the **[D2S]** and **[D2S]$_2$** macrocycles from the donor building block and there is no sign of the **A3** building block. Looking at the HPLC trace at 381 nm, the baseline is not a flat line and it starts to increase over time, which cannot be from the solvent because it does not absorb at 381 nm, therefore it is a sign of polymerisation. There is also a small peak at 25.7 min, which has low intensity (8 au in the presence of $NaNO_3$) and proves to be an impurity.

Different HPLC methods were tried, but none was successful in eluting the molecule from the column.

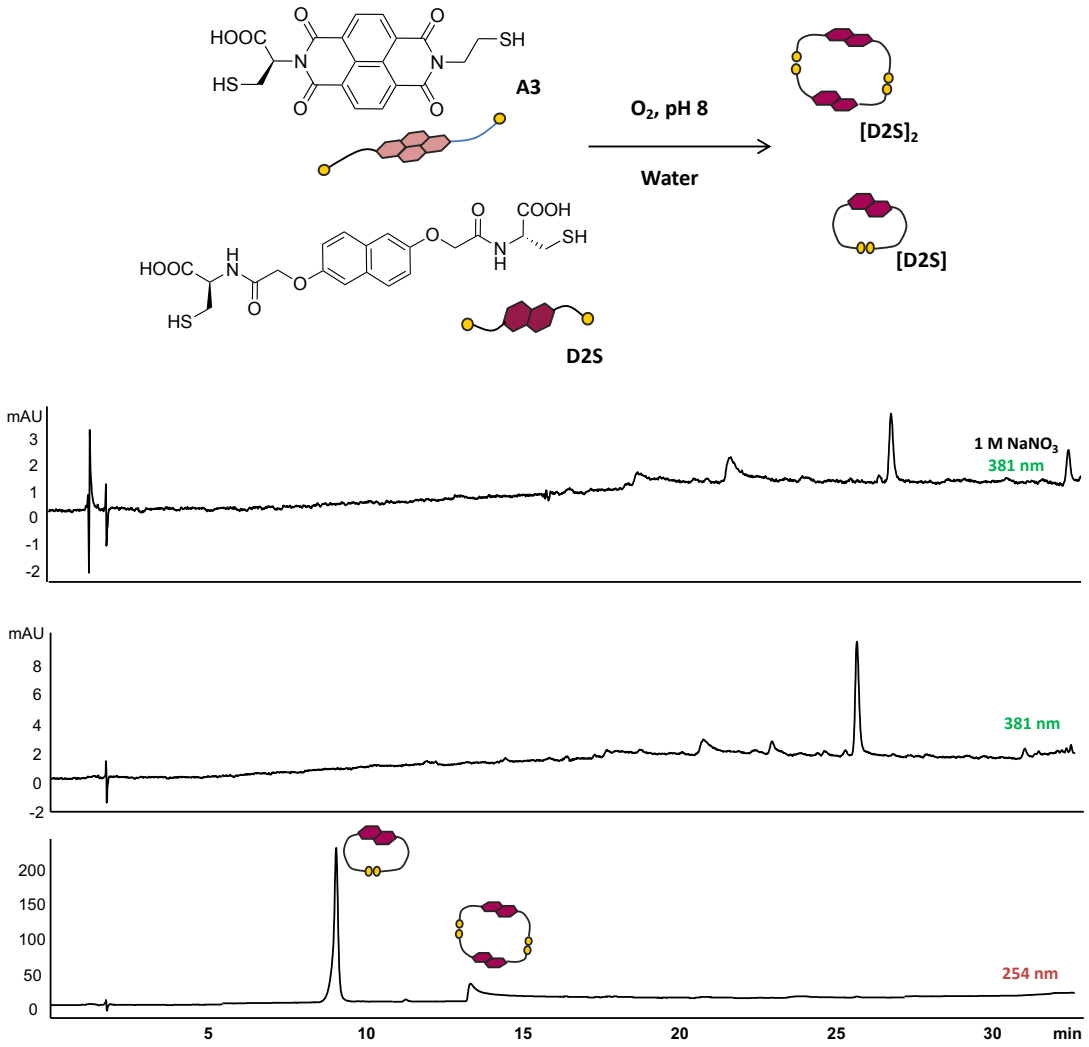

Figure 4-4. The HPLC analysis of **A3** and **D2S** DCL (1:1 molar ratio, 5 mM total concentration).

4.3 DCL of A3 with A1c

The analysis of DCL of **A3** and **A1c** building blocks has indicated that the fully oxidised library contains hydrated **A1c**, **[A1c]** cyclic monomer and **[A3]$_2$**. This library shows no sign of interaction between the two acceptor moieties (**A3** and **A1c**) and only macrocycle of **A1c** is observed. We emphasise again that this building block could polymerise and thus, be retained on the column and cannot be analysed by HPLC or MS.

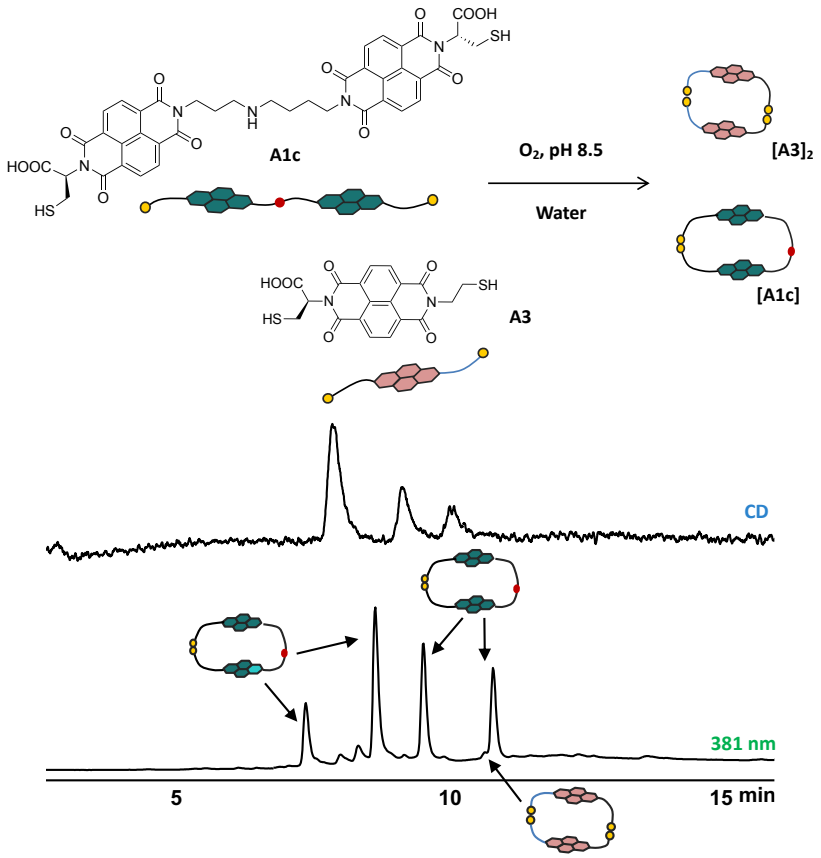

Figure 4-6. The HPLC analysis of **A1c** and **A3** DCL (1:2 molar ratio, 5 mM total concentration).

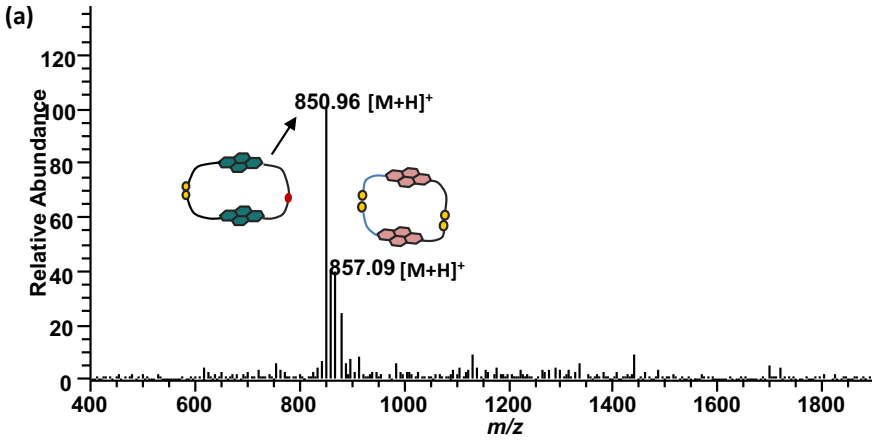

Figure 4-7. ESI-MS (+*ve*) spectra of (a) **[A1c]** and **[A3]$_2$** (as singly charged cations).

4.4 D-A DCL of A3, A1c with D2S

A new library was set up with **A3**, **A1c** and **D2S** in 1:1:2 ratio, and the LC-MS analysis of the D-A DCL has revealed that the fully oxidised library contains **[A3]$_2$** and **Cat5** [2]catenane up to 87%, along with other macrocycles of **A1c** and **D2S**. The **A3** molecule does not interact with **D2S** or the acceptor building block (**A1c**), and from the HPLC results, it shows that the compound retains on the column (a small peak represents the formation of **[A3]$_2$**). The HPLC result indicates that the **A3** acceptor slows the formation of **Cat5** and reduces the interaction between **A1c** and **D2S** (yield reduces to 87% from 93%). **A3** could be interacting with **D2S** and this can be associated to the formation of the **Cat5** in smaller yield, but the HPLC or MS cannot identify the molecule due to the polymerisation issue.

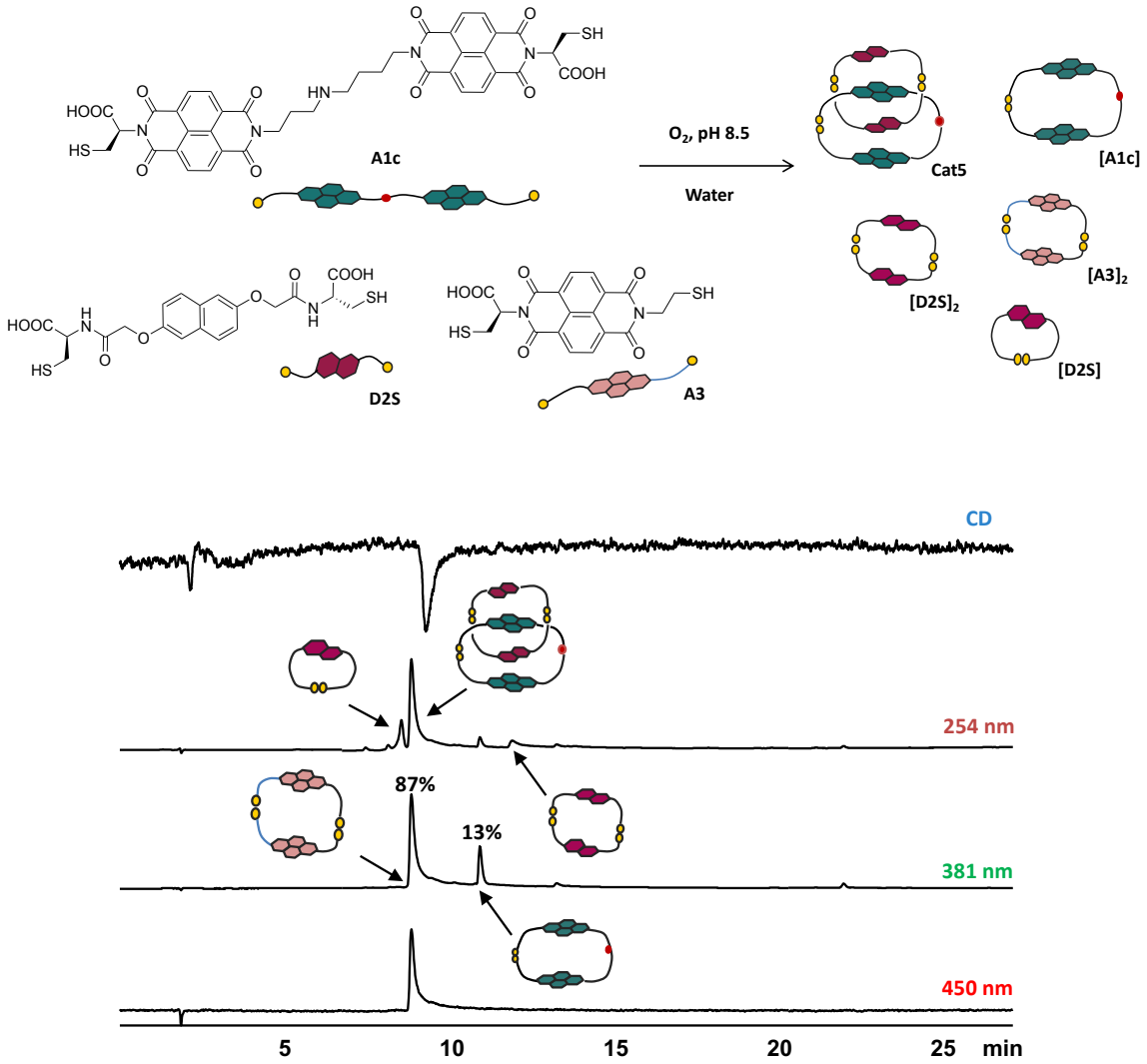

Figure 4-8. The HPLC analysis of **A3** with **A1c** and **D2S** DCL (1:1:2 molar ratio, 5 mM total concentration).

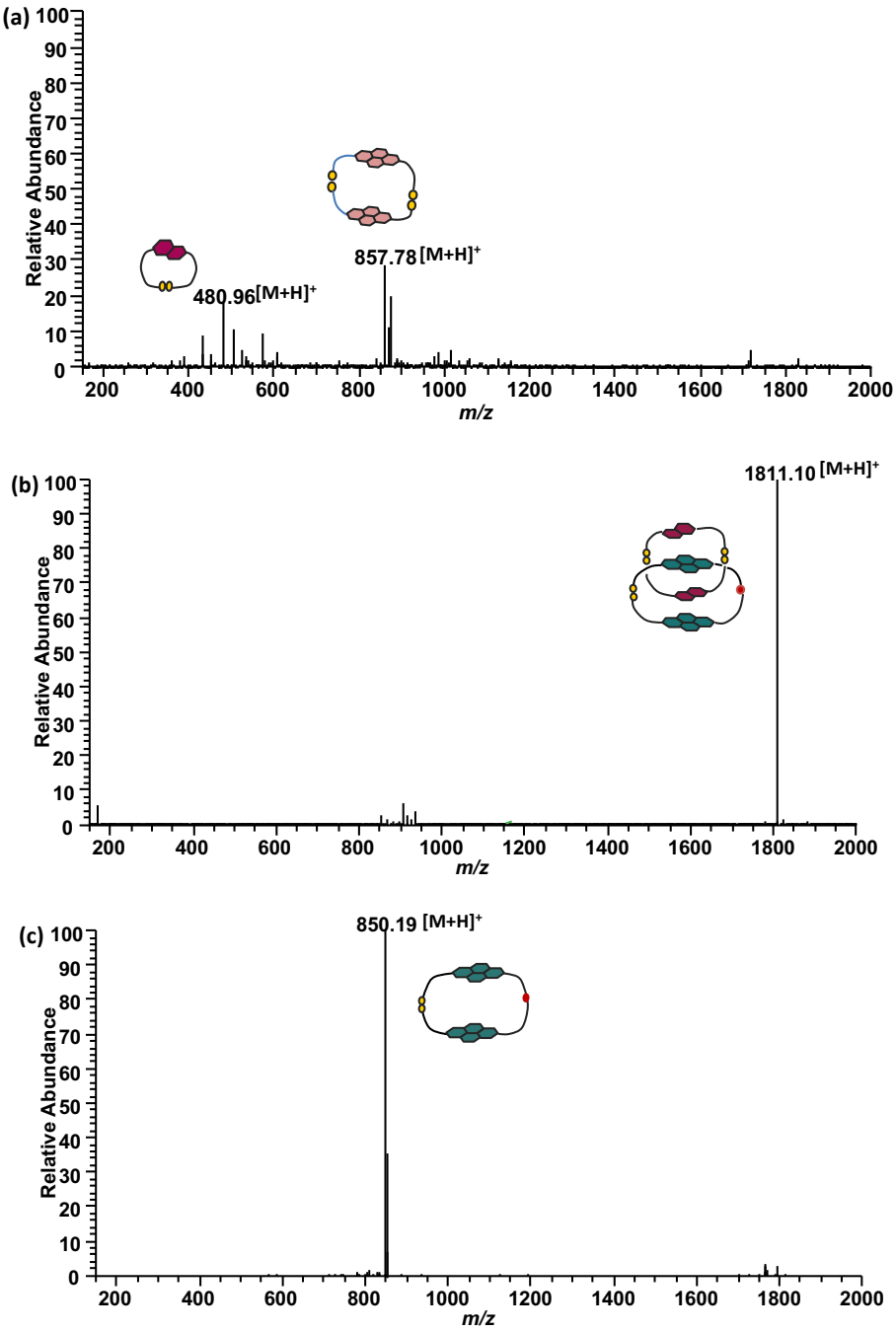

Figure 4-9. ESI-MS (+*ve*) spectra of (a) **[D2S]** and **[A3]**$_2$ (as singly charged cations), (b) **Cat5** (as singly charged cation) and (c) **[A1c]** (as singly charged cation).

4.5 D-A DCL of A3, A2a with D2S

The LC-MS analysis of D-A DCL of **A3**, **A2a** with **D2S** has showed that the fully oxidised library contains **[A3]$_2$** dimer only in 1%, and **Cat8** up to 72% in presence of $NaNO_3$. The formation of **Cat9** has, however, slightly been improved (9%) in comparison to the library with only **A2a** and **D2S** (5%).

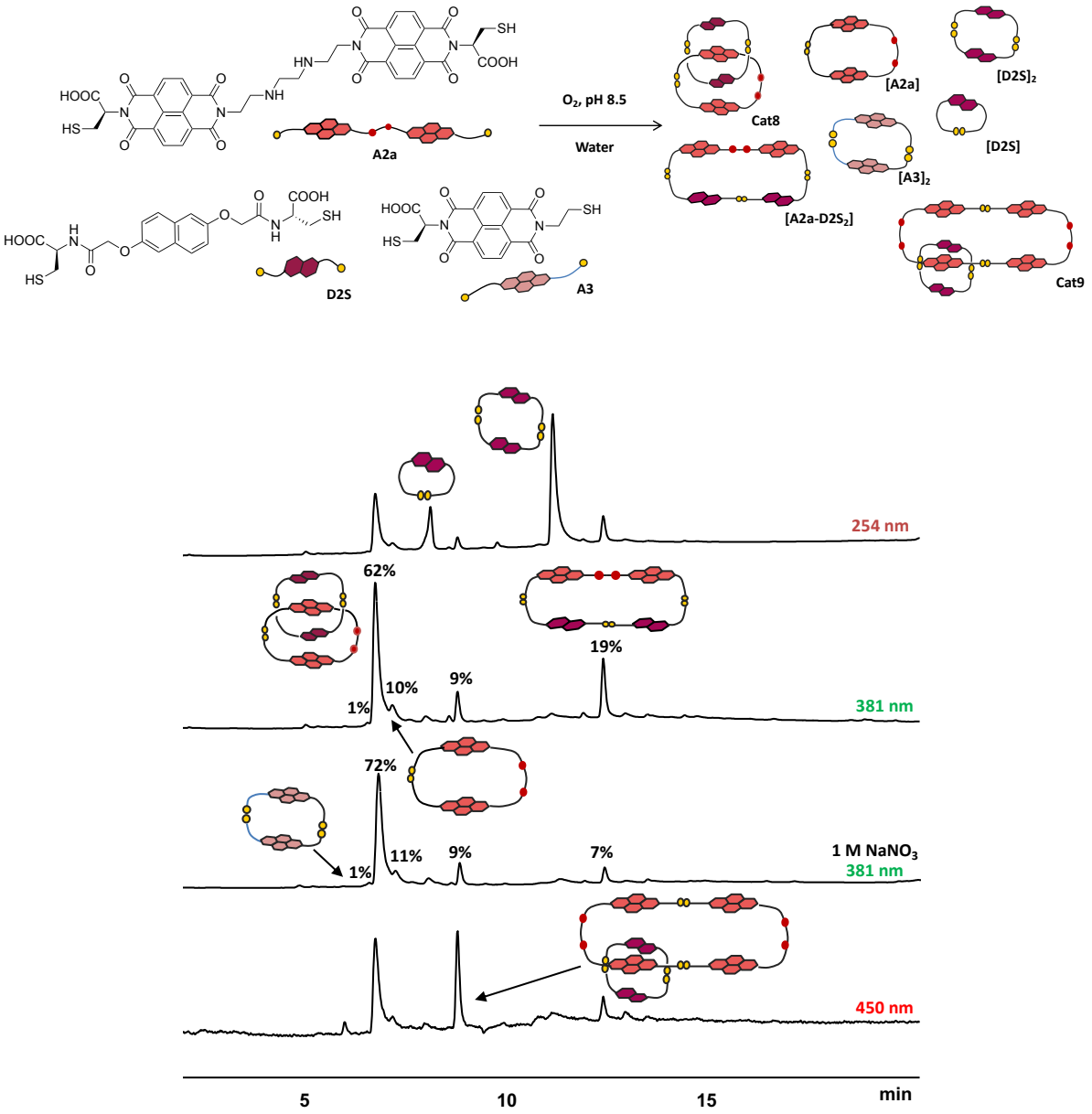

Figure 4-10. The HPLC analysis of **A3** with **A2a** and **D2S** DCL (1:1:2 molar ratio, 5 mM total concentration).

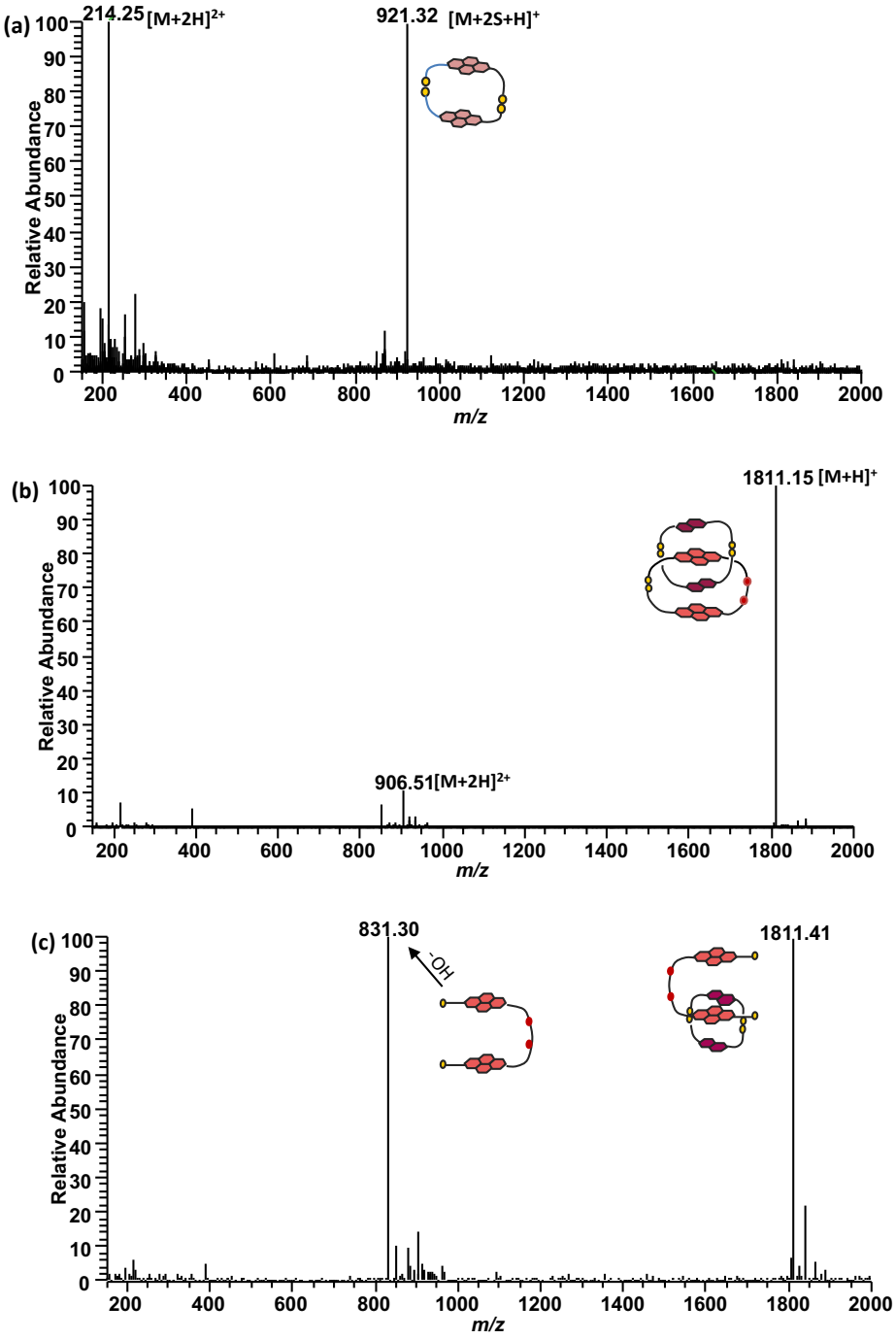

Figure 4-11. ESI-MS (+*ve*) spectra of (a) **[A3]$_2$** (as singly and doubly charged cation), (b) **Cat8** (as singly and doubly charged cations) and (c) the fragments of **Cat9**.

4.6 D-A DCL of A3, A2b with D2S

The LC-MS analysis of D-A DCL of **A3**, **A2b** with **D2S** has indicated that the fully oxidised library contains **[A3]$_2$** dimer, **Cat14** up to 74% along other macrocycles from **A2b** and **D2S**. This library, similarly to the previously studied, has showed that the **A3** does not interact with either **D2S** or **A2b** and it only forms a **[A3]$_2$**, which elutes early on the column.

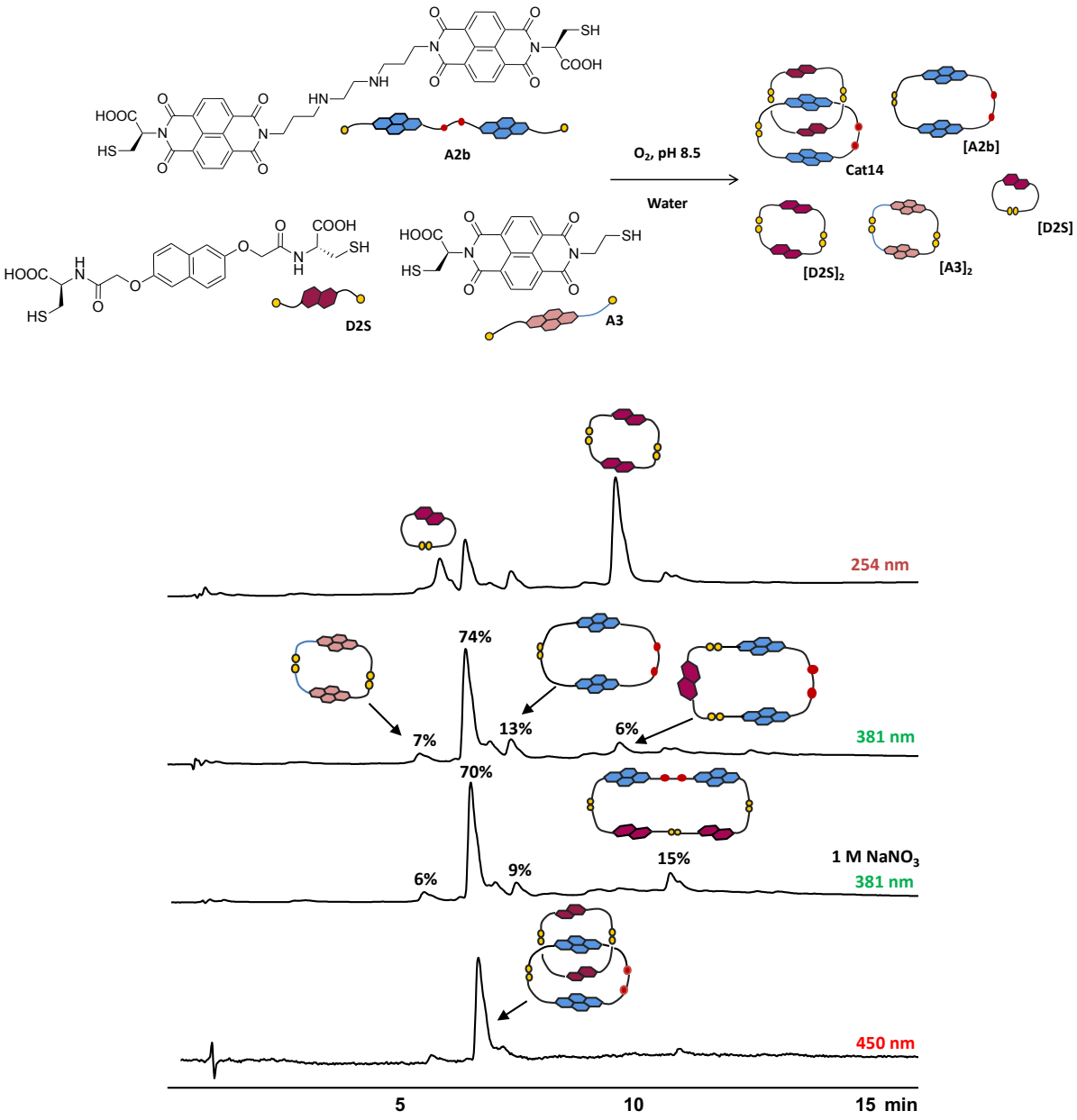

Figure 4-12. The HPLC analysis of **A3** with **A2b** and **D2S** DCL (1:1:2 molar ratio, 5 mM total concentration).

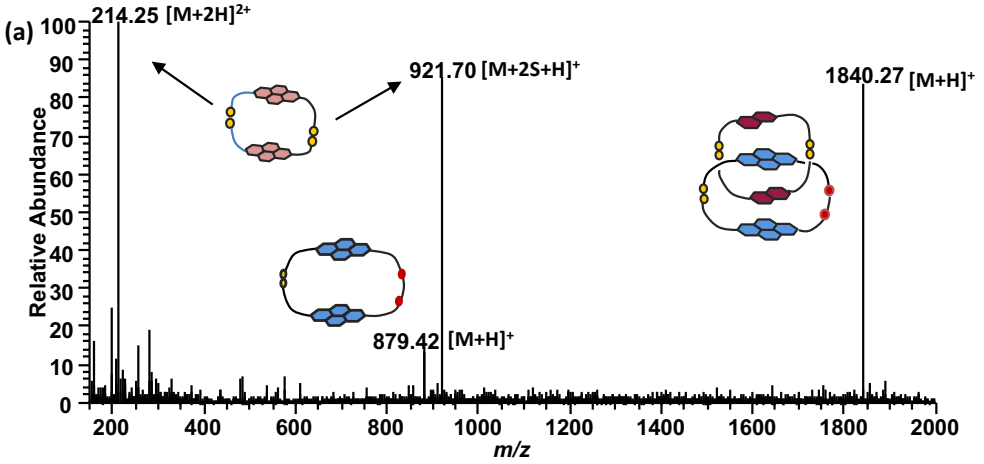

Figure 4-13. ESI-MS (+*ve*) spectra of (a) **[A3]$_2$** (as singly and doubly charged cation), **Cat14** (as singly charged cations) and **[A2b]$_2$** (singly charged cation).

In Figure 4-13, the MS result shows the mass of **[A3]$_2$**, **Cat14**, and **[A2b]** due to partial co-elution as the peaks are close to each other and their masses overlap.

4.7 D-A DCL of A3 and BDT

The LC-MS analysis of D-A DCL of **A3** and **BDT** as donor building block has indicated that the fully oxidised library contains **[BDT]$_2$** dimer in >90%. The MS and NMR results both confirm the formation of **[BDT]$_2$** and again no sign of **A3**, which means it is polymerising. (**BDT** building block can absorb at both 254 and 381 nm so for that reason we see a peak in both wavelengths).

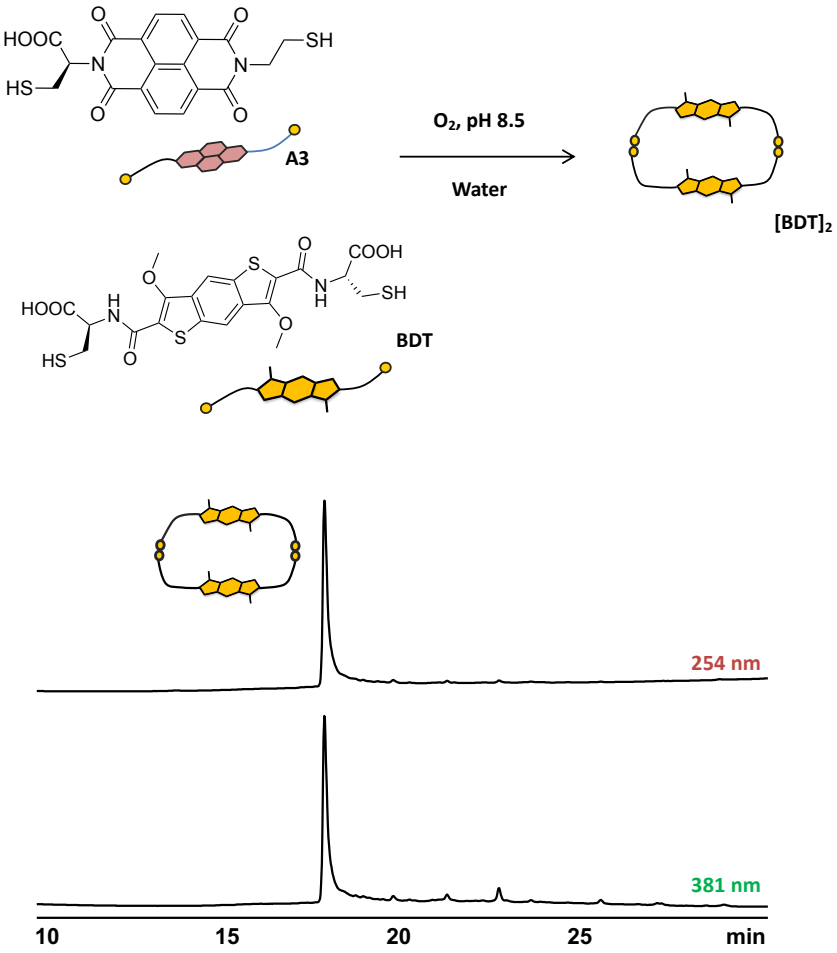

Figure 4-14. The HPLC analysis of **A3** with **BDT** DCL (1:1 molar ratio, 5 mM total concentration).

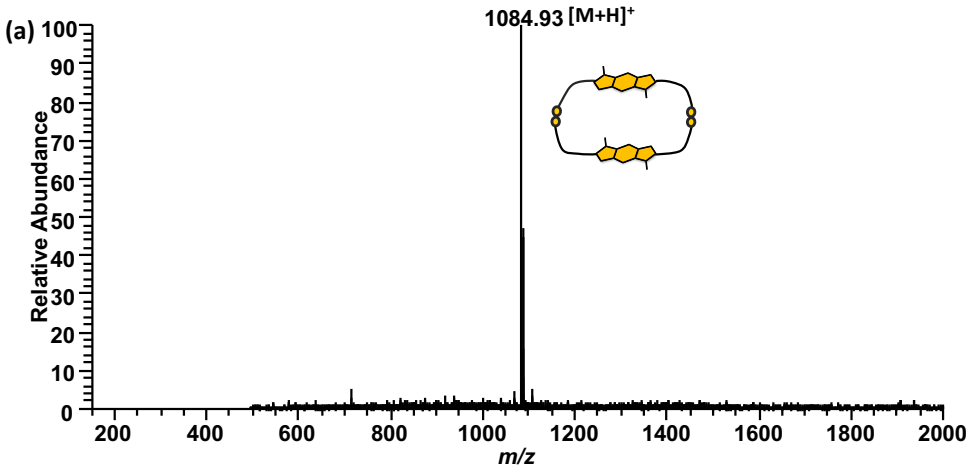

Figure 4-15. ESI-MS (+*ve*) spectrum of (a) **[BDT]$_2$** (as singly charged cation).

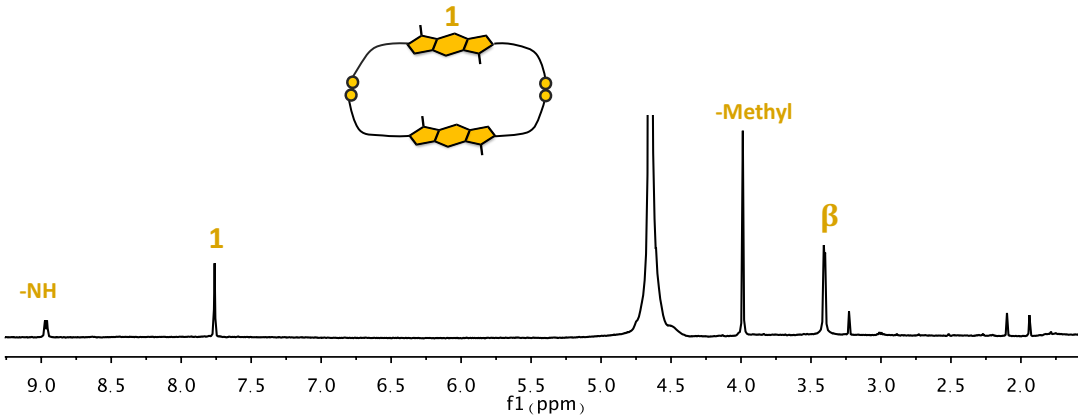

Figure 4-16. ^{1}H NMR spectrum of **A3-BDT** library in D_2O. The spectrum is referenced at 4.74 ppm.

4.8 Conclusion

This chapter describes the synthesis and analysis of a new NDI building block (which consists of one cysteine and one thiol linker) as well as DCLs preparation. The similarities between this molecule and the classical NDI have led to the assumption that this linker would generate similar libraries with the donor building block (*e.g.* **D2S**); however, this was not achieved as the molecule polymerised constantly with every building block used and did not make any interlocked structures with **D2S, BDT** or any of acceptor moieties (**A1c**, **A2a** and **A2b**).

This study is important as it illustrates how even a minor change in the structure (missing one carboxylic acid group) can have significant effect on library's distribution, suggesting that there are typical structural features required to form interlocked species. The chirality can also play a role here, as there is one chiral centre missing in the **A3** compare to the classical NDI. Even incorporating the new donor building block (**BDT**), it did not change how this molecule behaves and still only **[BDT]$_2$** was formed in the DCL.

Chapter 5

To conclude, this work confirms NDI-based building blocks are excellent acceptor building block for DCC applications. The design of the building blocks is an evolution of molecules previously studied by students in the Pantos and Sanders groups respectively. The acceptor molecules employed in this work are linked *via* various polyamines with different number of nitrogen atoms in their linker. The length of the polyamine has played a significant role in the distribution of the library. The shorter polyamines (n = 5, 6) have led to the formation of a series of macrocycles, whereas the longer polyamines (n = 8, 9 and 10) have generated [2]catenanes in good to remarkable yields. The length of the donor building blocks has also significantly influenced in diversity of the library. The 1,5-DN isomers with long or short arms have had different effects on the libraries. The long arm always generates catenanes in better yield than the short one.

This, however, has oppositely behaved to 2,6-DN-isomers, where the short DN formed catenanes in superior yields over the long 2,6-DN.

A new NDI-based dithiol building block has also been synthesised and studied with various acceptors and **D2S**. However, none of the libraries has led to the formation of any interlocked molecules because of polymerisation of the new building block.

This work reports the synthesis of a series of new D-A [2]catenanes, taking advantage of the DCC approach. In total twenty-three catenanes were synthesised in this work and six of those were isolated by semi-prep HPLC and fully characterised using solution techniques.

Chapter 6

6.1. Experimental

6.1.1. General Information

All reagents were purchased from commercial suppliers: Acros Organics, Alfa Aesar, Sigma Aldrich, TCI Europe, Gross, Fluorochem or Apollo Scientific, and used without further purification.

^{1}H and ^{13}C NMR spectra were performed on an Agilent Advance 500 (^{1}H 500 MHz, ^{13}C 125 MHz) instrument as stated. Chemical shifts are reported in parts per million (ppm) All spectra were referenced to the residual solvent peaks. Coupling constants are reported in Hertz (Hz) and signal multiplicity is denoted as singlet (s), doublet (d), doublet of doublet (dd), triplet (t), quartet (q), multiplet (m) and broad (br). All spectra were acquired at the specified temperatures and were referenced to the residual solvent peaks. The common solvent impurities in ^{1}H and ^{13}C NMR in very small amounts were water, Et_3N or DMF. COSY, NOESY and HSQC were performed on a Bruker Advance III HD 500 Cryo spectrometer.

The microwave reactions were carried out in either CEM Discover or CEM Explorer 12. HPLC analyses were carried out on Hewlett Packard 1050 or 1090 systems coupled to diode array detectors and a Jasco CD-2095 CD detector. The data was processed using Agilent's ChemStation software.

All the CD data was acquired either on an Applided Photophysics Chirascan spectrophotometer or on Module B of the B23 Beam line at Diamond Light Source, Harwell Complex, UK. The latter setup was used for the variable temperature experiments.

LC-MS studies were carried out on a Thermo Surveyor PDA Plus LC and LCQ classical ESI. Data was processed using the XCalibur software. The individual HPLC / LC-MS methods are detailed in the LC-MS Analysis section.

6.2. DCL Set-up

A 5 mM library was prepared by dissolving the building block in 10 mM aqueous NaOH, followed by titration with 100 mM NaOH to adjust the pH to 8 or 8.5 depending on solubility. The library solutions were stirred in close capped vials in room temperature and analysed by LC-MS, HPLC, NMR and CD. Preparative libraries (5 or 10 mL scale) were made using the same method as for the analytical libraries.

6.3. LC-MS Analysis of the DCLs

6.3.1. LC-MS Method:

ESI-MS spectra (positive ion) were acquired with drying temperature of 250 °C, spray current 6.20 μA, sheath gas flow of 50 arb, spray voltage was set to 4.5 kV and tube lens -15.0 V. The mass range was set from m/z 150-2000, the number of microscans in scan time was 5 and the maximum injection time was 300.0 ms.

All the yields calculated (presented above each peak) is based on HPLC integration.

6.4. HPLC and LC-MS methods for DCLs of Chapter 2, 3 and 4:

Method 1: Column: Kromasil C_8, 25.0 x 0.45 cm, 5 μm, 100 Å, Part No.: PSL847275
A CD detector was connected in series with the DAD detector, thus all the retention times in CD are 0.6 min longer than in DAD and the peaks are broader.

Injection volume	3 μL
Flow Rate	0.5 mL/min
Temperature	38 °C
Run Time	30 min
Elution Profile	Gradient elution by CH_3CN/Water (0.1% FA)

Time / min	**Water (0.1% FA)**	**CH_3CN (0.1% FA)**
0	80%	20%
25	35%	65%
30	80%	20%

The libraries analysed using Method 1

A1a Libraries: Figures 2.-7, 2.9, 2-16 and 2-19.

A1b Libraries: Figures 2-23, 2-25, 2-32 and 2-35.

A1c Libraries: Figures 2-39, 2-42, 2-80, 2-87 and 2-91.

A2a Libraries: Figures 3-3, 3-5, 3-13 and 3-16.

A2b Libraries: Figures 3-20, 3-22, 3.32 and 3-35.

A2c Libraries: Figures 3-39, 3-41, 3-67 and 3-69.

A3 Libraries: Figures 4-4, 4-6 and 4-14.

Method 2: Column: Kromasil C_8, 25.0 x 0.21 cm, 5 μm, 100 Å, Part No.: KR100-5C8-250AM

Injection volume	2 µL
Flow Rate	0.5 mL/min
Temperature	38 °C
Run Time	30 min
Elution Profile	Gradient elution by CH_3CN/Water (0.1% FA)

Time / min	**Water (0.1% FA)**	**CH_3CN (0.1% FA)**
0	85%	15%
25	40%	60%
30	85%	15%

The libraries analysed using Method 2

A1a Libraries: Figures 2-12.

A1b Libraries: Figures 2-28.

A1c Libraries: Figures 2-47, 2-63, 2-75, 2-77, 2-78 and 2-79.

A2a Libraries: Figures 3-6.

A2b Libraries: Figures 3-25.

A2c Libraries: Figures 3-44 and 3-60.

A3 Libraries: Figures 4-8, 4-10 and 4-12.

Method 3: Column: DevelosilC_{30} RPAqueous-3, 5.0 x 0.3 cm, 3 µm, 140 Å, Part No.: CH0-5999

Injection volume	2 µL
Flow Rate	0.5 mL/min
Temperature	38 °C
Run Time	30 min
Elution Profile	Gradient elution by CH_3CN/Water (0.1% FA)

Time / min	**Water (0.1% FA)**	**CH_3CN (0.1% FA)**
0	85%	15%
25	40%	60%
30	85%	15%

The libraries analysed using Method 3

A1c and **A1c*** Libraries: Figures 2-45, 2-65 and 2-67

6.5. Preparative method for separation of Cat5 and Cat5*

Column: Develosil C_{30} RPAqueous-3, 5.0 x 2.0 cm, 5 μm, 140 Å, Part No.: CH0-5904

Injection volume	300 μL
Flow Rate	4 mL/min
Temperature	38 °C
Run Time	40 min
Elution Profile	Gradient elution by CH_3CN/Water (0.1% FA)

Time / min	**Water (0.1% FA)**	**CH_3CN (0.1% FA)**
0	80%	20%
30	55%	45%
40	80%	20%

6.6. Preparative method for DCLs of Cat8, Cat14, Cat18 and Cat18* (5 mM):

Column: Kromasil 100-5 C_8, 25.0 x 0.8 cm, 5 μm, 100 Å, Part No.: KR100-5C8-250A

Injection volume	400 μL
Flow Rate	3 mL/min
Temperature	38 °C
Run Time	30 min
Elution Profile	Gradient elution by CH_3CN/Water (0.1% FA)

Time / min	**Water (0.1% FA)**	**CH_3CN (0.1% FA)**
0	75%	25%
30	55%	45%
40	75%	25%

6.7. Synthesis of Building Blocks

I have performed the synthesis of NMI molecules based on previously published protocol.[130]

L-NMI (1):

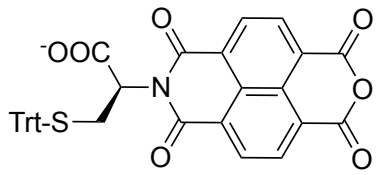

^{1}H NMR (500 MHz, $CDCl_3$, 300 K) δ (ppm): 8.80 (d, *J* = 7.6 Hz, 2 H, NDI), 8.73 (d, *J* = 7.6 Hz, 2 H, NDI), 7.33-7.10 (m, 15 H, Trt), 5.53 (dd, *J* = 10.5, 4.7 Hz, 1 H, α-Cys), 3.28-3.23 (m, 1 H, β-Cys), 3.19 (dd, *J* = 13.6, 4.6 Hz, 1 H, β-Cys). The ^{1}H NMR spectrum matches the literature data.

D-NMI (1*):

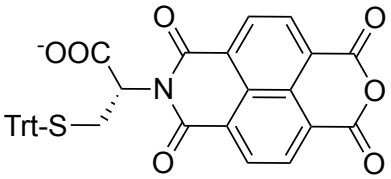

^{1}H NMR (500 MHz, $CDCl_3$, 300 K) δ (ppm): 8.83 (d, *J* = 7.6 Hz, 2 H, NDI), 8.78 (d, *J* = 7.6 Hz, 2 H, NDI), 7.38-7.11 (m, 15 H, Trt), 5.54 (dd, *J* = 10.4, 4.7 Hz, 1 H, α-Cys), 3.29-3.24 (m, 1 H, β-Cys), 3.18 (dd, *J* = 13.6, 4.7 Hz, 1 H, β-Cys). The ^{1}H NMR spectrum matches the literature data.

Synthesis of New Acceptor Building Blocks

A1a (Protected)

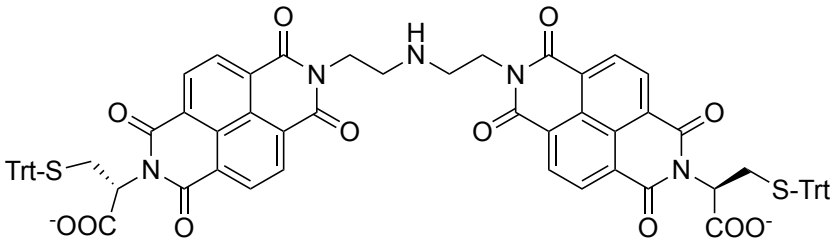

L-Cysteine naphthalenemonoimide (L-NMI) (200 mg, 3.27 x 10^{-4} mol) and dry Et_3N (0.2 mL) were dissolved in DMF (5 mL) in an 8 mL microwave tube. Diethylenetriamine (0.020 mL, 1.63 x 10^{-4} mol) was added to the solution. The suspension was sonicated until the mixture was homogenous, and then heated under microwave irradiation at 120 °C for 5 minutes. The solvent was removed under reduced pressure, and the residue was washed with Et_2O and dried *in vacuo*. Yield: (130 mg, 1.01 x 10^{-4} mol) 61%, M.p.: 185 °C (decomposed). ^{1}H NMR (500 MHz, $CDCl_3$ with Et_3N, 300 K) δ (ppm): 8.73-8.51 (m, 8 H, NDI), 7.35-6.98 (m, 30 H, Trt), 5.55-5.46 (m, 2 H, α-Cys), 4.31 (t, *J* = 6.3 Hz, 4 H, α-Alk), 4.21-4.16 (m, 2 H) 3.45-3.37 (m, 2 H, β-Cys), 3.22-3.15 (m, 2 H, β-Cys), 3.08 (t, *J* = 6.3 Hz, 2 H, β-Alk). ^{13}C NMR (125 MHz, $CDCl_3$ with Et_3N) δ (ppm): 173.0, 163.2, 162.4, 146.9 144.9, 130.0, 129.5, 127.9, 127.8, 127.6, 127.1 126.6, 126.3, 66.8, 59.2, 55.4, 47.2 and 31.8. The molecule did not ionise with different MS techniques (*e.g.* ESI, MALDI).

A1a (Deprotected)

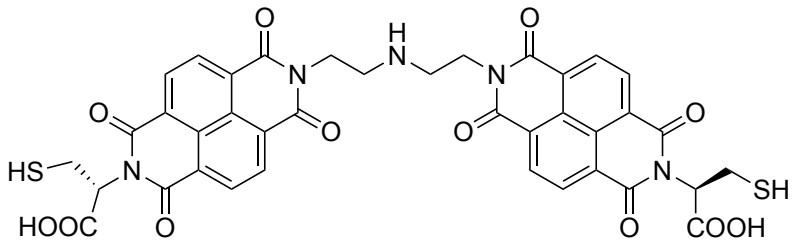

The protected **A1a** (120 mg, 9.28 x 10^{-5} mol) was added to a mixture of trifluoroacetic acid (2 mL), CH_2Cl_2 (2 mL), and triethylsilane (0.2 mL). After 30 min, all the volatiles were removed under reduced pressure. The residue was then suspended in Et_2O (20 mL), filtered using a

Büchner funnel and washed with Et_2O (20 mL) and dried *in vacuo* to yield a pink coloured solid. Yield: (75 mg, 8.13 x 10^{-5} mol), 87%, as TFA salt. M.p.: 198 °C (decomposed). ^{1}H NMR (500 MHz, DMSO-d_6, 300 K) δ (ppm): 13.19 (br, 2 H, COOH), 8.79-8.65 (m, 8 H, NDI), 5.74-5.65 (dd, J = 9.2 Hz, 5.3 Hz, 2 H, α-Cys), 4.38-4.30 (m, 4 H, α-Alk), 3.22-3.09 (m, 4 H, β-Cys), 2.64-2.60 (m, 2 H, SH) 2.63-2.60 (m, 2 H, β-Alk) and 2.58-2.55 (m, 2 H, β'-Alk). The ^{13}C NMR could not be obtained due to fast oxidation of thiols. Therefore, it was used as obtained from the deprotection reaction in DCLs.

A1b (Protected)

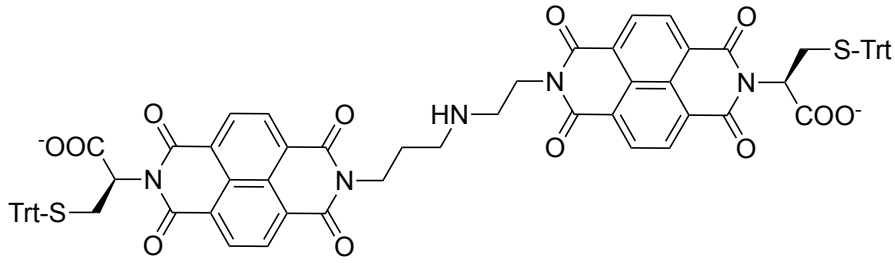

L-Cysteine naphthalenemonoimide (L-NMI) (401 mg, 6.56 x 10^{-4} mol) and dry Et_3N (0.4 mL) were dissolved in DMF (15 mL) in a 20 mL microwave tube. *N*-(2-Aminoethyl)-1,3-propanediamine (0.041 mL, 3.28 x 10^{-4} mol) was added to the solution. The suspension was sonicated until the mixture was homogenous, and then heated under microwave irradiation at 120 °C for 5 minutes. The solvent was removed under reduced pressure, and the residue was washed with Et_2O and dried *in vacuo*. Yield: (338 mg, 2.58 x 10^{-4} mol) 79%, M.p.: 160 °C (decomposed). ^{1}H NMR (500 MHz, $CDCl_3$ with Et_3N, 300 K) δ (ppm): 8.77-8.55 (m, 8 H, NDI), 7.36-6.98 (m, 30 H, Trt), 5.50 (dd, J = 11.0 Hz, 4.3 Hz, 2 H, α-Cys), 4.34 (t, J = 6.5 Hz, 2 H, α-Alk), 4.23 (t, J = 7.1 Hz, 2 H, α'-Alk), 3.44-3.39 (m, 2 H, β-Cys), 3.19-3.12 (m, 2 H, β-Cys), 3.01 (t, J = 6.5 Hz, 2 H, β-Alk), 2.78 (t, J = 6.6 Hz, 2 H, Alkyl), 1.94-1.89 (m, 2 H, γ-Alkyl). ^{13}C NMR (125 MHz, $CDCl_3$ with Et_3N) δ (ppm): 172.9, 163.1, 162.9, 147.0, 144.9, 130.7, 129.6, 129.5, 127.8, 127.7, 127.5, 127.0, 126.2, 66.7, 55.3, 55.4, 47.3 and 31.9. UltrafleXtreme MALDI: calcd. for $C_{77}H_{57}N_5O_{12}S_2$ $[M+H]^+$ (*m/z*): 1308.4, found: 1308.4

A1b (Deprotected)

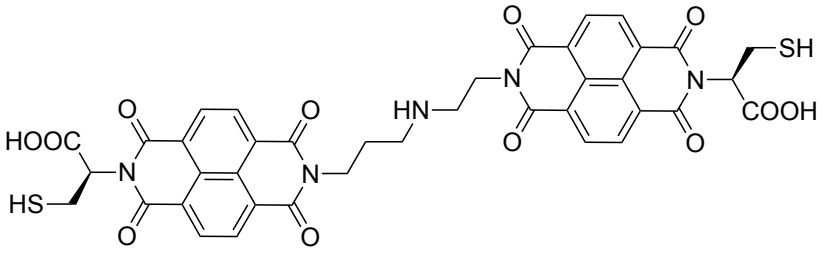

The protected **A1b** (200 mg, 1.53 x 10^{-4} mol) was added to a mixture of trifluoroacetic acid (2 mL), CH_2Cl_2 (2 mL), and triethylsilane (0.2 mL). After 30 min, all the volatiles were removed under reduced pressure. The residue was then suspended in Et_2O (20 mL), filtered using a Büchner funnel and washed with Et_2O (20 mL) and dried *in vacuo* to yield a pink coloured solid. Yield: (137 mg, 1.46 x 10^{-4} mol), 96%, as TFA salt. M.p.: 183 °C (decomposed). ^{1}H NMR (500 MHz, DMSO-d_6, 300 K) δ (ppm): 13.21 (br, 2 H, COOH), 8.83-8.59 (m, 8 H, NDI), 5.69 (dd, J = 9.2 Hz, 5.3 Hz, 2 H, α-Cys), 4.35 (br, 2 H, α-Alk), 4.13 (br, 2 H, α'-Alk), 3.39-3.34 (m, 4 H, Alkyl), 3.24-3.06 (m, 4 H, β-Cys), 2.72-2.65 (m, 2 H, SH) and 2.08-1.93 (m, 2 H, Alkyl). It was used as obtained from the deprotection reaction in DCLs.

A1c (Protected)

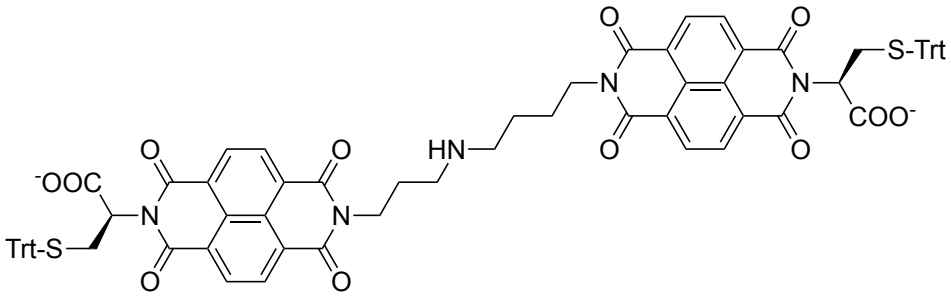

L-Cysteine naphthalenemonoimide (L-NMI) (180 mg, 2.95 x 10^{-4} mol) and dry EtN_3 (0.3 mL) were dissolved in DMF (5 mL) in an 8 mL microwave tube. Spermidine trihydrochloride (37 mg, 1.46 x 10^{-4} mol) was added to the solution. The suspension was sonicated until it became homogenous, and then heated under microwave irradiation at 120 °C for 5 minutes. The solvent was removed under reduced pressure, and the residue was washed with Et_2O and dried *in vacuo*. Yield: (167 mg, 1.25 x 10^{-4} mol) 86%, M.p.: 175-177 °C. ^{1}H NMR (500 MHz, $CDCl_3$ with Et_3N, 300 K) δ (ppm): 8.79-8.57 (m, 8 H, NDI), 7.39-7.01 (m, 30 H, Trt), 5.50 (dd, J =

10.7 Hz, 4.3 Hz, 2 H, α-Cys), 4.27 (t, *J* = 7.1 Hz, 2 H, α-Alk), 4.20 (t, *J* = 7.4 Hz, 2 H, α'-Alk), 3.46-3.37 (m, 2 H, β-Cys), 3.19-3-10 (m, 2 H, β-Cys), 2.73-2.69 (m, 4 H, under satellites of Et_3N), 2.01-1.89 (m, 2 H), 1.83-1.72 (m, 2 H), 1.66-1.55 (m, 2 H). ^{13}C NMR (125 MHz, $CDCl_3$ with Et_3N) δ (ppm): 172.9, 163.0, 162.4, 144.9, 130.7, 130.0, 129.7, 128.2, 127.8, 127.6, 126.3, 126.0, 66.7, 59.3, 55.4, 49.4, 43.4, 40.6, 38.8, 27.5 and 25.9. UltrafleXtreme MALDI: calcd. for $C_{79}H_{60}N_5O_{12}S_2$ $[M-H]^-$ (*m/z*): 1334.4, found: 1333.6.

A1c (Deprotected)

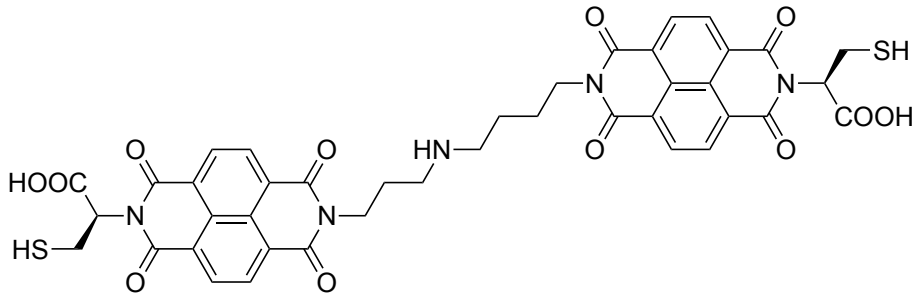

The protected **A1** (100 mg, 7.48 x 10^{-5} mol) was added to a mixture of trifluoroacetic acid (2 mL), CH_2Cl_2 (2 mL), and triethylsilane (0.1 mL). After 30 min, all the volatiles were removed under reduced pressure. The residue was then suspended in Et_2O (20 mL), filtered using a Büchner funnel and washed with Et_2O (20 mL) and dried *in vacuo* to yield a yellow coloured solid. Yield: (61 mg, 6.32 x 10^{-5} mol), 84%, as TFA salt. M.p.: 97 °C (decomposed). ^1H NMR (500 MHz, DMSO-d_6, 300 K) δ (ppm): 13.20 (br, 2 H, COOH), 8.78-8.65 (m, 8 H, NDI), 5.70 (dd, *J* = 10.7 Hz, 4.3 Hz, 2 H, α-Cys), 4.14 (t, *J* = 4.1 Hz, 2 H, α-Alk), 4.09 (t, *J* = 4.0 Hz, 2 H, α'-Alk), 3.24-3.14 (m, 2 H, β-Cys), 3.13-3.06 (m, 2 H, β'-Cys), 3.05-2.99 (m, 2 H, Alkyl) 2.98-2.91 (m, 2 H, Alkyl), 2.71-2.65 (m, 2 H, SH), 2.02 (q, *J* = 7.9, 7.5 Hz, 2 H), 1.77-1.62 (m, 4 H, Alkyl). It was used as obtained from the deprotection reaction in DCLs.

A1c* (Protected)

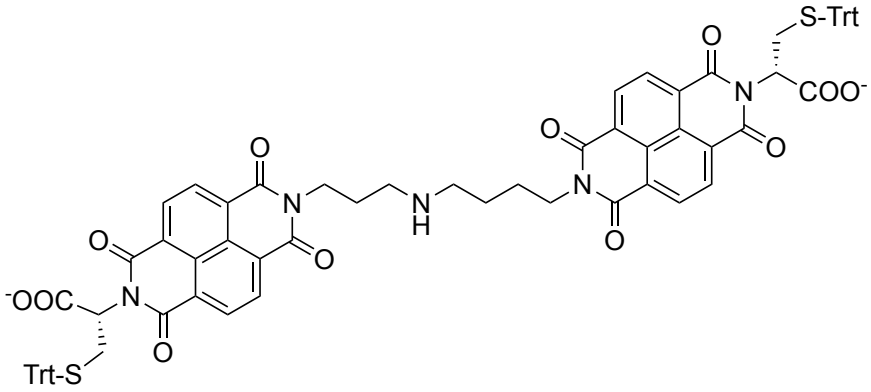

D-Cysteine naphthalenemonoimide (D-NMI) (200 mg, 3.27 x 10^{-4} mol) and dry Et_3N (0.2 mL) were dissolved in 5 mL DMF in an 8 mL microwave tube. Spermidine trihydrochloride (42 mg, 1.64 x 10^{-4} mol) was added to the solution. The suspension was sonicated until it became homogenous, and then heated under microwave irradiation at 120 °C for 5 minutes. The solvent was removed under reduced pressure, and the residue was washed with Et_2O and dried *in vacuo*. Yield: (166 mg, 1.21 x 10^{-4} mol) 73%, M.p.: 170 °C (decomposed). ^{1}H NMR (500 MHz, $CDCl_3$ with Et_3N, 300 K) δ (ppm): 8.78-8.60 (m, 8 H, NDI), 7.36-7.02 (m, 30 H, Trt), 5.51 (dd, *J* = 10.8 Hz, 4.3 Hz, 2 H, α-Cys), 4.28 (t, *J* = 7.0 Hz, 2 H, α-Alk), 4.21 (t, *J* = 7.5 Hz, 2 H, α-Alk), 3.45-3.39 (m, 2 H, β-Cys), 3.21-3.13 (m, 2 H, β-Cys), 2.75-2.71 (m, 4 H, under satellites of Et_3N), 2.01-1.92 (m, 2 H), 1.85-1.74 (m, 2 H), 1.68-1.57 (m, 2 H). ^{13}C NMR (125 MHz, $CDCl_3$ with Et_3N) δ (ppm): 172.9, 162.9, 162.3, 144.9, 130.7, 130.0, 129.6, 127.6, 127.3, 126.5, 126.2, 126.0, 66.7, 55.4, 49.4, 47.0, 43.7, 40.6, 38.8, 27.5, and 25.8. FTMS-NSI: calcd. for $C_{79}H_{60}N_5O_{12}S_2$ $[M-H]^-$ (*m/z*): 1334.3685, found: 1334.3693.

A1c* (Deprotected)

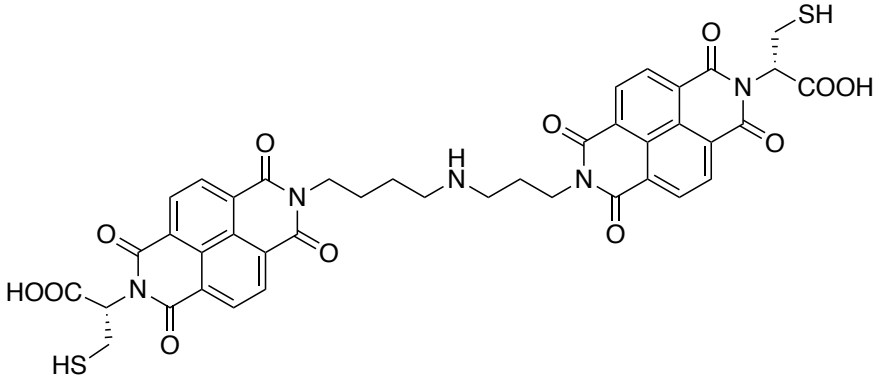

The protected **A1*** (128 mg, 9.58 x 10^{-5} mol) was added to a mixture of trifluoroacetic acid (2 mL), CH_2Cl_2 (2 mL), and triethylsilane (0.2 mL). After 30 min, all the volatiles were removed

under reduced pressure. The residue was then suspended in Et_2O (20 mL), filtered using a Büchner funnel and washed with Et_2O (20 mL) and dried *in vacuo* to yield a yellow coloured solid. Yield: (68 mg, 7.00 x 10^{-5} mol), 73%, as TFA salt. M.p.: 218 °C (decomposed). ^{1}H NMR (500 MHz, DMSO-d_6, 300 K) δ (ppm): 12.90 (br, 2 H, COOH), 8.98-8.10 (m, 8 H, NDI), 5.70 (dd, J = 9.2 Hz, 5.4 Hz, 2 H, α-Cys), 4.20-4.01 (m, 4 H, 2 α-Alk), 3.22-3.14 (m, 2 H, β-Cys), 3.12-3.06 (m, 2 H, β-Cys), 3.05-2.99 (m, 2 H), 2.98-2.88 (m, 2 H), 2.68 (t, J = 8.6 Hz, 2 H, SH), 2.02 (t, J = 8.3 Hz, 2 H), 1.78-1.60 (m, 4 H). It was used as obtained from the deprotection reaction in DCLs.

A2a (Protected)

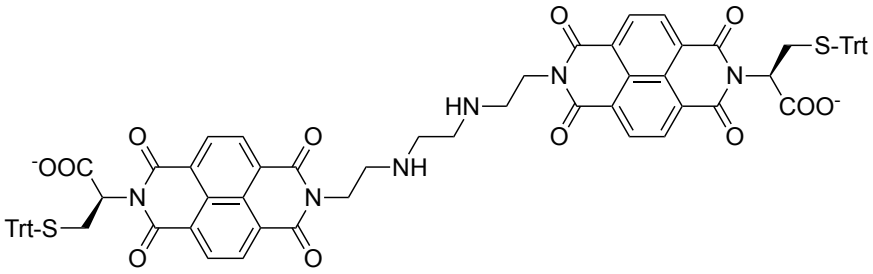

L-Cysteine naphthalenemonoimide (L-NMI) (405 mg, 6.56 x 10^{-4} mol) and dry Et_3N (0.4 mL) were dissolved in (10 mL) DMF in a 20 mL microwave tube. Triethylenetetramine (0.047 mL, 3.28 x 10^{-4} mol) was added to the solution. The suspension was sonicated until the mixture was homogenous, and then heated under microwave irradiation at 195 °C for 5 minutes. The solvent was removed under reduced pressure, and the residue was washed with Et_2O and dried *in vacuo*. Yield: (335 mg, 2.51 x 10^{-4} mol) 76%, M.p.: 162 °C (decomposed). ^{1}H NMR (500 MHz, $CDCl_3$ with Et_3N, 300 K) δ (ppm): 8.75-8.56 (m, 8 H, NDI), 7.35-6.99 (m, 30 H, Trt), 5.51 (dd, J = 10.9 Hz, 4.4 Hz, 2 H, α-Cys), 4.34 (t, J = 5.9 Hz, 2 H, α-Alk), 4.30 (t, J = 6.6 Hz, 2 H, α'-Alk), 3.44-3.41 (m, 2 H, β-Cys), 3.19-3.12 (m, 2 H, β-Cys), 3.01-2.98 (m, 2 H, Alkyl), 2.71 (br, 2 H, Alkyl). ^{13}C NMR (125 MHz, $CDCl_3$ with Et_3N) δ (ppm): 173.5, 162.9, 146.9, 144.9, 130.0, 129.7, 129.5, 128.2, 127.9, 127.8, 127.6, 126.1, 64.5, 59.3, 55.5, 40.0, 34.1 and 29.6. FTMS-NSI: calcd. for $C_{78}H_{60}N_6O_{12}S_2$ $[M-H]^-$ (*m/z*): 1335.3638, found: 1335.3637

A2a (Deprotected)

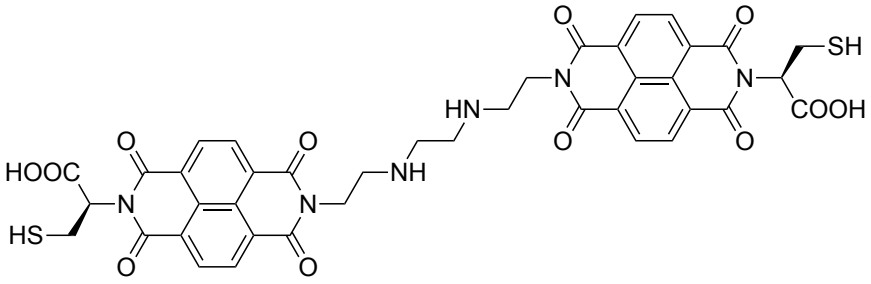

The protected **A2a** (200 mg, 1.50 x 10^{-4} mol) was added to a mixture of trifluoroacetic acid (2 mL), CH_2Cl_2 (2 mL), and triethylsilane (0.2 mL). After 30 min, all the volatiles were removed under reduced pressure. The residue was then suspended in Et_2O (20 mL), filtered using a Büchner funnel and washed with Et_2O (20 mL) and dried *in vacuo* to yield a pink coloured solid. Yield: (120 mg, 3.65 x 10^{-5} mol), 74%, as 2 x TFA salt. M.p.: 208 °C (decomposed). ^{1}H NMR (500 MHz, DMSO-d_6, 300 K) δ (ppm): 12.6 (br, 2 H, COOH), 8.81-8.66 (m, 8 H, NDI), 5.71 (dd, J = 9.3 Hz, 5.4 Hz, 2 H, α-Cys), 4.39 (t, J = 5.9 Hz, 4 H, α-Alk), 3.43-3.34 (m, 4 H, Alkyl), 3.30 (br, 2 H, alkyl), 3.22-3.07 (m, 4 H, β-Cys), 2.70-2.64 (m, 2 H, SH). It was used as obtained from the deprotection reaction in DCLs.

A2b (Protected)

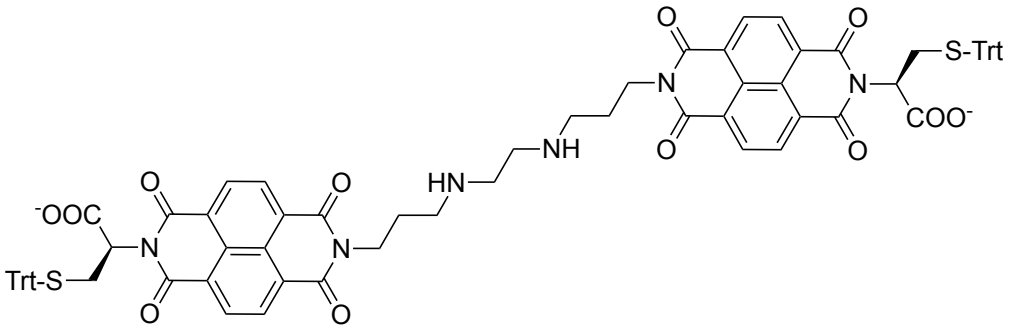

L-Cysteine naphthalenemonoimide (L-NMI) (403 mg, 6.56 x 10^{-4} mol) and dry Et_3N (0.3 mL) were dissolved in (10 mL) DMF in a 20 mL microwave tube. 1,2-Bis(3-aminopropylamino)ethane (0.059 mL, 3.28 x 10^{-4} mol) was added to the solution. The suspension was sonicated until the mixture was homogenous, and then heated under microwave irradiation at 120 °C for 5 minutes. The solvent was removed under reduced pressure, and the residue was washed with Et_2O and dried *in vacuo*. Yield: (343 mg, 2.52 x 10^{-4} mol) 76%, M.p.:

177 °C (decomposed). ^{1}H NMR (500 MHz, $CDCl_3$ with Et_3N, 300 K) δ (ppm): 8.75-8.56 (m, 8 H, NDI), 7.35-6.99 (m, 30 H, Trt), 5.51 (dd, *J* = 10.9 Hz, 4.4 Hz, 2 H, α-Cys), 4.28 (t, *J* = 7.1 Hz, 4 H, α-Alk), 3.44-3.39 (m, 2 H, β-Cys), 3.19-3.12 (m, 2 H, β-Cys), 2.77-2.68 (m, 6 H, Alkyl), 2.41-2.35 (m, 2H, Alkyl), 2.00-1.92 (m, 2 H, Alkyl). ^{13}C NMR (125 MHz, $CDCl_3$ with Et_3N) δ (ppm): 173.6, 162.2, 160.5, 147.1, 144.9, 129.6, 129.5, 128.1, 127.8, 127.7, 127.0, 126.5, 126.2, 66.1, 55.3, 39.3, 36.0 and 31.9. FTMS-NSI: calcd. for $C_{80}H_{64}N_6O_{12}S_2$ $[M-H]^-$ (*m/z*): 1363.3951, found: 1363.3862.

A2b (Deprotected)

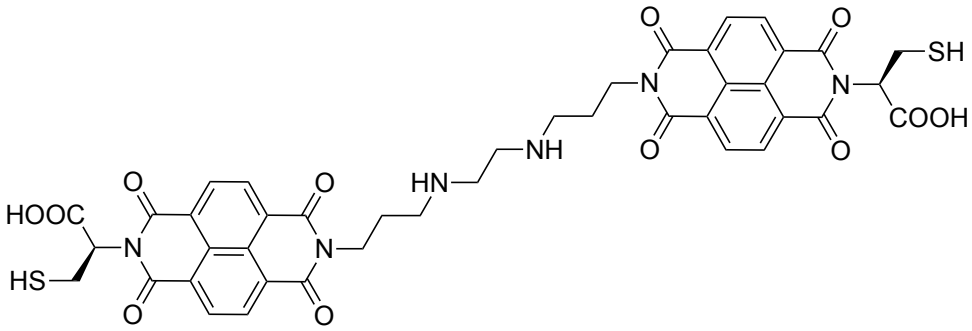

The protected **A2b** (200 mg, 1.47 x 10^{-4} mol) was added to a mixture of trifluoroacetic acid (2 mL), CH_2Cl_2 (2 mL), and triethylsilane (0.3 mL). After 30 min, all the volatiles were removed under reduced pressure. The residue was then suspended in Et_2O (20 mL), filtered using a Büchner funnel and washed with Et_2O (20 mL) and dried *in vacuo* to yield a pink coloured solid. Yield: (160 mg, 1.44 x 10^{-4} mol), 98%, as 2 x TFA salt. 195 °C (decomposed). ^{1}H NMR (500 MHz, DMSO-*d*$_6$, 300 K) δ (ppm): 12.10 (br, 2 H, COOH), 8.81-8.61 (m, 8 H, NDI), 5.68 (dd, *J* = 9.2 Hz, 5.1 Hz, 2 H, α-Cys), 4.18 (m, 4 H, α-Alk), 4.12 (bs, 4 H, α'-Alk), 3.22-3.13 (m, 2 H), 3.10-3.02 (m, 4 H, β-Cys), 2.70-2.64 (m, 2 H, SH), 2.37-2.33 (m, 2 H) and 2.05-1.95 (m, 2 H, Alkyl). It was used as obtained from the deprotection reaction in DCLs.

A2c (Protected)

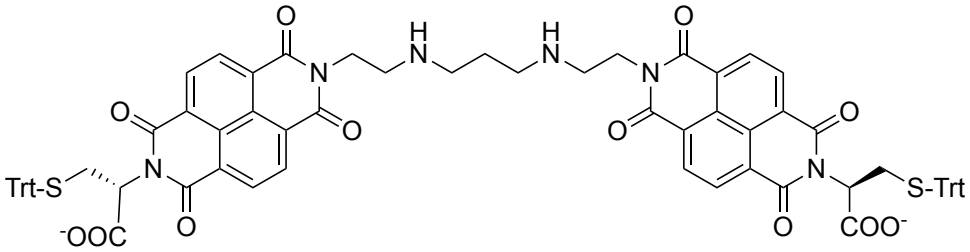

L-Cysteine naphthalenemonoimide (L-NMI) (300 mg, 4.90 x 10^{-4} mol) and dry Et_3N (0.3 mL) were dissolved in 5 mL DMF in an 8 mL microwave tube. 2-aminoethyl-1,3-propanediamine (0.041 mL, 2.40 x 10^{-4} mol) was added to the solution. The suspension was sonicated until the mixture was homogenous, and then heated under microwave irradiation at 120 °C for 5 minutes. The solvent was removed under reduced pressure, and the residue was washed with Et_2O and dried *in vacuo*. Yield: (285 mg, 2.11 x 10^{-4} mol) 88%, M.p.: 200 °C (decomposed). ^{1}H NMR (500 MHz, $CDCl_3$ with Et_3N, 300 K) δ (ppm): 8.75-8.50 (m, 8 H, NDI), 7.30-7.02 (m, 30 H, Trt), 5.50 (dd, *J* = 10.8 Hz, 4.6 Hz, 2 H, α-Cys), 4.28 (t, *J* = 6.5 Hz, 4 H, α-Alk), 3.40 (dd, *J* = 12.7 Hz, 4.3 Hz, 2 H, β-Cys), 3.17-3.08 (m, 2 H, β-Cys), 2.94 (t, *J* = 6.5 Hz, 2 H), 2.70 (t, *J* = 6.8 Hz, 2 H), 1.66-1.53 (m, 2 H), Some of the peaks are hidden under satellites of Et_3N. ^{13}C NMR (125 MHz, $CDCl_3$ with Et_3N) δ (ppm): 172.9, 163.2, 162.4, 144.9, 130.8, 129.7, 127.8, 127.6, 127.3, 126.5, 126.3, 126.0, 66.7, 59.3, 55.4, 48.8, 47.6 and 40.3. FTMS-NSI: calcd. for $C_{79}H_{60}N_6O_{12}S_2$ $[M-2H]^{2-}$ (*m/z*): 674.1861, found: 674.1851.

A2c (Deprotected)

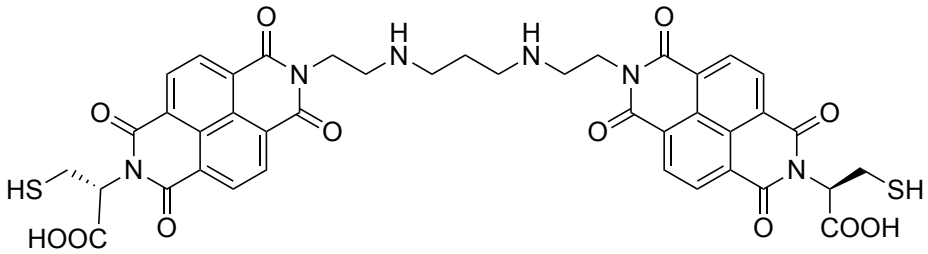

The protected **A2** (70 mg, 5.18 x 10^{-5} mol) was added to a mixture of trifluoroacetic acid (2 mL), CH_2Cl_2 (2 mL), and triethylsilane (0.2 mL). After 30 min, all the volatiles were removed under reduced pressure. The residue was then suspended in Et_2O (20 mL), filtered using a

Büchner funnel and washed with Et_2O (20 mL) and dried *in vacuo* to yield a pink coloured solid. Yield: (40 mg, 3.65 x 10^{-5} mol), 71%, as 2 x TFA salt. 195 °C (decomposed). ^{1}H NMR (500 MHz, DMSO-d_6, 300 K) δ (ppm): 13.18 (br, 2 H, COOH), 8.80-8.62 (m, 8 H, NDI), 5.74-5.65 (m, 2 H, α-Cys), 4.44-4.28 (m, 4 H, α-Alk), 3.55-3.46 (m, 2 H), 3.33-3.13 (m, 4 H, β-Cys), 3.07-3.02 (m, 4 H), 3.01-2.96 (m, 2 H), 2.68 (t, J = 9.0 Hz, 2 H, SH) 1.96-1.84 (m, 2 H). It was used as obtained from the deprotection reaction in DCLs.

A2c* (Protected)

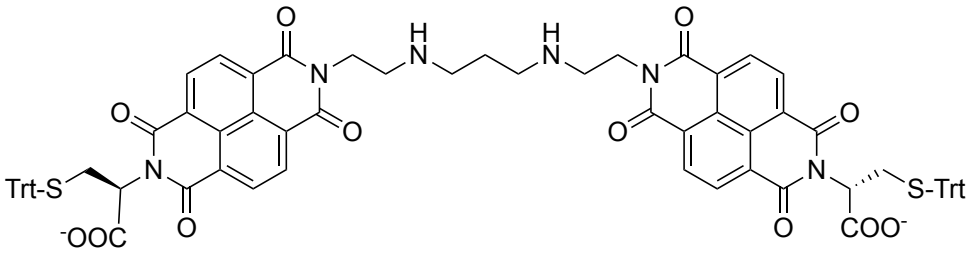

D-Cysteine naphthalenemonoimide (D-NMI) (100 mg, 1.64 x 10^{-4} mol) and dry Et_3N (0.1 mL) were dissolved in 5 mL DMF in an 8 mL microwave tube. 2-aminoethyl-1,3-propanediamine (0.013 mL, 7.60 x 10^{-5} mol) was added to the solution. The suspension was sonicated until the mixture was homogenous, and then heated under microwave irradiation at 120 °C for 5 minutes. The solvent was removed under reduced pressure, and the residue was washed with Et_2O and dried *in vacuo*. Yield: (88 mg, 6.5 x 10^{-5} mol) 86%, M.p.: > 235 °C (decomposed). ^{1}H NMR (500 MHz, $CDCl_3$ with Et_3N, 300 K) δ (ppm): 8.78-8.48 (m, 8 H, NDI), 7.40-6.97 (m, 30 H, Trt), 5.50 (dd, , J = 10.8 Hz, 4.6 Hz, 2 H, α-Cys), 4.30 (t, J = 6.5 Hz, 4 H, α-Alk), 3.43-3.36 (m, 2 H, β-Cys), 3.18-3.11 (m, 2 H, β-Cys), 2.96 (t, J = 6.5 Hz, 2 H), 2.70 (t, , J = 6.7 Hz, 2 H), 1.68-1.60 (m, 2 H), Some of the peaks are hidden under satellites of Et_3N. ^{13}C NMR (125 MHz, $CDCl_3$ with Et_3N) δ (ppm): 172.9, 163.2, 162.3, 144.9, 130.7, 130.0, 129.7, 127.9, 127.8, 127.6, 127.1, 126.3, 66.7, 59.3, 55.4, 48.0, 47.5, and 40.3. FTMS+NSI: calcd. for $C_{79}H_{63}N_6O_{12}S_2$ $[M+H]^+$ (*m/z*): 1351.3940, found: 1351.3954.

A2c* (Deprotected)

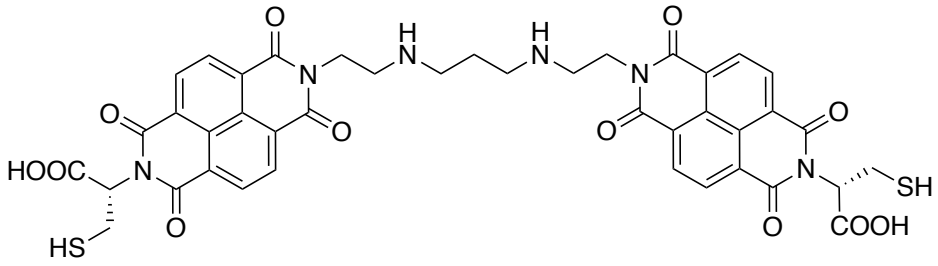

The protected A2* (88 mg, 6.51 x 10^{-5} mol) was added to a mixture of trifluoroacetic acid (2 mL), CH_2Cl_2 (2 mL), and triethylsilane (0.2 mL). After 30 min, all the volatiles were removed under reduced pressure. The residue was then suspended in Et_2O (20 mL), filtered using a Büchner funnel and washed with Et_2O (20 mL) and dried *in vacuo* to yield a pink coloured solid. Yield: (42 mg, 3.83 x 10^{-5} mol), 59%, as 2 x TFA salt. M.p.: > 119 °C (decomposed). ^{1}H NMR (500 MHz, DMSO-d_6, 300 K) δ (ppm): 13.20 (br, 2 H, COOH), 8.81-8.66 (m, 8 H, NDI), 5.70 (dd, J = 9.3 Hz, 5.5 Hz, 2 H, α-Cys), 4.43-4.34 (m, 4 H, α-Alk), 3.56-3.43 (m, 2 H), 3.23-3.12 (m, 4 H, β-Cys), 3.11-3.01 (m, 4 H), 3.00-2.93 (m, 2 H), 2.68 (t, J = 8.8 Hz, 2 H, SH) 1.95-1.81 (m, 2 H). It was used as obtained from the deprotection reaction in DCLs.

A3 (Protected)

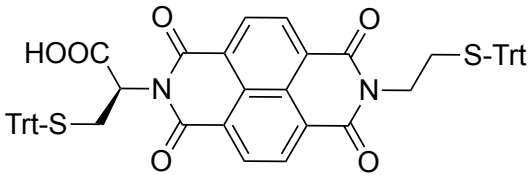

L-Cysteine naphthalenemonoimide (L-NMI) (150 mg, 2.46 x 10^{-4} mol) and dry Et_3N (0.2 mL) were dissolved in (5 mL) DMF in an 8 mL microwave tube. 2-Tritylsulfanylethanamine (87 mg, 2.46 x 10^{-4} mol) was added to the solution. Everything was dissolved in DMF giving a yellow solution, and then heated under microwave irradiation at 120 °C for 5 minutes. The solvent was removed under reduced pressure, and the residue was washed with Et_2O and dried *in vacuo*. Yield: (90 mg, 9.85 x 10^{-5} mol) 40%, M.p.: 150 °C (decomposed). ^{1}H NMR (500 MHz, DMSO-d_6, 300 K) δ (ppm): 12.05 (br, 1 H, COOH), 8.73-8.65 (m, 4 H, NDI), 7.44-7.09

(m, 30 H, Trt), 5.52 (dd, *J* = 10.5 Hz, 4.3 Hz, 1 H, α-Cys), 4.04 (t, *J* = 7.4 Hz, 2 H, α-Alk), 3.14-3.09 (m, 1 H, β-Cys), 2.94-2.89 (m, 1 H, β-Cys) and 2.59-2.53 (m, 2 H). ^{13}C NMR (125 MHz, DMSO-d_6,) δ (ppm): 162.7, 144.7, 144.4, 130.0, 129.4, 129.0, 128.5, 128.2, 127.9, 127.2, 127.9, 66.5, 45.6, 30.6, 29.7.

A3 (Deprotected)

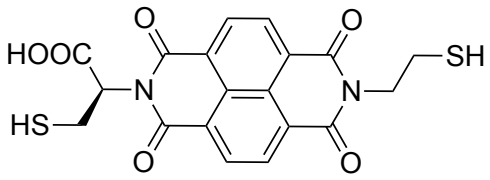

The protected **A3** (70 mg, 7.66 x 10^{-5} mol) was added to a mixture of trifluoroacetic acid (2 mL), CH_2Cl_2 (2 mL), and triethylsilane (0.2 mL). After 30 min, all the volatiles were removed under reduced pressure. The residue was then suspended in Et_2O (20 mL), filtered using a Büchner funnel and washed with Et_2O (20 mL) and dried *in vacuo* to yield a yellow coloured solid. Yield: (30 mg, 6.98 x 10^{-5} mol), 91%, M.p.: 132 °C (decomposed). The NMR obtained for **A3** deprotected gave broad signal in NDI region (could be a sign of polymerisation) and the region for α and β-Cys showed noisy signals. However, the peaks representing the trityl group were absent, which was the sign of deprotected sample. A3 was used as obtained from the deprotection reaction in DCLs.

Donor Building Blocks:

I have performed either the full or partial synthesis of all the DN molecules described in this thesis depending on the starting material available. The synthetic routes have been followed from previously reported protocols.[119] All the ^{1}H NMR data match the literature data.

D1S Protected

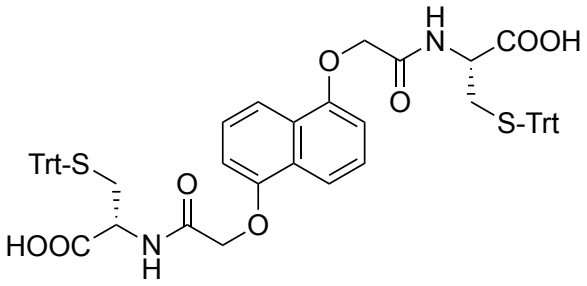

^{1}H NMR (500 MHz, DMSO-d_6, 300 K) δ (ppm): 12.74 (br, 2 H, COOH), 8.30 (d, J = 8.1 Hz, 2 H, NH), 7.60 (d, J = 8.9 Hz, 2 H, DN), 7.34–7.17 (m, 32 H, Trt, DN), 7.07 (d, J = 7.8, 2 H, DN), 4.61 (s, 4 H, OCH_2), 4.26 (dt, J = 8.2, 4.7 Hz, 2 H, α-Cys), 2.37 (dd, J = 12.2, 5.1 Hz, 2 H, β-Cys), 2.32-2.28 (m, 2 H, β-Cys). The ^{1}H NMR spectrum matches the literature data.

D1S Deprotected

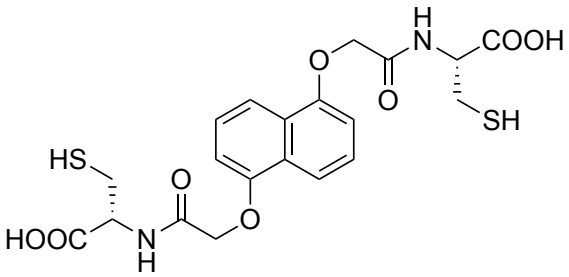

^{1}H NMR (500 MHz, DMSO-d_6, 300 K) δ (ppm): 8.36 (d, J = 7.9 Hz, 2 H, NH), 7.89 (d, J = 8.5 Hz, 2 H, DN), 7.41 (t, J = 8.1 Hz, 2 H, DN), 6.99 (d, J = 7.8 Hz, 2 H, DN), 4.77 (s, 4 H, OCH_2), 4.53 (m, 2 H, α-Cys), 2.93–3.00 (m, 2 H, β- Cys), 2.91-2.84 (m, 2 H, β-Cys), 2.42 (t, J = 8.5 Hz, 2 H, SH). The ^{1}H NMR spectrum matches the literature data.

D2S Protected

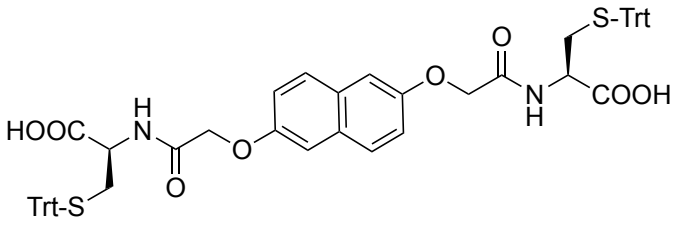

^{1}H NMR (500 MHz, DMSO-d_6, 300 K) δ (ppm): 12.89 (br, 2 H, COOH), 8.46 (d, J = 8.3 Hz, 2 H, NH), 7.61 (d, J = 8.9 Hz, 2 H, DN), 7.27-7.13 (m, 32 H, Trt, DN), 4.61 (s, 4 H, OCH_2), 4.24 (dt, J = 8.7, 4.7 Hz, 2 H, α-Cys), 2.65-2.60 (m, 4 H, β-Cys). The ^{1}H NMR spectrum matches the literature data.

D2S Deprotected

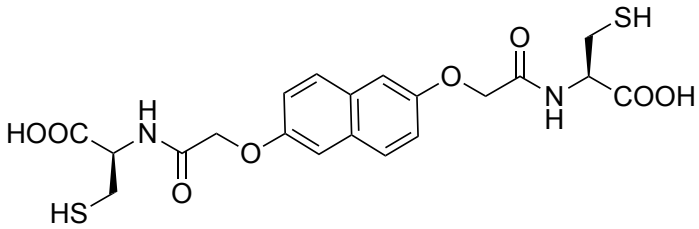

^{1}H NMR (500 MHz, DMSO-d_6, 300 K) δ (ppm): 8.35 (d, J = 8.3 Hz, 2 H, NH), 7.72 (d, J = 9.0 Hz, 2 H, DN), 7.29 (d, J = 2.6 Hz, 2 H, DN), 7.23 (dd, J = 8.9, 2.6 Hz, 2 H, DN), 4.66 (s, 4 H, OCH_2), 4.48 (dt, J = 7.6, 4.5 Hz, 2 H, α-Cys), 3.00-2.90 (m, 2 H, β-Cys), 2.90-2.83 (m, 2 H, β'-Cys), 2.42 (m, 2 H, SH). The ^{1}H NMR spectrum matches the literature data.

D1L Protected

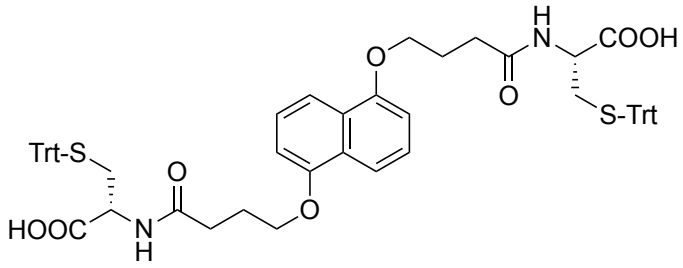

^{1}H NMR (500 MHz, DMSO-d_6, 300 K) δ (ppm): 12.81 (br, 2 H, COOH), 8.24 (d, J = 7.9 Hz, 2 H, NH), 7.73 (d, J = 8.4 Hz, 2 H, DN), 7.41-7.10 (m, 32 H, Trt, DN), 6.96 (d, J = 7.7 Hz, 2 H, DN), 4.40 (td, J = 7.7, 4. Hz, 2 H, α-Cys), 4.14 (t, J = 6.2, 4 H, $OCH_2CH_2CH_2$), 2.87-2.80 (m, 2 H, β-Cys), 2.77–2.68 (m, 2 H, β-Cys), 2.44-2.39 (m, 4 H, $OCH_2CH_2CH_2$), 2.16-2.04 (m, 4 H, $OCH_2CH_2CH_2$). The ^{1}H NMR spectrum matches the literature data.

D1L Deprotected

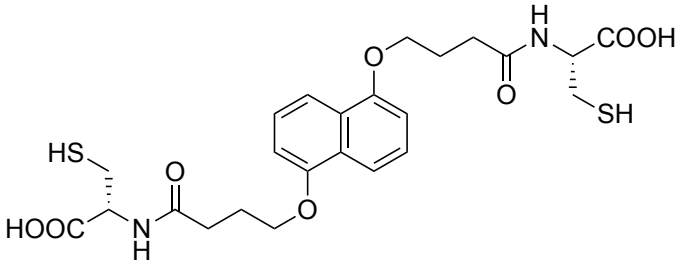

^{1}H NMR (500 MHz, DMSO-d_6, 300 K) δ (ppm): 8.24 (d, J = 7.9 Hz, 2 H, NH), 7.73 (d, J = 8.4 Hz, 2 H, DN), 7.37 (t, J = 8.0 Hz, 2 H, DN), 6.95 (d, J = 7.7 Hz, 2 H, DN), 4.40 (td, J = 7.7, 4.6 Hz, 2 H, α-Cys), 4.14 (t, J = 6.3, 4 H, $OCH_2CH_2CH_2$), 2.89-2.80 (m, 2 H, β-Cys), 2.76–2.70 (m, 2 H, β-Cys), 2.45-2.40 (m, 4 H, $OCH_2CH_2CH_2$), 2.11-2.04 (m, 4 H, $OCH_2CH_2CH_2$). The ^{1}H NMR spectrum matches the literature data.

D2L Protected

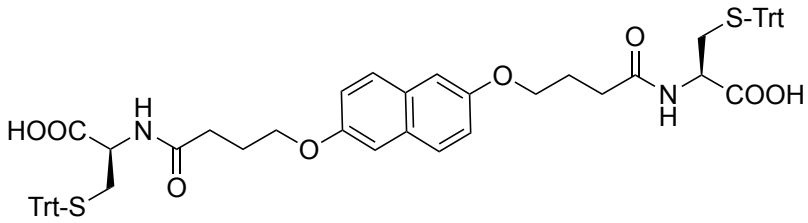

^{1}H NMR (500 MHz, DMSO-d_6, 300 K) δ (ppm): 12.62 (br, 2 H, COOH), 8.22 (d, J = 8.1 Hz, 2 H, NH), 7.59 (d, J = 9.0 Hz, 2 H, DN), 7.37-7.12 (m, 30 H, Trt), 7.07 (dd, J = 8.8, 2.4 Hz, 2 H, DN), 4.15 (td, J = 8.4, 4.9 Hz, 2 H, α-Cys), 4.02 (t, J = 6.6 Hz, 4 H, $OCH_2CH_2CH_2$), 2.40-2.34 (m, 4 H, β-Cys), 2.33-2.28 (m, 2 H, $OCH_2CH_2CH_2$), 2.01-1.90 (m, 4 H, $OCH_2CH_2CH_2$). The ^{1}H NMR spectrum matches the literature data.

D2L Deprotected

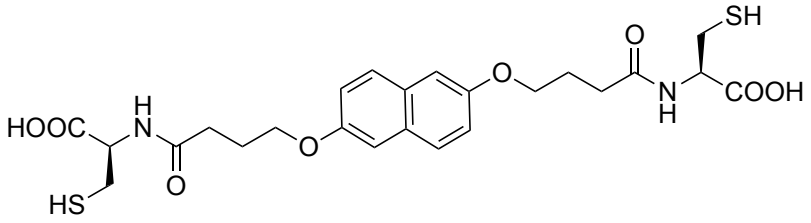

^{1}H NMR (500 MHz, DMSO-d_6, 300 K) δ (ppm): 8.20 (d, J = 7.9 Hz, 2 H, NH), 7.67 (d, J = 8.9 Hz, 2 H, DN), 7.22 (d, J = 2.6 Hz, 2 H, DN), 7.10 (dd, J = 8.8, 2.6 Hz, 2 H, DN), 4.38 (dt, J = 7.7, 4.6 Hz, 2 H, α-Cys), 4.03 (t, J = 6.5, 4 H, $OCH_2CH_2CH_2$), 2.88-2.81 (m, 2 H, β-Cys), 2.76–2.69 (m, 2 H, β-Cys), 2.39-2.32 (m, 4 H, $OCH_2CH_2CH_2$), 2.02-1.95 (m, 4 H, $OCH_2CH_2CH_2$). The ^{1}H NMR spectrum matches the literature data.

References

1 P. T. Corbett, J. Leclaire, L. Vial, K. R. West, J.-L. Wietor, J. K. Sanders and S. Otto, *Chem. Rev.*, 2006, **106**, 3652–3711.

2 F. B. L. Cougnon and J. K. M. Sanders, *Acc. Chem. Res.*, 2012, **45**, 2211–2221.

3 S. Otto, R. L. . Furlan and J. K. . Sanders, *Drug Discov. Today*, 2002, **7**, 117–125.

4 J. Li, P. Nowak and S. Otto, *J. Am. Chem. Soc.*, 2013, **135**, 9222–9239.

5 P. Dydio, P.-A. R. Breuil and J. N. Reek, *Isr. J. Chem.*, 2013, **53**, 61–74.

6 B. Rasmussen, A. Sørensen, S. R. Beeren and M. Pittelkow, *Dynamic Combinatorial Chemistry*, John Wiley & Sons: Hoboken, NJ, USA, 2014.

7 N. Giuseppone and J.-M. Lehn, *Chem. - Eur. J.*, 2006, **12**, 1715–1722.

8 L. A. Ingerman and M. L. Waters, *J. Org. Chem.*, 2009, **74**, 111–117.

9 N. Giuseppone and J.-M. Lehn, *Angew. Chem. Int. Ed.*, 2006, **45**, 4619–4624.

10 S. Otto, R. L. Furlan and J. K. Sanders, *Science*, 2002, **297**, 590–593.

11 C. Browne, T. K. Ronson and J. R. Nitschke, *Angew. Chem. Int. Ed.*, 2014, **53**, 10701–10705.

12 P. C. Haussmann, S. I. Khan and J. F. Stoddart, *J. Org. Chem.*, 2007, **72**, 6708–6713.

13 J. Wu, K. C.-F. Leung and J. F. Stoddart, *Proc. Natl. Acad. Sci.*, 2007, **104**, 17266–17271.

14 C. Dietrich-Buchecker and G. Rapenne, *Chem. Commun.*, 1997, 2053–2054.

15 S. Otto and K. Severin, in *Creative Chemical Sensor Systems*, ed. T. Schrader, Springer Berlin Heidelberg, Berlin, Heidelberg, 2007, vol. 277, pp. 267–288.

16 K. A. Clark, E. L. Krueger and D. A. Vanden Bout, *J. Phys. Chem. C*, 2014, **118**, 24325–24334.

17 S. Kirstein and S. Daehne, *Int. J. Photoenergy*, 2006, **2006**, 1–21.

18 J. E. A. Webb, M. J. Crossley, P. Turner and P. Thordarson, *J. Am. Chem. Soc.*, 2007, **129**, 7155–7162.

19 E. Wasserman, *J. Am. Chem. Soc.*, 1960, **82**, 4433–4434.

20 P. R. Ashton, C. L. Brown, E. J. T. Chrystal, T. T. Goodnow, A. E. Kaifer, K. P. Parry, D. Philp, A. M. Z. Slawin, N. Spencer, J. F. Stoddart and D. J. Williams, *J. Chem. Soc. Chem. Commun.*, 1991, 634.

21 D. B. Amabilino, P. R. Ashton, C. L. Brown, E. Cordova, L. A. Godinez, T. T. Goodnow, A. E. Kaifer, S. P. Newton and M. Pietraszkiewicz, *J. Am. Chem. Soc.*, 1995, **117**, 1271–1293.

22 P. R. Ashton, A. M. Heiss, D. Pasini, F. M. Raymo, A. N. Shipway, J. F. Stoddart and N. Spencer, *Eur. J. Org. Chem.*, 1999, **1999**, 995–1004.
23 H. Y. Au-Yeung, University of Cambridge, 2010.
24 J. E. Beves, B. A. Blight, C. J. Campbell, D. A. Leigh and R. T. McBurney, *Angew. Chem. Int. Ed.*, 2011, **50**, 9260–9327.
25 L. C. Gilday, T. Lang, A. Caballero, P. J. Costa, V. Félix and P. D. Beer, *Angew. Chem. Int. Ed.*, 2013, **52**, 4356–4360.
26 K. E. Griffiths and J. F. Stoddart, *Pure Appl. Chem.*, 2008, **80**, 485–506.
27 G. Schill and A. Lüttringhaus, *Angew. Chem. Int. Ed. Engl.*, 1964, **3**, 546–547.
28 N. Kameta, K. Hiratani and Y. Nagawa, *Chem. Commun.*, 2004, 466.
29 K. Hirose, K. Nishihara, N. Harada, Y. Nakamura, D. Masuda, M. Araki and Y. Tobe, *Org. Lett.*, 2007, **9**, 2969–2972.
30 J. P. Sauvage, *Acc. Chem. Res.*, 1990, **23**, 319–327.
31 J. F. Nierengarten, C. O. Dietrich-Buchecker and J. P. Sauvage, *J. Am. Chem. Soc.*, 1994, **116**, 375–376.
32 P. Mobian, J.-P. Collin and J.-P. Sauvage, *Tetrahedron Lett.*, 2006, **47**, 4907–4909.
33 H. L. Frisch and E. Wasserman, 1961, 7.
34 B. H. Jerome Vinograd, 1967, **216**, 647–652.
35 G. Gil-Ramírez, D. A. Leigh and A. J. Stephens, *Angew. Chem. Int. Ed.*, 2015, **54**, 6110–6150.
36 F. B. D. Nicholas R. Cozzarelli, *J. Biol. Chem.*, **260**, 4975–4983.
37 W. R. Wikoff, *Science*, 2000, **289**, 2129–2133.
38 N. Ponnuswamy, F. B. L. Cougnon, J. M. Clough, G. D. Pantoş and J. K. M. Sanders, *Science*, 2012, **338**, 783–785.
39 D. Cao, M. Amelia, L. M. Klivansky, G. Koshkakaryan, S. I. Khan, M. Semeraro, S. Silvi, M. Venturi, A. Credi and Y. Liu, *J. Am. Chem. Soc.*, 2009, **132**, 1110–1122.
40 M. B. Avinash, K. V. Sandeepa and T. Govindaraju, *Beilstein J. Org. Chem.*, 2013, **9**, 1565–1571, 7 pp.
41 S. Basu, A. Coskun, D. C. Friedman, M. A. Olson, D. Benítez, E. Tkatchouk, G. Barin, J. Yang, A. C. Fahrenbach, W. A. Goddard III and J. F. Stoddart, *Chem. - Eur. J.*, 2011, **17**, 2107–2119.
42 N. H. Evans, E. S. H. Allinson, M. D. Lankshear, K.-Y. Ng, A. R. Cowley, C. J. Serpell, S. M. Santos, P. J. Costa, V. Félix and P. D. Beer, *RSC Adv.*, 2011, **1**, 995.
43 G. T. Spence and P. D. Beer, *Acc. Chem. Res.*, 2013, **46**, 571–586.
44 N. H. Evans, C. J. Serpell and P. D. Beer, *Angew. Chem. Int. Ed.*, 2011, **50**, 2507–2510.

45 G. Rapenne, C. Dietrich-Buchecker and J.-P. Sauvage, *J. Am. Chem. Soc.*, 1999, **121**, 994–1001.

46 C. Dietrich-Buchecker and J.-P. Sauvage, *Chem. Commun.*, 1999, 615–616.

47 A. L. Kieran, A. D. Bond, A. M. Belenguer and J. K. M. Sanders, *Chem. Commun.*, 2003, 2674.

48 C. Lincheneau, B. Jean-Denis and T. Gunnlaugsson, *Chem. Commun.*, 2014, **50**, 2857.

49 F. Aparicio and L. Sánchez, *Chem. - Eur. J.*, 2013, **19**, 10482–10486.

50 D. A. Leigh, A. Murphy, J. P. Smart and A. M. Z. Slawin, *Angew. Chem. Int. Ed. Engl.*, 1997, **36**, 728–732.

51 F. G. Gatti, D. A. Leigh, S. A. Nepogodiev, A. M. Z. Slawin, S. J. Teat and J. K. Y. Wong, *J. Am. Chem. Soc.*, 2001, **123**, 5983–5989.

52 N. S. Simpkins, D. F. Weske, L. Male, S. J. Coles and M. B. Pitak, *Chem. Commun.*, 2013, **49**, 5010–5012.

53 P. R. Ashton, S. E. Boyd, A. Brindle, S. J. Langford, S. Menzer, L. Pe´rez-García, J. A. Preece, isco M. Raymo, N. Spencer, J. Fraser Stoddart, A. J. P. White and D. J. Williams, *New J. Chem.*, 1999, **23**, 587–602.

54 T. W. Anderson, G. D. Pantoş and J. K. M. Sanders, *Org. Biomol. Chem.*, 2011, **9**, 7547.

55 I. Aprahamian, O. Š. Miljanic, W. R. Dichtel, K. Isoda, T. Yasuda, T. Kato and J. F. Stoddart, *Bull. Chem. Soc. Jpn.*, 2007, **80**, 1856–1869.

56 G. Barin, A. Coskun, M. M. G. Fouda and J. F. Stoddart, *ChemPlusChem*, 2012, **77**, 159–185.

57 O. A. Bozdemir, G. Barin, M. E. Belowich, A. N. Basuray, F. Beuerle and J. F. Stoddart, *Chem. Commun.*, 2012, **48**, 10401–10403.

58 R. S. Forgan, J. J. Gassensmith, D. B. Cordes, M. M. Boyle, K. J. Hartlieb, D. C. Friedman, A. M. Z. Slawin and J. F. Stoddart, *J. Am. Chem. Soc.*, 2012, **134**, 17007–17010.

59 R. L. Furlan, S. Otto and J. K. Sanders, *Proc. Natl. Acad. Sci.*, 2002, **99**, 4801–4804.

60 R. F. Ludlow and S. Otto, *J. Am. Chem. Soc.*, 2010, **132**, 5984–5986.

61 M. M. Boyle, R. S. Forgan, D. C. Friedman, J. J. Gassensmith, R. A. Smaldone, J. F. Stoddart and J.-P. Sauvage, *Chem. Commun.*, 2011, **47**, 11870–11872.

62 C. Dietrich-Buchecker, B. Colasson, M. Fujita, A. Hori, N. Geum, S. Sakamoto, K. Yamaguchi and J.-P. Sauvage, *J. Am. Chem. Soc.*, 2003, **125**, 5717–5725.

63 J.-F. Ayme, J. E. Beves, C. J. Campbell and D. A. Leigh, *Angew. Chem. Int. Ed.*, 2014, **53**, 7823–7827.

64 J.-F. Ayme, J. E. Beves, C. J. Campbell, G. Gil-Ramírez, D. A. Leigh and A. J. Stephens, *J. Am. Chem. Soc.*, 2015, **137**, 9812–9815.

65 J.-F. Ayme, J. E. Beves, D. A. Leigh, R. T. McBurney, K. Rissanen and D. Schultz, *J. Am. Chem. Soc.*, 2012, **134**, 9488–9497.

66 S. Erbas-Cakmak, D. A. Leigh, C. T. McTernan and A. L. Nussbaumer, *Chem. Rev.*, 2015, **115**, 10081–10206.

67 M. von Delius, E. M. Geertsema and D. A. Leigh, *Nat. Chem.*, 2010, **2**, 96–101.

68 S. Kassem, A. T. L. Lee, D. A. Leigh, A. Markevicius and J. Solà, *Nat. Chem.*, 2015, **8**, 138–143.

69 E. H. A. Beckers, Z. Chen, S. C. J. Meskers, P. Jonkheijm, A. P. H. J. Schenning, X.-Q. Li, P. Osswald, F. Wuerthner and R. A. J. Janssen, *J. Phys. Chem. B*, 2006, **110**, 16967–16978.

70 C. A. Hunter and J. K. M. Sanders, *J. Am. Chem. Soc.*, 1990, **112**, 5525–5534.

71 R. M. Parrish and C. D. Sherrill, *J. Am. Chem. Soc.*, 2014, **136**, 17386–17389.

72 M. S. Cubberley and B. L. Iverson, *J. Am. Chem. Soc.*, 2001, **123**, 7560–7563.

73 R. Foster, *J. Phys. Chem.*, 1980, **84**, 2135–2141.

74 S. Burattini, H. M. Colquhoun, J. D. Fox, D. Friedmann, B. W. Greenland, P. J. F. Harris, W. Hayes, M. E. Mackay and S. J. Rowan, *Chem. Commun.*, 2009, 6717–6719.

75 P. M. Alvey, J. J. Reczek, V. Lynch and B. L. Iverson, *J. Org. Chem.*, 2010, **75**, 7682–7690.

76 G. Griffini, J. D. Douglas, C. Piliego, T. W. Holcombe, S. Turri, J. M. J. Frechet and J. L. Mynar, *Adv. Mater.*, 2011, **23**, 1660–1664.

77 V. L. Gunderson, A. L. Smeigh, C. H. Kim, D. T. Co and M. R. Wasielewski, *J. Am. Chem. Soc.*, 2012, **134**, 4363–4372.

78 M. E. El-Khouly, C. A. Wijesinghe, V. N. Nesterov, M. E. Zandler, S. Fukuzumi and F. D'Souza, *Chem. - Eur. J.*, 2012, **18**, 13844–13853.

79 M. Fujitsuka, H. Shimakoshi, Y. Tei, K. Noda, S. Tojo, Y. Hisaeda and T. Majima, *Phys. Chem. Chem. Phys.*, 2013, **15**, 5677–5683.

80 H. Y. Au-Yeung, G. D. Pantoş and J. K. M. Sanders, *J. Org. Chem.*, 2011, **76**, 1257–1268.

81 P. R. Ashton, A. M. Z. Slawin, N. Spencer, J. F. Stoddart and D. J. Williams, *J. Chem. Soc. Chem. Commun.*, 1987, 1066–1069.

82 B. L. Allwood, N. Spencer, H. Shahriari-Zavareh, J. F. Stoddart and D. J. Williams, *J. Chem. Soc. Chem. Commun.*, 1987, 1064–1066.

83 G. J. Moody, R. K. Owusu, A. M. Z. Slawin, N. Spencer, J. F. Stoddart, J. D. R. Thomas and D. J. Williams, *Angew. Chem. Int. Ed. Engl.*, 1987, **26**, 890–892.

84 G. Koshkakaryan, L. M. Klivansky, D. Cao, M. Snauko, S. J. Teat, J. O. Struppe and Y. Liu, *J. Am. Chem. Soc.*, 2009, **131**, 2078–2079.

85 J. C. Barnes, M. Juríček, N. L. Strutt, M. Frasconi, S. Sampath, M. A. Giesener, P. L. McGrier, C. J. Bruns, C. L. Stern, A. A. Sarjeant and J. F. Stoddart, *J. Am. Chem. Soc.*, 2012, **135**, 183–192.

86 P. R. Ashton, T. T. Goodnow, A. E. Kaifer, M. V. Reddington, A. M. Z. Slawin, N. Spencer, J. F. Stoddart, C. Vicent and D. J. Williams, *Angew. Chem. Int. Ed. Engl.*, 1989, **28**, 1396–1399.

87 F. M. Raymo, M. D. Bartberger, K. N. Houk and J. F. Stoddart, *J. Am. Chem. Soc.*, 2001, **123**, 9264–9267.

88 M. Asakawa, P. R. Ashton, V. Balzani, A. Credi, C. Hamers, G. Mattersteig, M. Montalti, A. N. Shipway, N. Spencer, J. F. Stoddart, M. S. Tolley, M. Venturi, A. J. P. White and D. J. Williams, *Angew. Chem. Int. Ed.*, 1998, **37**, 333–337.

89 Y. Liu, P. A. Bonvallet, S. A. Vignon, S. I. Khan and J. F. Stoddart, *Angew. Chem.*, 2005, **117**, 3110–3115.

90 G. Koshkakaryan, D. Cao, L. M. Klivansky, S. J. Teat, J. L. Tran and Y. Liu, *Org. Lett.*, 2010, **12**, 1528–1531.

91 P. R. Ashton, C. L. Brown, E. J. T. Chrystal, T. T. Goodnow, A. E. Kaifer, K. P. Parry, A. M. Z. Slawin, N. Spencer, J. F. Stoddart and D. J. Williams, *Angew. Chem. Int. Ed. Engl.*, 1991, **30**, 1039–1042.

92 D. B. Amabilino, P. R. Ashton, A. S. Reder, N. Spencer and J. F. Stoddart, *Angew. Chem. Int. Ed. Engl.*, 1994, **33**, 433–437.

93 D. B. Amabilino, P. R. Ashton, S. E. Boyd, J. Y. Lee, S. Menzer, J. F. Stoddart and D. J. Williams, *Angew. Chem. Int. Ed. Engl.*, 1997, **36**, 2070–2072.

94 D. B. Amabilino, P. R. Ashton, A. S. Reder, N. Spencer and J. F. Stoddart, *Angew. Chem. Int. Ed. Engl.*, 1994, **33**, 1286–1290.

95 K. Wang, C.-C. Yee and H. Y. Au-Yeung, *Chem. Sci.*, 2016, **7**, 2787–2792.

96 P. L. Privalov and S. J. Gill, *Pure Appl. Chem.*, 1989, **61**, 1097–1104.

97 N. Muller, *Acc. Chem. Res.*, 1990, **23**, 23–28.

98 K. A. Silverstein, A. D. J. Haymet and K. A. Dill, *J. Am. Chem. Soc.*, 1998, **120**, 3166–3175.

99 Y. Furusho, T. Oku, T. Hasegawa, A. Tsuboi, N. Kihara and T. Takata, *Chem. - Eur. J.*, 2003, **9**, 2895–2903.

100 J. Leclaire, L. Vial, S. Otto and J. K. M. Sanders, *Chem. Commun.*, 2005, 1959–1961.

101 J. Canadell, H. Goossens and B. Klumperman, *Macromolecules*, 2011, **44**, 2536–2541.

102 S. P. Black, J. K. M. Sanders and A. R. Stefankiewicz, *Chem Soc Rev*, 2014, **43**, 1861–1872.

103 R. T. S. Lam, *Science*, 2005, **308**, 667–669.
104 Z. Rodriguez-Docampo and S. Otto, *Chem. Commun.*, 2008, 5301–5303.
105 M. E. Belowich and J. F. Stoddart, *Chem. Soc. Rev.*, 2012, **41**, 2003–2024.
106 M. E. Bracchi and D. A. Fulton, *Chem Commun*, 2015, **51**, 11052–11055.
107 M. Ciaccia and S. Di Stefano, *Org. Biomol. Chem.*, 2015, **13**, 646–654.
108 R. J. Sarma, S. Otto and J. R. Nitschke, *Chem. - Eur. J.*, 2007, **13**, 9542–9546.
109 K. Caprice, M. Pupier, A. Kruve, C. A. Schalley and F. B. L. Cougnon, *Chem. Sci.*, , DOI:10.1039/C7SC04901C.
110 H. Hioki and W. C. Still, *J. Org. Chem.*, 1998, **63**, 904–905.
111 K. R. West, R. F. Ludlow, P. T. Corbett, P. Besenius, F. M. Mansfeld, P. A. G. Cormack, D. C. Sherrington, J. M. Goodman, M. C. A. Stuart and S. Otto, *J. Am. Chem. Soc.*, 2008, **130**, 10834–10835.
112 N. Ponnuswamy, F. B. L. Cougnon, G. D. Pantoş and J. K. M. Sanders, *J. Am. Chem. Soc.*, 2014, **136**, 8243–8251.
113 K. Jalani, M. Kumar and S. J. George, *Chem. Commun.*, 2013, **49**, 5174–5176.
114 S. G. Ramkumar and S. Ramakrishnan, *Macromolecules*, 2010, **43**, 2307–2312.
115 C. Tsiamantas, X. de Hatten, C. Douat, B. Kauffmann, V. Maurizot, H. Ihara, M. Takafuji, N. Metzler-Nolte and I. Huc, *Angew. Chem. Int. Ed.*, 2016, **55**, 6848–6852.
116 T. Iijima, S. A. Vignon, H.-R. Tseng, T. Jarrosson, J. K. M. Sanders, F. Marchioni, M. Venturi, E. Apostoli, V. Balzani and J. F. Stoddart, *Chem. - Eur. J.*, 2004, **10**, 6375–6392.
117 H. Y. Au-Yeung, G. D. Pantoş and J. K. M. Sanders, *Angew. Chem. Int. Ed.*, 2010, **49**, 5331–5334.
118 H. Y. Au-Yeung, G. D. Pantoş and J. K. M. Sanders, *Proc. Natl. Acad. Sci. U. S. A.*, 2009, **106**, 10466–10470.
119 H. Y. Au-Yeung, G. D. Pantoş and J. K. M. Sanders, *J. Am. Chem. Soc.*, 2009, **131**, 16030–16032.
120 H. Y. Au-Yeung, F. B. L. Cougnon, S. Otto, G. D. Pantoş and J. K. M. Sanders, *Chem Sci*, 2010, **1**, 567–574.
121 F. B. Cougnon, University of Cambridge, 2012.
122 F. B. L. Cougnon, H. Y. Au-Yeung, G. D. Pantoş and J. K. M. Sanders, *J. Am. Chem. Soc.*, 2011, **133**, 3198–3207.
123 F. B. L. Cougnon, N. A. Jenkins, G. D. Pantoş and J. K. M. Sanders, *Angew. Chem. Int. Ed.*, 2012, **51**, 1443–1447.
124 Fabien B. L. Cougnon, Cambridge, 2011.

125 W. Wang, L. Wang, B. J. Palmer, G. J. Exarhos and A. D. Q. Li, *J. Am. Chem. Soc.*, 2006, **128**, 11150–11159.

126 Nandhini Ponnuswamy, Cambridge, 2012.

127 J.-F. Ayme, J. E. Beves, D. A. Leigh, R. T. McBurney, K. Rissanen and D. Schultz, *Nat. Chem.*, 2012, **4**, 15–20.

128 J. J. Danon, A. Krüger, D. A. Leigh, J.-F. Lemonnier, A. J. Stephens, I. J. Vitorica-Yrezabal and S. L. Woltering, *Science*, 2017, **355**, 159–162.

129 S. P. Black, A. R. Stefankiewicz, M. M. J. Smulders, D. Sattler, C. A. Schalley, J. R. Nitschke and J. K. M. Sanders, *Angew. Chem. Int. Ed.*, 2013, **52**, 5749–5752.

130 P. Pengo, G. D. Pantos, S. Otto and J. K. M. Sanders, *J. Org. Chem.*, 2006, **71**, 7063–7066.